Probing the Physics of the Intracluster Medium

by

Ian G. McCarthy
B.Sc., Saint Mary's University, 2000

A Dissertation Submitted in Partial Fulfillment of the
Requirements for the Degree of

DOCTOR OF PHILOSOPHY

in the Department of Physics and Astronomy

Supervisor: Dr. Arif Babul

ABSTRACT

Clusters of galaxies are the largest and most massive virialized objects in the universe. And because structure formation in the universe occurs hierarchically, clusters represent the end points of this process. As a result, these systems contain a wealth of cosmological information including a detailed fossil record of the structure formation process. However, in order to fully exploit clusters for cosmological purposes, it is necessary to model the internal properties of these systems in detail, particularly the baryonic component. Although much progress has been made on this front, there remain several important outstanding issues in our understanding of the properties of the intracluster medium (ICM), a diffuse plasma that fills clusters and dominates (by mass) the baryonic component of these systems. In particular, very little is presently known about the potential role of non-gravitational ICM physics such as radiative cooling, thermal conduction, and heating via outflows from supermassive black holes (i.e., active galactic nuclei - AGN) that are often located at the centers of clusters.

In this dissertation, we have attempted to shed light on this important issue. In particular, we have developed physically-motivated analytic models of the ICM in order to assess the role that non-gravitational processes, such as radiative cooling and heating from AGN, play in mediating the observed properties of clusters. We have carried out detailed and systematic comparisons between our models and the observed global and structural X-ray and Sunyaev-Zeldovich (SZ) effect properties of clusters. From this comparison we conclude the following. As expected, a pure gravitational model (i.e., the standard self-similar model) fails to match the observed properties of clusters. A model that invokes radiative cooling but no sources of non-gravitational heating also fails, as it has no hope of avoiding the so-called "cooling crisis" or of explaining the origin of "non-cooling flow" clusters. On the other hand, a model that includes non-gravitational heating but that

does not take into account the effects of radiative cooling fails to account for the observed global and structure properties of "cooling flow" clusters and obviously has no hope of explaining galaxy or star formation in clusters. We find that in order to account for the global X-ray and SZ effect scaling relations (including their intrinsic scatter), it is necessary to invoke both radiative cooling and a distribution in the level of non-gravitational heating experienced by clusters. Under this scenario, clusters that were severely heated early on likely evolved into "non-cooling flow" clusters, whereas clusters that were heated by only mild amounts likely evolved into "cooling flow" clusters. This conclusion is reinforced by comparisons to new spatially-resolved entropy, temperature, and surface brightness profiles derived from Chandra and XMM-Newton X-ray data.

Supervisor: Dr. A. Babul, (Department of Physics and Astronomy)

Contents

List of Tables

List of Figures

ACKNOWLEDGEMENTS

There are a great many people that I would like to thank for their contributions (both direct and indirect) to this work and/or for their support throughout the years. However, it is inevitable that I will miss someone along the way and for that I apologize.

First, I would like to thank my primary collaborators, in particular my thesis advisor Arif Babul, Michael Balogh, Gilbert Holder, Doug Johnstone, Andreea Font, and Greg Poole. Arif has provided excellent guidance throughout my time at UVic, including teaching me the delicate art of balancing science with human psychology. Also, I thank him for pushing me to "sell my product" to the outside community. Without that, I am sure I would not have had nearly as much success in terms of postdoc employment. I am deeply indebted to Michael Balogh and Gilbert Holder for answering a barrage of my stupid/silly questions throughout my time at UVic. I only hope that I can live up to their example of kindness and patience towards young researchers in the coming years. I would also like to thank Doug Johnstone for enlightening me on a completely different subject and on a different perspective to doing astronomy. In particular, his approach to astronomy (and life in general) has reminded me of the true reason I got into this field in the first place; it's fun! I thank Andreea Font, the research collaborator, for her hard work and her ability to motivate me and instill in me the desire to do things right and well. Lastly, I thank fellow grad student Greg Poole for putting up with my constant rants about research and dispensing useful ideas and suggestions.

I would like to thank the members UVic Astronomy Group. In particular, I would like to acknowledge David Hartwick, Chris Pritchet, Don Vandenberg, Ann Gower, Doug Johnstone, Arif Babul, and recent additions Sara Ellison, Jon Willis, and Henk Hoekstra for making my experience at UVic a generally enjoyable one. I give big thanks to the secretarial staff, especially Geri, Susan, Rosemary, Tracey, and Chantal, for helping me out on countless occasions. Of course, I also have to thank the graduate students and postdocs for making my time here real fun. Here

goes: thank you Chris B., James C., Mark F., Andreea F., Wes F., Rachel F., Jon G., Aida G. Z., Melissa G., Stephen G., Eric H., Eric H. (the new one), Anudeep K., Helen K., Jeff L., Aaron L., Margaret M., Greg P., Jeff S., Karun T., and Brian Y.

There are many friends and family who have provided support and encouragement throughout the years (not just limited to my time at UVic). In terms of close friends, I offer my sincere thanks to Steve S., Stephen G., Kip B., Pete L., and newbies Chris B., Anudeep K., John M., Kelly R., Julie W., Ramona D., and Kent T. Of course, none of this would have been possible without the loving support of my family: Larry, Georgie, Lori, and Leanne. Also, thank you Jaime, Cathy, Meaghan, Keith, Shaaron, John and many others.

Finally, I would like to give a special 'thank you' to Andreea Font. She has shown continuous support and stuck by me through thick and thin. More than anyone else, Andreea has shown me, through her actions both at school and at home, what it means to work hard, to persevere in tough times, and, at the same time, maintain integrity and honesty. I am infinitely impressed by her strength of character and how easily/naturally she gives in order to help others in need without any concern for herself. Thank you, Andreea, for being you.

For my grandmother, Margaret McCarthy

Chapter 1

Introduction

1.1 A Brief Primer on Clusters

Our understanding of galaxy clusters, the largest and most massive gravitationally bound objects in the universe, has advanced tremendously over the past few decades. This is due in large part to our increasing ability to study clusters from differing perspectives via new and innovative techniques. For example, thanks to the development of satellite technology for astronomical purposes, it was discovered some 30 years ago that clusters are profuse emitters of high energy X-radiation. It was later determined that the X-ray emission is due mainly to free-free emission from an extremely hot, diffuse intracluster medium (ICM). It turns out that the X-ray properties of clusters contain a wealth of information about the physical processes that govern the formation and evolution of these systems. This will be demonstrated in great detail throughout this dissertation. The development of sensitive wide-field optical CCD cameras has also opened up an entirely different probe of clusters, namely that of gravitational lensing. Because the potential wells of clusters are so deep, they deflect the light of background galaxies toward our line of sight. Depending on the degree of deflection, the result is either "strong" lensing (characterized by large arcs and multiple images of background galaxies) or

"weak" lensing (a small tangential distortion of background galaxies). Both types of lensing yield valuable information about the mass structure of clusters. At the same time, sensitive optical imaging and spectroscopic observations, particularly with large ground-based telescopes such as Keck and Gemini, have continually been refining our understanding of the baryonic component of clusters locked up in stars and galaxies. As a result, a great deal has been uncovered about the star formation histories of clusters, for example. Accurately measured cluster galaxy luminosity functions have been used to test theories of galaxy formation (among other things). Major advances have also been made at radio/mm wavelengths, particularly regarding observations of the Sunyaev-Zeldovich (SZ) effect. The SZ effect is a distortion of the cosmic microwave background (CMB) in the direction of clusters that arises from the scattering of CMB photons off of high energy electrons contained within the potential wells of clusters. Traditionally, detecting (much less mapping the SZ effect in detail) has been challenging (expressed in temperature units, the typical SZ effect distortion of the 3 Kelvin CMB background is only of order a few hundred micro Kelvin). However, the past few years have seen huge leaps in detector technology and innovative observing strategies (e.g., using radio GHz receivers on interferometers originally designed for mm-wavelength observations of the local universe) that have clearly demonstrated that mapping the SZ effect is not only feasible but is potentially a very powerful observational tool for probing clusters.

Spurred on by many recent observational achievements (such as those briefly outlined above), the theoretical modelling of galaxy clusters has also been proceeding at a rapid pace over the past few decades. One of the most notable developments has been the emergence of sophisticated numerical simulation codes. Nowadays, such simulations are capable of accurately and self-consistently following the gravitational growth and development of clusters from small density perturbations in the nearly-uniform high redshift universe to the highly concentrated, massive ($\sim 10^{15} M_{\odot}$) structures we see today (each of which can often contain in excess of

a thousand individual galaxies). Not only are such simulations able to track the gravitational collapse of the baryons and dark matter that comprise clusters, but they are also able to realistically capture the gravitationally-driven hydrodynamic processes that influence the baryons (e.g., shock heating of the gas as its infall kinetic energy is converted into thermal energy). Comparisons of such simulations to observations (e.g., X-ray observations) yield reasonable agreement. For example, the mass profiles of clusters are well-described by the cuspy profiles predicted by high resolution simulations (e.g., Pointecouteau et al. 2005), as are the observed temperature profiles of the ICM in clusters (with the exception of the central regions of clusters; e.g., Loken et al. 2002), and so on. In short, comparisons of simulations and observations have confirmed our basic ideas about the formation and evolution of clusters.

Although a general picture for the formation and evolution of clusters has been firmly established, many important details have yet to be worked out. This is particularly the case for the baryonic component of clusters. Even though this component is rather insignificant in comparison to the dark matter in a dynamical sense, it is extremely important that we be able to model the baryons correctly. The reason, of course, is that it is the baryons, not the dark matter, that we observe with our X-ray, optical, and radio telescopes. Unfortunately, modelling the baryons is much more complicated than modelling the dark matter. This may sound rather odd at first, given that we know exactly what constituents make up the baryonic matter but are essentially ignorant of the nature of dark matter (see below). But there is a perfectly good explanation for this. Even though we are unable to directly detect dark matter in a laboratory, all current (astronomical) indications point to the fact that dark matter is collisionless and responds only to the gravitational force. This makes dark matter relatively simple to model. Baryons, on the other hand, are collisional and respond to both the gravitational and the electromagnetic forces. Thus, for the baryons one must worry about complicated processes such as radiative cooling, thermal conduction, viscosity, and so on. This potentially makes

life very difficult for theorists. However, we hope to demonstrate throughout this dissertation that much progress can be (and has been) made in modelling the baryonic component of clusters, especially with regards to the ICM (which, in terms of mass, dominates the baryons locked up in stars and galaxies in clusters).

Presently, there are at least two major unresolved issues in our understanding of the properties of intracluster gas. The first is often termed the "cooling crisis". In short, simple analytic calculations involving the cooling time of the gas in clusters lead to the conclusion that a significant fraction of the ICM should have cooled down to very low temperatures (and formed molecular gas and stars) over a cluster's lifetime (e.g., Balogh et al. 2001). Numerical simulations that attempt to model the radiative cooling of the ICM in a more realistic way also lead to the same conclusion (e.g., Davé et al. 2002). However, observations indicate that only a very small fraction of the baryons in clusters are in the form of cold gas and stars (e.g., Roussel et al. 2000; Cole et al. 2001; Lin et al. 2003). This problem has recently been exacerbated by high resolution X-ray observations from *Chandra* and *XMM-Newton*. In particular, spectral data from these satellites indicates that there is very little gas cooling below a few keV or so (which corresponds to a few times 10^7 K) let alone down to temperatures typical of molecular clouds ($\sim$ 100 K). In the X-ray regime, the cooling crisis is often referred to as the "cooling flow" problem, even though the cooling flow problem is just one aspect of the more general cooling crisis (which affects not only clusters but also galaxy groups and individual galaxies as well).

The second major issue may be summarized as follows. If only gravitational-induced processes (e.g., shock heating and compression) are important in dictating the properties of the ICM, then specific well-defined relationships are expected between various global properties of clusters (e.g., the X-ray luminosity should scale as the square of the mean temperature of the ICM). Observations indeed indicate relationships between the global properties of clusters, but they typically have different slopes and normalizations than predicted and also exhibit a surprising

degree of intrinsic scatter. However, simple "self-similar" predictions such as these neglect processes such as radiative cooling, which almost certainly have important consequences for the observed scaling relations of clusters. On the other hand, radiative cooling by itself cannot be the solution since it's clear that some form of non-gravitational heating must be offsetting the effects of cooling (i.e., the "cooling crisis" outlined above).

The central goal of my research is to help shed some light on both of these important issues. But before outlining how we have attempted to do this, it would be useful to provide some further motivation for why astrophysicists should care about modelling the ICM accurately.

1.2 Why care about ICM Physics?

1.2.1 Precision Cosmology with Clusters

The field of cosmology has recently achieved an impressive milestone. A variety of different observational tests (on a range of different physical scales) now appear to support a single model for the overall geometry and matter and energy content of the universe. This "concordance" model is characterized by a spatially flat (or very nearly flat) geometry, implying that the universe has a total energy density that is extremely close to the critical value required to close the universe. Observations indicate that the total energy density is dominated by two components: non-baryonic dark matter, which accounts for approximately 25% of the total energy density, and a poorly understood form of dark energy, which accounts for approximately 70% of the total energy density (e.g., Spergel et al. 2003) and whose negative pressure is currently causing the expansion of the universe to accelerate. Ordinary baryonic matter (e.g., protons, neutrons, electrons), of which stars, planets, and even people are comprised, plays a negligible role in terms of the dynamics of the universe. Our best estimates suggest that baryonic matter

accounts for only about 4% of the total energy density (e.g., Burles et al. 2001).

Even though the concordance model is quite successful at explaining many different cosmological observations, at present it's not a completely satisfactory model. Until the nature of dark matter and dark energy is revealed, it will probably remain this way. Additionally, many aspects of the process of galaxy formation remain poorly understood. For example, debates are currently raging in the literature over the observed and predicted density profiles of galaxies and over the observed and predicted numbers of satellite galaxies orbiting massive galaxies such as the Milky Way. At present, it's unclear whether these (apparent) discrepancies are signalling that there are problems with the concordance model or if they are simply telling us that not all of the relevant physical processes that influence baryonic matter have been incorporated into the theoretical models. (It should be noted that the theoretical models referred to here are often represented by dark matter-only simulations, whereas the observations probe just the baryonic component of galaxies).

In any case, it would be useful to further tie down and understand the parameters of the currently-accepted cosmological model. One way of doing this is with clusters of galaxies, which contain a wealth of cosmological information. A robust prediction of the concordance model is that structure formation occurred (and continues to occur) hierarchically, with the smallest objects forming first and then merging with other objects to create successively larger and larger objects. Clusters, which are the largest bound systems in the universe, are therefore the most recent class of objects to have formed and, as a result, directly trace the process of structure formation in the universe.

Not only do clusters preserve a fossil record of the general process of structure formation, but they also potentially shed direct light on a number of important cosmological parameters. For example, clusters can be used in several different ways to measure the energy density of the universe in the form of matter (both baryons and dark matter). One method involves making use of the fact that clusters are

"typical" regions of the universe. By typical, we mean that because clusters are so large and their potential wells are so deep they are essentially closed boxes and, therefore, the ratio of baryon mass to total mass of a cluster should be equivalent (or very nearly so) to the ratio of these two components for the universe as a whole (i.e., $M_{gas}/M_{tot} = \Omega_b/\Omega_m$). Thus, if one can measure the baryonic and dark matter masses of a cluster (say, from its X-ray properties) and has external information about Ω_b (e.g., from a combination of Big Bang Nucleosynthesis calculations and deuterium measurements from quasar absorption lines), it is straightforward to deduce the matter density of the universe, Ω_m. Another method for measuring Ω_m involves simply counting clusters above a certain mass threshold. For example, upcoming SZ effect experiments should be capable of detecting *every cluster in the observable universe* with masses above a few times $10^{14} M_{\odot}$ (e.g., Holder et al. 2000). This will allow for amazingly tight constraints on Ω_m, since the total number of clusters in the universe is quite sensitive to this parameter. A plethora of other interesting cosmological tests involving clusters also exist, including: combining X-ray and SZ effect observations to measure Hubble's constant (e.g., Reese et al. 2002), using the SZ effect power spectrum of clusters to constrain the properties of the dark energy and normalization of the matter power spectrum (e.g., Holder, McCarthy, & Babul in prep.), using the 2-point correlation of clusters to measure Ω_m (among other parameters), combining the X-ray luminosity (or temperature) functions of clusters with the mass-luminosity (or mass-temperature) relation to measure the mass function of clusters and, hence, constrain the normalization of the matter power spectrum (e.g., Balogh et al. 2005), and so on.

The majority of cluster cosmological tests require high precision mass estimates (or, alternatively, a precise estimate of the survey mass threshold). Unfortunately, it is not possible to directly observe the mass of a cluster, or of any other astronomical object for that matter. (Note that this is the case even when using gravitational lensing, which is sensitive not to the mass of the system of interest but to the total mass along the line of sight). Instead, some other observable (e.g.,

luminosity, temperature, velocity dispersion, and so on) must be used as a proxy for mass. As a result, various assumptions about the physical state of the system must be relied upon in order to convert the observable into a mass estimate. For example, a common method employed to measure the mass of galaxy clusters is to use the gas density and temperature profiles of the ICM (as inferred from X-ray observations) coupled with the assumption that the ICM is in hydrostatic equilibrium. Another commonly used method involves combining the observed velocity dispersion of cluster galaxies with the virial theorem in order to yield a mass estimate. These sorts of analyses are probably safe for present day massive clusters, which are likely to be in equilibrium (or nearly so) and where it is often possible to accurately determine the radial profiles for the gas density and temperature (for example). However, for high redshift systems of similar mass (which potentially provide the tightest constraints on cosmological parameters) the likelihood that a particular cluster is in equilibrium decreases, as we are witnessing clusters at an earlier stage in their formation. Furthermore, it becomes increasingly difficult to accurately map the observable in question, as the flux is diminished owing to the increased distance (and also to cosmological dimming) and resolving the object becomes more difficult as well (except beyond a redshift of $z \sim 1.3$, where the angular size of an object of fixed physical size actually begins to increase). Thus, for distant clusters, it will likely be necessary to resort to using theoretical relations between "integrated" observables (such as total luminosity, mean temperature, cluster richness, and so on) and mass in order to do cosmology. As highlighted in §1.1, such relations are sensitive to non-gravitational processes like radiative cooling and AGN heating. It is therefore absolutely essential that we accurately model the physics of the ICM in nearby clusters if we have any hope of using high redshift clusters to constrain cosmological models.

1.2.2 Clues to the Riddle of Galaxy Formation

As alluded to in §1.2.1, there are a number of potentially serious issues with our current understanding of galaxy formation. The "cusp-core" and "missing satellite" controversies are two of the most well-known examples. However, other issues exist as well, including the so-called "angular momentum problem" (i.e., the fact that disk galaxies formed in simulations tend to have lower angular momenta, and hence are smaller, than those observed), the "missing baryon problem" (i.e., the ratio M_b/M_{tot} for the Milky Way is substantially smaller than Ω_b/Ω_m), and what will we term the "dwarf metallicity problem" (i.e., local dwarf galaxies have a much different α/F_e ratio than the disk of the Milky Way, which appears to be at odds with a hierarchical formation scenario for the Galaxy). These issues have led some astronomers to speculate that the concordance model fails on small scales. Others, however, point to the excellent agreement between the predictions of the concordance model and numerous other (usually extragalactic) observations and suggest that there must be an alternative explanation. The most plausible candidate proposed thus far is that of relevant baryonic physics missing from the theoretical models. Examples include multiphase cooling, thermal conduction, efficient heating from supernovae and/or AGN, and so on. In fact, it might be expected that all of these processes (and others as well) are simultaneously shaping the baryonic properties of galaxies.

Of course, many of the same processes that affect the baryons in galaxies will also affect the baryons in clusters. Thus, by studying cluster formation one might hope to learn about the process of galaxy formation as well. The advantage of this approach is that clusters represent a much cleaner environment than galaxies for studying baryonic physics. First, the atmospheres of clusters are completely ionized due to the extreme temperatures. So, one need not worry about the complication of a two phase neutral-ionized medium. Second, because most of the baryons in clusters are diffuse (i.e. have not cooled significantly and formed neutral gas or stars), it is possible to study the properties of clusters all the way out to their

virial radii. This, of course, is not possible with galaxies (e.g., it is only possible to observe out to $\sim$10% of the virial radius for the Milky Way). Third, because the baryons are distributed throughout the cluster potential well (as opposed to being condensed at the center), they play a negligible dynamical role. In other words, cuspy density profiles derived from dark-matter only simulations match observed clusters perfectly well. So, the gravitational potential is a given. Forth, the baryons are in hydrostatic equilibrium (or very nearly so). These and other neat features of clusters potentially make it easier to separate out the effects of the various processes that influence baryons.

To give but one example of how cluster gas physics is directly linked to galaxy formation, consider the galaxy luminosity function. It is well known that the observed galaxy luminosity function dives off at high luminosities (i.e., masses) much faster than predicted by simple analytic models rooted in the standard ΛCDM cosmology. In other words, really luminous/massive galaxies appear to be much more rare than predicted. Of course, some of the most massive galaxies in the universe are located at the centers of rich galaxy clusters. It is, therefore, quite likely that whatever source of non-gravitational heating that is causing the cooling crisis in clusters is also, at least partially, responsible for the high luminosity cut-off in the galaxy luminosity function.

1.2.3 It's fun!

Of course, the most important reason for studying ICM physics is that it's fun! There are plenty of problems to solve and a myriad of rich physical phenomena to study in these massive systems. And unlike star formation, and possibly galaxy formation as well, the problems are likely solvable within my lifetime (whoa, that was a cheap shot). But let's hope it doesn't happen before I get a chance to be tenured somewhere!

1.3 Our approach: Analytic Modelling

Detailed descriptions of our analytic models are provided in Chapters 2-7. However, these are basically technical descriptions and don't provide much in the way of motivation for why we have adopted this general approach. We attempt to provide that motivation here.

There are two general theoretical approaches that astrophysicists use in order to study structure formation and evolution; analytic modelling and numerical simulations. Both approaches have advantages and disadvantages. Consider the case of analytic modelling. The primary advantages of this approach are perhaps fairly obvious. First, its inherent simplicity can often allow one to gain deep physical insight about the various processes that are competing to shape the evolution of the system in question. Second, analytic modelling is normally very computationally-inexpensive. This potentially means that it can be used to study many different realizations of the same process in order to build-up a solid statistical picture. It also allows one to study many different physical phenomena over a large range of physical scales. This could be particularly important for galaxy clusters, since it is now believed accretion onto a supermassive black hole (i.e., where the typical size scale is of order an AU, i.e., $\sim 10^{11}$ cm) is feeding jets which may be capable of offsetting radiative losses of the ICM out to a few hundred kpc ($\sim 10^{21}$ cm). This is a huge dynamic range that will probably never be accessible to numerical simulations.

On the other hand, because of its inherent simplicity, analytic models do not self-consistently follow important nonlinear phenomena such as the hierarchical formation of structure. For example, it is common for analytic modellers in this field to ignore the effects of substructure and mass growth of the system. "Semi-analytic" modelling, which generally refers to a statistical approach commonly used to track the formation of objects (e.g., galaxies or clusters) through the accretion and merging of smaller objects (e.g., with the Extended Press-Schechter

formalism), is an attempt to ameliorate this problem, but it is not a completely satisfactory approach either. In terms of modelling galaxy clusters, other questionable assumptions are often implemented as well. Some of the obvious ones include: (1) neglecting the baryon contribution to the gravitational potential, which could become important if enough baryons are able to cool and condense at the cluster center (although, one can attempt to take this into account through an approach called 'adiabatic contraction' - which we have experimented with in Chapters 6 and 7); (2) spherical symmetry, which might apply in average sense, but that could introduce important scatter into the observed properties of clusters; and (3) hydrostatic equilibrium, which almost certainly does not apply to the outer regions of clusters or to clusters in general at high redshift. With analytic modelling, therefore, it becomes a question of which problems you want to solve and how accurately you want to know the answer.

Numerical simulations, on the other hand, can self-consistently track the build-up of clusters, explicitly take into account the coupling of the baryons and the dark matter, and do not need to make questionable assumptions such as spherical symmetry of the system or hydrostatic equilibrium of the gas. In this respect, they have an obvious advantage over analytic models. However, such numerical simulations are quite time-consuming. So, for example, because clusters are so large and fairly rare, it is quite difficult to simulate a big enough region of the universe (with adequate resolution) such that a reasonably large sample of massive clusters are contained there. In other words, it is difficult to achieve a sound statistical picture of galaxy clusters with current cosmological simulations. Furthermore, many of the processes that are likely to influence the baryonic component of clusters (e.g., star formation, AGN heating, turbulence, and so on) are "sub-grid"; i.e., they cannot be resolved with current simulations. As a result, processes such as star formation and AGN heating are difficult to implement in a self-consistent manner and, instead, are often incorporated through ad hoc recipes (e.g., Katz 1992; Di Matteo et al. 2005). Even some baryonic processes that are not sub-grid are

very difficult to implement. For example, in the case of radiative cooling, one can often achieve very different results depending on which numerical method is implemented, a Eulerian approach (i.e., a mesh code) or a Lagrangian approach (i.e., a particle code). So, as in the case of analytic modelling, there are various advantages and disadvantages to the use of numerical simulations.

The above should not be viewed as a list of complaints about analytic models and numerical simulations. Rather, it should demonstrate the complementary nature of these two approaches. Detailed comparisons of the results of these two approaches, which is beginning to become a regular occurrence now, will help provide a more complete picture of clusters. In fact, it could well be that in a few years there will be an explicit amalgamation of these two approaches; i.e., a hybrid model. But we will leave a discussion of this for Chapter 8 (Conclusions and Future Work).

1.4 Dissertation Overview

Before moving on to the actual research, a brief description of the six main chapters of this dissertation [each of which are based on articles published in (or to be published in) the Astrophysical Journal (ApJ)], including a discussion of the main results and conclusions, is presented below. This should hopefully serve as a guide to the motivation behind each of the chapters and how they are related to one another.

1.4.1 The Cluster $M_{gas} - T$ Relation

The X-ray luminosity-temperature ($L - T$) relation of clusters has been known to deviate from the predictions of the standard self-similar model (that incorporates gravitational processes only) for over a decade now (e.g., Kaiser 1991). This is firm evidence that some form of non-gravitational physics is modifying (or has modified) the properties of the ICM. Babul et al. (2002) demonstrated that one

could account for slope and normalization of of the $L-T$ relation by heating the ICM prior to cluster formation (i.e., "preheating"). Furthermore, a constant level of heating for all clusters (i.e., the simplest heating model one can explore) was consistent with the data. Independent analyses of the $L-T$ relation by a variety of other groups also led to similar conclusions. However, the level of heating inferred by the various groups differed quite significantly in some cases. In order track down the nature of this discrepancy, we decided to examine the effects of preheating on another X-ray scaling relation, namely the ICM gas mass-temperature ($M_{gas}-T$) relation. This scaling relation had just recently been demonstrated to also deviate from the predictions of the standard self-similar model (e.g., Neumann & Arnaud 2001). So, it was interesting to see, first, whether or not a preheating model could account for this scaling relation and, second, how the inferred level of heating compared with our estimates based on analysis of the $L-T$ relation. This is exactly what we looked at in McCarthy et al. (2002).

The main results and conclusions of this study are as follows. We demonstrated that preheating models could indeed account for this relationship. In fact, the model successfully reproduced three different $M_{gas}-T$ relations, corresponding to observational estimates of M_{gas} at three different radii. Furthermore, we again inferred that a high level of heating, completely consistent with that deduced from the $L-T$ relation, was required. A detailed examination of a few of the other theoretical studies that found lower levels of heating was performed. Most of the discrepancy in the inferred heating level could be attributed to the fact that these studies focused solely on matching the slopes of the $L-T$ and $M_{gas}-T$ relations and not on matching the normalizations of those relations. However, we demonstrated that the slopes of these (and indeed most) X-ray scaling relations are not nearly as sensitive as the normalizations to the level of heating. Thus, a variety of heating levels can all lead to very similar slopes but produce significantly different normalizations.

1.4.2 Sunyaev-Zeldovich Effect Scaling Relations

The results of McCarthy et al. (2002) appeared to suggest that there was a single model that could explain the bulk of the global X-ray properties of clusters. However, studies of the ICM are not limited to X-ray wavelengths. The Sunyaev-Zeldovich, a distortion of the CMB caused by the inverse Compton scattering of CMB photons off hot intracluster electrons, potentially offers an independent probe of the ICM. Furthermore, it probes the ICM in a different way. Namely, the X-ray surface brightness of a cluster is proportional to $n_e^2 T^{1/2}$, whereas the SZ "surface brightness" is proportional to $n_e T$, i.e., the pressure of the ICM (or thermal energy density). The SZ effect also has the added advantage of not being subject to cosmological dimming (since it is nothing but a fractional change in intensity or, equivalently, temperature of the CMB). This is particularly important for high redshift clusters. In fact, because of this feature, the SZ effect is perhaps our best hope of doing cosmology with high redshift clusters.

Unfortunately, because the SZ effect is quite weak only a relatively small number of clusters have measured SZ "fluxes". However, this number is rapidly increasing and, therefore, we thought it would be prudent to make predictions for the SZ effect properties of our preheated clusters. In McCarthy et al. (2003a), we derived a number of scaling relations between SZ effect properties and SZ effect and X-ray properties. Furthermore, we provided accurate fitting formulae for these relations as a function of redshift and preheating level. We concluded that the SZ effect is a fairly sensitive probe to non-gravitational heating. In fact, we estimated (surprisingly) that even the current sample of 30-40 clusters observed with the *BIMA* and *OVRO* arrays should be able to distinguish the self-similar model from the preheating models and perhaps even place reasonably tight constraints on the level of heating. A comparison of our theoretical models to the current sample of SZ effect clusters was presented in a companion paper (McCarthy et al. 2003b; next chapter).

1.4.3 The Sunyaev-Zeldovich Effect: Theory vs. Observations

Given the results of McCarthy et al. (2003a), we were quite excited to see what implications the current sample of SZ effect clusters had for our preheating models. As far as we are aware, this is the first time the SZ effect had been used to probe cluster non-gravitational physics (almost all previous studies were restricted to measuring Hubble's constant or the baryon fraction of clusters). A detailed comparison of our theoretical models to the SZ effect data (via 7 different scaling relations) in McCarthy et al. (2003b) yielded very similar results to that derived in our previous studies of X-ray scaling relations (in terms of the amount of preheating required). Thus, both the X-ray and Sunyaev-Zeldovich effect properties of clusters generally appeared to support the preheating scenario.

A significant portion of this paper was also devoted to making mock SZ effect observations of our preheated clusters for the upcoming Sunyaev-Zeldovich Array (SZA). By folding in the expected instrumental response of this interferometer into our theoretical models, we demonstrated it will soon be possible to use the SZ effect to probe the non-gravitational physics of the ICM up to redshifts in excess of $z \sim 2$.

One of the most important results of this particular study, although we didn't fully appreciate it at the time, was that there were several significant outliers that could not be explained by our model. Furthermore, these outliers all happened to be massive "cooling flow" clusters, i.e., simple analytic estimates based on *ROSAT* and *ASCA* X-ray data indicated that these clusters ought to be cooling out approximately $\sim 1000 M_{\odot}$ yr^{-1}. Like many in the community, we were quite skeptical of such calculations (and of the cooling flow model in general) since the vast quantities of cold gas and stars predicted have never been found. However, the SZ effect scaling relations examined in McCarthy et al. (2003b) indicated that there indeed appeared to be a real physical difference between "cooling flow" and "non-cooling

flow" clusters. A likely explanation for why an analogous trend was not seen in our previous explorations of X-ray scaling relations is that the data used in those studies had been "cooling flow corrected". Basically, cooling flow correction is an adjustment made to the X-ray temperatures and luminosities of clusters by excising the central regions of clusters when fitting spectral and surface brightness models to the X-ray data. It was previously shown that this correction results in much tighter scaling relations, implying that the outer regions of clusters are all similar but that the central regions can vary significantly from cluster to cluster. Of course, reducing the intrinsic scatter in the X-ray scaling relations is potentially useful if one is attempting to do cosmology with clusters (note, however, that this is not possible for high redshift clusters where the "cooling flow" regions of clusters are unresolved), but it is a real hindrance when one is attempting understand the physics of the ICM. What we hadn't fully appreciated (up until this point) was just how large of an impact cooling flow correction was.

1.4.4 Cooling Flows, Bubbles, and Projection Effects

Spurred on by the results of McCarthy et al. (2003b), we decided to examine the properties of "cooling flow" clusters in more detail. By this time, spatially-resolved X-ray temperature and entropy profiles derived from *Chandra* and *XMM-Newton* data were beginning to become available. Indeed, these new X-ray observations confirmed in exquisite detail significant differences between "cooling flow" and "non-cooling flow" clusters, especially in regards to their temperature profiles. Another interesting development was the discovery of X-ray surface brightness depressions in the cores of many "cooling flow" clusters (whereas such depressions have never been observed in "non-cooling flow" clusters). These depressions were often observed to be surrounded by bright rims (or shells) of cool X-ray emission. Comparisons with radio synchrotron observations showed that the depressions coincided closely with large radio lobes. This, combined with the fact that the X-ray depressions normally were observed in pairs symmetric about the cluster center

(like the radio lobes) quickly convinced the community that the depressions were bubbles of extremely hot, perhaps relativistic, plasma blown by the central AGN (the plasma is so hot that any X-rays produced by it would go unobserved by *Chandra*, since it is sensitive to 'soft' X-rays only - hence the X-ray depressions). The cool rims surrounding the bubbles are hypothesized to be cool gas entrained by the bubbles as they rise buoyantly through the cluster atmosphere.

An examination of the azimuthally-averaged temperature profiles of some "cooling flow" clusters that also happened to contain obvious bubbles led to a startling discovery. To explain, "cooling flow" clusters are often noted to have a dip in their temperature profiles near the cluster center (i.e., a positive temperature gradient). We noted that the dip in the temperature profiles of some clusters happened to begin almost at the exact same radius as where the cool rims of the bubbles began (most bubbles are observed to be within the central 50 kpc of clusters). This led us to speculate that the temperature dip seen in many clusters might not be due to radiative cooling but, rather, to the azimuthal averaging of cool rims surrounding bubbles.

In McCarthy et al. (2003c), we used a simple toy model to experiment with placing bubbles (with properties guided by the observations) in our preheated clusters. We showed that one could explain the "cooling flow" properties entirely of some clusters (such as A2052) with this simple model. However, it also became apparent that some "cooling flow" clusters could not be explained with this model. In particular, the central dips in some massive clusters are observed to extend out to 150 kpc. The typical bubble size, on the other hand, is only 30-50 kpc (diameter). Therefore, in order to explain such clusters, it would be necessary to place several sets of bubbles at specific radii in order to reproduce the observations. This may be the case for some clusters, but it seems rather unlikely that this can explain all (or most) "cooling flow" clusters.

1.4.5 Models of the ICM with Heating and Cooling

The results of McCarty et al. (2003b; 2003c) forced us to conclude that, even though there is no evidence for gas cooling down to very low temperatures (i.e., optical, mm, and radio searches for neutral gas and/or increased star formation have always resulted in negative or, at best, very modest results), radiative cooling must be significantly influencing the X-ray (and SZ effect) properties of clusters. With this mind, we were determined to include a realistic treatment of radiative cooling in our theoretical models. Up to this point, several other groups had been examining the effects of cooling with analytic models. However, the treatment of cooling in these studies was very crude. In particular, it was commonly assumed in these models that all of the gas within the cooling radius cooled out and that the gas outside the cooling radius (which was assumed to be unaffected by cooling) simply flowed in to the cluster center adiabatically. However, it's clear that this is not a physically reasonable model. Gas that was originally outside the cooling radius will be compressed as it flows toward the cluster center. As a result, the cooling rate (which scales as gas density squared) of this gas will increase. Consequently, the entropy of this gas will be reduced through radiative cooling (i.e., the flow cannot be considered adiabatic). This point was underscored by Voit et al. (2002), who examined a variety of different analytic treatments of radiative cooling.

To remedy this problem, we decided to develop what is essentially a 1-D hydrodynamic code. A brief description of our cooling treatment is as follows. We specified the initial clusters conditions (prior to cooling) using either the standard self-similar model or the preheating models. We then calculated the reduction in entropy of the the ICM due to radiative cooling for a small time step. Using this new entropy profile together with our adopted dark matter potential (which remained unchanged), we solved the hydrostatic equilibrium equation to determine the new density and temperature profiles of the ICM. At the same time, the gas was allowed to flow inward. Strictly speaking, therefore, our clusters were quasi-hydrostatic systems. We repeated this procedure over and over for each successive

time step until the cluster had cooled for a Hubble time. While this procedure is much more tedious and computationally-expensive than that used in previous analytic cooling models, it also represents a much realistic model of cooling (see Chapter 7 for further discussion this).

Given that we had expended a fair deal of effort in developing a realistic model of cooling, we wanted to ensure that our models be compared with X-ray data that had not been corrected for the effects of "cooling flows". By this time, several large 'raw' X-ray samples were available, including the ASCA Cluster Catalog (ACC) which contains nearly 300 nearby, massive clusters. In addition, more and more spatially-resolved *Chandra* and *XMM-Newton* radial profiles (e.g., temperature and entropy) were also becoming available. As such, in McCarthy et al. (2004) we undertook a large study to compare in detail our analytic cooling + heating models to the global and structural X-ray properties of clusters (i.e., scaling relations and radial profiles).

The main results and conclusions of this study are as follows. In order to account for the large amount of intrinsic scatter in the raw luminosity-temperature and luminosity-mass relations of clusters it is necessary to include the effects of radiative cooling as well as a distribution of initial preheating levels. In particular, "cooling flow" clusters typically require minor amounts of heating (plus cooling), whereas "non-cooling flow" clusters typically require large amounts of heating. A consequence of this prediction is that "non-cooling flow" clusters should have large central entropy cores, whereas "cooling flow"clusters should not. Our examination of the entropy profiles derived from *Chandra* and *XMM-Newton* confirmed this picture both in a qualitative and a quantitative sense. In addition, we demonstrated that our model could also account for the temperature and surface brightness profiles of both classes of clusters.

1.4.6 The Physics of Radiative Cooling

McCarthy et al. (2004) found that, given enough time, radiative cooling is capable of completely washing away the effects of any initial preheating. Furthermore, these authors found that cooling tends to naturally establish near powerlaw entropy profiles in the cores of clusters, independent of the initial entropy distribution of the gas. We were intrigued by this result and decided to look into it further. During our investigation we came across an excellent article by Bertschinger that was written about 15 years ago but, apparently, went unnoticed (or was forgotten). Bertschinger performed a self-similarity analysis of cooling flows in clusters that had powerlaw gravitational potentials. He showed that one could relate the shapes of the density and temperature profiles of the ICM in the central regions of clusters to the shape of the gravitational potential and (to a lesser extent) to the shape of the cooling function. Since the entropy of the ICM is just a function of its density and temperature, it too should be explainable in this way.

Using the 1-D code developed in McCarthy et al. (2004), we confirmed Bertschinger's results for powerlaw clusters (but in a more rigorous fashion). However, real cluster don't have pure powerlaw gravitational potentials. Rather they have cuspy profiles that are characterized by a scale radius, where the profile changes from relatively shallow ($\rho \propto r^{-\alpha}$, with $1 \lesssim \alpha \lesssim 1.5$) to relatively steep ($\alpha = 3$). Furthermore, the cooling function is not a powerlaw either (as assumed by Bertschinger), owing to line emission. So, we experimented with relaxing both of these assumptions. In turns out that, to a large extent, these assumptions have only a very minor effect. First, for temperatures above approximately 2 keV (which describes almost all of the gas within the cooling radius of a massive, $10^{15} M_{\odot}$ cluster), the cooling function is dominated by thermal bremsstrahlung (as opposed to line emission). Thermal bremsstrahlung is characterized by pure powerlaw cooling function $\Lambda(T) \propto T^{\beta}$ with $\beta = 1/2$. However, the shape of the cooling flow entropy profile is a more sensitive function to the shape of gravitational potential than it is to the shape of the cooling function. But, because the typical scale radius of a massive

cluster is much larger than the cooling radius (typically, 400 kpc $\lesssim r_s \lesssim$ 700 kpc, whereas 100 kpc $\lesssim r_{cool} \lesssim$ 200 kpc), the central cooling flow essentially only feels a powerlaw gravitational potential. This work is presented in McCarthy et al. (2005).

An analysis of the shapes of entropy profiles of observed massive "cooling flow" clusters lead us to conclude that: (1) outside the central 20 kpc or so, the profiles are indeed well described by powerlaws; (2) the inferred shapes of the gravitational potentials are consistent those derived using the standard hydrostatic equilibrium method and with the cuspy profiles found in numerical simulations. The implication of this result is that real honest-to-goodness cooling flows appear to be operating in "cooling flow" clusters. That is, at least outside a radius of 20 kpc or so. Inside this radius, some kind of non-gravitational heating (e.g., AGN heating) must be continually preventing the buildup of large amounts of cold gas and stars. Alternatively, if it is distributed all of the way out to the cooling radius, the heating must be distributed in just such a way as to precisely balance cooling. In either case, this is likely giving us an important clue about the nature of the heating source in "cooling flow" clusters.

A brief review of the general conclusions of this dissertation and of future work is presented in Chapter 8. Enjoy.

Chapter 2

The Cluster $M_{gas} - T_X$ Relation: Evidence for a High Level of Preheating?

Abstract

Recent X-ray observations have been used to demonstrate that the cluster gas mass - temperature relation is steeper than theoretical self-similar predictions drawn from numerical simulations that consider the evolution of the cluster gas through the effects of gravity and shock heating alone. One possible explanation for this is that the gas mass fraction is not constant across clusters of different temperature, as is usually assumed. Observationally, however, there is no compelling evidence for gas mass fraction variation, especially in the case of hot clusters. Seeking an alternative physical explanation for the observed trends, we investigate the role that preheating of the intracluster medium has on gas mass - temperature relation for massive clusters with temperatures of $T_X \gtrsim 3$ keV. Making use of the physically-motivated, analytic models developed in 2002 by Babul and coworkers, we find that preheating does, indeed, lead to a steeper relation. This is in agreement with previous theoretical studies on the relation. However, in apparent conflict with these studies, we argue that a "high" level of entropy injection is required

to match observations. In particular, an entropy floor of $\gtrsim 300$ keV cm^2 is required. We also present a new test, namely, the study of the relation within different fixed radii. This allows one to indirectly probe the density profiles of clusters, since it samples different fractions of the virial radius for clusters of different temperature. This test also confirms that a high level of preheating is required to match observations.

2.1 Introduction

Analytic models and numerical simulations of clusters of galaxies have been used to predict the existence of scaling relations between various observable quantities, such as the well-known luminosity (L_X) - temperature (T_X) and mass (M) - temperature relations, where $L_X \propto T_X^2$ and $M \propto T_X^{1.5}$, respectively. However, it is now fairly well established that X-ray properties of clusters do not scale in such a fashion. Most notable of these is the $L_X - T_X$ relationship, which is observed to be much steeper than predicted, $L_X \propto T_X^{2.6-3.0}$ (e.g., Markevitch 1998; Allen & Fabian 1998; Arnaud & Evrard 1999).

Considerable effort has recently been directed towards explaining why the observed relations deviate from their predicted scalings (e.g., Tozzi & Norman 2001; Davé et al. 2001; Babul et al. 2002, hereafter BBLP02). In particular, it is the $L_X - T_X$ relation that has grabbed most of the spotlight because there is a wealth of published observational studies on the luminosities and temperatures of clusters with which to compare models and simulations. However, another important scaling relation is the cluster gas mass (M_{gas}) - T_X relation. Neumann & Arnaud (2001) have suggested that a deviation from the self-similar scaling of $M_{gas} \propto T_X^{1.5}$ might "explain" the observed deviation in the $L_X - T_X$ relation. Indeed, a number of observational studies have indicated that the relation is much steeper, with $M_{gas} \propto T_X^{1.6-2.0}$ (Vikhlinin et al. 1999; Mohr et al. 1999, hereafter MME99; Neumann & Arnaud 2001). If the gas density profile is roughly self-similar, this does lead to consistency with the observed $L_X - T_X$ relation. However, we still need a

physical explanation for why the relationship between a cluster's gas mass and its temperature deviates from its self-similar scaling.

Expressing the total gas mass within the cluster as $M_{gas} = f_{gas}M$, a steepening of the $M_{gas} - T_X$ relation can be interpreted as a dependence of f_{gas} on cluster mass. That is, if $M \propto T_X^{1.5}$, as suggested by the self-similar model, then the observed $M_{gas} - T_X$ relation implies that $f_{gas} \propto T_X^{0.1-0.5}$. A varying gas mass fraction is expected if the efficiency of galaxy formation varies systematically across clusters of different mass. Observational support for this has been claimed recently by Bryan (2000). However, this is still controversial, and there is no compelling evidence for a variation of f_{gas} with cluster temperature (but see Arnaud & Evrard 1999; MME99). This is especially true for the systems that we are specifically interested in: hot clusters with $T_X \gtrsim 3$ keV. This is apparent, for example, in Figure 1 (top) of Balogh et al. (2001), who carry out an accounting of stars and gas to estimate the fraction of cooling baryons in clusters. Moreover, Roussel, Sadat, & Blanchard (2000) have carried out a careful analysis of group and cluster X-ray data to estimate f_{gas} directly and have found no trends. More recently, Grego et al. (2001) have analysed Sunyaev-Zeldovich effect observations of 18 hot clusters and have also found no correlations between a hot cluster's gas mass fraction and its temperature. Finally, observational studies of the *total* cluster mass (M) - temperature relation have indicated that $M \propto T_X^{1.6-2.0}$ (Horner et al. 1999; Ettori & Fabian 1999; Nevalainen et al. 2000; Finoguenov et al. 2001), which, given the observed $M_{gas} - T_X$ relation, is consistent with f_{gas} being constant.

Theoretically, it is only now becoming possible to reliably investigate the dependence of f_{gas} on temperature with the inclusion of radiative cooling, star formation, feedback, and other relevant processes in numerical simulations (e.g., Lewis et al. 2000; Pearce et al. 2000; Muanwong et al. 2001; Davé et al. 2001). As of yet, however, there is little agreement in the approaches adopted to model these processes and prevent the so-called cooling crisis (compare, for example, the findings of Lewis et al. 2000 with those of Pearce et al. 2000). This is not surprising.

As discussed in detail by Balogh et al. (2001), attempting to model the effects of cooling across the wide range of halo masses found in clusters is inherently very difficult. The addition of "sub-grid" processes, such as star formation and feedback, further complicates matters. Thus, the effects that these additional physical processes have on the gas mass fraction of clusters will not be fully realized until such issues are resolved.

In this paper, however, we show that the observed variation of the $M_{gas} - T_X$ relation(s) arises quite naturally within the class of models that invoke preheating of the intracluster medium during the early stages of cluster formation. In these models, f_{gas} is constant on cluster scales ($T_X \gtrsim 3$ keV), and the self-similarity is instead broken by an entropy floor generated by early non-gravitational heating events. Preheating has previously been shown to bring consistency between a number of other observed and predicted scaling relations for groups and clusters (e.g., BBLP02), and therefore one might expect that the $M_{gas} - T_X$ relation should also be modified.

The preheating model was originally put forward by Kaiser (1991) and has subsequently been investigated by a number of authors (e.g., Evrard & Henry 1991, Bower 1997, Cavaliere et al. 1997; 1998; 1999; Balogh et al. 1999, Wu, Fabian, & Nulsen 2000; Loewenstein 2000, Tozzi & Norman 2001; Borgani et al. 2001; Thomas et al. 2002; BBLP02). If the ICM is injected with enough thermal energy, the hot X-ray emitting gas will become decoupled from the dark halo potential and break the self-similar scaling relations. The best estimates suggest that a substantial amount of energy (~ 1 keV per particle) is required to reproduce the observed relations (mainly the $L_X - T_X$ relation). It is not yet known what source(s) could inject such a large amount of energy into the ICM. Both galactic winds (driven by supernovae) and ejecta from active galactic nuclei have been proposed, but because of the complexity of the physics, the exact details have yet to be worked out. For an in-depth discussion of potential sources of preheating and of alternative possibilities for reproducing the observed relations we refer the

reader to BBLP02.

In this paper, we adopt the physically motivated, analytic model developed in BBLP02 to explore the impact of cluster preheating on the $M_{gas} - T_X$ relation. In comparison with the $L_X - T_X$ and $M - T_X$ relations, it has drawn very little attention by theoretical studies. The only studies to have examined the effects of entropy injection on the $M_{gas} - T_X$ relation to date are Loewenstein (2000) and Bialek et al. (2001). To be specific, Loewenstein (2000) considered models where the entropy injection occurs at the centers of groups and clusters, after the latter have formed whereas Bialek et al (2001), like BBLP02, investigated preheated models. For reasons that will be described below (in §2.5), we believe our work greatly improves upon both of these studies. The prevailing apathy by theorists is perhaps due in part to a near absence of published observational studies on the gas masses of clusters. However, in light of the recent important observations discussed above (e.g., Vikhlinin et al. 1999; MME99; Neumann & Arnaud 2001) and the new influx of high resolution data from the *Chandra* and *XMM-Newton* X-ray satellites, which will likely provide even tighter constraints, we believe that a thorough examination of the $M_{gas} - T_X$ relation is timely.

The models we consider below were developed in a flat Λ-CDM cosmology with $\Omega_m = 0.3$, $h = 0.75$, and a nucleosynthesis value $\Omega_b = 0.019h^{-2}$ (Burles & Tytler 1998). They are computed for a number of different preheating levels, corresponding to entropy constants of $K_0 = 100$, 200, 300, & 427 keV cm^2. These span the range required to match the observed $L_X - T_X$ relations of groups and hot clusters (e.g., Ponman et al. 1999; Lloyd-Davies et al. 2000; Tozzi & Norman 2001; BBLP02). For the purposes of comparison, we also implement an "isothermal" model (see Section 2.3 in BBLP02), which mimics the self-similar result deduced from numerical simulations (e.g., Evrard et al. 1996).

2.2 Cluster models

Since an in-depth discussion of the preheated cluster models can be found in BBLP02, we present only a brief description of the models here.

The preheated models can be summarized as follows: the dominant dark matter component, which is unaffected by the energy injection, collapses and virializes to form bound halos. The distribution of the dark matter in such halos is assumed to be the same as found in recent ultra-high resolution numerical simulations (Moore et al. 1998; Klypin et al. 1999; Lewis et al. 2000) and is described by

$$\rho_{dm}(r) = \rho_{dm,0}\left(\frac{r}{r_s}\right)^{-n}\left(1+\frac{r}{r_s}\right)^{n-3} \tag{2.1}$$

where n = 1.4, $\rho_{dm,0}$ is the profile normalization, and r_s is the scale radius. While the dark component is unaffected by energy injection, the collapse of the baryonic component is hindered by the pressure forces induced by preheating. If the maximum infall velocity due purely to gravity of the dark halo is subsonic, the flow will be strongly affected by the pressure and it will not undergo accretion shocks. It is assumed that the baryons will accumulate onto the halos *isentropically* at the adiabatic Bondi accretion rate (as described in Balogh et al. 1999). This treatment, however, is only appropriate for low mass halos. If the gravity of the dark halos is strong enough (as it is expected to be in the hot clusters being considered here) so that the maximum infall velocity is transonic or supersonic, the gas will experience an additional (generally dominant) entropy increase due to accretion shocks. In order to trace the shock history of the gas, a detailed knowledge of the merger history of the cluster/group is required but is not considered by BBLP02. Instead, it is assumed that at some earlier time the most massive cluster progenitor will have had a mass low enough such that shocks were negligible in its formation, similar to the low mass halos discussed above. This progenitor forms an isentropic core of radius r_c at the cluster center. The entropy of gas outside of the core, however, will be affected by shocks. Recent high resolution numerical simulations suggest that the entropy profile for gas outside this core can be adequately represented

by a simple analytic expression given by $\ln K(r) = \ln K_0 + \alpha \ln (r/r_c)$ (Lewis et al. 2000), where $\alpha \sim 1.1$ for the massive, hot clusters ($T_X \gtrsim 3$ keV) of interest here (Tozzi & Norman 2001; BBLP02). It should be noted that in the case of these massive systems, the accretion of gas is limited by gravitational infall, and hence they accrete their full complement of baryons [i.e., $M_{gas} = (\Omega_b/\Omega_m)M$]. It is assumed that the mass of baryons locked up in stars is negligible (as suggested by, for example, Roussel et al. 2000; Balogh et al. 2001).

Following this prescription and specifying the parameters r_c, $\rho_{gas}(r_c)$, and α (as discussed in BBLP02) completely determines the models. Under all conditions, the gas is assumed to be in hydrostatic equilibrium within the dark halo potential. The effects of radiative cooling are neglected by these models.

2.3 How Preheating Affects the $M_{gas} - T_X$ Relation

Preheating will affect the $M_{gas} - T_X$ relation in two ways: (1) by altering the temperature profile and increasing the emission-weighted gas temperature of a cluster and (2) by altering the gas density profile and reducing the gas mass in the cluster core. We are interested in the strength of these effects and whether or not they can be distinguished by current or future observational data. First, we consider the effect of preheating on the temperature of a cluster.

Figure 2.1 is a plot of T_X as a function of entropy floor level (i.e., K_0) for three clusters of different *total* masses. The thin line represents a cluster with $M \approx 5.6 \times 10^{14} M_\odot$, the next thickest line represents a cluster with $M \approx 10^{15} M_\odot$, and the thickest line represents a cluster with $M \approx 1.8 \times 10^{15} M_\odot$. As expected, the gas temperature of a cluster increases as the level of preheating is increased. On average, an increase in T_X of about 1 keV (10 - 25%) occurs when a cluster is preheated to the level of $K_0 \gtrsim 300$ keV cm^2 (over the range 3 keV $\lesssim T_X \lesssim$ 10 keV). This effect will primarily manifest itself as a normalization shift in the $M_{gas} - T_X$

relation.

Figure 2.2 presents the dimensionless gas density profile of a cluster with $T_X = 4$ keV (left panel) and a cluster with $T_X = 8$ keV (right panel) as a function of the level of preheating. The dot-dashed line is the self-similar result (i.e., isothermal model of BBLP02). The long-dashed, short-dashed, dotted, and solid lines represent the preheated models of BBLP02 with $K_0 = 100$, 200, 300, and 427 keV cm^2, respectively. Preheating reduces the gas density, and therefore the gas mass, in the central regions of a cluster. In §2.4, we investigate the $M_{gas} - T_X$ relation within three different radii: $r = 0.25h^{-1}$ Mpc and $0.50h^{-1}$ Mpc and r_{500} (the radius within which the mean dark matter mass density is 500 times the mean critical density ρ_{crit} at $z = 0$). These radii are indicated in Figure 2.2 by the open squares, pentagons, and triangles, respectively. Clearly, the effect on the $M_{gas} - T_X$ relation will be strongest when M_{gas} is evaluated within $r = 0.25h^{-1}$ Mpc.

Furthermore, because $r = 0.25h^{-1}$ Mpc is a fixed radius that samples different fractions of the virial radius (R_{halo}) for clusters of different temperature, the (fractional) reduction in gas mass within that radius will be largest for the lowest temperature systems. This will lead to both a normalization shift and a steepening of the $M_{gas} - T_X$ relation. To illustrate how strong the effect is, we examine the reduction of gas mass within $r = 0.25h^{-1}$ Mpc, $0.50h^{-1}$ Mpc and r_{500} for a low mass cluster with a *total* mass of $M \approx 5.6 \times 10^{14} M_\odot$ and for a high mass cluster with $M \approx 1.8 \times 10^{15} M_\odot$. We find that when the low mass cluster has undergone preheating at the level of $K_0 = 100$ keV cm^2 it has $\approx 32\%$ more mass in gas within $r = 0.25h^{-1}$ Mpc than when the same cluster has undergone preheating at the level of $K_0 = 427$ keV cm^2. Using the same test on the $M \approx 1.8 \times 10^{15} M_\odot$ cluster, however, yields a difference of only 22%. When we probe the larger radius $r = 0.50h^{-1}$ Mpc, we find the effect is less pronounced (as expected). The difference in M_{gas} between the $K_0 = 100$ keV cm^2 model and $K_0 = 427$ keV cm^2 model is 8% for the low mass cluster and 7% for the high mass cluster. Finally, when the gas mass is evaluated within r_{500}, the difference is 4% for the low mass cluster as

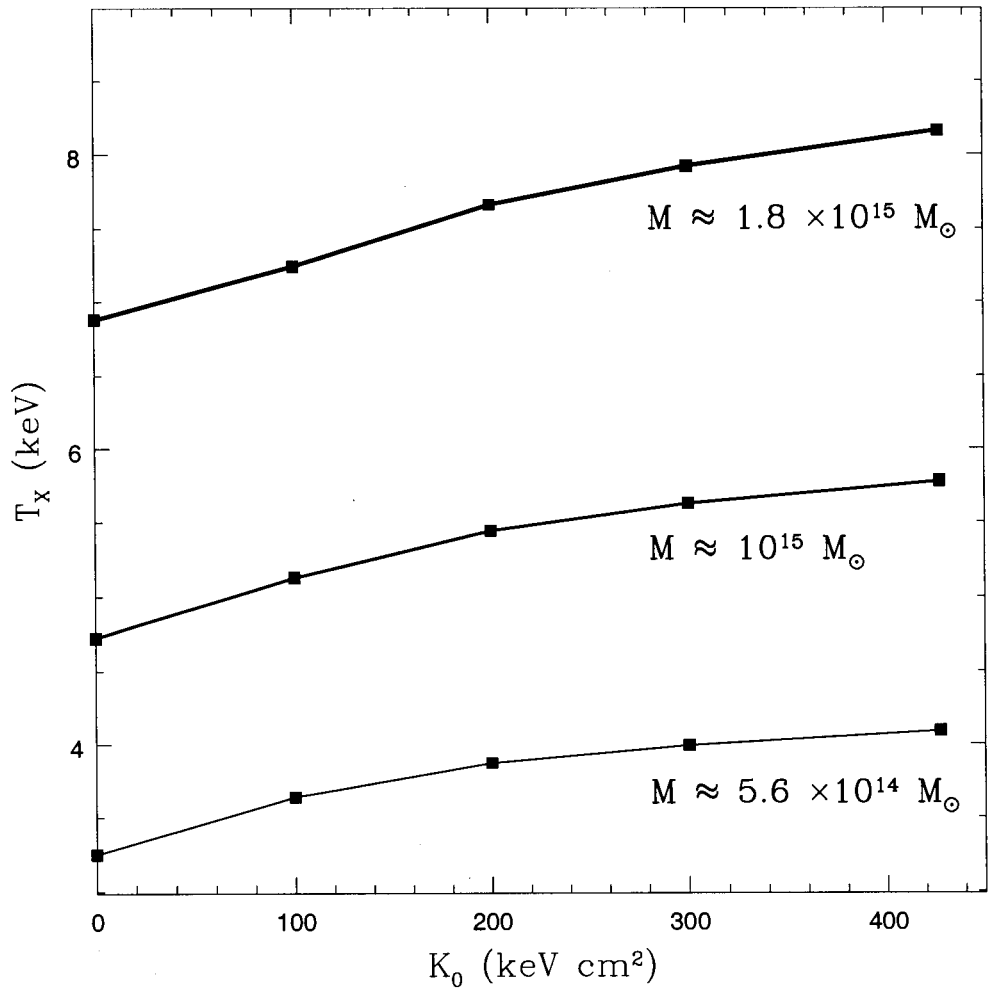

Figure 2.1: Effect of preheating on a cluster's temperature. The thin line, the next thickest line, and the thickest line represent clusters with $M \approx 5.6 \times 10^{14}$, 10^{15}, and $1.8 \times 10^{15} M_\odot$, respectively. The solid squares indicate the discrete points where the model was actually evaluated.

opposed to 2% for the high mass cluster.

In summary, preheating will significantly affect the $M_{gas} - T_X$ relation by increasing the emission-weighted gas temperature of clusters. Whether or not the relation is also affected by the reduction of gas mass in the cores of clusters de-

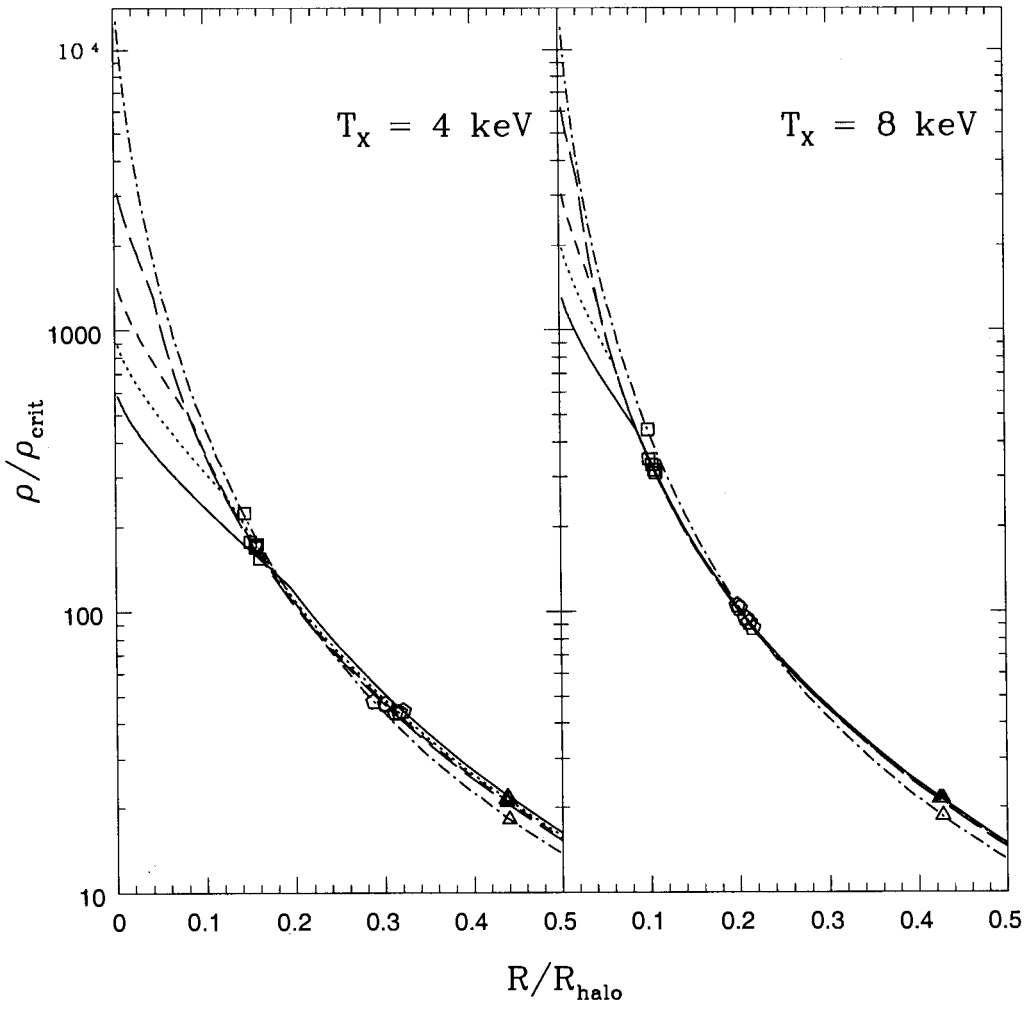

Figure 2.2: Effect of preheating on a cluster's gas density profile. *Left*: Cluster with $T_X = 4$ keV. *Right*: Cluster with $T_X = 8$ keV. The dot-dashed line is the self-similar result. The long-dashed, short-dashed, dotted, and solid lines represent the preheated models of BBLP with $K_0 = 100$, 200, 300, and 427 keV cm^2, respectively. The squares, pentagons, and triangles indicate the radii $r = 0.25h^{-1}$ Mpc and $0.50h^{-1}$ Mpc and r_{500}, respectively, for each of the models.

pends on within which radius M_{gas} is evaluated and what temperature regime is being probed. The effect will be strongest for low temperature systems and when M_{gas} is probed within small radii (e.g., $r = 0.25h^{-1}$ Mpc). An evaluation of the

$M_{gas} - T_X$ relation within large radii, such as r_{500}, however, probes the integrated properties of a cluster and will be sensitive only to the temperature shift.

In the next section, we compare the results of the BBLP02 preheated models to genuine observational data. As we show below, only models with $K_0 \gtrsim 300$ keV cm^2 are consistent with the data.

2.4 Results

In Figure 2.3 we present the $M_{gas} - T_X$ relation as predicted by the BBLP02 preheated models within r_{500}. The radius r_{500} is typically comparable in size to the *observed* radius of a cluster and represents the boundary between the inner, virialized region and recently accreted, still settling outer region of a cluster (Evrard et al. 1996). Thus, as already mentioned, the $M_{gas}(r_{500}) - T_X$ relation can be regarded as a probe of the integrated properties of a cluster and can be directly compared with the self-similar result of $M_{gas} \propto T_X^{1.5}$.

In Figures 2.4 and 2.5 we present the $M_{gas} - T_X$ relation as predicted by the BBLP02 preheated models within the fixed radii $r = 0.25h^{-1}$ Mpc and $r = 0.50h^{-1}$ Mpc, respectively. As mentioned above, the determination of the $M_{gas}-T_X$ relation within some fixed radius, such as $r = 0.25h^{-1}$ Mpc or $r = 0.50h^{-1}$ Mpc, can be used as an indirect probe of the gas density profiles of clusters because it samples different fractions of the virial radius for clusters of different temperature. For the purposes of clarity, we discuss the $M_{gas}-T_X$ relation at these three radii separately.

2.4.1 Test 1: $M_{gas}(r_{500}) - T_X$

The solid squares in Figure 2.3 represent the gas mass determinations of MME99 within r_{500} using surface brightness profile fitting (with isothermal β models) of *ROSAT* Position Sensitive Proportional Counter data and mean emission-weighted temperatures from the literature, for clusters with $T_X \geq 3$ keV and whose error bars are 1 keV or smaller. We compare this with the self-similar result repre-

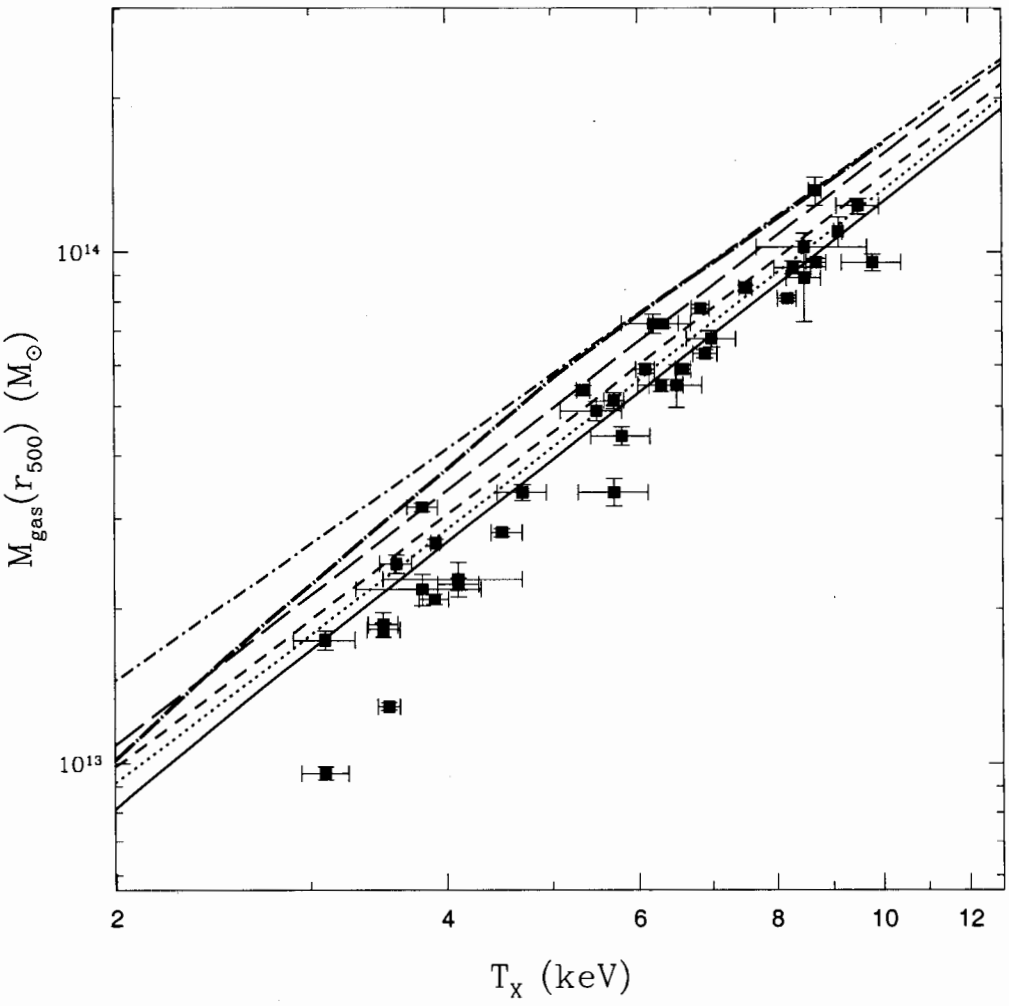

Figure 2.3: Comparison of $M_{gas}(r_{500}) - T_X$ relations. Squares represent the gas mass determinations of Mohr et al. (1999) within r_{500}. The dot-short-dashed, long-dashed, short-dashed, dotted, and solid lines represent the self-similar model and preheated models of BBLP02 with K_0 = 100, 200, 300, and 427 keV cm^2, respectively. The dot-long-dashed (thick) line represents the best-fit heated model of Loewenstein (2000).

sented by the "isothermal" model of BBLP02 (dot-short-dashed line). Finally, the long-dashed, short-dashed, dotted, and solid lines represent the preheated models of BBLP02 with K_0 = 100, 200, 300, and 427 keV cm^2, respectively. The thick dot-long-dashed line represents the predictions of the best-fit heated model

of Loewenstein (2000). This model is discussed further in §2.5.1.

It is readily apparent that only the preheated models of BBLP02 with $K_0 \gtrsim 200$ keV cm^2 have a reasonable chance of being consistent with the data of MME99. The normalization clearly indicates that the observed gas temperature of clusters with a given gas mass is hotter than predicted by models with entropy floors of $K_0 \lesssim 100$ keV cm^2. We note that this discrepancy may be remedied by assuming a smaller value of Ω_b/Ω_m. However, a similar offset, in the same sense, is seen in the correlation with *total* dark matter mass and gas temperature (Horner et al. 1999; Nevalainen et al. 2000; Finoguenov et al. 2001). This will not be reconciled by lowering Ω_b/Ω_m. The reason why the preheated models with $K_0 \gtrsim 200$ keV cm^2 are better able to match the normalization of the observational data than models with $K_0 \lesssim 100$ keV cm^2 is, as mentioned above, because an increase in the amount of preheating directly leads to an increase in the emission-weighted gas temperature.

We have attempted to quantify how well (or poorly) the preheated and self-similar models match the observational data. We have fit both the theoretical results and the observational data with simple linear models of the form $\log M_{gas} = m \log T_X + b$ over the range 3 keV $\lesssim T_X \lesssim$ 10 keV. For the theoretical results, we calculate the best-fit slope and intercept using the ordinary least squares (OLS) test. We stress that the results of these fits, which are presented in Table 2.1, are only valid for clusters with $T_X \gtrsim 3$ keV. At lower temperatures, the role of preheating becomes much more important [as M_{gas} becomes less than $(\Omega_b/\Omega_m)M$] and as a result, the relations steepen dramatically. For example, the preheated model with $K_0 = 427$ keV cm^2 is well approximated by a power-law with $M_{gas} \propto T_X^{1.68}$ over the range 3 keV $\lesssim T_X \lesssim$ 10 keV but is significantly steeper over the range 1 keV $\lesssim T_X \lesssim 3$ keV with $M_{gas} \propto T_X^{1.94}$. *Thus, it is absolutely essential that comparisons between theoretical models and observations are done over the same range in temperatures.*

To fit the observational data of MME99, we have used a linear regression tech-

Table 2.1: Results of linear regression fits to $M_{gas}(r_{500}) - T_X$ data

Model	Entropy Floor (keV cm^2)	m^a	b^a
Isothermal model	0	1.50	12.72
Preheated models	100	1.65	12.54
	200	1.66	12.48
	300	1.67	12.45
	427	1.68	12.42
MME99 data	?	1.93 ± 0.16	12.21 ± 0.13
MME99 data minus 2 clusters	?	1.82 ± 0.14	12.31 ± 0.12

Note.— Models of the form $\log M_{gas} = m \log T_X + b$ were fit over the range 3 keV $\lesssim T_X \lesssim$ 10 keV.

[a]Uncertainties correspond to the 90% confidence level.

nique that takes into account measurement errors in both coordinates as well as intrinsic scatter (the BCES test of Akritas & Bershady 1996). As a consistency check, we have also employed 10,000 Monte Carlo bootstrap simulations. No significant deviations between the two tests were found. The results of the linear regression fits to the observational data are also presented in Table 2.1.

For all 38 clusters taken from MME99, we derive a best fit that is inconsistent with the results of *all* of the theoretical models considered at greater than the 90% confidence level[1]. However, as is apparent from Figure 2.3, the slope and intercept of the best-fit line are sure to be heavily dependent upon the two low temperature clusters with the lowest measured gas masses (and gas mass fractions): the Hya I cluster (Abell 1060) and the Cen cluster (Abell 3526). A number of other studies (both optical and X-ray) have also identified very unusual properties in both clusters. For example, Fitchett & Merritt (1988) were unable to fit a spherical equilibrium model to the kinematics of galaxies in the core of Hya I. They suggest that substructure is present and is likely why Hya I does not lie

[1]Our best fit differs slightly from MME99's best fit to their own data because we implemented a different selection criteria. Namely, we have used only clusters with $T_X \geq 3$ keV and whose error bars are 1 keV or smaller.

along the $L_X - \sigma$ relation for galaxy clusters. More recently, Furusho et al. (2001) have found that the metal abundance distribution implies that the gas in Hya I is well-mixed (i.e., it does not contain an obvious metallicity gradient), suggesting that a major merger event may have occurred sometime after the enrichment of the ICM. Measurements of the bulk motions of the intracluster gas in the Cen cluster (through Doppler shifting of X-ray spectral lines) reveal strange gas velocity gradients indicative of a large merger event in the not too distant past (Dupke & Bregman 2001). This picture has also been supported by Furusho et al. (2001), who found large temperature variations across the cluster's surface. Thus, neither Hya I nor Cen can be regarded as typical "relaxed" clusters and are probably not representative of the majority of low temperature systems.

One way to ameliorate the impact of the two clusters would be to increase the number of systems of this temperature. However, there are very few published gas mass estimates of cool clusters and groups within r_{500}. X-ray emission from groups is usually only detected out to a small fraction of this radius. The one study that does present group gas masses for a radius at fixed overdensity, Roussel et al. (2000), does so for r_{200} and is not directly comparable to the results presented in Figure 2.3. Also, in that study, gas masses were determined by extrapolating the surface brightnesses far outside the limiting radius for which X-ray emission was actually detected. This can lead to biases in determining group/cluster properties (see Mulchaey 2000; Balogh et al. 2001).

In recognition of the above, we have tried removing Hya I and Cen from the sample and fitting the remaining 36 clusters using the same procedure. We find that the preheated model with $K_0 = 427$ keV cm^2 is then consistent with the data at the 90% level. The $K_0 = 200$ and 300 keV cm^2 models are marginally inconsistent with the MME99 data. The isothermal model is ruled out at $\gtrsim 99\%$ confidence irrespective of whether these clusters are dropped or not.

The other two observational studies that have investigated the $M_{gas} - T_X$ relation, Neumann & Arnaud (2001) and Vikhlinin et al. (1999), unfortunately did

not present gas mass determinations within r_{500} for individual clusters in a table or graphically. They did, however, present their best-fit values for the slope of the relation. These were deduced from samples of clusters that have temperatures spanning roughly the same range as that considered in Figure 2.3. The best-fit slopes of the preheated models are shallower than the best-fit claimed by Neumann & Arnaud (2001) of $M_{gas} \propto T_X^{1.94}$ for a sample of 15 hot clusters. However, an estimate of the uncertainty on this result was not reported; thus we are unable to say whether this result is inconsistent with the predictions of the preheated models. The predicted slopes of all four preheated models studied here are in excellent agreement with the findings of Vikhlinin et al. (1999), who report $M_{gas} \propto T_X^{1.71\pm0.13}$ for their sample of 39 clusters. We also note that the results of Neumann & Arnaud (2001) and Vikhlinin et al. (1999) differ significantly from the predictions of the self-similar model.

In summary, we find that the class of models that invoke preheating are much better able to match the observed $M_{gas}(r_{500}) - T_X$ of hot clusters than that of the isothermal self-similar model, which is ruled out with a high level of confidence. A careful analysis of the MME99 data also suggests that only those models that invoke a "high" level of energy injection (i.e., $K_0 > 300$ keV cm^2) are able to match observations.

2.4.2 Test 2: $M_{gas}(r = 0.25h^{-1}$ Mpc) - T_X

The solid triangles and pentagons in Figure 2.4 represent the gas mass determinations within $r = 0.25h^{-1}$ Mpc of Peres et al. (1998) and White et al. (1997), respectively. These data were obtained using surface brightness profile fitting of *ROSAT* data (Peres et al. 1998) and *Einstein* data (White et al. 1997) and emission-weighted temperatures from the literature, for clusters with $T_X \geq 3$ keV and whose error bars are 1 keV or smaller. The predictions of the isothermal self-similar model are represented by the dot-dashed line. Once again, the long-dashed, short-dashed, dotted, and solid lines represent the preheated models of BBLP02

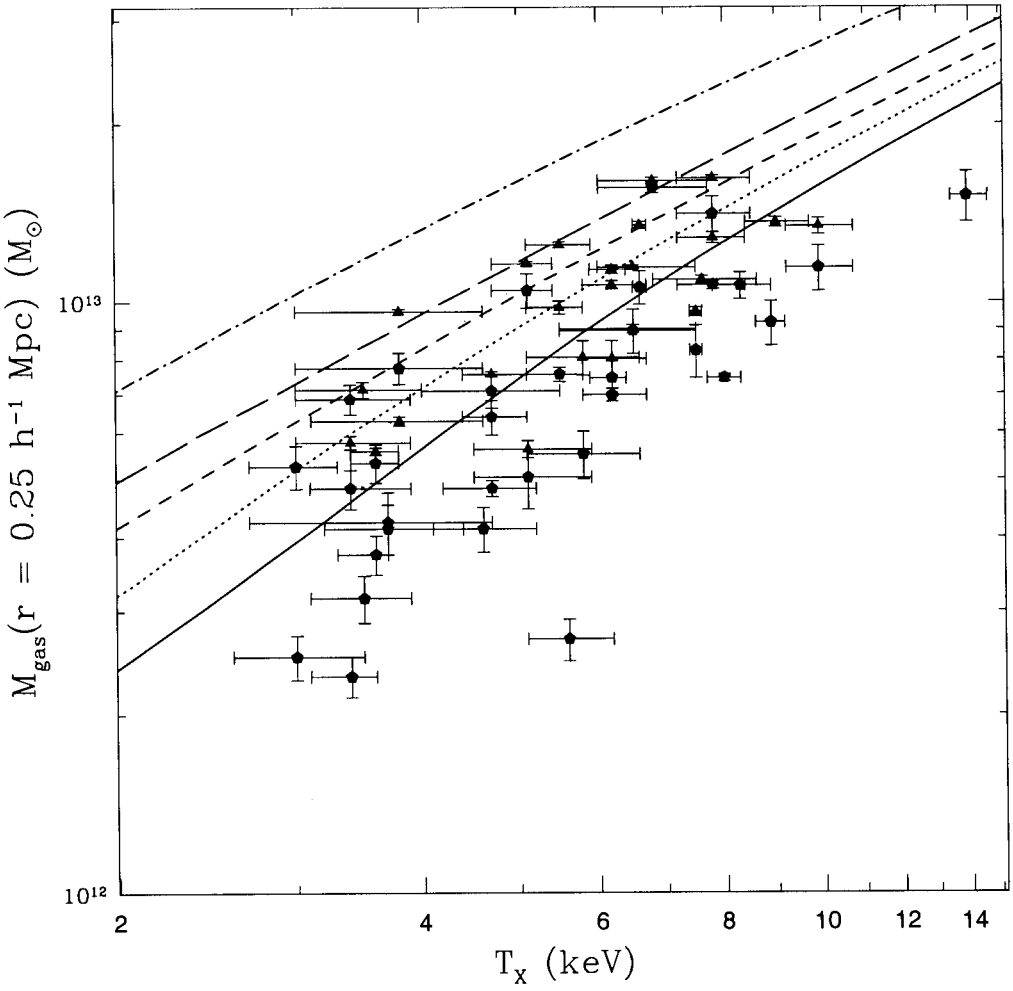

Figure 2.4: Comparison of $M_{gas}(r = 0.25h^{-1}$ Mpc$)$–T_X relations. The solid triangles and pentagons represent the gas mass determinations Peres et al. (1998) and White et al. (1997) within $r = 0.25h^{-1}$ Mpc, respectively. The dot-dashed line is the self-similar result. The long-dashed, short-dashed, dotted, and solid lines represent the preheated models of BBLP02 with $K_0 = 100$, 200, 300, and 427 keV cm^2, respectively.

with $K_0 = 100$, 200, 300, and 427 keV cm^2, respectively.

In spite of the scatter, it is apparent that only those preheated models with entropy floors of $K_0 \gtrsim 300$ keV cm^2 are consistent with the 57 clusters plotted in Figure 2.4. As with the $M_{gas}(r_{500}) - T_X$ relation, the normalization of the self-

Table 2.2: Results of linear regression fits to $M_{gas}(r = 0.25h^{-1}$ Mpc) - T_X data

Model	Entropy Floor (keV cm^2)	m[a]	b[a]
Isothermal model	0	0.84	12.61
Preheated models	100	0.91	12.43
	200	0.95	12.34
	300	1.06	12.21
	427	1.19	12.03
Peres et al. and White et al. data	?	1.11 ± 0.22	12.06 ± 0.17

Note.— Models of the form $\log M_{gas} = m \log T_X + b$ were fit over the range 3 keV $\lesssim T_X \lesssim$ 10 keV.

[a]Uncertainties correspond to the 90% confidence level.

similar model and the preheated model with $K_0 = 100$ keV cm^2 suggests that ICM is observed to be much hotter than predicted by either of these models. Fitting both the theoretical predictions and observational data in a manner identical to that presented in the previous subsection, we find that only the preheated models with $K_0 \geq 300$ keV cm^2 have both slopes and intercepts that are consistent with the observational data (see Table 2.2). On the basis of normalization (intercept), the self-similar model is ruled out with greater than 99% confidence.

In §2.3 we briefly discussed the potential of the gas density profile to affect the $M_{gas}(r = 0.25h^{-1}$ Mpc) - T_X relation. This effect is obvious in Figure 2.4, with mild breaks at $T_X \approx 10$ keV for the $K_0 = 427$ keV cm^2 model and at $T_X \approx 5$ keV for the $K_0 = 300$ keV cm^2 model. However, with the large scatter obscuring any potential breaks in the $M_{gas} - T_X$ relation, all we can conclude is that the data are consistent with predicted profiles of the BBLP02 preheated models with $K_0 \gtrsim 300$ keV cm^2.

The exact nature of the scatter in Figure 2.4 is unclear. While some of the scatter is likely attributable to the large uncertainties in the temperature measurements made using *Einstein*, *Ginga*, and *EXOSAT* data, some of it may also be due to unresolved substructure (e.g., cooling flows) and point sources. Such issues

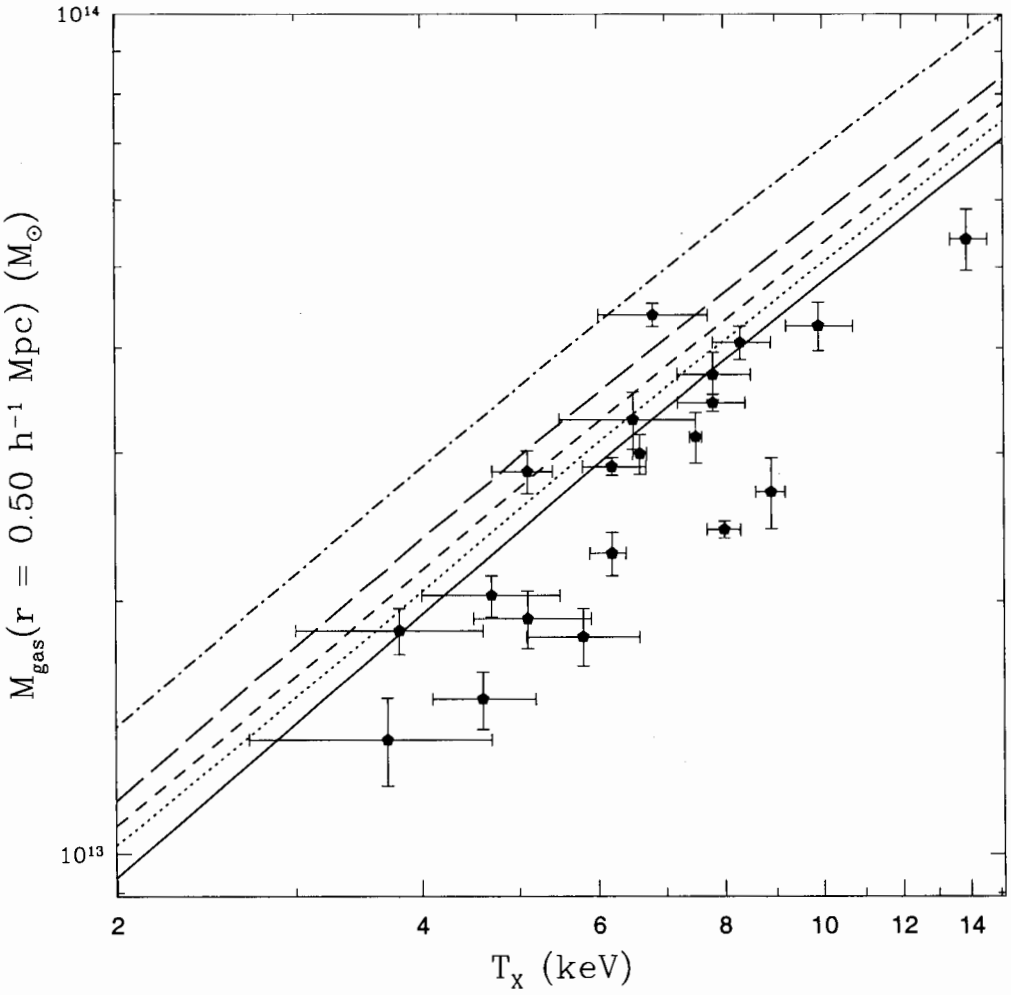

Figure 2.5: Comparison of $M_{gas}(r = 0.50h^{-1}\ \mathrm{Mpc})$–$T_X$ relations. The solid pentagons represent the gas mass determinations of White et al. (1997) within $r = 0.50h^{-1}$ Mpc. The dot-dashed line is the self-similar result. The long-dashed, short-dashed, dotted, and solid lines represent the preheated models of BBLP02 with $K_0 = 100$, 200, 300, and 427 keV cm^2, respectively.

become particularly important when investigating the central regions of clusters as opposed to its integrated properties. Indeed, new high-resolution data obtained by *Chandra* support this idea (see, e.g., Stanford et al. 2001). We anticipate that future data obtained by both *Chandra* and *XMM-Newton* will place much tighter

Table 2.3: Results of linear regression fits to $M_{gas}(r = 0.50h^{-1}$ Mpc) - T_X data

Model	Entropy Floor (keV cm^2)	m^a	b^a
Isothermal model	0	0.97	12.87
Preheated models	100	0.98	12.78
	200	0.98	12.75
	300	0.99	12.72
	427	1.01	12.68
White et al. data	?	1.12 ± 0.25	12.53 ± 0.20

Note.— Models of the form $\log M_{gas} = m \log T_X + b$ were fit over the range 3 keV $\lesssim T_X \lesssim$ 10 keV.

[a]Uncertainties correspond to the 90% confidence level.

constraints on the $M_{gas}(r = 0.25h^{-1}$ Mpc) - T_X relation and possibly even allow one to probe the mild break in the relationship predicted by the preheated models.

2.4.3 Test 3: $M_{gas}(r = 0.50h^{-1}$ Mpc) - T_X

The solid pentagons in Figure 2.5 represent the gas mass determinations of White et al. (1997) within $r = 0.50h^{-1}$ Mpc using surface profile fitting of *Einstein* data and emission-weighted gas temperatures from the literature, for clusters with $T_X \geq 3$ keV and whose error bars are 1 keV or smaller. Again, the predictions of the isothermal self-similar model are represented by the dot-dashed line while the long-dashed, short-dashed, dotted, and solid lines represent the preheated models with $K_0 = 100$, 200, 300, and 427 keV cm^2, respectively.

A linear regression fit to the 20 clusters taken from White et al. (1997) yields a best-fit slope and intercept that is consistent with only the $K_0 = 300$ and 427 keV cm^2 preheated models (90% confidence; see Table 2.3). Once again, the isothermal model is ruled out with greater than 99% confidence. This follows the same general trend discovered in the previous tests.

As expected, the influence of the gas density profile on the $M_{gas}(r = 0.50h^{-1}$ Mpc) - T_X is minimal. Only a very modest break is detectable at $T_X \approx 4.5$ keV for the $K_0 = 427$ keV cm^2 preheated model. Like the $M_{gas}(r_{500}) - T_X$ relation,

this relation is mostly sensitive to the temperature shift (at least for clusters with $T_X \gtrsim 3$ keV).

2.5 Comparison with previous theoretical studies

Only two other theoretical studies have examined the effects on the $M_{gas} - T_X$ relation of entropy injection into the ICM: Loewenstein (2000) and Bialek et al. (2001). Both studies investigated the $M_{gas}(r_{500}) - T_X$ relation and demonstrated that entropy injection does, indeed, steepen the relation, in agreement with the present work (however, neither implemented the $M_{gas} - T_X$ at fixed radii test). These studies suggest that models that produce an entropy floor with a level that is consistent with measurements of groups ($K_0 \sim 100$ keV cm^2; Ponman et al. 1999; Lloyd-Davies et al. 2000) are capable of matching the observations of even hot clusters (up to 10 keV). This is in apparent conflict with the results presented in §2.3 that suggest that a high entropy floor of $K_0 \gtrsim 300$ keV cm^2 is required to match the observations of hot clusters. A low value of the entropy floor is also in apparent conflict with a number of other studies that have focused mainly on the $L_X - T_X$ relation of hot clusters. For example, da Silva et al. (2001), Tozzi & Norman (2001) and BBLP02 have all concluded that such low levels of entropy injection do not bring consistency between observations and theoretical models of *hot clusters*. As such, a closer analysis of Loewenstein (2000) and Bialek et al. (2001) studies is warranted.

2.5.1 The Loewenstein (2000) Models

To model the observed deviations of the cluster X-ray scaling relations, Loewenstein (2000) has constructed a suite of hydrostatic polytropic models (which are normalized to observations of high-temperature clusters and numerical simula-

tions), and then modified them by adding various amounts of heat per particle at the cluster center. Strictly speaking, the Loewenstein (2000) models cannot be characterized as *preheated* models, since the injection of entropy into the ICM occurs after the cluster has formed. Thus, a straightforward comparison between the Loewenstein (2000) and BBLP02 models is not trivial. However, success in matching the $M_{gas}(r_{500}) - T_X$ relation (the data of MME99) is claimed by Loewenstein (2000) for a model that "produces an entropy - temperature relation with the observed entropy floor at $\approx$ 100 keV cm^2." Regardless of how the entropy floor actually arose, this contradicts the results presented in §2.3, which suggest that an entropy floor of $\gtrsim$ 300 keV cm^2 is required to match the observations. Can the analysis of Loewenstein (2000) and that of the present work be reconciled?

A closer investigation of Figure 2.4 of Loewenstein (2000) reveals that first of all, his heated models were not compared to the actual data but rather to points that represent MME99's best-fit power-law match to their data. Second, this power-law relationship was assumed to hold true and hence, extrapolated to span a wider range in temperatures than considered by MME99. Of the 45 clusters studied by MME999, only one had a temperature below 3 keV (it was 2.41 keV), yet Loewenstein (2000) compared his heated models to the best-fit relation of MME99 over the range 1 keV $\lesssim T_X \lesssim$ 10 keV. As previously mentioned, however, entropy injection preferentially affects low-temperature systems and, therefore, extrapolating scaling relations derived from high-temperature systems down to the low-temperature regime is not safe.

In Figure 2.3, we compare the best-fit heated model of Loewenstein (2000) (his $\epsilon = 0.35$ model, as the thick dot-long-dashed line) with the predictions of BBLP02 models and the data of MME99. The plot clearly demonstrates that his best-fit model does not match the data of MME99 nearly as well as the BBLP02 preheated models with $K_0 \gtrsim$ 300 keV cm^2, especially at the high temperature end. The difference in temperature ranges examined by Loewenstein (2000) and the present study (whose range of temperatures were purposely chosen to match

the observational data) has likely led to an underestimation of the entropy floor in these clusters by Loewenstein (2000). We once again re-iterate that it is extremely important that comparisons between theoretical models and observations are done over the same range in temperatures.

2.5.2 The Bialek et al. (2001) simulations

In similarity to the present work, Bialek et al. (2001) investigated the impact of preheating on the $M_{gas} - T_X$ relation for a number of different levels of entropy injection, spanning the range 0 keV cm^2 $\lesssim K_0 \lesssim$ 335 keV cm^2. Fitting their $M_{gas}(r_{500}) - T_X$ simulation data over the range 2 keV $\lesssim T_X \lesssim$ 9 keV, which is similar (but not identical) to the MME99 sample, they claim success in matching the observations of MME99 for models with entropy injection at the level of 55 keV cm^2 $\lesssim K_0 \lesssim$ 140 keV cm^2, at least on the basis of slope. Their models with higher levels of entropy injection, apparently, predict relations much too steep to be consistent with the data of MME99. These predictions are inconsistent with the results of the BBLP02 analytic models with similar levels of entropy injection (e.g., for $K_0 \approx 300$ keV cm^2, BBLP02 predict $M_{gas} \propto T_X^{1.67}$ while Bialek et al. find $M_{gas} \propto T_X^{2.67}$) . However, we believe the difference in the predictions (and conclusions) of Bialek et al. (2001) and the present work can be reconciled.

As noted by Neumann & Arnaud (2001), Bialek et al. (2001) have simulated very few hot clusters and, although they fit their $M_{gas}(r_{500}) - T_X$ simulation data over a range similar to MME99, the results are too heavily weighted by the cool clusters ($T_X \lesssim 3$ keV) to be properly compared with the data of MME99. As an example, we consider their "S6" sample of 12 clusters that have $K_0 = 335$ keV cm^2. According to the present study, this model should give a reasonably good fit to the MME99 observational data, much better than that of a model with $K_0 \approx 100$ keV cm^2. Although the normalization of the S6 model is in excellent agreement with the MME99 data (as is apparent in Table 3 of Bialek et al. and the general trends in their Figure 1) they rule this model out based on the fact that the

predicted slope is 2.67, much steeper than the 1.98 found by MME99. However, a closer analysis reveals that the fraction of cool clusters in the simulation data set is much higher than fraction of cool clusters in the MME99 sample. For example, in the MME99 sample of 45 clusters, only one cluster has a temperature below 3 keV. In the Bialek et al. (2001) S6 set, however, 5 of the 12 clusters have temperatures below 3 keV. In addition, the mean temperature of clusters in the MME99 sample is $\approx$ 5.5 keV, while it is only about 3.8 keV in the Bialek et al. (2001) S6 data set. As previously mentioned, preheating preferentially affects low temperature systems and, therefore comparisons between theory and observations should be done over the same range in temperatures. To illustrate the problems of comparing theoretical models and observations that span different temperature ranges, we tried to reproduce the fit of Bialek et al. (2001) to their S6 data set. We used data presented in their Table 2 for clusters with $T_X > 2$ keV (we use their preferred "processed" temperatures) and fit it with a linear model and found $M_{gas} \propto T_X^{2.42\pm0.17}$. This is slightly different from the value listed in their Table 3, presumably because Table 2 is based on data within r_{200} while Table 3 is based on data within r_{500} (they note that a change of up to 6% in the predicted slope can occur when switching between the two). To match the conditions of the present work, we then discarded all simulated cluster data below 3 keV (the mean temperature for the remaining 7 clusters was then 5.1 keV, similar to the MME99 data) and found a best fit of $M_{gas} \propto T_X^{1.99\pm0.30}$. This is excellent agreement with the results of MME99 and only marginally inconsistent with the BBLP02 models of similar entropy injection.

What about their favored models? We have tried the same type of test on their S3 data set ($K_0 \approx 100$ keV cm^2). Fitting all simulated clusters with $T_X \gtrsim 2$ keV (mean temperature of 3.8 keV) we find $M_{gas} \propto T_X^{1.86\pm0.12}$, which is in good agreement with the results of MME99. When we remove all clusters below 3 keV (mean temperature of 4.9 keV), however, the best fit is $M_{gas} \propto T_X^{1.77\pm0.38}$. In this case, the best-fit relation is not very constraining. It is even indistinguishable

from the self-similar result. It is apparent from their Figure 1, however, that the predicted normalization for this model (and all other low entropy models) does not match the observations of MME99. This is noted by the authors themselves. They claim the difference in the zero point may be resolved by reducing the baryon fraction by $\sim 20\%$. As we noted earlier, however, a similar normalization offset is also seen in the total cluster mass - temperature ($M - T_X$) relation and this cannot be resolved by reducing the baryon fraction. This suggests that the problem lies with the temperature, rather than the gas mass. Alternatively, Bialek et al. also suggest that rescaling their simulations for $H_o = 70$ km s^{-1} Mpc^{-1} (instead of 80 km s^{-1} Mpc^{-1}) would bring consistency between the normalization of this model and the observations. This would be true only if the baryon fraction was held fixed at 0.1 and not rescaled for the new cosmology. Given that they assume $\Omega_m = 0.3$, this would imply $\Omega_b = 0.015h^{-2}$ which is roughly 30% lower than observed in quasar absorption spectra (Burles & Tytler 1998). Thus, while the normalization offset between their theoretical model and the observations of MME99 is directly reduced by decreasing the value of h, it is indirectly increased by roughly the same proportion through the increased value of Ω_b/Ω_m.

In summary, as with the Loewenstein (2000) models, we find that the difference in the results and conclusions of Bialek et al. (2001) and the present work can be explained on the basis that different temperature ranges were examined. In particular, we have shown that the fraction of cool clusters in Bialek et al.'s simulated data set is much larger than that found in the MME99 sample and this has likely led to an underestimation of the entropy floor in these clusters. In order to safely and accurately compare the preheated models of BBLP02 with observations we have paid special attention to only those hot clusters with $T_X \gtrsim 3$ keV. As such, we believe our comparison is more appropriate.

2.6 Discussion & Conclusions

Motivated by a number of observational studies that have suggested that the $M_{gas} - T_X$ relation of clusters of galaxies is inconsistent with the self-similar result of numerical simulations and by the launch of the *Chandra* and *XMM-Newton* satellites, which will greatly improve the quality of the observed $M_{gas} - T_X$ relation, we have implemented the analytic model of BBLP02 to study the impact of preheating on $M_{gas} - T_X$ relation. The predictions of the model have previously been shown to be in very good agreement with observations (e.g., $L_X - T_X$ relation and $L_X - \sigma$ relation).

In agreement with the previous theoretical studies of Loewenstein (2000) and Bialek et al. (2001), our analysis indicates that injecting the intracluster medium with entropy leads to a steeper relationship than predicted by the self-similar result of numerical simulations of clusters that evolve through the effects of gravity alone. Loewenstein (2000) and Bialek et al. (2001) have found that models that produce an entropy floor of $K_0 \sim 100$ keV cm^2, which is consistent with measurements of galaxy groups, are capable of reproducing the $M_{gas} - T_X$ relation of hot clusters. This is inconsistent with our analysis, which indicates that a "high" level of entropy injection ($K_0 \gtrsim 300$ keV cm^2) is required to match the observational data of hot clusters of White et al. (1997), Peres et al. (1998), and MME99. It is also inconsistent with BBLP02's best-fit value of $K_0 \approx 330$ keV cm^2 found via an investigation of the $L_X - T_X$ relation of both groups and hot clusters. They note that the strongest constraints for a high entropy floor comes from hot clusters. Moreover, a high value of K_0, one that is inconsistent with the predictions of the best-fit models of Loewenstein (2000) and Bialek et al. (2001), has also been reported by Tozzi & Norman (2001). Finally, da Silva et al. (2001) used numerical simulations with a "low" value of $K_0 \sim 80$ keV cm^2 (which is similar to the predictions of the best-fit models of Loewenstein 2000 and Bialek et al. 2001) and found that they *could not* reproduce the observed X-ray scaling relations.

Our result, on the other hand, is consistent with the results of BBLP02, Tozzi & Norman (2001), and da Silva et al. (2001). As discussed in §2.5, we believe the difference between the studies of Loewenstein (2000) and Bialek et al. (2001) and present work can be explained by considering the difference in temperature ranges studied. In particular, we have focused only on hot clusters in an attempt to match the majority of the observational data as closely as possible. The results and conclusions of the other two studies, however, are strongly influenced by their low temperature model data.

We have proposed that the $M_{gas} - T_X$ relation can be used as a probe of the gas density profiles of clusters if it is evaluated at different fixed radii. This is a new test. The preheated models of BBLP02 predict a mild break in the scaling relations when small fixed radii (such as $r = 0.250h^{-1}$ Mpc) are used. The scatter in the current observational data is consistent with the predictions of the BBLP02 models with $K_0 \gtrsim 300$ keV cm^2; however, the exact shape of the gas density profiles is not tightly constrained. We anticipate that large samples of clusters observed by *Chandra* and *XMM-Newton* will place much stronger constraints on the gas density profiles of clusters and allow for further testing of the preheating scenario.

Finally, the high level of energy injection inferred from our analysis has important implications for the possible sources of this excess entropy. Valageas & Silk (1999), Balogh et al. (1999), and Wu et al. (2000) have all shown that galactic winds driven by supernovae can only heat the intracluster/intergalactic medium at the level of $\lesssim 0.3 - 0.4$ keV per particle. This is lower than the $1 - 2$ keV per particle result found here. Thus, if the BBLP02 preheated models provide an accurate description of the ICM, supernovae winds alone cannot be responsible for the excess entropy. It has also been speculated that quasar outflows may be responsible (e.g., Valageas & Silk 1999; Nath & Roychowdhury 2002). This remains an open possibility.

The role of radiative cooling also remains an open issue. Recently, it has been

suggested that *both radiative cooling and preheating together* could be actively involved in shaping the X-ray scaling relations (e.g., Voit & Bryan 2001; Voit et al. 2002). Radiative cooling (and subsequent star formation) would serve to remove the lowest entropy gas, which in turn would help to compress the highest entropy gas, thus increasing the emission-weighted gas temperature and steepening the $M_{gas} - T_X$ relation (cf. the discussion of entropy in the Cool+SF simulation of Lewis et al. 2000). In this way, the combination of cooling and preheating may reduce the best-fit entropy level, perhaps even to a level that can be provided by supernovae winds (Voit et al. 2002). Further study is required to determine the relative roles that both preheating and cooling have on cluster evolution.

Chapter 3

Cluster Sunyaev-Zeldovich Effect Scaling Relations

Abstract

X-ray observations of an "entropy floor" in nearby groups and clusters of galaxies offer evidence that important non-gravitational processes, such as radiative cooling and/or "preheating", have strongly influenced the evolution of the intracluster medium (ICM). We examine how the presence of an entropy floor modifies the thermal Sunyaev-Zeldovich (SZ) effect. A detailed analysis of scaling relations between X-ray and SZ effect observables and also between the two primary SZ effect observables is presented. We find that relationships between the central Compton parameter and the temperature or mass of a cluster are extremely sensitive to the presence of an entropy floor. The same is true for correlations between the integrated Compton parameter and the X-ray luminosity or the central Compton parameter. In fact, if the entropy floor is as high as inferred in recent analyses of X-ray data, a comparison of these correlations with both *current* and future SZ effect observations should show a clear signature of this excess entropy. Moreover, because the SZ effect is redshift-independent, the relations can potentially be used to track the evolution of the cluster gas and possibly discriminate between the possible sources of the excess entropy. To facilitate comparisons with observations, we

provide analytic fits to these scaling relations.

3.1 Introduction

Correlations between the global X-ray properties of galaxy clusters have proven to be important probes of the intracluster medium (ICM). Studies of the relation between the X-ray luminosity (L_X) and the emission-weighted temperature (T_X) have been particularly powerful. Numerical simulations and analytic models that take into account the effects of gravity and shock heating of the gas only (i.e., the so-called "self-similar" models) predict that $L_X \propto T_X^2$ for massive clusters, yet the observed relation is much steeper; $L_X \propto T_X^{2.6-3.0}$ (e.g., Markevitch 1998; Allen & Fabian 1998; Arnaud & Evrard 1999). A number of other observed X-ray scaling relations, for example the total cluster mass (M_{tot})-T_X and total ICM mass (M_{gas})-T_X relations, have also recently been shown to deviate from their predicted scalings (e.g., Horner et al. 1999; Ettori & Fabian 1999; Mohr et al. 1999; Vikhlinin et al. 1999; Nevalainen et al. 2000; Finoguenov et al. 2001; McCarthy et al. 2002a, hereafter MBB02). These discrepancies between theory and observations have motivated a number of authors to examine the potential role of "additional" gas physics. For example, the heating of the ICM by galactic winds and/or quasar outflows has been investigated by Kaiser (1991) and also by a whole host of subsequent authors (e.g., Evrard & Henry 1991; Bower 1997; Balogh et al. 1999; Wu et al. 2000; Loewenstein 2000; Tozzi & Norman 2001; Borgani et al. 2001; Babul et al. 2002, hereafter BBLP02; MBB02; Nath & Roychowdhury 2002; Lloyd-Davies et al. 2002). Recently, the effects of radiative cooling on X-ray scaling relations have also been explored (e.g., Bryan 2000; Voit & Bryan 2001; Wu & Xue 2002; Thomas et al. 2002; Voit et al. 2002; Davé et al. 2002). These studies find that both heating and cooling can act in a similar manner, by raising the mean entropy of the intracluster gas and, in some cases, establishing a core in the entropy profile. This, in turn, modifies the X-ray scaling relations of

clusters and ameliorates, or possibly eliminates, the discrepancies between theory and observations. It also potentially explains the emerging observational evidence for an "entropy floor" in nearby groups and low mass clusters (Ponman et al. 1999; Lloyd-Davies et al. 2000).

Thus far, X-ray observations alone have provided evidence for the entropy floor and it has come almost entirely from low redshift ($z \lesssim 0.2$) groups/clusters. Observations of higher redshift clusters are hindered by cosmological dimming [the bolometric X-ray surface brightness of a cluster scales as $(1+z)^{-4}$]. An additional, *independent* probe which could be used to confirm the presence of this excess entropy in low/intermediate redshift clusters and also provide new tests for their high redshift counterparts would be quite useful. Here, we show that scaling relations based on the thermal Sunyaev-Zeldovich effect (Sunyaev & Zeldovich 1972; 1980) - hereafter referred to as the "SZ effect" - can provide such a probe.

The SZ effect is a fractional change in the temperature/intensity of the cosmic microwave background (CMB) caused by the inverse-Compton scattering of CMB photons off high energy electrons in the ICM. On average, the photons gain a small amount of this energy from the scatterings and this results in a slight spectral distortion of the CMB towards clusters. At frequencies of $\nu \lesssim 218$ GHz, the SZ effect appears as a decrement in the temperature of the CMB, while at higher frequencies it appears as an increment. The magnitude of the SZ effect is determined by the integrated gas pressure along the line-of-sight through the cluster. Since heating/cooling modifies the entropy of the gas, it should be expected that the gas pressure and, thus, the SZ effect will also be modified by these processes. Therefore, it can be expected that SZ effect scaling relations will tell us something about the entropy history of the gas. Unlike the X-ray surface brightness of a cluster, the SZ effect is not subject to cosmological dimming and can be used to study the effects of excess entropy in the ICM out to arbitrarily high redshift. This makes scaling relations based on the SZ effect particularly interesting and attractive tests.

Traditionally, detecting and mapping the SZ effect has been quite difficult.

This is because the effect is very weak, with typical beam-averaged decrements in the CMB temperature of only a few hundred μK (see Birkinshaw 1999 for a recent compilation). Recently, however, extraordinary leaps in detector technology and new observing strategies have allowed observers to make reliable and routine pointed observations of the effect (for recent data see, e.g., Grego et al. 2001; Grainge et al. 2002a; Reese et al. 2002). With this advance, we feel a detailed study of SZ effect scaling relations and what new insights they can give us on the thermal and spatial characteristics of the ICM, especially in high redshift clusters, is timely.

In this paper, we construct SZ effect scaling relations for massive clusters both with and without excess entropy and focus on how these correlations are modified by the presence of an entropy floor. Along the way, we also discuss the potential for both current and future observations to measure these relations and constrain the entropy floor level. Constraining the entropy floor level out to high redshift could possibly yield information about the source(s) of the excess entropy, whether it be "preheating" by quasar outflows, radiative cooling, or some other non-gravitational process. In a companion paper (McCarthy et al. 2003b), we compare the scaling relations derived here to high redshift SZ effect data from the literature.

To date, only a few other theoretical studies have investigated the role of excess entropy on the SZ effect. White et al. (2002), Springel et al. (2001), da Silva et al. (2001), Cavaliere & Menci (2001), and Holder & Carlstrom (2001) have all looked at how *universal* SZ effect properties, such as the SZ effect angular power spectrum, SZ effect cluster source counts, and/or the mean universal Compton parameter, are modified by an entropy floor. However, measurements of most of these quantities are not feasible with current instrumentation and, therefore, estimates of the entropy floor level of clusters via observations of universal SZ effect quantities will have to wait until the next generation of instruments [e.g., the Sunyaev-Zeldovich Array (*SZA*), the Arcminute MicroKelvin Imager (*AMI*), and the Array for Microwave Background Anisotropy (*AMiBA*)] come online. In

a spirit similar to that of the present study, however, Holder & Carlstrom (2001) and Cavaliere & Menci (2001) have also examined a few SZ effect scaling relations for *individual* clusters. We briefly compare our findings to the results of these two studies in §3.5.

The present paper is outlined as follows: in §3.2, we briefly describe the analytic cluster models developed in BBLP02 and employed here; in §3.3, we discuss in a general sense how and why entropy injection is expected to influence the SZ effect and how this can be explored with current and future observations through comparisons with predicted scaling relations. In §3.4, we derive theoretical scaling relations based on SZ effect observables and quantify how excess entropy modifies these relations. We start by examining scaling relations consisting only of SZ effect observables. These relations are most interesting because they potentially offer a completely (X-ray-)independent way of probing the intracluster gas. Next, we explore scaling relations between the various SZ effect observables and a cluster's mass. These relations, too, can potentially be measured independent of X-ray observations, since clusters can be weighed via gravitational lensing or galaxy velocity dispersion measurements. Finally, we construct and analyse scaling relations between the various SZ effect and X-ray observables (i.e., X-ray luminosity and emission-weighted temperature). In §3.5, we discuss and summarize our findings.

The models we consider below were developed in a flat Λ-CDM cosmology with $h = 0.75$, $\Omega_m = 0.3$, and $\Omega_b = 0.020h^{-2}$ (Burles et al. 2001). They are computed for a number of different entropy floor levels spanning the range $K_0 \approx 100 - 430$ keV cm^2. This is approximately the range found to match the observed $L_X - T_X$ relations of both groups and hot clusters (e.g., Ponman et al. 1999; Lloyd-Davies et al. 2000; Tozzi & Norman 2001; BBLP02; MBB02). We work in physical units throughout the paper (e.g., $M_\odot$ rather than $h^{-1}M_\odot$).

3.2 Galaxy Cluster Models

Since an in-depth discussion of the cluster models can be found in BBLP02, we present only a brief description of the models here. We note that the model clusters derived here represent high mass ($M_{tot} \gtrsim 3 \times 10^{14}$ $M_{\odot}$), high temperature ($T_X \gtrsim 3$ keV) clusters only. Such a range reflects all of the clusters observed to date through the SZ effect and is approximately the range expected to be probed by upcoming interferometric surveys (e.g., Holder et al. 2000).

3.2.1 The Self-Similar Model

To mimic the standard self-similar result deduced from numerical simulations, we implement the "isothermal" model of BBLP02. In this model, the ICM is assumed to be isothermal and is in hydrostatic equilibrium with the dark halo potential. The distribution of the dark matter in these clusters is assumed to be the same as found in recent high resolution numerical simulations (Moore et al. 1998; Lewis et al. 2000). This model will serve as our "baseline" model for assessing how an entropy floor modifies the SZ effect. The isothermal model has been tested extensively (BBLP02; MBB02) to make sure it provides a good match to the results of genuine self-similar numerical simulations, such as those done by Evrard et al. (1996).

3.2.2 The Entropy Floor Models

To test the effects of an entropy floor on the SZ effect, we make use of the entropy injection (preheated) models of BBLP02. The models can be summarized as follows: the dominant dark matter component, which is unaffected by the energy injection, collapses and virializes to form bound halos. The distribution of the dark matter in such halos is assumed to be the same as for the self-similar clusters described above. While the dark component is unaffected by energy injection, the collapse of the baryonic component is hindered by the pressure forces induced by

entropy injection. If the maximum infall velocity due purely to gravity of the dark halo is subsonic, the flow will be strongly affected by the pressure and it will not undergo accretion shocks. It is assumed that the baryons will accumulate onto the halos *isentropically* at the adiabatic Bondi accretion rate (as described in Balogh et al. 1999). This treatment, however, is only appropriate for low mass halos. If the gravity of the dark halos is strong enough (as it is expected to be in the hot clusters being considered here) that the maximum infall velocity is transonic or supersonic, the gas will experience an additional (generally dominant) entropy increase due to accretion shocks. In order to trace the shock history of the gas, a detailed knowledge of the merger history of the cluster/group is required but is not considered by BBLP02. Instead, it is assumed that at some earlier time the most massive cluster progenitor will have had a mass low enough such that shocks were negligible in its formation, similar to the low mass halos discussed above. This progenitor forms an isentropic gas core of radius r_c at the cluster center. The entropy of gas outside of the core, however, will be affected by shocks. Recent high resolution numerical simulations suggest that the "entropy" profile for gas outside this core can be adequately represented by a simple analytic expression given by $\ln K(r) = \ln K_0 + \alpha \ln (r/r_c)$ (Lewis et al. 2000), where $K \equiv kT_e n_e^{-2/3}$. For the massive, hot clusters ($T_X \gtrsim 3$ keV) of interest here, $\alpha \sim 1.1$ (Tozzi & Norman 2001; BBLP02).

Following this prescription and specifying the parameters r_c, $\rho_{gas}(r_c)$, and α (as discussed in BBLP02) completely determines the models. Under all conditions, the gas is assumed to be in hydrostatic equilibrium within the dark halo potential. The complicated effects of radiative cooling are neglected by these models.

3.3 Entropy Injection and the SZ Effect

The amplitude of the SZ effect is directly proportional to the "Compton parameter" (y) which is given by

$$y(\theta) = \frac{\sigma_T}{m_e c^2} \int P_e(\vec{r}) dl \tag{3.1}$$

where θ is the projected position from the cluster center, σ_T is the Thomson cross-section, and $P_e(\vec{r}) \equiv n_e(\vec{r}) k T_e(\vec{r})$ is the electron pressure of the ICM at the 3-dimensional position $\vec{r}$. The integral is performed over the line-of-sight (l) through the cluster.

All of the physics of the SZ effect is contained within the Compton parameter. It is the SZ effect analog of the X-ray surface brightness of a cluster and is a measure of the average fractional energy gain of a photon due to inverse-Compton scattering while passing through a cloud of gas (in this case, the ICM) with an electron pressure profile of $P_e(\vec{r})$. As discussed by BBLP02 and MBB02, the presence of excess entropy will modify both a cluster's density and temperature profiles. In the case where it is preheating that gives rise to an entropy core, as in the present study, the temperature of the gas near the center of the cluster is increased and, therefore, so is the global emission-weighted temperature of the cluster (e.g., Fig. 1 of MBB02). At the same time, the density of the gas at the cluster center is dramatically reduced (e.g., Fig. 2 of MBB02). It turns out that, relatively speaking, preheating has a stronger influence on the density than it does on the temperature, at least at the centers of massive clusters. The result is that the gas pressure in central regions of a cluster is reduced by preheating and, consequently, so is the cluster's Compton parameter. To demonstrate this, we plot cluster pressure profiles ($z = 0.2$) for several values of the entropy floor in Figure 3.1 (R_{halo} is the radius of the cluster). The addition of an entropy floor leads to a decrease in the gas pressure near the cluster core. The gas pressure in the outer regions of the clusters, however, remains relatively unchanged as the entropy increase due to gravitational shock heating dominates the non-gravitational entropy injection. Also of note is that the *relative* difference between the various models is greatest for the lower mass cluster. This is expected since the lower mass cluster has a

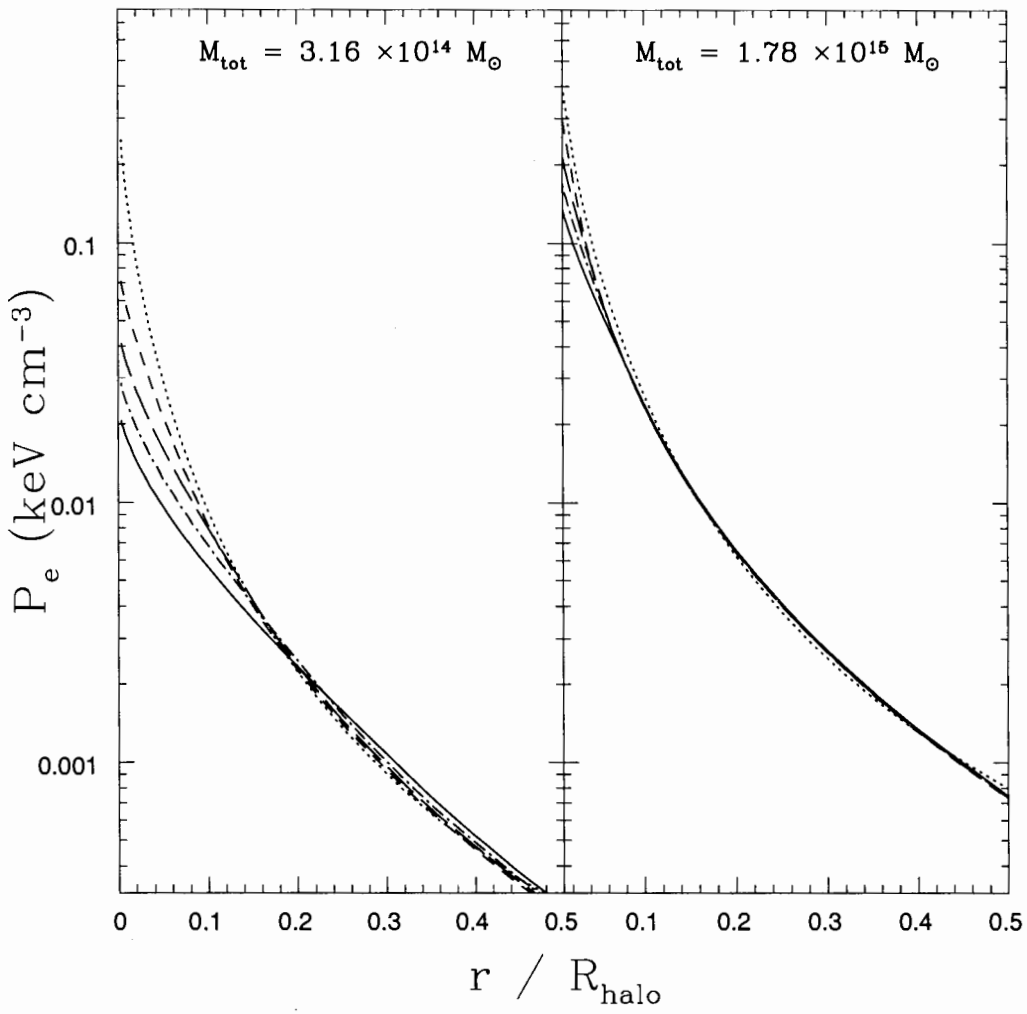

Figure 3.1: Effects of an entropy floor on cluster pressure profiles. *Left:* Cluster with total mass $M_{tot} = 3.16 \times 10^{14} M_{\odot}$. *Right:* Cluster with total mass $M_{tot} = 1.78 \times 10^{15} M_{\odot}$. The dotted line is the standard self-similar result. The short-dashed, long-dashed, dot-dashed, and solid lines represent the models of BBLP02 with entropy floor constants of $K_0 = 100$, 200, 300, and 427 keV cm^2, respectively.

shallower potential well and, thus, is more strongly influenced by the presence of an entropy floor.

With an entropy floor significantly affecting the pressure of the ICM near the center of a cluster, the Compton parameter will be most strongly modified if it is

evaluated within the smallest possible projected radius [i.e., the *central* Compton parameter, $y(\theta = 0) \equiv y_0$]. Integrating (or averaging) the Compton parameter within larger projected radii (for example, R_{halo}, the radius of the cluster), on the other hand, will diminish (though not completely remove) the effects of entropy injection. Which of these quantities, the central or integrated Compton parameters, will be the most useful for constructing scaling relations that are sensitive to the value of K_0 will depend upon which other cluster observables are used in the relations. For example, in §3.4.3, we show that a comparison of y_0 with T_X provides a more sensitive test of entropy injection than a comparison of the integrated Compton parameter with T_X. On the other hand, a scaling relation between the integrated Compton parameter and L_X is more sensitive to the entropy floor level than is a scaling relation between y_0 and L_X. Ultimately, one would like to directly image the entire cluster out to the virial radius with high angular resolution and directly compare theoretical models to the images over the entire cluster profile.

The observability of these quantities will obviously depend on the details of the instrument and observing strategy. Generically, observations of the SZ effect filter large-scale emission while finite resolution smears out small-scale structures. Fitting to a model (such as the isothermal β model; Cavaliere & Fusco-Femiano 1976; 1978) provides a method for effectively deconvolving these effects and estimating the central and integrated Compton parameters, but it is important to keep in mind that such quantities are inferred and model-dependent. Provided the smallest angular scale resolved is comparable to the typical scale over which the cluster varies, the inferred y_0 will be reliable, while inferred integrated Compton parameters will not be reliable when extrapolated beyond the filtering scale of the observations. For current interferometric observations [such as those obtained with the Berkeley Illinois Maryland Association (*BIMA*) and Owens Valley Radio Observatory (*OVRO*) arrays and the Ryle telescope], the highest angular resolution for SZ measurements is typically smaller than the core radius of most clusters observed to date ($\sim 30''$) while the typical large-scale filtering becomes important on

scales larger than about 2'. Therefore, it can be expected that the inferred values of y_0 should be reasonably accurate while any integrated Compton parameter/flux density reported on scales larger than 2' will be suspect.

In recognition of the above, we construct scaling relations between central Compton parameter, the integrated Compton parameter within the central 1' (which is a conservative choice for the filtering scale of current interferometers), and various X-ray observables. However, we also explore relations involving the integrated Compton parameter within R_{halo}, as future experiments, such as *SZA*, will probe angular scales larger than that of current experiments.

3.4 SZ Effect and SZ Effect-X-ray Scaling Relations

3.4.1 100% SZ Effect: The $S_\nu - y_0$ Relation

We start our discussion of SZ effect scaling relations by first examining relations between SZ effect quantities only (i.e., the central and integrated Compton parameters). In principle, these relations are completely independent of X-ray results, in that the latter depend on the combination of $n_e^2\epsilon(T_e)$ [where $\epsilon(T_e)$ is the X-ray emissivity] whereas the SZ effect depends on n_eT_e. For this reason, scaling relations which depend only on SZ effect quantities have the potential of providing new insights into both the thermal and spatial properties of the ICM. As such, we will invest a little bit more effort discussing and expanding on the nature of these relations than the SZ effect-X-ray relations discussed later in §3.4.2-3.4.5.

First, because the SZ effect flux density of a cluster is most commonly reported in observational studies and not the integrated Compton parameter, we convert the integrated Compton parameter (symbolized as y_{int}), which is given by

$$y_{int}(\leq \theta) = 2\pi \int_0^{\theta} y(\theta')\theta' d\theta' \tag{3.2}$$

into flux density (S_ν) via

$$S_\nu = j_\nu(x) y_{int} \tag{3.3}$$

where $j_\nu(x)$ describes the shape of the SZ effect spectrum and is a function of the dimensionless frequency $x = h\nu/kT_{CMB}$. The mean temperature of the present-day cosmic microwave background, T_{CMB}, is 2.728 K (Fixsen et al. 1996) and $j_\nu(x) = 2(kT_{CMB})^3(hc)^{-2} f_\nu(x)$, with

$$f_\nu(x) = \frac{x^4 e^x}{(e^x - 1)^2}\left(\frac{x}{\tanh(x/2)} - 4\right) \tag{3.4}$$

where $f_\nu \approx -2x^2$ at long wavelengths (the Rayleigh-Jeans limit).

Since our aim here is to achieve a *physical* understanding of the relationship between S_ν and y_0, we remove the frequency dependence of the integrated SZ effect flux density by dividing it by the quantity f_ν given in (4). Then a comparison of the quantity S_ν/f_ν with genuine observations at any observing frequency ν can be made simply by multiplying by the conversion factor f_ν. For reasons discussed in §3.3, we investigate the frequency-independent SZ effect flux density within a fixed angular radius of 1 arcminute (which we symbolize as $S_{\nu,arc}/f_\nu$) and within R_{halo}, the radius of the cluster (which we symbolize as $S_{\nu,halo}/f_\nu$).

In Figure 3.2, we plot scaling relations between the (frequency-independent) SZ effect flux densities and the central Compton parameter. The dotted lines are the self-similar results. The short-dashed, long-dashed, dot-dashed, and solid lines represent the results of the models of BBLP02 with entropy floor constants of K_0 = 100, 200, 300, and 430 keV cm^2, respectively. The top panel is for the SZ effect flux density within central one arcminute, while the bottom panel is the total SZ

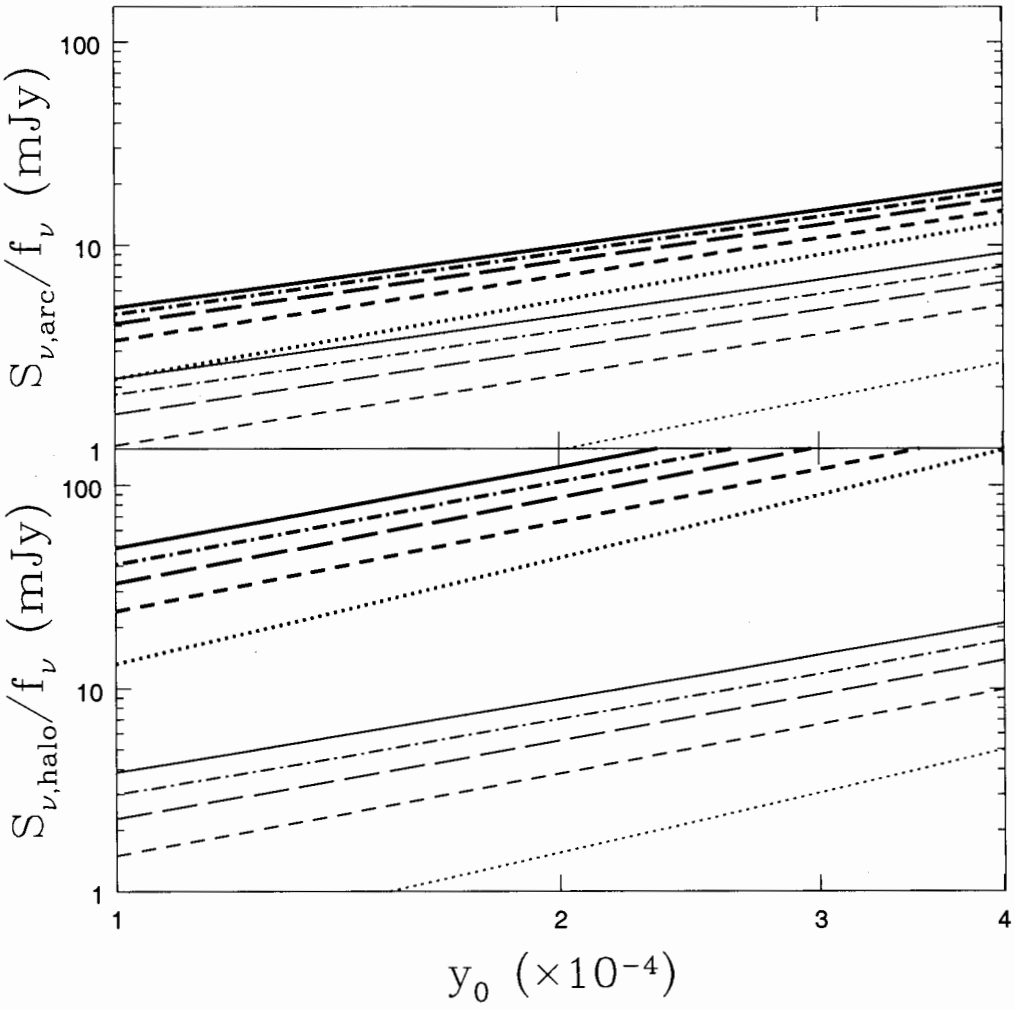

Figure 3.2: Comparison of the $S_\nu/f_\nu - y_0$ relations. The short-dashed, long-dashed, dot-dashed, and solid lines represent the models of BBLP02 with entropy floor levels K_0 = 100, 200, 300, and 427 keV cm^2, respectively. The dotted lines are the isothermal self-similar result. The thick lines are for $z = 0.2$ and the thin lines are for $z = 1.0$. The top panel is for the SZ effect flux density within the central one arcminute and the bottom panel is for the total SZ effect flux density of the cluster.

effect flux density of the cluster (out to R_{halo}). The thick lines are for $z = 0.2$ and the thin lines are for $z = 1.0$.

We start by considering the dependence of $S_{\nu,arc}/f_\nu - y_0$ on K_0 and z in the

top panel of Figure 3.2. First, as discussed in §3.3, entropy injection leads to a decrease in the gas pressure near the cluster core (Fig. 3.1). This, in turn, reduces the magnitude of both $S_{\nu,arc}/f_\nu$ and y_0. However, the relative reduction in both of these quantities is not equal. $S_{\nu,arc}/f_\nu$ is derived within larger physical radii than y_0 and, therefore, is less affected by the entropy floor. The result is an increase in the normalization of the $S_{\nu,arc}/f_\nu - y_0$ relation as the value of K_0 is increased. For example, at $z = 0.2$, a cluster with a fixed value $\log y_0 \approx -3.7$ ($\Delta T_0 \approx$ -1060 μK at 30 GHz) will have an integrated decrement of $S_{\nu,arc}/f_\nu \approx 5.5$ mJy ($S_\nu \approx -11$ mJy at 30 GHz) if no entropy floor is present but will have $S_{\nu,arc}/f_\nu \approx 10$ mJy ($S_\nu \approx -20$ mJy at 30 GHz) if $K_0 \approx 430$ keV cm^2. Furthermore, this trend is amplified at higher redshifts since the SZ effect flux density within a fixed angular size probes larger physical regions at higher redshifts (and, therefore, is less affected by the entropy floor). Compare the difference between the models for the $z = 0.2$ lines and the $z = 1.0$, for example.

The slope of $S_{\nu,arc}/f_\nu - y_0$ relation is also modified by the presence of an entropy floor. For example[1], at $z = 0.2$ and 1.0 (respectively), the self-similar model approximately predicts

$$S_{\nu,arc}/f_\nu \propto y_0^{1.3,\ 1.4} \tag{3.5}$$

while the $K_0 = 300$ keV cm^2 model approximately predicts

$$S_{\nu,arc}/f_\nu \propto y_0^{1.0,\ 1.1} \tag{3.6}$$

A more precise analytic expression for the $S_{\nu,arc}/f_\nu - y_0$ relation at any $z \lesssim 1$ and any entropy floor in the range $K_0 \approx 100 - 700$ keV cm^2 is presented in Table 3.1.

[1]Throughout the paper we often compare scaling relations at $z = 0.2$ and 1.0 for the self-similar and $K_0 = 300$ keV cm^2 models. The choice in redshift is motivated by the fact that most interferometric observations are of clusters with $0.2 \lesssim z \lesssim 1.0$, while the choice in entropy floor level is motivated by X-ray observations which require $K_0 \gtrsim 300$ keV cm^2 for massive clusters.

At a fixed redshift, the presence of an entropy floor flattens the relationship between $S_{\nu,arc}/f_\nu$ and y_0 because clusters with small values of y_0 (i.e., low mass clusters) are more strongly influenced (relatively speaking) by entropy injection than clusters with large values of y_0.

It is worth noting that, for the most part, the $S_{\nu,arc} - y_0$ relations (and, in fact, virtually every relation discussed in the paper) exhibit almost perfect power-law behavior. This may seem rather surprising in light of the fact that most X-ray scaling relations show some kind of a break from power-law trends (see BBLP02, for example). We note, however, that the break in the $L_X - T_X$ relation, for example, occurs at the transition between groups and clusters (roughly $T_X \lesssim 1$ keV). This is below the range of temperatures (and central Compton parameters) studied in the present paper. We verify that a break does occur for low mass systems (i.e., for systems with $y_0 \lesssim 10^{-5}$) but, because such low mass systems have very weak integrated SZ effect signals, there is little hope of observing this feature in the near future.

In the bottom panel of Figure 3.2, we plot the $S_{\nu,halo}/f_\nu - y_0$ relations. With the quantity $S_{\nu,halo}/f_\nu$ only slightly affected by the presence of an entropy floor (and, therefore, the relative difference in the normalizations of the models are at a maximum), these relations are more sensitive to entropy injection than those plotted in the top panel of Figure 3.2. For example, for a $z = 0.2$ cluster with a fixed value of $\log y_0 \approx -3.7$, the $K_0 = 430$ keV cm^2 models predicts a flux density that is roughly three times larger than that predicted by the self-similar model (as opposed to being only about two times larger for the relation presented in the top panel).

The steepness of the relation is also altered by an entropy floor. Using simple scaling arguments, one can easily arrive at the predicted self-similar result. Combining $S_{\nu,halo}/f_\nu \propto T_X R^3$ and $y_0 \propto T_X R$ with $R \propto T_X^{0.5}$ (which is just the virial theorem) yields

Table 3.1: Parameters for SZ scaling relations: $Y = A(1+z)^{\gamma} K_2^{\alpha} X^{\beta}$

Relation: Y - X		parameters
$S_{\nu,arc}/f_\nu - y_0$		
	A	5.807×10^4
	γ	$-0.244 - 4.812 \log K_2 + 1.787(\log K_2)^2$
	α	$0.148 + 0.620z - 0.007z^2$
	β	$1.016 - 0.017 \log K_2 + 0.150z - 0.186z \log K_2$
$S_{\nu,halo}/f_\nu - y_0$		
	A	7.893×10^7
	γ	$-7.486 - 140.076 \log K_2 - 0.689(\log K_2)^2$
	α	$0.527 + 52.220z - 10.589z^2$
	β	$1.478 - 0.269 \log K_2 - 0.058z - 0.026z \log K_2$
$y_0 - M(r_{500})$		
	A	3.568×10^{-21}
	γ	$-1.956 - 88.996 \log K_2 - 7.675(\log K_2)^2$
	α	$-3.397 + 35.984z - 8.293z^2$
	β	$1.130 + 0.243 \log K_2 + 0.041z + 0.032z \log K_2$
$y_0 - T_X$		
	A	5.668×10^{-6}
	γ	$0.188 + 1.287 \log K_2 - 0.558(\log K_2)^2$
	α	$-0.734 - 0.451z + 0.089z^2$
	β	$1.880 + 0.287 \log K_2 + 0.070z - 0.003z \log K_2$
$y_0 - L_X$		
	A	6.659×10^{-41}
	γ	$1.504 + 24.922 \log K_2 + 4.478(\log K_2)^2$
	α	$0.887 - 11.117z + 3.057z^2$
	β	$0.805 - 0.022 \log K_2 - 0.005z - 0.010z \log K_2$

$K_2 \equiv K_0/100$ keV cm^2.

Note. — The relations are accurate to better than the $\approx 5\%$ level over the ranges $0.1 \lesssim z \lesssim 1$ and 100 keV cm^2 $\lesssim K_0 \lesssim$ 700 keV cm^2.

$$S_{\nu,halo}/f_\nu \propto y_0^{5/3}, \tag{3.7}$$

in excellent agreement with the predictions of the BBLP02 isothermal model. However, injection of entropy flattens the relation and at $z = 0.2$ and 1.0, the $K_0 = 300$ keV cm^2 model approximately predicts

$$S_{\nu,halo}/f_\nu \propto y_0^{1.3,\ 1.2} \tag{3.8}$$

An analytic expression for the $S_{\nu,halo}/f_\nu - y_0$ relation at any $z \lesssim 1$ and any entropy floor between 100 keV cm^2 $\lesssim K_0 \lesssim$ 700 keV cm^2 is given in Table 3.1.

Since the $S_{\nu,halo}/f_\nu - y_0$ relation is more sensitive to entropy injection (relatively speaking) than the $S_{\nu,arc}/f_\nu - y_0$ relation, this means that observations obtained with future experiments, such as the *SZA*, *AMiBA*, and *AMI* (which will probe larger angular scales than that of current interferometers), will (at least in theory) have the best chance of placing tight constraints on the non-gravitational entropy of high redshift clusters.

We note that most of the dependence of the relations plotted in Figure 3.2 (both the top and bottom panels) on the entropy floor level, K_0, is due to the central Compton parameter, y_0. A completely resolved central decrement formally requires infinite resolution and there is little to be gained by increasing the resolution beyond the smallest scale on which the cluster structure varies. For diffuse emission, higher resolution normally means less signal per resolution element, so pushing to very high resolution will not lead to much new information. Alternatively, the central Compton parameter can be estimated by fitting a model (e.g., the isothermal β model) to the the observed SZ effect surface brightness and extrapolating it to the cluster center (as discussed briefly in §3.3). This method is widely used to estimate y_0 (e.g., Carlstrom et al. 1996; Holzapfel et al. 1997; Grego et al. 2000; 2001; Reese et al. 2000; 2002; Pointecouteau et al. 2001; 2002; Jones et al. 2005; Grainge et al. 2002a). While the *statistical* measurement error on y_0 for current data is typically only of order 100 μK (which is relatively small compared to the differences between the models plotted in Figure 3.2, assuming S_ν/f_ν is known), it has yet to be demonstrated that the *systematic* error (due to assuming an incorrect surface brightness model) for current data is negligible. If the models employed in the extrapolation provide poor descriptions of the surface brightness profiles, then one would expect the results to vary as a function of instrument characteristics (e.g., resolution, field of view). However, a comparison of the results of various studies (which made use of different instruments; e.g., *Ryle*

telescope, *BIMA/OVRO*, and *SuZIE*) of the same clusters reveals that the agreement is quite good, often within one sigma statistical uncertainty (see Holzapfel et al. 1997, Reese et al. 2002, and Jones et al. 2005, for example). Thus, the extrapolation procedure seems to be a viable way estimating the central Compton parameter at current sensitivity. By modeling "mock" (future) *SZA* observations, we also demonstrated that this extrapolation procedure is an accurate way of estimating the true underlying values of y_0 and S_ν of the BBLP02 cluster models (see McCarthy et al. 2003b).

Finally, we point out that part of the motivation for our study of the $S_\nu - y_0$ relations (and the other scaling relations involving these quantities) comes from the fact that observational studies often use either S_ν or y_0 to characterize a cluster's SZ effect but not usually both. For example, integrated SZ effect flux densities are often associated with large-beam single-dish experiments, while estimates of the central Compton parameter normally come from high resolution interferometric observations. However, if one is able to determine $y(\theta)$ (i.e., the SZ effect "surface brightness" profile) from a single dataset then, strictly speaking, it isn't necessary to use scaling relations to probe the entropy of the ICM. For example, the SZ effect surface brightness profile could be used together with the X-ray surface brightness profile (if it is known) to determine the true 3-dimensional entropy distribution of the gas (with some assumptions about the geometry of the cluster). The disadvantages of this method are: (1) it requires X-ray observations, and (2) it probably cannot be used for the most distant clusters, since the X-ray signal-to-noise ratio falls sharply with increasing z. Alternatively, the entropy distribution could be constrained by comparing the observed SZ effect surface brightness profile with theoretically predicted profiles. This is similar to using scaling relations, since the entropy distribution is being inferred and not measured, but with the important difference that all of the available SZ effect information, $y(\theta)$, is being used in the comparison. We are in the process of exploring these methods and they will be addressed in detail in a subsequent paper. For now, we stick with the

scaling relations derived above, which are more readily comparable with available observations.

3.4.2 The $y_0 - M(r_{500})$ relation

In Figure 3.3, we present scaling relations between y_0 and the total cluster dark matter mass within the radius r_{500} [i.e., $M(r_{500})$]. This is the radius within which the mean dark matter mass density is 500 times the critical density at $z = 0$. The lines hold the same meaning as in Figure 3.2. For clarity, we plot the $z = 0.2$ predictions in the left-hand panel and the $z = 1.0$ predicts in the right-hand panel.

It is apparent that entropy injection has a substantial effect on the $y_0 - M(r_{500})$ relation. Both the normalization and the steepness of the relation are modified. First, the normalizations imply that, for a cluster of given mass at a given redshift, entropy injection tends to diminish the strength of y_0. For example, at $z = 0.2$, a cluster with $M(r_{500}) \approx 9 \times 10^{14} M_{\odot}$ will have $y_0 \approx 4 \times 10^{-4}$ in the absence of an entropy floor, but the central Compton parameter is only half this value for an entropy floor of $K_0 \approx 430$ keV cm^2. This corresponds to a difference of nearly $1060 \mu K$ at 30 GHz (which is large compared to the typical *BIMA/OVRO* statistical measurement error of $100 - 200 \mu K$; Reese et al. 2000; 2002). Of course, there will also be a measurement error associated with the cluster mass. Typically, X-ray-determined masses have associated statistical uncertainties of about 20% (Nevalainen et al. 2000; Finoguenov et al. 2001). Therefore, based on Figure 3.3, it should be possible to constrain K_0 to within about ± 100 keV cm^2 with current data.

Physically, the diminution in the normalization $y_0 - M(r_{500})$ relation can be understood since entropy injection greatly reduces the pressure of the cluster gas near the core (and therefore y_0; see Figure 3.1) but does not affect its dark matter mass. It is also worth noting that the normalizations of the individual models are a function of redshift. For example, the $K_0 = 100$ keV cm^2 at $z = 0.2$ predicts a relation somewhat similar to that of the $K_0 = 200$ keV cm^2 at $z = 0.5$ or

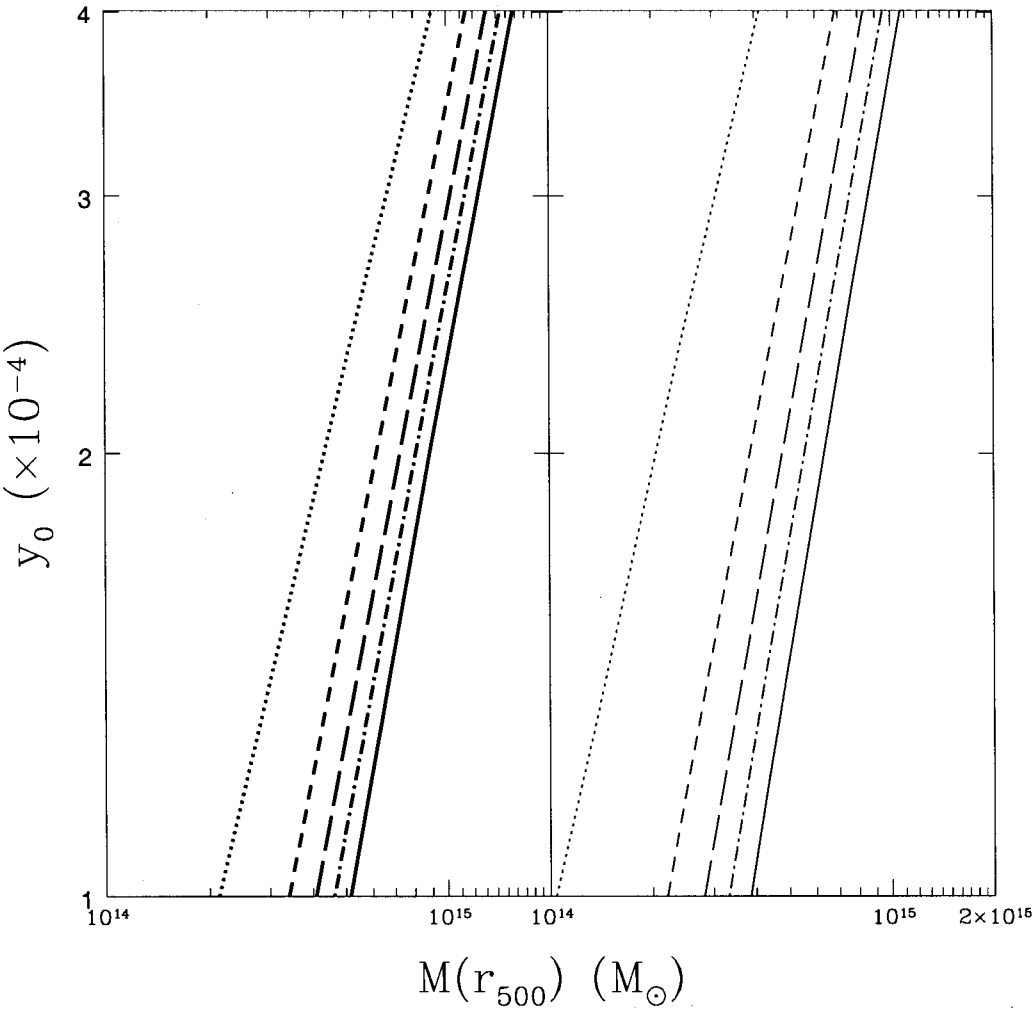

Figure 3.3: Comparison of the $y_0 - M(r_{500})$ relations. The lines hold the same meanings as in Fig. 3.2. The left-hand panel is for $z = 0.2$ and the right-hand panel is for $z = 1.0$.

the $K_0 = 430$ keV cm^2 at $z = 1.0$. So, it is extremely important to consider the evolution of galaxy clusters when comparisons are made to observational data (i.e., information about the redshift of the clusters is required in order to constrain the level of the entropy floor).

Another interesting point is that the difference between the normalizations of the models becomes greater at higher redshift. For example, the difference between

y_0 for the isothermal and $K_0 = 100$ keV cm^2 models of a $M(r_{500}) \approx 5.6 \times 10^{14} M_\odot$ cluster at $z = 1.0$ is about 3.7 times larger than at $z = 0.2$. This is a result of the fact that the physical size of the isentropic core (r_c; discussed in §3.2) is a larger fraction of the cluster virial radius at higher redshifts. This trend of increasing r_c/R_{halo} with redshift can be understood as follows. In BBLP02, it was pointed out that there is a critical mass threshold which determines the importance of gravitational shock heating. For clusters with masses above this threshold, shock heating significantly increases the entropy of the intracluster gas and it begins to dominate the injected non-gravitational entropy (except for in the very central regions of the clusters). For clusters with masses below this threshold, shock heating is unimportant. The critical mass also sets size of the isentropic core, r_c. Incorporating the results of recent high resolution hydrodynamic simulations (Lewis et al. 2000), BBLP02 defined the critical mass to be that which gives rise to a gas temperature at R_{halo} that is equal to one half of the cluster virial temperature. Using this constraint, it is relatively straightforward to show that the critical mass (for a fixed entropy floor level) increases with redshift and, therefore, so does the ratio r_c/R_{halo}. For gas in the core of the cluster (with entropy equal to K_0), $P_{core} \propto \rho_{core}^{5/3}$ and, therefore, $T_{core} \propto \rho_{core}^{2/3}$. At high redshifts, the cluster gas is denser and, in the case of an $\Omega_m = 1$ universe (assumed here for simplicity), scales as $\rho \propto (1+z)^3$. Therefore, the temperature of the gas in the core scales as $T_{core} \propto (1+z)^2$. The gas temperature at the virial radius, on the other hand, scales as $T_{halo} \propto (1+z)$. Thus, the ratio T_{core}/T_{halo} increases with redshift and in order to match the temperature constraint described above, the critical mass threshold and r_c/R_{halo} must increase with z as well.

The steepness of the $y_0 - M(r_{500})$ relation is also affected by an entropy floor. If clusters are self-similar, then $y_0 \propto T_X R$, $R \propto T_X^{0.5}$, and $M(r_{500}) \propto T_X^{1.50}$ (Evrard et al. 1996). This leads to

$$y_0 \propto M(r_{500}) \tag{3.9}$$

while at $z = 0.2$ and 1.0, the $K_0 = 300$ keV cm^2 model predicts

$$y_0 \propto M(r_{500})^{1.3,\ 1.3} \tag{3.10}$$

A more precise form the $y_0 - M(r_{500})$ relation as a function of both the entropy floor (K_0) and redshift is presented in Table 3.1 [valid for $M(r_{500}) \gtrsim 1.5 \times 10^{14} M_\odot$].

The steepening of the relation with the increase in the level of the entropy floor can also be understood in an intuitive sense. It stems from the fact that the relative decrease in the gas pressure at the cluster center is strongest for low mass clusters (which have the shallowest potential wells; see Figure 3.1).

Again, because of the increasing importance of entropy injection as one goes to low masses, a break from power-law behavior in the $y_0 - M(r_{500})$ relation occurs at the transition between groups and clusters (not shown). For entropy floors of $K_0 \gtrsim 300$ keV cm^2, the break becomes quite noticeable for systems with $M(r_{500}) \lesssim 8 \times 10^{13} M_\odot$, which is below the range of system masses that we are most interested in and far below the range of system masses that can be observed presently.

We have found that, at least theoretically, the best hope for testing galaxy clusters for the presence of excess entropy using the $y_0 - M(r_{500})$ relation is at high redshift, although our results reveal that the relation is sensitive to the entropy floor level even at low redshifts. The quantity $M(r_{500})$ is usually determined through X-ray observations (e.g., Ettori & Fabian 1999) and, hence, we have placed it in the "y_0-X-ray scaling relations" subsection. However, gravitational lensing has also been used recently to trace the mass profiles of clusters out to radii near or exceeding that of r_{500} with statistical uncertainties similar to that of X-ray-determined masses (e.g., Clowe & Schneider 2001; Gray et al. 2002; Athreya et al. 2002). So, like the $S_\nu - y_0$ relation, the $y_0 - M(r_{500})$ relation can also potentially be measured completely independent of X-ray results.

3.4.3 The $y_0 - T_X$ relation

In Figure 3.4, we present scaling relations between y_0 and the mean emission-weighted gas temperature (T_X) of a cluster. The lines hold the same meaning as in Figure 3.2. Of the scaling relations presented thus far, the $y_0 - T_X$ relation is the most sensitive to the entropy floor level. There is a two-fold effect in that entropy injection diminishes y_0 but also *increases* T_X for a cluster of mass M (see, e.g., Fig. 1 of MBB02). For example, at $z = 0.2$, a cluster that has $T_X \approx 7$ keV and no entropy floor will have a value of y_0 that is about 3.5 times larger than a cluster (also with $T_X \approx 7$ keV) that has an entropy floor of $K_0 \approx 430$ keV cm^2. At 30 GHz, this corresponds to a difference of $\approx 1300\mu K$. Current SZ effect and X-ray data can constrain the central decrement (Compton parameter) and emission-weighted temperature of massive clusters at about the 10% level (e.g., Reese et al. 2002), making the $y_0 - T_X$ relation an extremely promising test of non-gravitational entropy injection. Furthermore, the difference in the normalizations becomes progressively larger with increasing redshift.

The slopes of the predicted relations are also very sensitive to the level of entropy injection. Combining $y_0 \propto T_X R$ with $R \propto T_X^{0.5}$, yields the self-similar result

$$y_0 \propto T_X^{3/2} \tag{3.11}$$

while at $z = 0.2$ and 1.0, the $K_0 = 300$ keV cm^2 model predicts

$$y_0 \propto T_X^{2.0,\ 2.1} \tag{3.12}$$

An analytic expression for the $y_0 - L_X$ relation as a function of both the entropy floor (K_0) and redshift is presented in Table 3.1 (valid for $T_X \gtrsim 3$ keV).

Lastly, we note that a break in slope of the relations occurs at $T_X \lesssim 1$ keV, in good qualitative agreement with the position and steepness of the break found in

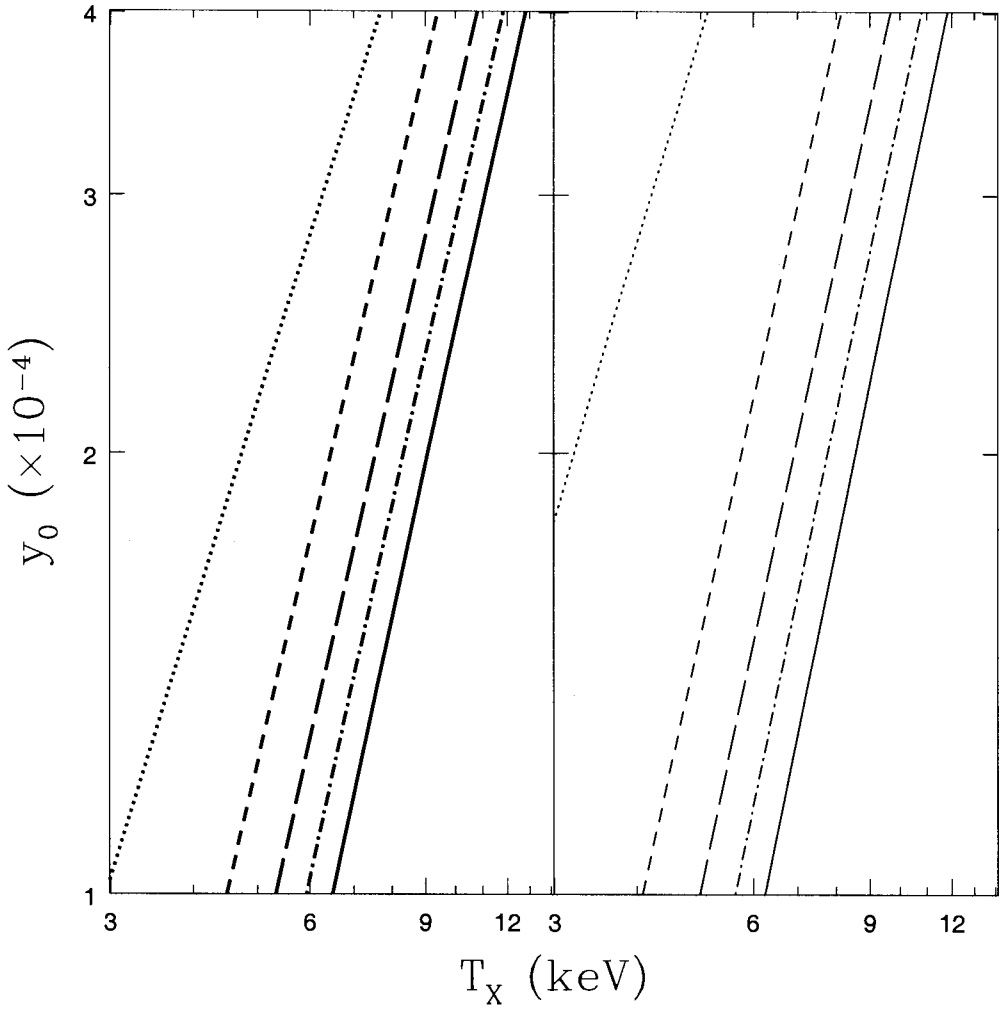

Figure 3.4: Comparison of the $y_0 - T_X$ relations. The lines hold the same meanings as in Fig. 3.2. The left-hand panel is for $z = 0.2$ while the right-hand panel is for $z = 1.0$.

the $y - T$ relation of Cavaliere & Menci (2001; see their Figure 4). Unfortunately, present SZ effect observations are essentially limited to systems with $T_X \gtrsim 5$ keV.

3.4.4 The $y_0 - L_X$ relation

In Figure 3.5, we plot scaling relations between the central y parameter and the total bolometric X-ray luminosity (L_X) of a cluster. The lines hold the same mean-

ing as in Figure 3.2. These relations are more complicated than those presented immediately above because both of the coordinates, y_0 and L_X, are affected by entropy injection. Very interestingly, however, the $y_0 - L_X$ relation is almost unchanged by the addition of an entropy floor. Both the self-similar and entropy floor models predict very similar slopes and normalizations (at all redshifts). At first sight, this may seem rather surprising. However, the predicted $y_0 - L_X$ relations can be understood as follows. The luminosity of a cluster of fixed mass is reduced by entropy injection because $L_X \propto n_e^2$ and entropy injection greatly reduces the gas density near the cluster core, where most of the X-ray emission originates. In the case of the BBLP02 entropy floor models, the result is that $L_X \propto M^{1.5}$, roughly (instead of $L_X \propto M^{4/3}$ in the self-similar case). On the other hand, we showed in §3.4.2 that an increase in the entropy floor level strongly diminishes y_0 for a cluster of fixed mass and this leads to $y_0 \propto M^{1.3}$. This implies that entropy injection gives rise to $y_0 \propto L_X^{0.8}$ (roughly), which is very close to the self-similar scaling of

$$y_0 \propto L_X^{3/4} \tag{3.13}$$

A precise analytic expression for the $y_0 - L_X$ relation as a function of both the entropy floor (K_0) and redshift is presented in Table 3.1 (valid for $L_X \gtrsim 10^{44}$ ergs s^{-1}).

Despite being insensitive to the entropy floor level, the $y_0 - L_X$ relation has at least two other potential uses. First, it could be used as a consistency check of other X-ray and SZ effect scaling relations. Second, it could allow one to deduce the X-ray luminosity of clusters in cases where only SZ effect observations are available (or vice-versa) without having to worry about the role of "additional" gas physics. The accuracy of this will be limited by the relatively large amount of intrinsic scatter present in the X-ray luminosities of clusters (see, e.g., studies of the $L_X - T_X$ relation; Markevitch 1998; Novicki et al. 2002) and by the measurement errors associated with y_0.

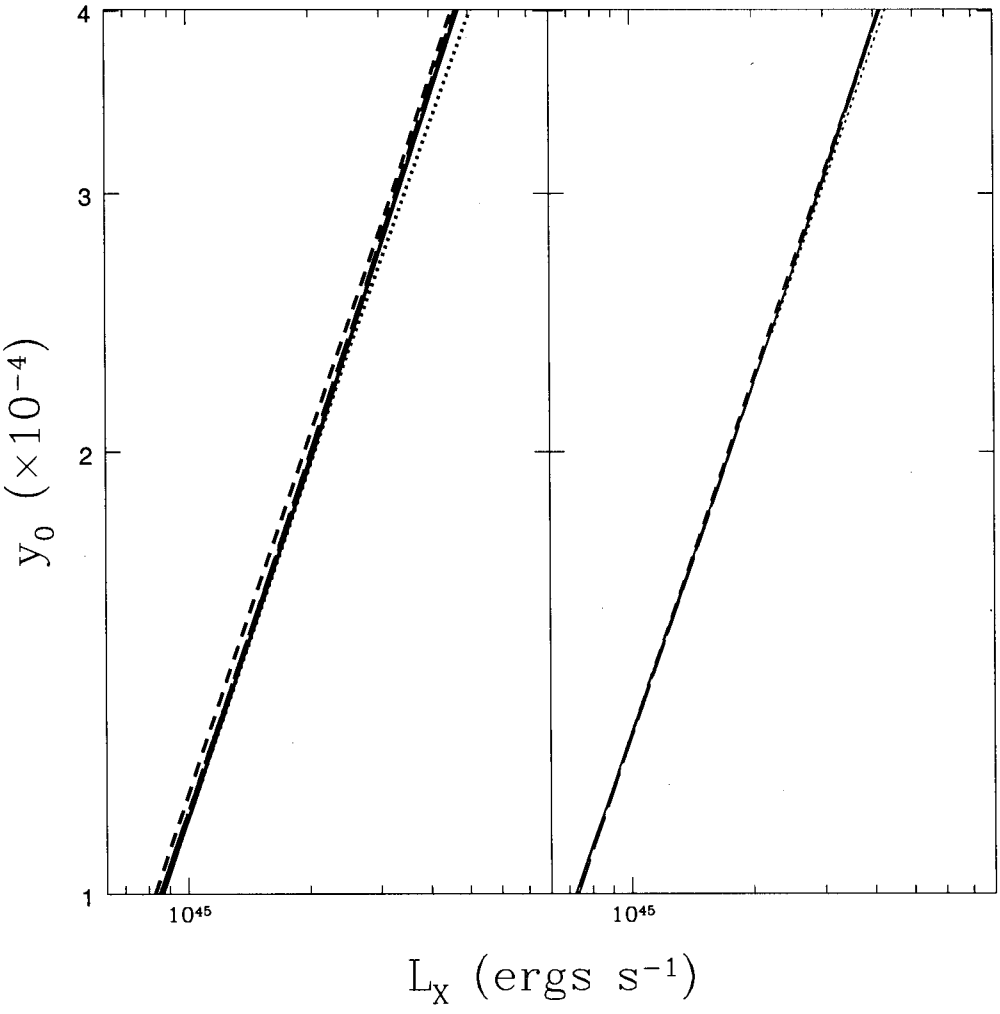

Figure 3.5: Comparison of the $y_0 - L_X$ relations. The lines hold the same meanings as in Fig. 3.2. The left-hand panel is for $z = 0.2$ while the right-hand panel is for $z = 1.0$.

3.4.5 S_ν-X-ray scaling relations

Apart for the central y parameter, we also investigated theoretical scaling relations between the frequency-independent integrated SZ effect flux density and the X-ray observables $M(r_{500})$, L_X, and T_X. Again, we evaluated S_ν/f_ν within a fixed angular radius of one arcminute and within R_{halo}. Since these relations can be reconstructed from Figures 3.2 - 3.5 or Table 3.1, we summarize the important

points here only.

For the very same reasons discussed in §3.4.2, the $S_\nu/f_\nu - M(r_{500})$ relation has its normalization decreased by entropy injection and, also, the relation becomes steeper. How large these effects will be depends upon which radius S_ν/f_ν is evaluated within. Because the dark matter mass is unaffected by entropy injection, the $S_\nu/f_\nu - M(r_{500})$ relation will *always* be most strongly modified if S_ν/f_ν is evaluated within small projected radii (where entropy injection is most prevalent). Thus, evaluating S_ν/f_ν within the central 1 arcminute provides a more sensitive test of the entropy floor than if S_ν/f_ν is measured within R_{halo}. Of course, it follows that $y_0 - M(r_{500})$ relation is the most sensitive to the entropy floor level of any and all of the SZ effect-$M(r_{500})$ relations. The $S_\nu/f_\nu - M(r_{500})$ relation, however, could offer a useful consistency check.

The $S_\nu/f_\nu - T_X$ relation also becomes steeper and has its normalization decreased with increasing values of K_0 (S_ν/f_ν is diminished while T_X is increased). The maximum (relative) difference between the various models occurs when the SZ effect flux densities are measured within small projected radii, although the increase in T_X is large enough such that the relation is sensitive to the entropy floor level even when S_ν/f_ν is measured within R_{halo}. Again, these relations offer useful consistency checks of the more entropy floor-sensitive $y_0 - T_X$ relation.

Finally, entropy injection has an interesting effect on the $S_\nu/f_\nu - L_X$ relation[2]. Both the SZ effect flux density and the luminosity are reduced as the level of entropy injected is increased, similar to the $y_0 - L_X$ relation. However, in the case of the present relation, the reduction in the luminosity is greater than the reduction in the SZ effect flux density (relatively speaking). This is because S_ν is much less sensitive than y_0 to the entropy floor level, K_0. The result is that the normalization of the $S_\nu/f_\nu - L_X$ relation is increased by entropy injection. The sensitivity of this relation to the entropy floor level depends on what radius the flux density is evaluated within. It is most sensitive when S_ν is integrated out to R_{halo}, since the relative reduction in S_ν is at a minimum. It is least sensitive when

the SZ effect is evaluated at zero projected radius (i.e., $y_0 - L_X$).

3.5 Discussion & Conclusions

Comparisons of observed and predicted cluster X-ray scaling relations has led to suggestions that important (non-gravitational) gas physics is being neglected in analytic models and numerical simulations. It has been found that the presence of a core in the entropy profiles of clusters (which may be generated through heating and/or cooling processes) can account for the deviations between observations and theory (e.g., Bower 1997; Balogh et al. 1999; Ponman et al. 1999; Wu et al. 2000; Lloyd-Davies et al. 2000; Tozzi & Norman 2001; Bialek et al. 2001; Borgani et al. 2001; Voit & Bryan 2001; BBLP02; MBB02; Voit et al. 2002; Davé et al. 2002; Lloyd-Davies et al. 2002). So far, X-ray observations have provided the only evidence for this excess entropy and it has come from low redshift ($z \lesssim 0.2$) clusters alone. Cosmological dimming is partially responsible for the lack of information on the entropy of more distant groups/clusters.

In the interest of achieving a better physical understanding of important non-gravitational processes in high redshift clusters (and how these processes affect cluster formation and evolution), we have derived a number of theoretical scaling relations based on SZ effect quantities and have analyzed how these relations are modified by the addition of an entropy floor. We find that entropy injection reduces the gas pressure in the cores of clusters and, therefore, diminishes the amplitude of both the central and integrated Compton parameters (which are directly proportional to the SZ effect). This translates to a steepening of- and a reduction in the normalization of the $y_0 - M(r_{500})$ and $S_\nu/f_\nu - M(r_{500})$ relations. Scaling relations between the Compton parameter(s) and X-ray temperature or luminosity are more complicated because both T_X and L_X are also affected by entropy injec-

[2]Note — there is an error in Figure 12 of the original BBLP02 publication. The self-similar predictions were incorrectly plotted.

tion (whereas the cluster mass M is not). Because T_X is increased by an entropy floor, the $y_0 - T_X$ and $S_\nu/f_\nu - T_X$ relations have their normalizations severely reduced by entropy injection. These relations are also considerably steeper than in the case where no entropy floor is present (i.e., the isothermal self-similar model). On the other hand, because L_X is decreased with entropy injection, the $y_0 - L_X$ relation is almost unaffected by entropy injection, while the normalization of the $S_\nu/f_\nu - L_X$ relation is increased by entropy injection. Finally, the $S_\nu/f_\nu - y_0$, a relation that can (in principle) be measured entirely through SZ effect observations, has its normalization increased by an entropy floor (the relative reduction in y_0 is much greater than in S_ν/f_ν). The relation is also slightly flattened. Analytic expressions for these relations as a function of entropy floor level and redshift can be found in Table 3.1.

We are aware of only two other studies that have examined the effects of an entropy floor on cluster SZ effect scaling relations: Holder & Carlstrom (2001) and Cavaliere & Menci (2001). Using simplified cluster models, Holder & Carlstrom (2001) illustrated the potential power of high-z SZ effect observations when it comes to studying the physics of ICM. Their Figure 1 shows the impact of an entropy floor on the central SZ effect decrement-cluster core radius relation at $0.5 \leq z \leq 2.0$. They find that the addition of an entropy floor tends to decrease the central decrement and increase the cluster core radius for clusters of a fixed total mass. This is in very good qualitative agreement with our Figure 3.3, which illustrates that the normalization of the $y_0 - M(r_{500})$ is decreased by entropy injection, and also with our Figure 3.2, which demonstrates that for clusters of a fixed y_0, the SZ effect flux density is increased by an entropy floor and, therefore, the SZ effect surface brightness becomes less centrally peaked (i.e., the core radius grows).

Cavaliere & Menci (2001), on the other hand, implemented a semi-analytic model of galaxy formation and clustering and computed a *present-day* $y - T_X$ scaling relation and analyzed how it was modified by entropy injection from stellar

winds and supernovae blasts. In qualitative agreement with the results presented in §3.4, these authors found that entropy injection tends to diminish the Compton parameter for a cluster of given mean emission-weighted temperature, T_X. However, our theoretical results are not directly comparable to those of Cavaliere & Menci (2001) since their focus was mainly on nearby ($z = 0$) groups, whereas we have investigated massive, distant clusters such as those regularly observed by the *BIMA/OVRO* arrays and the *Ryle* telescope. We also point out that the majority of clusters expected to be found in upcoming "blind" surveys will be at high redshift ($z \sim 1$; Holder et al. 2000). Finally, the Cavaliere & Menci (2001) cluster models only invoked low levels of entropy injection ($K_0 < 100$ keV cm^2) consistent with measurements of nearby groups (Ponman et al. 1999; Lloyd-Davies et al. 2000), whereas we have generally focused on higher levels of entropy injection (which are required to match X-ray observations of nearby massive clusters; Tozzi & Norman 2001; BBLP02; MBB02).

One thing we have not addressed in the present study is the effect of radiative cooling on SZ effect scaling relations. Correctly modeling the effects of radiative cooling in numerical simulations and analytic cluster models is a daunting task (see for Balogh et al. 2001 for a detailed study of the "cooling crisis"). Cooling can significantly modify not only the ICM density and temperature distributions but it can also modify the underlying dark matter distribution of clusters (see Fig. 12 of Lewis et al. 2000, for example). In addition, cooling gives rise to other "sub-grid" processes such as star formation, outflows, and supernovae explosions. These, too, will also modify the ICM's structure and appearance. While modeling this is quite difficult, we know from both optical and X-ray observations of clusters that cooling must be occurring, at least at some level, and, ultimately, must be modeled correctly in order to attain a deep physical understanding of the observed properties of clusters. Numerical simulations and analytic models which attempt to take this complicated process into account (e.g., Voit & Bryan 2001; da Silva et al. 2001; Wu & Xue 2002; Voit et al. 2002; Davé et al. 2002; White et al. 2002)

are apparently able to match many of the features of the X-ray scaling relations of nearby clusters. In this sense, cooling has very similar effects on the ICM to those induced by "preheating". Cooling has an advantage over preheating in that it does not require some (as of yet) unknown source to transfer large amounts of energy into the ICM. However, cooling alone leads to an expected amount of cooled gas in groups and clusters that far exceeds what is observed (Balogh et al. 2001). Feedback, be it through preheating or heating after cluster formation, must also be an important process.

We are currently in the process of adding radiative cooling to the BBLP02 analytic models (McCarthy et al. 2004) with the intention of exploring how SZ effect and X-ray scaling relations are modified by it. As far as we know, the effects of cooling on SZ effect scaling relations have not yet been examined. While, in general, we do not expect the results of the present study to change significantly with the inclusion of cooling (since cooling affects the ICM in a very similar way to that of preheating), in detail, we do anticipate subtle (or perhaps not so subtle) differences to be present. This may also lead to a way of separating out the relative contributions of cooling and heating to cluster scalings.

Finally, we note that with the recent release of the Reese et al. (2002) data, there are now enough SZ effect observations to begin testing the "entropy floor" hypothesis by mapping out the various correlations involving the SZ and X-ray observables, and comparing these to their theoretical counterparts derived in this paper. It would be most interesting to see if these correlations also favor the existence of an entropy floor, and whether the level of this floor is comparable to that required to explain the X-ray trends. This will be the focus of McCarthy et al. (2003b), a companion paper to this one.

We thank the referee for very useful comments and suggestions. We also thank Peng Oh, Kathy Romer, and Mark Voit for helpful discussions. A. B. would like to acknowledge the hospitality extended to him by the Canadian Institute for Theo-

retical Astrophysics during his tenure as CITA Senior Fellow. I. G. M. is supported by a postgraduate scholarship from the Natural Sciences and Engineering Research Council of Canada (NSERC). A. B. is supported by an NSERC operating grant, G. P. H. is supported by the W. M. Keck Foundation, and M. L. B. is supported by a PPARC rolling grant for extragalactic astronomy and cosmology at the University of Durham.

Chapter 4

The Sunyaev-Zeldovich Effect Signature of Excess Entropy in Distant, Massive Clusters

Abstract

Studies of cluster X-ray scaling relations have led to suggestions that non-gravitational processes, e.g., radiative cooling and/or "preheating", have significantly modified the entropy of the intracluster medium (ICM). For the first time, we test this hypothesis through a comparison of predicted thermal Sunyaev-Zeldovich (SZ) effect scaling relations with available data from the literature. One of the relations that we explore, in principle, depends solely on SZ effect observations, thus offering an X-ray independent probe of the ICM. A detailed comparison of the theoretical relations with the largest compilation of high-z SZ effect data to date indicates that the presence of an entropy floor is favored by the data. Furthermore, the inferred level of that floor, $K_0 \gtrsim 300$ keV cm^2, is comparable to that found in studies of X-ray scaling relations of nearby massive clusters. Thus, we find no evidence for significant evolution of the entropy floor out to $z \sim 0.7$. We further demonstrate that the high quality data to be obtained from the upcoming Sunyaev-Zeldovich Array (*SZA*) and the (soon-to-be) upgraded Owens Valley Radio Observatory (*OVRO*) array will open powerful new windows into the properties

of the ICM. Specifically, the new measurements will allow for accurate measurements of the ICM entropy for even the most distant galaxy clusters.

4.1 Introduction

The failure of theoretical self-similar X-ray scaling relations to match observed trends has led to suggestions that important non-gravitational processes, such as radiative cooling and/or "preheating", are significantly affecting the structure and appearance of the intracluster medium (ICM). Models and simulations of clusters which attempt to explicitly take into account the effects of cooling and/or heating produce clusters which have higher mean entropies ("excess" entropy) than those produced by models which neglect these processes. In some cases, the model clusters possess cores in their entropy profiles commonly referred to as the "entropy floor". The presence of this entropy floor, in turn, modifies the predicted X-ray scaling relations, bringing them in to much closer agreement with the observed correlations (e.g., Kaiser 1991; Evrard & Henry 1991; Bower 1997; Balogh et al. 1999; Wu et al. 2000; Bryan 2000; Tozzi & Norman 2001; Borgani et al. 2001; Voit & Bryan 2001; Babul et al. 2002; McCarthy et al. 2002a; Thomas et al. 2002; Voit et al. 2002; Davé et al. 2002; Lloyd-Davies et al. 2003). Direct observational evidence for an "entropy floor" in nearby groups and low mass clusters has been presented by Ponman et al. (1999) and Lloyd-Davies et al. (2000).

To date, only X-ray observations have yielded information about the entropy floor but because the X-ray surface brightnesses of groups/clusters suffer the effects of cosmological dimming [the bolometric surface brightness scales as $(1+z)^{-4}$], both direct and indirect studies of the entropy floor via X-ray observations have generally been limited to low redshift ($z \lesssim 0.2$) systems. An *independent* test of the entropy floor hypothesis which could also provide information on *high redshift* clusters and, therefore, the evolution of the non-gravitational processes that give rise to the entropy floor, would be extremely useful. In a companion paper (McCarthy

et al. 2003a, hereafter MBHB03), we argued that a number of scaling relations based entirely or in part on thermal Sunyaev-Zeldovich effect (Sunyaev & Zeldovich 1972; 1980; hereafter, referred to as the SZ effect) observables can, potentially, be used for both of these purposes. Our analysis indicated that even current SZ effect observational data from, for example, the Berkeley Maryland Illinois Association (*BIMA*) and Owens Valley Radio Observatory (*OVRO*) arrays and the Ryle Telescope, when compared to the predicted correlations, can be used to tell us something about the entropy floors of distant, massive clusters.

The primary focus of the present paper is a comparison of these predicted scaling relations with available data from the literature to determine if the SZ effect data favor the existence of an entropy floor and how the inferred level of the entropy floor compares with that required to explain local X-ray trends (which require $K_0 \gtrsim 300$ keV cm^2 for massive clusters; Tozzi & Norman 2001; Babul et al. 2002; McCarthy et al. 2002a). *This is the first time that the SZ effect has been used as a probe of non-gravitational entropy in galaxy clusters.*

A number of new SZ experiments, which will greatly improve the quality of the observations, are being planned or are already under construction. An additional goal of the present study, therefore, is to examine the efficacy of two of these experiments, the Sunyaev-Zeldovich Array (*SZA*) and the (soon to be) upgraded *OVRO* array, to constrain the properties of the excess entropy in distant clusters. By constructing and analysing "mock" observations which take explicit account of the expected instrumental responses of these arrays, we quantify the accuracy with which the level of the entropy floors of distant clusters can be inferred by future data as a function of redshift.

The present paper is outlined as follows: in §4.2, we discuss and select available data from the literature; in §4.3, we compare these data to our theoretical scaling relations; in §4.4, we assess the ability of the upcoming *SZA* and upgraded *OVRO* array to probe the entropy floors of distant clusters; and in §4.5; we discuss and summarize our results. We assume $\Omega_m = 0.3$, $\Omega_\Lambda = 0.7$, and $H_0 = 75$ km s^{-1}

Mpc^{-1} and work in physical units (e.g., $M_{\odot}$ rather than $h^{-1}M_{\odot}$) throughout the paper.

4.2 Observational data

Observations of the SZ effect have advanced tremendously over the last decade or so and routine high signal-to-noise measurements of the effect are now being made with a variety of instruments (including both single-dish and interferometric experiments) at a variety of wavelengths (spanning radio down to the submillimeter). There now exist published data for some 30-40 clusters (e.g., Jones et al. 1993; Herbig et al. 1995; Carlstrom et al. 1996; Myers et al. 1997; Holzapfel et al. 1997; Hughes & Birkinshaw 1998; Pointecouteau et al. 1999; 2001; 2002; Patel et al. 2000; Holzapfel et al. 2000; Joy et al. 2001; Mason et al. 2001; Grego et al. 2001; Grainge et al. 2002a; Grainge et al. 2002b; Jones et al. 2005; Reese et al. 2002; Cotter et al. 2002; LaRoque et al. 2003; Cantalupo et al. 2003). With this influx of new data, the sample is large enough to make statistically significant comparisons between observed and theoretically predicted SZ effect scaling relations. Such comparisons test our understanding of the ICM and clusters in general. In this section, we compile and discuss cluster SZ effect data from the literature with the intention of comparing it to theoretically predicted scaling relations in §4.3.

Of the 30-40 clusters that have published SZ effect data, we are particularly interested in those clusters which lie at high redshift. As already mentioned, the vast majority of studies on the *X-ray* scaling relations of clusters have been for low redshift ($z \lesssim 0.2$) systems but information on the entropy floors of more distant clusters is scant. Because the SZ effect is not subject to cosmological dimming, SZ effect scaling relations potentially offer a way of probing the non-gravitational entropy of even the most distant galaxy clusters.

A search of the literature for high redshift clusters with SZ effect data yields 22 different clusters in the range $0.14 \lesssim z \lesssim 0.78$, many of which were observed

Table 4.1: SZ effect observational data

Cluster	z	$\log y_0$	$\log S_{\nu,arc}/f_\nu$	Ref.
A1413	0.143	$-3.794^{+0.053}_{-0.060}$	$0.954^{+0.062}_{-0.070}$	a (b)
A2204	0.152	$-3.744^{+0.111}_{-0.150}$	—	c
A1914	0.171	-3.798	0.934	b
A2218	0.176	$-3.862^{+0.056}_{-0.081}$	$0.922^{+0.060}_{-0.086}$	a (b)
A665	0.182	$-3.864^{+0.081}_{-0.100}$	$0.939^{+0.084}_{-0.104}$	a
A1689	0.183	$-3.489^{+0.029}_{-0.027}$	$1.169^{+0.038}_{-0.036}$	a
A520	0.199	$-3.906^{+0.058}_{-0.067}$	$0.914^{+0.065}_{-0.075}$	a
A2163	0.203	$-3.448^{+0.031}_{-0.033}$	$1.363^{+0.034}_{-0.036}$	a (d,e)
A773	0.217	$-3.626^{+0.052}_{-0.059}$	$1.132^{+0.080}_{-0.103}$	a (b,f)
A2261	0.224	$-3.497^{+0.048}_{-0.054}$	$1.137^{+0.085}_{-0.087}$	a
A1835	0.253	$-3.328^{+0.029}_{-0.027}$	$1.146^{+0.048}_{-0.050}$	a (g)
A697	0.282	$-3.577^{+0.052}_{-0.052}$	$1.179^{+0.082}_{-0.091}$	a (b)
A611	0.288	$-3.795^{+0.066}_{-0.066}$	$0.807^{+0.141}_{-0.179}$	a
Zwicky 3146	0.291	$-3.792^{+0.066}_{-0.077}$	—	c
A1995	0.319	$-3.717^{+0.032}_{-0.037}$	$0.943^{+0.092}_{-0.125}$	a
MS1358.4+6245	0.327	$-3.832^{+0.047}_{-0.053}$	$0.720^{+0.083}_{-0.090}$	a
A370	0.375	$-3.628^{+0.154}_{-0.083}$	$1.145^{+0.204}_{-0.180}$	a
RXJ2228+2037	0.421	-3.620	1.024	h
RXJ1347.5-1145	0.451	$-3.130^{+0.037}_{-0.040}$	$1.245^{+0.069}_{-0.072}$	a (i,j)
Cl0016+16	0.546	$-3.632^{+0.035}_{-0.038}$	$1.056^{+0.054}_{-0.059}$	a (k,l)
MS0451.6-0305	0.550	$-3.571^{+0.027}_{-0.031}$	$1.041^{+0.076}_{-0.091}$	a
MS1137.5+6625	0.784	$-3.814^{+0.048}_{-0.055}$	$0.608^{+0.243}_{-0.365}$	a (m)

Note. — $S_{\nu,arc}/f_\nu$ expressed in mJy.

[a]Reese et al. (2002); [b]Jones et al. (2005); [c]Holzapfel (1996); [d]Holzapfel et al. (1997); [e]Lamarre et al. (1998); [f]Saunders et al. (2003); [g]Mauskopf et al. (2000); [h]Pointecouteau et al. (2002); [i]Pointecouteau et al. (2001); [j]Komatsu et al. (1999); [k]Grainge et al. (2002a); [l]Hughes & Birkinshaw (1998); [m]Cotter et al. (2002)

multiple times. The clusters are listed in Table 4.1 along with their redshifts, central Compton parameters (y_0), frequency-independent integrated SZ effect flux densities within the central 1 arcminute ($S_{\nu,arc}/f_\nu$), and the bibliographic references (references in parentheses indicate that the cluster was observed multiple times). We are particularly interested in y_0 and $S_{\nu,arc}/f_\nu$ because a number of scaling relations based on these two quantities are expected to be quite sensitive to the

entropy floor level of galaxy clusters (see MBHB03).

Below, we discuss how we extract y_0 and $S_{\nu,arc}/f_\nu$ from the observational data. At present, it is not possible to directly measure either of these quantities. Observations of the SZ effect filter large-scale emission while finite resolution smears out small-scale structures. As discussed in MBHB03, fitting a model (such as the isothermal β model; Cavaliere & Fusco-Femiano 1976; 1978) to the SZ effect data provides a method for effectively removing these effects and estimating y_0 and $S_{\nu,arc}/f_\nu$, but it should be kept in mind that such quantities are inferred and model-dependent. Provided the smallest angular scale resolved is comparable to the typical scale over which the cluster varies, the estimated central Compton parameter will be reliable, while inferred flux densities will be suspect when extrapolated beyond the filtering scale of the observations. For current interferometric observations [such as those obtained with the *BIMA* and *OVRO* arrays and the Ryle telescope], the highest angular resolution for SZ measurements is typically smaller than the core radius of the cluster ($\sim$ 30 arcseconds) while the large-scale filtering normally becomes important on scales larger than about 2 arcminutes. Therefore, it can be expected that the inferred values of y_0 and $S_{\nu,arc}/f_\nu$ (the flux density within the central 1 arcminute) should be accurate.

To calculate the total frequency-independent SZ effect flux density within the central 1 arcminute for each of these clusters, we must reconstruct each of the SZ effect "surface brightness" profiles, $y(\theta)$. The majority of the clusters listed in Table 4.1 were modeled using the spherical isothermal β model. In this model, the ICM is assumed to be isothermal and has a density distribution described by

$$n_e(r) = n_{e0}\left(1 + \frac{r^2}{r_c^2}\right)^{-3\beta/2} \tag{4.1}$$

were n_{e0} is the central electron density, r_c is the cluster core radius, and β is the power-law index. This leads to a SZ effect surface brightness profile

$$y(\theta) = y_0\left(1 + \frac{\theta^2}{\theta_c^2}\right)^{1/2-3\beta/2} \tag{4.2}$$

where $y(\theta)$ is the Compton parameter evaluated at a projected position $\theta = r/D_a$ from the cluster center and is proportional to the integrated pressure along the line-of-sight through the cluster. In addition, $\theta_c = r_c/D_a$ (D_a is the angular diameter distance).

The central Compton parameters, y_0, are converted from the central SZ effect temperature decrements (references are given in col. 5) using the relation

$$\frac{\Delta T_0}{T_{CMB}} = y_0\left(\frac{x}{\tanh x/2} - 4\right) \tag{4.3}$$

where ΔT_0 is the central SZ effect temperature decrement and $x = h\nu/kT_{CMB}$ is the dimensionless frequency (T_{CMB} is the temperature of the present-day cosmic microwave background — 2.728 K; Fixsen et al. 1996, and ν is the observing frequency). We ignore the complication of relativistic effects, which only modify the Compton parameter of the hottest clusters by a few percent (Itoh et al. 1998; Nozawa et al. 2000).

We use the best-fit β model parameters [y_0 (ΔT_0), β, and θ_c] from the literature (discussed below) to reconstruct $y(\theta)$. The surface brightnesses are then numerically integrated within the central 1 arcminute (the result is symbolized by y_{int}) via

$$y_{int}(\leq \theta = 1') = 2\pi \int_0^{\theta=1'} y(\theta')\theta' d\theta' \tag{4.4}$$

and, finally, converted into a frequency-independent flux density through

$$S_{\nu,arc}/f_\nu = y_{int}\left[\frac{2(kT_{CMB})^3}{(hc)^2}\right] \tag{4.5}$$

where f_ν is a function of the dimensionless frequency x and is defined in MBHB03.

Ideally, the three β model parameters would be determined by fitting the model to the SZ effect data. However, current SZ effect data cannot tightly constrain these parameters when all three are left to vary independently (e.g., Carlstrom et al. 1996; Grego et al. 2000; 2001; Pointecouteau et al. 2001; 2002). This problem is often circumvented by adopting the best-fit values of β and θ_c (the "shape" parameters) determined from fitting to the *X-ray* surface brightness profile of the cluster and leaving only the normalization, y_0, to be determined from fitting to the SZ effect data (e.g., Pointecouteau et al. 1999; 2001; 2002; Patel et al. 2000; Jones et al. 2005; LaRoque et al. 2003; Grainge et al. 2002b). In the case of clusters with moderate redshifts (which is a good description of most of the clusters in Table 4.1), X-ray data still provide better constraints on β and θ_c than do SZ effect data. Thus, in the cases of A1914 and RXJ2228+2037, we use the X-ray-determined values of these parameters to calculate $S_{\nu,arc}/f_\nu$. However, a better approach is to use all available data (both the SZ effect and X-ray data) to constrain these parameters. In estimating Hubble's constant from a sample of 18 distant clusters, Reese et al. (2002) did just this. The shape parameters, central X-ray surface brightness, and y_0 were all determined simultaneously by using a joint maximum-likelihood analysis of both SZ effect and X-ray data. Because their sample is large (in fact, it is the largest sample of SZ effect clusters observed to date) and homogeneously analysed and their method takes advantage of all ICM imaging data, we preferentially use the values of y_0, β, and θ_c measured by Reese et al. (2002) when multiple measurements for a particular cluster are available (which is the case for roughly half of the clusters listed in Table 4.1). We note that the agreement between different studies is reasonably good (estimates of y_0 differ by $\lesssim 20\%$ from study to study, e.g., Holzapfel et al. 1997; Jones et al. 2005). Using the best-fit parameters of Reese et al. (2002), we calculate $S_{\nu,arc}/f_\nu$ for these 18 clusters. Published values for the shape parameters of the two remaining clusters in Table 4.1, A2204 and Zwicky 3146, are not available.

To calculate the uncertainty associated with the SZ effect flux density, we vary y_0, β, and θ_c within their allowable ranges (each of the three free parameters has an associated statistical uncertainty) to determine the maximum and minimum possible flux density of the cluster. This method actually *overestimates* the uncertainty associated with the flux density as there is a known correlation between the β and θ_c parameters for current SZ effect data (e.g., Grego et al. 2000; 2001).

We are also interested in mapping out correlations between SZ effect and X-ray observables. In Table 4.2, we list the total dark matter masses within r_{500} [$M(r_{500})$], the mean emission-weighted gas temperatures (T_X), and bolometric X-ray luminosities (L_X) of these clusters. We also list whether the cluster has a sharp centrally-peaked X-ray surface brightness profile which presumably indicates of the presence of a cooling flow (CF indicates the cluster is a "cooling flow cluster", NCF indicates that it is not; Allen 2000; Reese et al. 2002) and the references for $M(r_{500})$, T_X, and L_X (respectively). Below, we discuss the X-ray data in columns 2-4 of Table 4.2.

For the total dark matter masses within r_{500} (col. 2), we turn to the study of Ettori & Fabian (1999). By constructing X-ray surface brightness profiles that are based on the "universal" dark matter density (NFW) profile (Navarro et al. 1997) and comparing these to data from *ROSAT*, these authors were able to model the underlying dark matter density for nine of the clusters listed in our Table 4.1. We use their best-fit parameters (listed in their Tables 1 and 2) to recover the dark matter density profiles of these clusters. We take care to properly scale these parameters for our assumed cosmology. We then integrate the density profiles out to r_{500} to determine the total dark matter mass within that radius. We are unable to estimate the uncertainty on the masses, as there is no reported uncertainty for the best-fit NFW parameters of these clusters.

The most recently determined values for the ICM temperatures of these clusters are also listed in Table 4.2 (col. 3). Of the 21 clusters with reported temperatures, 16 have temperatures determined via fitting to *ASCA* X-ray spectral data (Allen

Table 4.2: X-ray observational data

Cluster	$\log M(r_{500})$	$\log T_X$	$\log L_X$	Type	Ref.
A1413	14.86	$0.929^{+0.062}_{-0.043}$	$45.082^{+0.018}_{-0.018}$	CF	a,b,c
A2204	14.88	$0.964^{+0.104}_{-0.055}$	45.407	CF	a,b,c
A1914	—	$0.934^{+0.018}_{-0.020}$	—	NCF	d
A2218	14.73	$0.839^{+0.030}_{-0.033}$	$44.974^{+0.018}_{-0.018}$	NCF	a,e,c
A665	14.83	$0.944^{+0.042}_{-0.047}$	$45.124^{+0.013}_{-0.013}$	NCF	a,f,c
A1689	15.06	$1.000^{+0.049}_{-0.036}$	$45.423^{+0.010}_{-0.010}$	CF	a,b,c
A520	14.75	$0.921^{+0.038}_{-0.036}$	45.070	NCF	a,b,c
A2163	15.11	$1.090^{+0.044}_{-0.041}$	45.732	NCF	a,f,c
A773	—	$0.968^{+0.016}_{-0.016}$	45.278	NCF	b,g
A2261	—	$1.037^{+0.188}_{-0.098}$	45.447	CF	b,h
A1835	—	$0.991^{+0.092}_{-0.062}$	45.725	CF	b,g
A697	—	$1.009^{+0.074}_{-0.090}$	—	NCF	i
A611	—	$0.836^{+0.029}_{-0.030}$	—	CF	i
Zwicky 3146	14.91	$1.053^{+0.180}_{-0.119}$	45.525	CF	a,b,g
A1995	—	$1.016^{+0.053}_{-0.053}$	$45.241^{+0.010}_{-0.010}$	CF	j,j
MS1358.4+6245	14.81	$0.875^{+0.289}_{-0.097}$	$45.093^{+0.014}_{-0.014}$	CF	a,b,j
A370	—	$0.848^{+0.031}_{-0.032}$	$45.236^{+0.010}_{-0.010}$	NCF	i,j
RXJ2228+2037	—	—	—	NCF	—
RXJ1347.5-1145	—	$1.422^{+0.112}_{-0.272}$	$46.093^{+0.003}_{-0.003}$	CF	b,j
Cl0016+16	—	$0.911^{+0.041}_{-0.045}$	—	NCF	i
MS0451.6-0305	—	$0.908^{+0.041}_{-0.045}$	45.610	NCF	k,k
MS1137.5+6625	—	$0.799^{+0.027}_{-0.028}$	45.158	NCF	k,k

Note. — Masses, temperatures, and bolometric luminosities are expressed in $M_\odot$, keV and ergs s^{-1}, respectively.

[a]Ettori & Fabian (1999); [b]Allen (2000); [c]White, Jones, & Forman (1997); [d]Jones et al. (2005); [e]Machacek et al. (2002); [f]Markevitch & Vikhlinin (2001); [g]Mushotzky & Scharf (1997); [h]Allen & Fabian (1998); [i]White (2000); [j]Novicki, Sornig, & Henry (2002);[k]Vikhlinin et al. (2002)

2000; White 2000; Novicki, Sornig, & Henry 2002; Jones et al. 2005) and five have measurements based on fits to new *Chandra* X-ray spectral data (Markevitch & Vikhlinin 2001; Machacek et al. 2002; Vikhlinin et al. 2002). The cluster RXJ2228+2037 does not have a temperature deduced from X-ray spectral analysis, although its central temperature was estimated by a combined analysis of

X-ray and SZ effect *imaging* data (Pointecouteau et al. 2002). In the interest of homogeneity, however, we do not include this cluster in our analysis of scaling relations involving the emission-weighted gas temperatures because it is unclear how the reported temperature is related to the X-ray emission-weighted temperature. For the clusters that have sharp centrally-peaked X-ray surface brightnesses and apparently harbor massive cooling flows (Allen 2000; Reese et al. 2002; see col. 5), we use cooling flow-corrected temperatures. The temperatures were corrected by fitting the X-ray spectra with a multi-phase plasma model that explicitly takes into account the cooler emission from the cluster core (Allen 2000). We note that for the clusters in this sample, cooling flow correction only slightly increases the temperature of a cluster (by about 10% or 1 keV) and does not significantly affect our results.

Finally, column 4 lists the bolometric X-ray luminosities of these clusters. We preferentially select data that has published uncertainties (e.g., White, Jones, & Forman 1997; Novicki, Sornig, & Henry 2002). For data without published uncertainties, we select on the basis of X-ray satellite in the following order: *Chandra/XMM-Newton*, *ASCA*, and *ROSAT/Einstein*. Of the 17 clusters that have published bolometric luminosities, seven were determined using *Einstein* imaging data (White, Jones, & Forman 1997), one was determined using *ROSAT* imaging data (Allen & Fabian 1998), seven were determined using *ASCA* imaging data (Mushotzky & Scharf 1997; Novicki, Sornig, & Henry 2002), and two were determined using new *Chandra* imaging data (Vikhlinin et al. 2002). Unfortunately, cooling flow-corrected luminosities (which normally entails excising the central 100-200 kpc of the CF cluster; e.g., Markevitch 1998; Vikhlinin et al. 2002) were not available for the CF clusters in Table 4.2.

Tables 4.1 and 4.2 comprise the largest compiled sample of high redshift SZ effect clusters to date. We note that the current compilation is not statistically complete or homogeneous, as discussed in Reese et al (2002). Clusters with bright radio point sources were avoided, for the most part, and targets were selected

primarily on the basis of X-ray luminosity. This compilation can not be simply defined as being flux-limited or luminosity-limited, for example, and it is not complete over the range of redshifts studied. Without a simple selection function it is difficult to assess possible systematic effects that could be introduced by not having a sample that adequately reflects the demographics of the general population of galaxy clusters.

Below, we compare the data in Tables 4.1 and 4.2 to our theoretically predicted scaling relations (see Table 1 of MBHB03) and attempt to determine if the data require an entropy floor (similar to that of X-ray data of nearby clusters) and, if so, what is the level of that entropy floor.

4.3 Results

4.3.1 Comparing Theory to Observations

A detailed analysis of how the presence of excess entropy alters SZ effect scaling relations was presented in the companion paper MBHB03. These relations were derived using the entropy injection (preheated) models developed by Babul et al. (2002). Following standard practice, we fitted simple power-law models to the theoretical scaling relations. Since a number of the relations were quite sensitive to redshift and existing SZ effect data span a wide range in z (see Table 4.1), we fitted power-law models which were an explicit function of both redshift and entropy floor level (K_0) to the theoretical relations; i.e., for arbitrary cluster parameters X and Y (e.g., y_0 and T_X)

$$\log_{10} Y = a(K_0, z) \log_{10} X + b(K_0, z) \tag{4.6}$$

With these relations, it is possible to quickly and accurately compute how various cluster properties scale with the SZ effect of the Babul et al. (2002) model clusters at any redshift between $0.1 \lesssim z \lesssim 1$ and with any entropy floor in the

range 100 keV cm^2 $\lesssim K_0 \lesssim$ 700 keV cm^2 (see the Table 1 of MBHB03). This is the only way a fair comparison can be made between the existing data and the theoretical models.

We compare the theoretical scaling relations to the observational data compiled in Tables 4.1 and 4.2 with a χ^2 statistic

$$\chi^2 = \sum_{i=1}^{N} \frac{[\log Y_i - a(K_0, z) \log X_i - b(K_0, z)]^2}{\sigma_{Y_i}^2 + a(K_0, z)^2 \sigma_{X_i}^2} \tag{4.7}$$

where $\sigma_{Y_i}^2$ and $\sigma_{X_i}^2$ are the measurement errors in log-space and are estimated by multiplying the measurement errors in linear-space by the weighting factors $(Y_i \log e)^{-1}$ and $(X_i \log e)^{-1}$, respectively (see, e.g., Press et al. 1992).

We specify the optically-determined redshifts for each of the clusters and then determine the best-fit value of entropy floor level, K_0, by minimizing the χ^2 (assuming that the value of K_0 is the same for all clusters). Unless stated otherwise, quoted error bars are for the 95.4% (2σ) confidence level (corresponding to $\Delta\chi^2 = 4$). We assess the quality of the fit by calculating the reduced-χ^2 (χ_ν^2). For the self-similar model (whose scaling relations depend on z only; i.e., there are no free parameters), we calculate the χ^2 and χ_ν^2 and compare this with that of the best-fit entropy floor model.

Below, we examine seven different scaling relations involving the two primary SZ effect observables (the central Compton parameter and the integrated flux density). First, we explore the trend that exists between the two SZ effect observables. This is an extremely interesting test since it can potentially be measured entirely independent of X-ray observations. In fact, in §4.4, we show that future data from the *SZA* and the upgraded *OVRO* array will allow one to constrain the central entropy distribution of clusters all the way out to $z \sim 2$ using this relation. The next two trends that we study, between the two SZ effect observables and the mass of a cluster, are also interesting because they too can potentially be measured independent of X-ray observations. Aside from X-ray observations, one can

estimate the mass of a cluster via gravitational lensing or through galaxy velocity dispersion measurements. We expect that the $y_0 - M(r_{500})$ relation, in particular, will be very sensitive to the presence of excess entropy. Finally, the four remaining correlations that we look at are between the two SZ effect observables and the two primary X-ray observables, i.e., the mean emission-weighted temperature (T_X) and the bolometric luminosity (L_X). The correlations between the SZ effect observables and the cluster temperature are expected to be excellent probes of the central entropy of clusters and, as such, we discuss these ahead of those involving L_X.

4.3.2 A SZ Effect Only Relation

We start by examining the correlation between the two SZ effect quantities, $S_{\nu,arc}/f_\nu$ and y_0 (see Fig. 2 of MBHB03). Even though theoretical arguments suggest that this relation is not as sensitive to the presence of excess entropy as some of the other relations we will discuss later, it is by far the most interesting. As we already mentioned, this relation can potentially be measured entirely through SZ effect observations, offering a completely X-ray-independent probe of the intracluster gas. This is discussed in more detail below.

Fitting all 20 clusters in Table 4.1 for which we have estimates of both $S_{\nu,arc}/f_\nu$ and y_0, we find a best-fit entropy floor level of $K_0 = 540^{+170}_{-165}$ keV cm^2 with a χ^2_ν $= 37.77/19 = 1.99$. A residual plot demonstrating the quality of our best-fit entropy floor model is presented in Figure 4.1 (top panel). The residuals from a comparison between the self-similar model and the data in Table 4.1 is presented in the bottom panel ($\chi^2_\nu = 244.15/20 = 12.21$). Note that the residuals in the top panel are generally consistent with the zero line (indicating a relatively good fit), whereas the residuals in the bottom panel are systematically too high, indicating that the self-similar model predicts values of $S_{\nu,arc}/f_\nu$ (for a fixed y_0) that are systematically lower than observed. This is equivalent to saying that the self-similar model predicts clusters that have SZ effect surface brightness profiles that are too

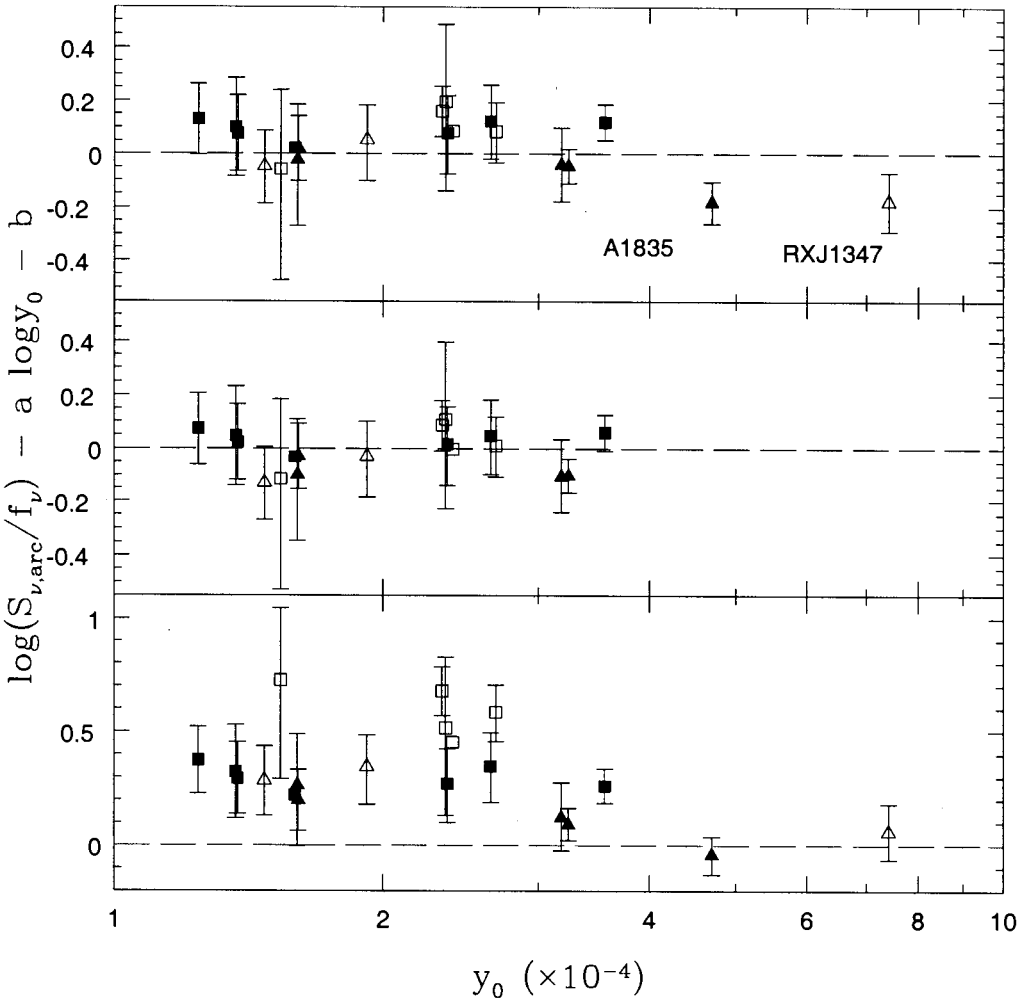

Figure 4.1: Residual plots for the $S_{\nu,arc}/f_\nu - y_0$ relation. *Top:* Residuals from a comparison between the entropy floor model with $K_0 = 540$ keV cm^2 and the data in Table 4.1 ($\chi^2_\nu = 1.99$). *Middle:* Neglecting A1835 and RXJ1347.5-1145 - for reasons discussed in the text - greatly improves the fit: $K_0 = 570$ keV cm^2 with $\chi^2_\nu = 0.99$. *Bottom:* Residuals from a comparison between the self-similar model and the data in Table 4.1 ($\chi^2_\nu = 12.21$). Filled symbols represent low redshift ($z < 0.3$) clusters, open symbols represent high redshift ($z > 0.3$) clusters, triangles represent cooling flow clusters, and squares represent non cooling flow clusters. For clarity, error bars for the abscissa are not displayed.

centrally-peaked. The entropy floor models are able to match the observations much better because the addition of an entropy floor flattens the pressure profiles of clusters (e.g., Fig. 1. of MBHB03) and since the SZ effect is proportional to integrated line-of-sight pressure of the cluster, this leads to flatter surface brightness profiles.

There is little doubt that the best-fit entropy floor model provides a much better fit than the self-similar model to the observational data, but the best-fit entropy floor model itself does not provide a statistically acceptable fit to the data (note the high value of the χ^2_ν). However, the residuals in the top panel of Figure 4.1 clearly show two obvious outliers, A1835 and RXJ1347.5-1145. Neglecting these two clusters, the quality of the fit to the whole sample is significantly improved: we find $K_0 = 575^{+150}_{-155}$ keV cm^2 with $\chi^2_\nu = 16.79/17 = 0.99$. The residuals for this fit are plotted in the middle panel of Figure 4.1. This result is consistent with that determined from studies of X-ray scaling relations of nearby massive clusters, which require $K_0 \gtrsim 300$ keV cm^2 (e.g., Tozzi & Norman 2001; Babul et al. 2002; McCarthy et al. 2002a).

It is interesting that the two outliers, A1835 and RXJ1347.5-1145, have extraordinarily large cooling flow mass deposition rates. Both apparently deposit several thousand solar masses of gas each year and are among the most massive cooling flow clusters known (Allen 2000). In fact, a closer inspection of the residuals (particularly in the left-hand panel) reveals that there is a small systematic difference between cooling flow clusters (triangles) and non cooling flow clusters (squares), even if one neglects these two outliers. While in principle the SZ effect should be less susceptible than the X-ray emission to the effects of cooling flows (because SZ effect is proportional to n_e, whereas the X-ray emission is proportional to n_e^2), recall that both of the SZ effect quantities used in Figure 4.1 were inferred through fitting to both X-ray and SZ effect data. Thus, the strong central surface brightness peaks present in the X-ray images of these cooling flow clusters will have an impact on the implied SZ effect observables. Excluding A1835 and RXJ1347.5-

1145, however, there is no statistical evidence for a difference in K_0 when fitting to the cooling flow and non cooling flow clusters separately or to the whole sample. Therefore, it appears that only the most extreme cooling flow clusters could have significantly different entropy histories.

Because the sample in Table 4.1 is reasonably large and spans a wide range of redshifts, it is possible to use the catalog to get some idea of how the entropy floor level of clusters evolved with cosmic time. We split the sample up into two large redshift bins: (1) "low" redshift clusters ($z < 0.3$), and (2) "high" redshift clusters ($z > 0.3$). Fitting only the low redshift clusters, we derive $K_0 = 505^{+220}_{-210}$ keV cm^2 ($\chi^2_\nu = 10.46/10 = 1.05$), which is consistent with the value derived from fitting to the entire sample. The high redshift clusters, however, prefer a slightly elevated entropy floor with $K_0 = 640^{+205}_{-215}$ keV cm^2 ($\chi^2_\nu = 5.84/6 = 0.97$), although the difference between the low and high redshift clusters is not statistically significant. Thus, there is no good evidence that K_0 evolves significantly out to $z \sim 0.7$, at least on the basis of this test. A stronger test of this hypothesis will soon be possible, as the list of high redshift clusters observed through the SZ effect is growing rapidly (Carlstrom and Joy and collaborators, for example, have now made detections in 21 clusters with $z > 0.45$; Reese et al. 2002).

Finally, to what extent the present $S_{\nu,arc}/f_\nu - y_0$ relation studied here is independent of previous X-ray results is debatable. Both $S_{\nu,arc}/f_\nu$ and y_0 were *inferred* by fitting a model to the SZ effect surface brightness profiles of clusters and, furthermore, this surface brightness model (the isothermal β model) had two of its three free parameters constrained to be the same as that deduced from X-ray observations (Jones et al. 2005; Pointecouteau et al. 2002) or from X-ray and SZ effect observations (Reese et al. 2002). Yet, it is also clear that this test is different from any other scaling relation examined to date. Ideally, both $S_{\nu,arc}/f_\nu$ and y_0 could be measured directly or, failing that, determined from fitting a model to only the SZ effect data. Current SZ effect data alone, however, cannot tightly constrain these quantities. In §4.4, we show that the high quality data to be produced by the

upcoming *SZA* and the (soon to be) upgraded *OVRO* array will make it possible to accurately measure these quantities for massive clusters at virtually any redshift and without having to use any X-ray results.

4.3.3 The SZ effect-$M(r_{500})$ Relations

The next set of scaling relations we examine are the SZ effect - cluster mass relations. Theoretical arguments suggest that these relations should be very sensitive to the presence of entropy floor, at least when the SZ effect is measured near the cluster center (e.g., y_0). Interestingly, these trends too can also potentially be measured independent of X-ray results. Future SZ effect observations will allow one to estimate y_0 and $S_{\nu,arc}/f_\nu$ accurately purely through SZ effect surface brightness profiles (see §4.4), while both strong and weak lensing are increasingly being used to measure the mass profiles of clusters out to radii comparable in size to that of r_{500} (e.g., Clowe & Schneider 2001). At present, however, only a few of the clusters in our sample have been weighed using lensing.

In Figure 4.2, we plot the observed $y_0 - M(r_{500})$ relation. This is superimposed on the predicted $z = 0.2$ $y_0 - M(r_{500})$ relations for the self-similar model (dotted line) and the $K_0 = 100$ (short-dashed), 300 (long-dashed), 500 (dot-dashed), and 700 keV cm^2 (solid) entropy floor models. Because the majority of the clusters with published masses in Tables 4.1 and 4.2 lie in a narrow redshift range around $z \sim 0.2$, it is possible to *qualitatively* compare the theoretical models to the data "by eye" before using the quantitative method outlined in §4.3.1. A simple, neat, and fair qualitative comparison was not possible for the previous relation ($S_{\nu,arc}/f_\nu - y_0$), as the data spanned a wide range of redshifts and because that relation is especially sensitive to z (S_ν scales as $1/D_a^2$).

By visual inspection of Figure 4.2, it is obvious that only the high entropy floor models ($K_0 \gtrsim 300$ keV cm^2) provide a reasonable fit to the observational data. In addition, the observed correlation does not seem to depend on the cooling flow status or redshift of the clusters, although the sample is far too small to make

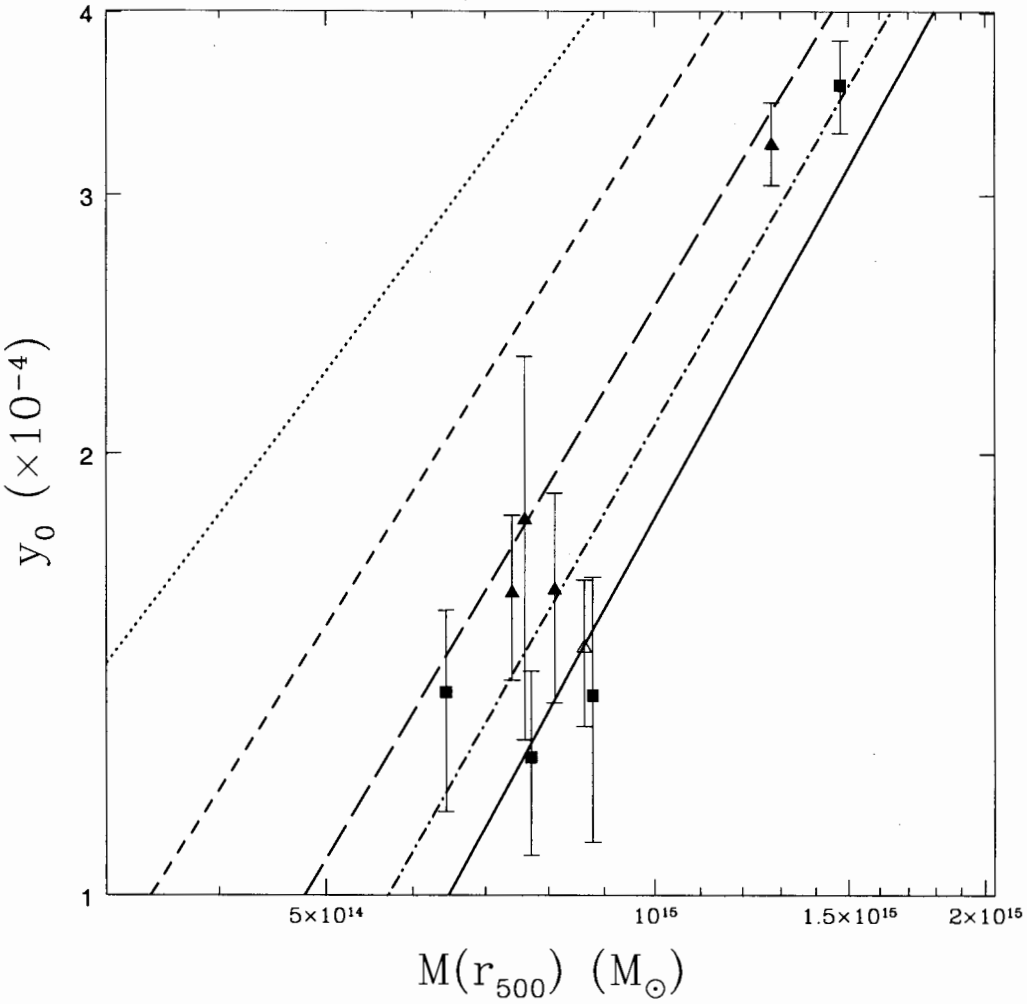

Figure 4.2: The observed and predicted $y_0 - M(r_{500})$ relations. The symbols have the same meaning as in Figure 4.1. The dotted, short-dashed, long-dashed, dot-dashed, and solid lines represent the self-similar and K_0 = 100, 300, 500, and 700 keV cm^2 entropy floor models, respectively.

any robust conclusions to this effect. Fitting all nine clusters with the method outlined in §4.3.1, our best-fit entropy floor level is $K_0 = 500^{+65}_{-65}$ keV cm^2 with χ^2_ν = 8.02/8 = 1.00. This is consistent with the results derived in §4.3.2 and with X-ray observations of nearby massive clusters. A plot of the residuals between the

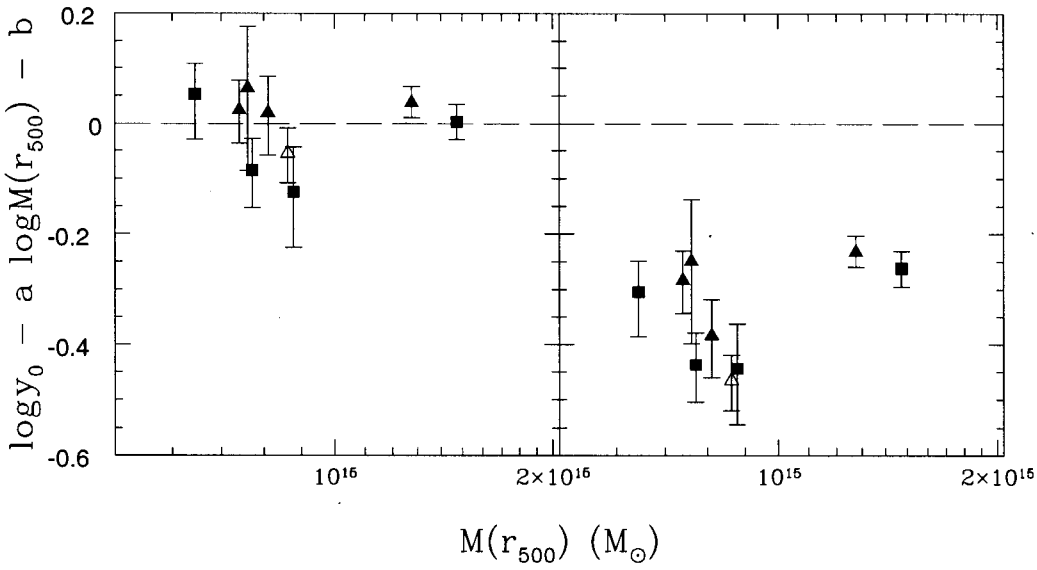

Figure 4.3: Residual plots for the $y_0 - M(r_{500})$ relation. *Left:* Residuals from a comparison between the entropy floor model with $K_0 = 500$ keV cm^2 and the observational data ($\chi^2_\nu = 1.00$). *Right:* Residuals from a comparison between the self-similar model and the observational data ($\chi^2_\nu = 41.80$). The symbols have the same meaning as in Figure 4.1. For clarity, error bars for the abscissa are not displayed.

data and the $K_0 = 500$ keV cm^2 model is shown in the left-hand panel of Figure 4.3. Also shown (right-hand panel) are the residuals of a comparison between the data and the self-similar model ($\chi^2_\nu = 376.05/9 = 41.80$). The residuals for the $K_0 = 500$ keV cm^2 model display a tight scatter about the zero line, while the residuals for the self-similar model indicate that y_0 is observed to be much lower [for a fixed value of $M(r_{500})$] than predicted by this model. The entropy floor models with $K_0 \sim 500$ keV cm^2 are able to provide a good match to the data because the addition of an entropy floor reduces the gas pressure near the centers of clusters (see MBHB03 for a detailed discussion). This, in turn, reduces the magnitude of y_0. The mass within r_{500}, however, is unaffected by the modification of the gas entropy.

Although the available $y_0 - M(r_{500})$ data exhibit only a very small amount of

scatter about the $K_0 \sim 500$ keV cm^2 relation (and the χ^2_ν indicates a very good fit), the estimated error bars on our best-fit value of K_0 from this relation are almost certainly too small. We say this because (1) we were unable to calculate any uncertainty for $M(r_{500})$ as there were no published error bars for the best-fit NFW parameters for the clusters in Figures 4.2 and 4.3, and (2) the sample is too small to get any kind of a handle on the systematic errors associated with the cluster masses. For example, estimates of cluster masses from gravitational lensing very often differ from those determined from X-ray data (sometimes by up to a factor of two; e.g., Miralda-Escudé & Babul 1995; Wu & Fang 1997; Ota et al. 2004) and it is not yet clear why this happens to be the case. There could be a systematic problem with the X-ray determined masses (e.g., Allen 1998).

Aside from the $y_0 - M(r_{500})$ relation, we also explore the $S_{\nu,arc}/f_\nu - M(r_{500})$ trend. This trend could provide a consistency check of the results discussed immediately above. Unfortunately, the available SZ effect flux density - mass data do not constrain K_0. This is not completely unexpected since the $S_{\nu,arc}/f_\nu - M(r_{500})$ relation is much less sensitive than the $y_0 - M(r_{500})$ relation to the entropy floor level of clusters (MBHB03). Future data from, for example, the *SZA* will allow for much more precise determinations of the SZ effect flux densities of clusters and we expect that the future $S_{\nu,arc}/f_\nu - M(r_{500})$ relation will place much tighter constraints on K_0.

4.3.4 The SZ effect$-T_X$ Relations

Plotted in Figure 4.4 is the observed $y_0 - T_X$ relation. In addition to the observational data, we have also plotted the $z = 0.2$ (thick lines) and $z = 0.5$ (thin lines) theoretical relations. The various line types (e.g., solid, dotted) have the same meanings as in Figure 4.2. Again, because the theoretical relations are not a strong function of redshift, a preliminary visual comparison of the data and models is feasible.

First, it is clear that the data indicate that there is a fairly tight correla-

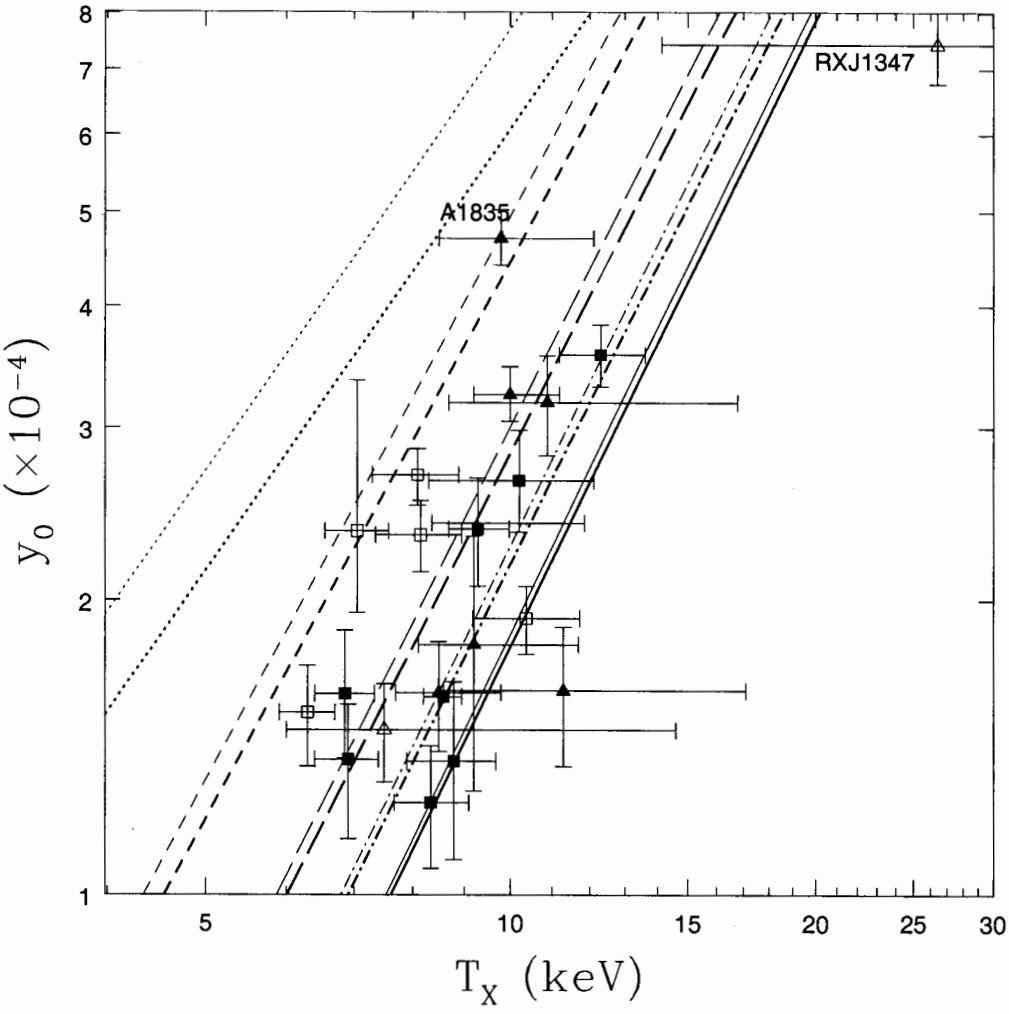

Figure 4.4: The observed and predicted $y_0 - T_X$ relations. The symbols have the same meaning as in Figure 4.1. The dotted, short-dashed, long-dashed, dot-dashed, and solid lines represent the self-similar and $K_0 = 100$, 300, 500, and 700 keV cm^2 entropy floor models, respectively. Thin lines are for $z = 0.2$ and thick lines are for $z = 0.5$. As discussed in the text, the models with $K_0 \sim 300$ keV cm^2 provide the best description of the observations.

tion between a cluster's central Compton parameter and its emission-weighted gas temperature. This correlation seems to hold true irrespective of whether the clusters have cooling flows or not. This may be expected since we have used cool-

ing flow-corrected temperatures. However, even without this correction the data still exhibit a tight trend. For the clusters in this sample, cooling flow correction only slightly increases the temperature of a cluster (by about 10% or 1 keV) and, therefore, does not significantly affect the results. There is also a hint of a slight systematic difference in the $y_0 - T_X$ relations for low and high redshift clusters (filled and open symbols, respectively). In particular, the relation for the high redshift clusters has a normalization that is slightly higher than that of the relation for low redshift clusters (ignoring RXJ1347, whose temperature is quite uncertain). This is discussed in more detail below.

Comparing the various theoretical relations to the observational data, it is apparent that the standard self-similar model predicts a $y_0 - T_X$ relation which is a poor match to the data. In particular, the normalizations of the self-similar relations are roughly 2.5 times larger than observed (over the range 6 keV $\lesssim T_X \lesssim$ 12 keV). The entropy floor models with $K_0 \sim 300$ keV cm^2, on the other hand, provide a very good qualitative fit to the data. In MBHB03, we found that injecting the ICM with non-gravitational entropy tends to decrease y_0 and, at the same time, increase T_X. This reduces the normalization of the predicted trend between these two quantities and, as is apparent from Figure 4.4, brings close agreement between theory and observations.

Fitting all 21 clusters in Tables 4.1 and 4.2 via the method outlined in §4.3.1, we obtain a best-fit entropy floor of $K_0 = 300^{+80}_{-60}$ keV cm^2 with $\chi^2_\nu = 26.36/20 = 1.32$. The residuals of a comparison between the $K_0 = 300$ keV cm^2 entropy floor model and the self-similar model with the observation data are plotted in Figure 4.5. Note the striking separation between the residuals of the two models. Theoretically, the $y_0 - T_X$ relation is the most sensitive to the entropy floor level of any and all scaling relations that we have explored.

If we exclude A1835 and RXJ1347.5-1145 from the fit, the entropy floor is essentially unchanged ($K_0 = 305^{+80}_{-65}$ keV cm^2) but the fit is improved ($\chi^2_\nu = 22.37/18 = 1.24$). In addition, we verify that splitting the sample by cooling flow status does

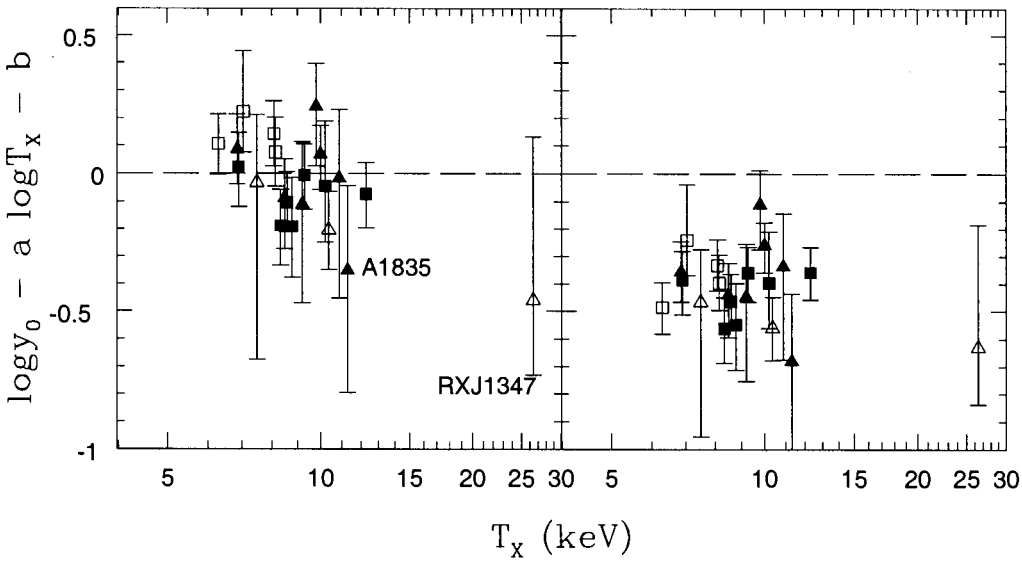

Figure 4.5: Residual plots for the $y_0 - T_X$ relation. *Left:* Residuals from a comparison between the entropy floor model with $K_0 = 300$ keV cm^2 and the observational data ($\chi^2_\nu = 1.32$). Neglecting A1835 and RXJ1347.5-1145, we find a best fit of $K_0 = 305$ keV cm^2 with $\chi^2_\nu = 1.24$. *Right:* Residuals from a comparison between the self-similar model and the observational data ($\chi^2_\nu = 21.41$). The symbols have the same meaning as in Figure 4.1. For clarity, error bars for the abscissa are not displayed.

not significantly modify the best-fit value of K_0. As mentioned above, there appears to be a slight difference in the normalizations of the $y_0 - T_X$ relations for low and high redshift clusters. Is this difference significant? If we restrict the fit to low redshift ($z < 0.3$) clusters only, we find a best-fit value of $K_0 = 370^{+130}_{-95}$ keV cm^2 ($\chi^2_\nu = 9.69/12 = 0.81$). This is consistent with the best-fit for the whole sample. Fitting only high redshift ($z > 0.3$) clusters we find a best-fit value of $K_0 = 220^{+100}_{-70}$ keV cm^2 ($\chi^2_\nu = 7.64/5 = 1.53$). Therefore, there is only a marginal statistical difference between the best-fit values of K_0 from the low and high redshift clusters. A very similar result is deduced from an examination of the $S_{\nu,arc}/f_\nu - T_X$ relation (which is not as sensitive as the $y_0 - T_X$ relation to the entropy floor; MBHB03), where the low redshift clusters are best fit by entropy floor models with $K_0 \sim 300$

keV cm^2 while the high redshift clusters are best fit by entropy floor models with $K_0 \sim 200$ keV cm^2.

4.3.5 The SZ effect$-L_X$ Relations

The theoretical $y_0 - L_X$ relations have the interesting properties that they do not evolve strongly with redshift and, more importantly, are virtually insensitive to the presence of an entropy floor. The reason why this happens to be the case is not because the individual quantities, y_0 and L_X, are unaffected by an entropy floor (on the contrary, they are greatly modified), but because they are both affected in a very similar manner. Therefore, this correlation is less than ideal when it comes to probing the non-gravitational entropy of galaxy clusters. However, the relation is still of great interest because it provides a valuable consistency check of the other scaling relations studied here.

Figure 4.6 is a plot of the observed $y_0 - L_X$ relation. This is superimposed on the predicted $z = 0.2$ (thick lines) and $z = 0.5$ (thin lines) relations for the self-similar model (dotted) and the $K_0 = 100$ (short-dashed), 300 (long-dashed), 500 (dot-dashed), and 700 keV cm^2 (solid) entropy floor models. Since the theoretical $y_0 - L_X$ relations do not evolve strongly with redshift (compare the thin and thick lines), a qualitative "by eye" comparison is possible.

A clear correlation between a cluster's central Compton parameter and its bolometric X-ray luminosity is apparent in Figure 4.6. The relation is quite tight and follows the predicted trends. Even the two massive cooling flow clusters A1835 and RXJ1347.5-1145 seem to follow the predicted trends. Thus, the observed $y_0 - L_X$ relation gives us confidence that our general understanding of ICM is basically correct. That being said, the quality of the fit is not great in a statistical sense ($\chi^2_\nu = 67.36/16 = 4.21$). The high value of χ^2_ν undoubtedly arises from the random scatter present in the observed relation. The presence of this scatter may be inconsistent with theoretical predictions. We note, however, that observational systematic uncertainties for y_0 and L_X are on the order of 10% each (Reese et al.

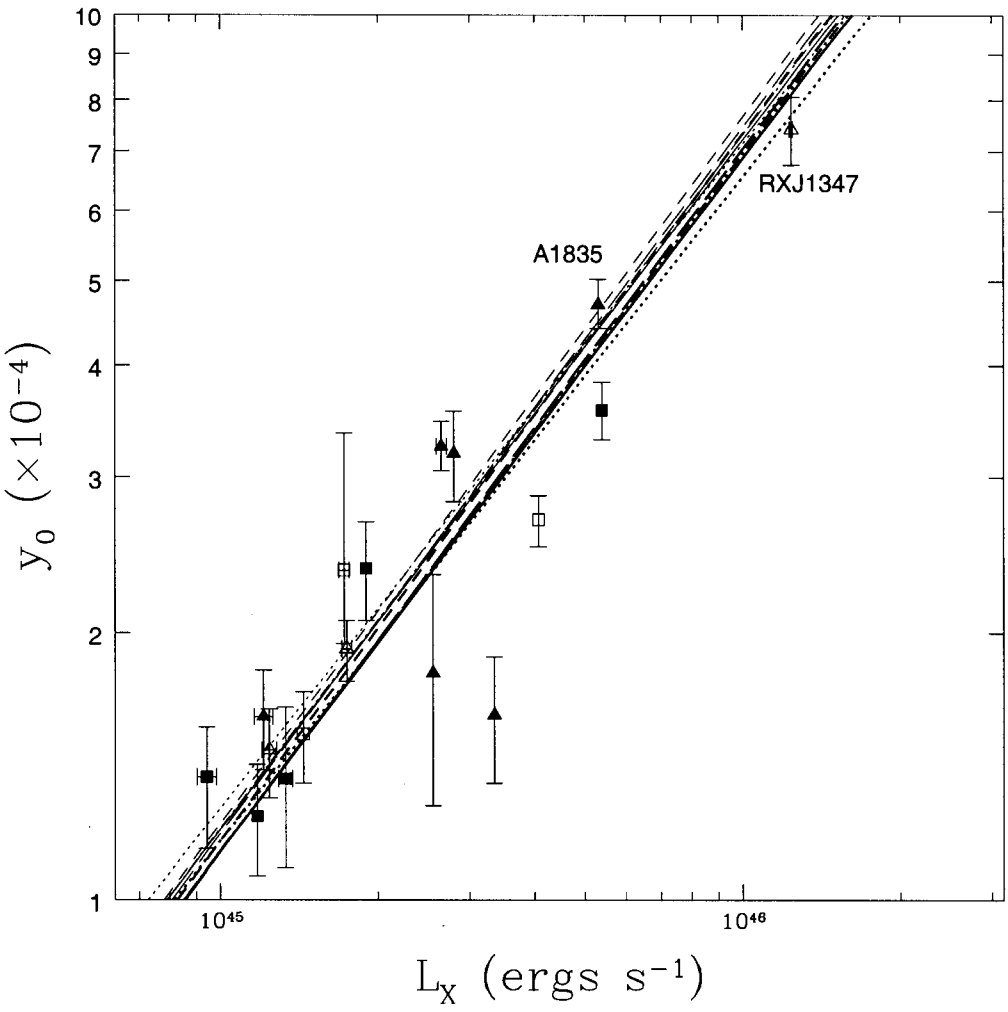

Figure 4.6: The observed and predicted $y_0 - L_X$ relations. The symbols have the same meaning as in Figure 4.1. The dotted, short-dashed, long-dashed, dot-dashed, and solid lines represent the self-similar and $K_0 = 100$, 300, 500, and 700 keV cm^2 entropy floor models, respectively. Thin lines are for $z = 0.2$ and thick lines are for $z = 0.5$.

2002). In addition, Mushotzky & Scharf (1997) have found that estimates of the X-ray luminosities of clusters can vary from study to study by up to 20%, most likely attributable to different measurement techniques. Conservatively estimating the *total* uncertainty on L_X to be 20%, we find a significantly improved fit of

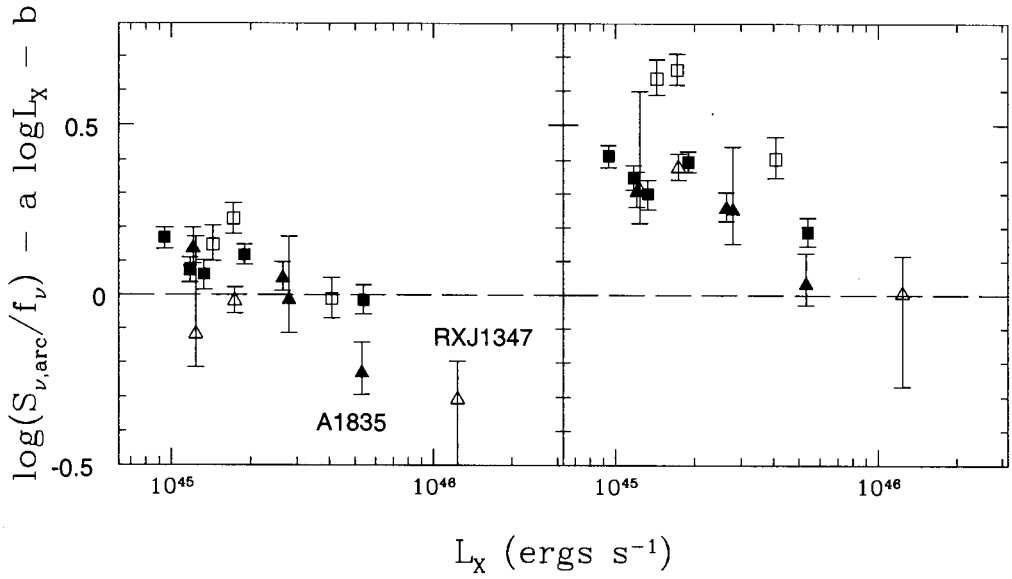

Figure 4.7: Residual plots for the $S_{\nu,arc}/f_\nu - L_X$ relation. *Left:* Residuals from a comparison between the entropy floor model with $K_0 = 310$ keV cm^2 and the observational data ($\chi^2_\nu = 4.27$). Neglecting the two massive "cooling flow" clusters, A1835 and RXJ1347.5-1145, we converge on $K_0 = 385$ keV cm^2 as the best-fit model with $\chi^2_\nu = 1.15$. *Right:* Residuals from a comparison between the self-similar model and the observational data ($\chi^2_\nu = 17.30$). The symbols have the same meaning as in Figure 4.1. For clarity, error bars for the abscissa are not displayed.

$\chi^2_\nu = 19.76/16 = 1.24$. As expected, the entropy floor level is not constrained by the data.

While the $y_0 - L_X$ relation is insensitive to the entropy floor level, the $S_{\nu,arc}/f_\nu - L_X$ relation is not. Fitting all 15 clusters for which we have estimates of both the luminosity and SZ effect flux density, we find a best-fit entropy floor level of $K_0 = 310^{+70}_{-70}$ keV cm^2. However, the fit is not a good one, as is evident from the residuals plotted in Figure 4.7 and the calculated reduced-χ^2 ($\chi^2_\nu = 34.34/14 = 4.27$). The two massive cooling flow clusters A1835 and RXJ1347.5-1145 are obvious outliers. Ignoring these two clusters, we obtain $K_0 = 385^{+75}_{-70}$ keV cm^2 (2σ error bars) and a significantly improved fit ($\chi^2_\nu = 13.79/12 = 1.15$). This best-fit value of K_0 is

consistent with the results of §4.3.2 and §4.3.3 and also with X-ray observations of nearby massive clusters. Splitting the sample into two redshift bins (< 0.3 and > 0.3), we also find there to be no difference in the entropy floors of "nearby" and "distant" galaxy clusters. This is the same as was found for the $S_{\nu,arc}/f_\nu - y_0$ relation.

4.3.6 Summary of Scaling Relations

Every single SZ effect scaling relation that we have examined is consistent with or requires a high value for the entropy floor level, K_0. In fact, several of the trends, such as the $y_0 - T_X$, $y_0 - M(r_{500})$, and $S_{\nu,arc}/f_\nu - y_0$ relations, rule out the standard self-similar model at many sigma. Neither of the relations show any convincing evidence for strong evolution in K_0 out to the limit to which our sample extends ($z \sim 0.7$).

It is interesting that the estimates of K_0 from the various relations do not always agree. For example, the best-fit entropy floors from the $y_0 - T_X$ and $S_{\nu,arc}/f_\nu - T_X$ trends are consistent with results from studies of X-ray scaling relations of nearby massive clusters (e.g., Babul et al. 2002) and the results of our SZ effect-luminosity relations but are marginally lower than the results from our $S_{\nu,arc}/f_\nu - y_0$ and $y_0 - M(r_{500})$ relations. A conservative estimate of the *true* value of K_0, however, must fall in between the results of each of the individual relations; i.e., 300 keV cm^2 $\lesssim K_0 \lesssim$ 600 keV cm^2. This is clearly illustrated in Figure 4.8 through a plot of $\Delta\chi^2$ vs. K_0 for the relations we have examined ($\Delta\chi^2 \equiv \chi^2 - \chi^2_{BF}$ where χ^2_{BF} is the χ^2 for the best-fit power-law model for each of the scaling relations). A naive simultaneous fit to all of the relations, ignoring correlated variables and errors, yields $K_0 = 430^{+60}_{-55}$ keV cm^2 (99% level), which is remarkably similar to that derived solely from X-ray data (c.f. Babul et al. 2002).

At present, it is unclear why some of the scaling relations do not converge on the same value of K_0. A more detailed analysis of this would require taking into account all of the observational and analysis biases (associated with both X-ray and

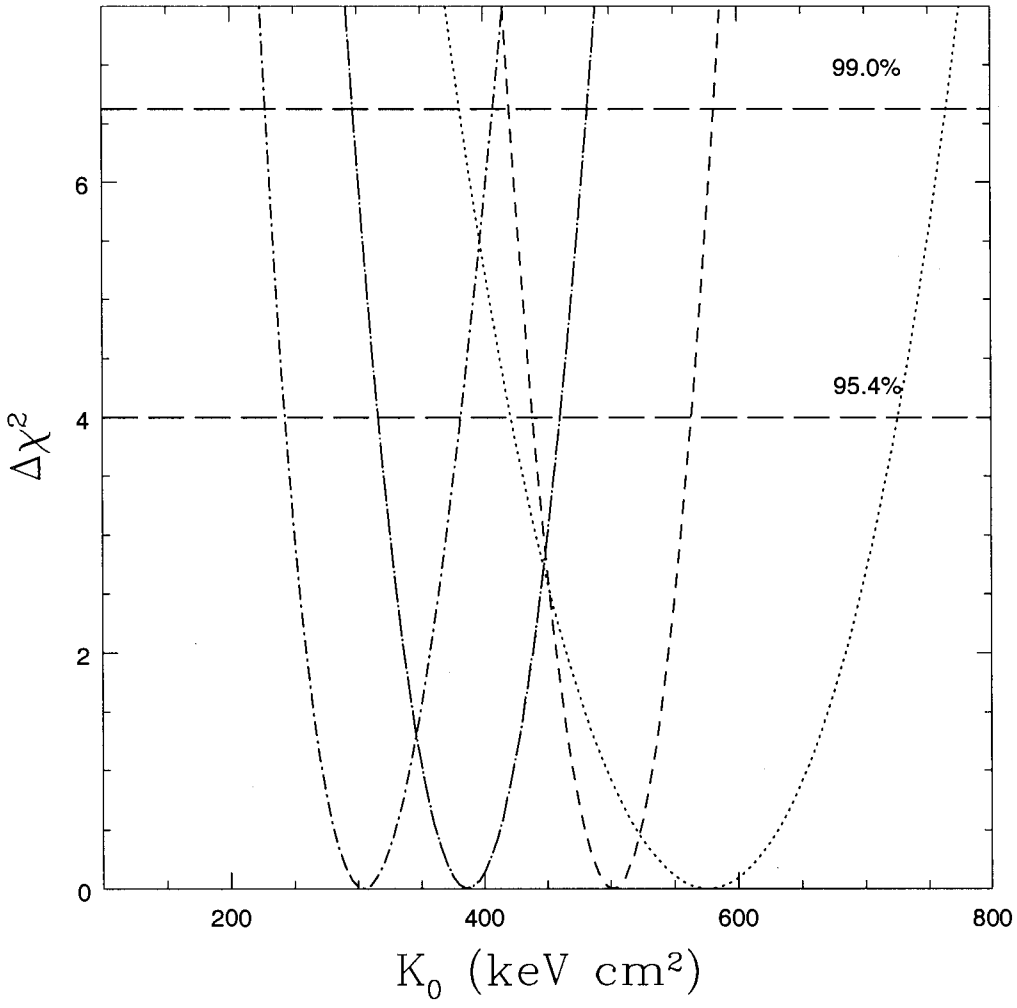

Figure 4.8: Constraints on K_0. The dot-short-dashed, dot-long-dashed, dashed, and dotted lines represent the $y_0 - T_X$, $S_{\nu,arc}/f_\nu - L_X$, $y_0 - M(r_{500})$, and $S_{\nu,arc}/f_\nu - y_0$ relations (the four most entropy floor-sensitive relations), respectively. The cooling flow clusters A1835 and RXJ1347.5-1145 have been excluded from the fits.

SZ effect), which is beyond the scope of this paper. We expect that it will be possible to get a much more firm handle on these differences in the near future. First, the number of high redshift clusters observed through the SZ effect is increasingly rapidly (see Reese et al. 2002) and with it comes improved statistics. Second, and perhaps more important, a number of new experiments (or substantial upgrades

to existing ones) are already under construction and will greatly improve the quality of the SZ effect observations. For example, the bandwidths of the future *SZA* and the upgraded *OVRO* array are expected to be nearly an order of magnitude larger than that of current interferometers and, as such, will lead to substantial improvements in the signal-to-noise ratios of SZ effect data. Tighter constraints on the SZ effect surface brightness profiles of clusters will then be possible and, in turn, more stringent limits can be placed on the entropy distributions of these clusters. Indeed, we demonstrate below that observations with the *SZA* and the upgraded *OVRO* array will allow one to constrain the amount of excess entropy in clusters all the way out to $z \sim 2$ and, best of all, without the need for any X-ray results.

4.4 The Future: Observations with SZA/OVRO

It was briefly discussed in §4.3.1 that current SZ effect data alone cannot tightly constrain the three parameters of the surface brightness β model. A large degeneracy is present in the shape parameters, β and θ_c (e.g., Carlstrom et al. 1996; Grego et al. 2000; 2001). A number of authors have dealt with this problem by using the values of β and θ_c obtained from modeling the *X-ray* surface brightness of the cluster (e.g., Patel et al. 2000; Grainge et al. 2002a; 2002b; LaRoque et al. 2003). In the case of low/intermediate redshift clusters, X-ray observations provide tighter constraints on these parameters than do SZ effect observations. However, a truly X-ray-independent probe of the ICM requires that only SZ effect data be used in the analysis. By using a joint maximum-likelihood fit to both the X-ray and SZ effect surface brightnesses of clusters, Reese et al. (2000; 2002) found a compromise between these two scenarios. Pushing the analysis of the ICM to higher redshifts than considered by Reese et al. (2000; 2002), however, will likely bring us into a regime that is uniquely accessible to SZ effect observations. Fortunately, substantial upgrades are planned for currently operational arrays [for

example, the current *BIMA* and *OVRO* arrays are being upgraded and merged into the Combined Array for Research in Millimeter-wave Astronomy (*CARMA*)[1]] and a number of new interferometers are planned as well (e.g., *SZA*[2], *AMiBA*, and *AMI*; Holder et al. 2000; Lo et al. 2000; Kneissl et al. 2001). These experiments will substantially improve the quality of SZ effect observations. Below, we compare the expected performance of the *SZA* and the (soon to be) upgraded *OVRO* array with the currently operational *BIMA/OVRO* arrays. We show that the degeneracy in the $\beta - \theta_c$ plane is greatly reduced with data from the *SZA* or the upgraded *OVRO* array and this will allow for accurate determinations of y_0 and S_ν and without the need for any X-ray results.

4.4.1 Mock Observations

To compare the arrays, we first generate "mock" observations of model galaxy clusters. We follow a method similar to that outlined by Holder et al. (2000). First, we create a Compton parameter map, $y(\theta_x, \theta_y)$, for each model cluster. These maps are converted into SZ effect intensity decrement maps. Before we can do this, however, we must assume an observing frequency for each of the interferometers. The current *BIMA* and *OVRO* arrays use amplifiers which operate over the range $26 - 36$ GHz (Reese et al. 2000). We assume a frequency centered on 30 GHz for these arrays. The upgraded *OVRO* array and the *SZA* are expected to have amplifiers which operate at $26 - 36$ GHz and at $85 - 115$ GHz. We assume frequencies centered on 30 and 90 GHz for these arrays. Thus, we generate six different decrement maps for each model cluster: 30 GHz maps for the current *BIMA/OVRO* arrays and 30 and 90 GHz maps for the *SZA* and upgraded *OVRO* array.

Interferometers do not image the sky. Rather, they measure the Fourier transform of the SZ effect intensity decrement multiplied by the primary beam. A

[1]For information on the *CARMA* see http://www.mmarray.org

[2]For information on the *SZA* see http://astro.uchicago.edu/sze/survey.html

particular value of this observable is referred to as a "visibility" and is given by

$$V(u,v) = j_\nu \int y(\theta_x,\theta_y) A(\theta_x,\theta_y) e^{2\pi i(u\theta_x + v\theta_y)} d\theta_x d\theta_y \tag{4.8}$$

where u and v are the conjugate variables, θ_x and θ_y are the projected sky coordinates, and $A(\theta_x,\theta_y)$ is the primary beam. At 30 GHz, the sensitivity patterns for the primary beams of the *BIMA* and *OVRO* arrays (both current and upgraded) and the *SZA* are, or will be, well-represented by Gaussians with FWHM $\approx$ 6.6 arcminutes, 4.2 arcminutes, and 10-12 arcminutes, respectively. We assume a FWHM = 10.8 arcminutes for the SZA. For more on the above formalism see White et al. (1999).

We multiply the SZ effect maps by the Gaussian primary beams described above and Fourier transform the result. We discard all visibilities for baselines ($R_{u,v} \equiv \sqrt{u^2+v^2}$) that are not probed by these interferometers. At 30 GHz, the *BIMA* and *OVRO* arrays probe multipole moments of $\ell = 2\pi R_{u,v} \gtrsim 4000$ and 7000, respectively. We assume uniform coverage over the ranges $4200 \lesssim \ell \lesssim 20000$ and $7200 \lesssim \ell \lesssim 20000$ for these arrays, respectively. The smaller 3.5 m dishes of the *SZA* will be able to probe shorter baselines (larger angular scales) and are expected to sample $\ell \gtrsim 2000$. We assume uniform coverage over the range $2400 \lesssim \ell \lesssim 20000$ (also at 30 GHz).

Finally, we add random Gaussian noise to each of the mock observations. At 30 GHz, we assume system temperatures (scaled to the atmosphere) of 45 K for the *BIMA* and *OVRO* arrays and 30 K for the *SZA*. At 90 GHz, we assume system temperatures of 100 K for the *SZA* and for the upgraded *OVRO* array. The current *BIMA/OVRO* arrays have effective noise bandwidths of approximately 550/1000 MHz, while both the upgraded *OVRO* array and the SZA are expected to have bandwidths of 8 GHz. A total integration time of 40 hours is assumed for each of the arrays at both 30 and 90 GHz. For specificity, the mock observations for the current *BIMA* and *OVRO* arrays have rms noise levels of approximately 150 μJy

beam^{-1} and 70 μJy beam^{-1}, respectively, while the upgraded *OVRO* array has noise levels of 25 μJy beam^{-1} and 50 μJy beam^{-1} at 30 and 90 GHz (respectively) and the *SZA* has noise levels of 40 μJy beam^{-1} and 140 μJy beam^{-1} at 30 and 90 GHz, respectively.

4.4.2 Analysing the Mock Observations

To analyse the mock observations, we follow the method described in a number of observational papers based on genuine *BIMA/OVRO* data (e.g., Carlstrom et al. 1996; Grego et al. 2000; 2001; Reese et al. 2000; 2002; Joy et al. 2001; LaRoque et al. 2003). We model the observations with the isothermal β models[3]. We create model SZ effect maps for for various choices of the three free parameters (y_0, θ_c, and β), multiply the maps by the appropriate primary beams, Fourier transform the maps, and compare the results to the mock observations in §4.4.1 via a χ^2 statistic. The best-fit parameters are those which result in the minimum value of χ^2. Note that the comparisons between the β models and the mock observations are done in the Fourier domain (also referred to as the $u-v$ plane), where the noise characteristics and spatial filtering of the interferometers are well understood. Like the observers, we do not "deconvolve" the mock observations for analysis.

To demonstrate the quality of the data to be produced by the *SZA* and the upgraded *OVRO* array, we plot in Figure 4.9 confidence contours for the β and θ_c parameters from "observations" of a $T_X = 6.7$ keV ($M_{tot} \approx 5.6 \times 10^{14} M_\odot$) cluster at $z = 1$. The third free parameter, y_0, is allowed to assume its best-fit value at each pair of β and θ_c (i.e., the plot is a projection of the confidence "volume" onto the $\beta - \theta_c$ plane). The contours correspond to a $\Delta\chi^2$ and the filled squares indicate the best-fit models. The projection of $\Delta\chi^2 = 1$ line onto the axes gives the 68% confidence interval for each of the two parameters. The contour labeled "current" is the result of fitting the SZ effect surface brightness model to the mock

[3]Note. — we do not assume that the model cluster used to make the mock observations is necessarily isothermal.

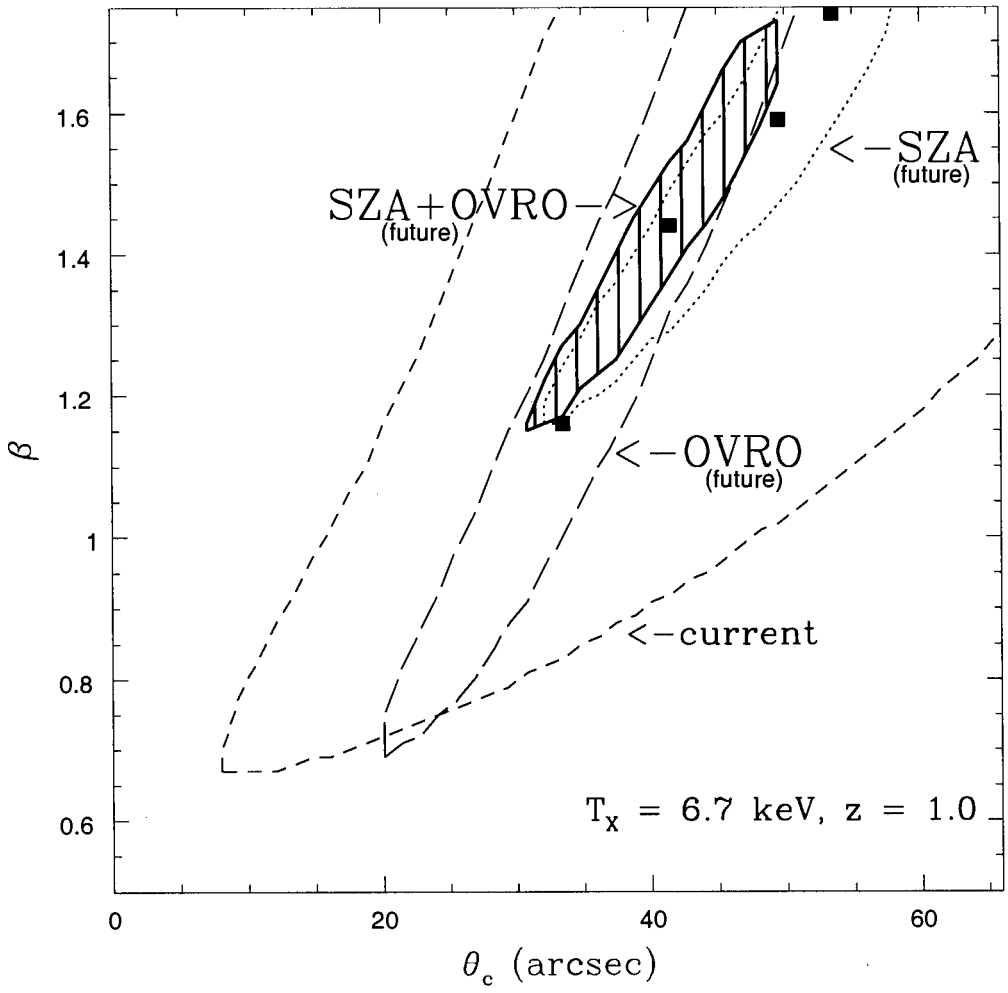

Figure 4.9: Comparison of constraints on the surface brightness profile of a distant, massive cluster. The filled squares indicate the best-fit parameters from modeling "mock" observations of the model cluster (the square at $\beta = 1.74$ is for "current" data while the square at $\beta = 1.59$ is for "SZA" data). The contours give the 68% confidence regions on the two parameters ($\Delta\chi^2 = 1$). The normalization, y_0, is allowed to assume its best-fit value at each point in the plot (see text).

observations with the currently operational *BIMA/OVRO* arrays (both arrays have similar sensitivity patterns). The contours labeled "SZA" and "OVRO" are the results of simultaneously fitting the surface brightness model to the mock 30 and

90 GHz *SZA* observations and the mock 30 and 90 GHz upgraded *OVRO* observations, respectively. Lastly, the contour labeled "SZA+OVRO" is the result of simultaneously fitting all four upgraded OVRO and SZA mock observations.

First, it is obvious that the "current" mock observational data do not tightly constrain β and θ_c and, furthermore, these parameters are strongly correlated, as found when modeling genuine *BIMA/OVRO* data (see, e.g., Fig. 3 of Grego et al. 2000; Fig. 2 of Grego et al. 2001). This gives us confidence that we have produced realistic mock observations. The large degeneracy in the $\beta - \theta_c$ plane is why a number authors elect to use X-ray constraints on these parameters instead or, in the case of Reese et al. (2000; 2002), use a simultaneous fit to both X-ray and SZ effect data. However, data from the upcoming *SZA* and the upgraded *OVRO* array will be able to place much tighter constraints on these parameters (compare the "OVRO" and "SZA" contours with the "current" contour). Note that the correlation between β and θ_c remains for the *SZA* and *OVRO* "data", but its size has been dramatically reduced. A simultaneous fit to both the *SZA* and upgraded *OVRO* data yields even better constraints on these parameters (shaded region).

To get an idea of how well the future SZ effect data can constrain K_0, the entropy floor level, we use the 68% confidence volume (β, θ_c, y_0) for the "SZA+OVRO" contour to "measure" y_0 and $S_{\nu,arc}/f_\nu$. The inferred statistical uncertainty associated with the central Compton parameter and integrated SZ effect flux density within the central 1 arcminute for this cluster is only about 10% and 15%, respectively. Comparing this to the predicted $S_{\nu,arc}/f_\nu - y_0$ relations (Figure 2 of MBHB03), it should, therefore, be possible to constrain the entropy floor level of this cluster to within 50-75 keV cm^2 or so. This is comparable with statistical uncertainties associated with X-ray measurements of nearby clusters. This is remarkable considering that no X-ray "data" was used in the analysis and the cluster lies at $z = 1$. We also find that reasonably accurate measurements of K_0 are possible for clusters all the way out to $z \sim 2$.

The *SZA* and upgraded *OVRO* array will be excellent tools for probing the

non-gravitational entropy of distant clusters. Because X-ray data will not be required to constrain the shapes of the SZ effect surface brightness profiles of clusters observed with these planned interferometers, comparisons of data to predicted scalings (such as $S_{\nu,arc}/f_\nu - y_0$) will provide *independent* constraints on the properties of the intracluster gas. It will then also be possible to take advantage of the redshift-independence of the SZ effect and monitor the evolution of non-gravitational processes in clusters right back to the epoch of cluster formation itself.

4.5 Discussion

Up until now, measurements (both direct and indirect) of the entropy floors of massive galaxy clusters have been limited to X-ray observations. Furthermore, these past X-ray studies have generally focused on nearby ($z \sim 0$) clusters and, as such, little is known about the evolution of the entropy floor (and the non-gravitational processes that produce it) with cosmic time. In the companion paper, we explored the extent to which the thermal Sunyaev-Zeldovich effect is modified by the presence of an entropy floor. Because it depends differently on the temperature and density of ICM and, also, because it is redshift-independent, the SZ effect could potentially be a very powerful, independent test of the entropy floors of even the most distant galaxy clusters.

The central focus of the present paper was to compare our theoretical relations from MBHB03 (including one that can potentially be measured through SZ effect observations only) to available high redshift SZ effect data from the literature to determine if the SZ effect data support the presence of an entropy floor and, if so, how does the inferred level of that floor compare with that required to match local X-ray trends. This is the first time such a comparison has been done and we have made use of the largest compilation of high z SZ effect clusters to date. A detailed analysis of seven different SZ effect scaling relations indicates that the

entropy floor in clusters with $0.14 \lesssim z \lesssim 0.78$ is between 300 keV cm^2 $\lesssim K_0 \lesssim$ 600 keV cm^2 and there are no strong indications for evolution in K_0 over that redshift interval. Our estimate for the value of K_0 is remarkably similar to that derived from studies of X-ray scaling relations of nearby ($z \sim 0$) massive clusters, which suggest that $K_0 \gtrsim 300$ keV cm^2 (e.g., Tozzi & Norman 2001; Babul et al. 2002; McCarthy et al. 2002a).

At present, the source (or sources) of the "excess" entropy is still not known. What constraints can be placed on the possible sources by the results of the present study? First, as in previous studies of X-ray scaling relations, our analysis indicates that the entropy of the ICM has been significantly raised by some non-gravitational process(es). In terms of thermal energy, this corresponds to a few keV per particle for massive clusters. This means that supernovae explosions probably cannot be the sole contributor to the entropy floor, since they are expected to impart $\lesssim 0.3$ keV per particle (e.g., Valageas & Silk 1999; Balogh et al. 1999; Wu et al. 2000). This was previously known but the present study, which offers an independent examination of the ICM, reinforces this conclusion. Recently, it has been speculated that quasar outflows could be source of the excess entropy (e.g., Nath & Roychowdhury 2002). The entropy requirements deduced in the present study (and previous X-ray studies) are probably met by quasar outflows but it isn't yet known what mechanism (if any) couples the outflows to the ambient ICM. Alternatively, and somewhat paradoxically, radiative cooling has also been shown to raise the mean entropy of ICM. It is possible that cooling in combination with supernovae and/or quasar outflows could be responsible for the observed SZ effect and SZ effect-X-ray relations. Whatever the source may be, it must reproduce the fact that K_0 does not change significantly out to $z \sim 0.7$. It could well be that this trend will become a critical piece of information for discriminating between the various theoretical models currently being proposed. An unchanging value of K_0 with redshift is obviously consistent with the generic "preheating" scenario; however, it remains to be seen whether it is consistent with more realistic heating models that distribute

entropy non-uniformly and over an extended periods of time. Without a detailed analysis, it is difficult to say whether or not it is consistent with radiative cooling contributing significantly to the excess entropy. We are currently in the process of examining the effects of radiative cooling on SZ effect scaling relations (c.f. the discussion in the companion paper, MBHB03).

Current SZ effect data cannot tightly constrain the surface brightness profiles of clusters. This prevents the SZ effect from being used as an independent (of X-ray) probe of the entropy floor and the ICM in general. Thus, any advantages that the SZ effect has over the X-ray emission (e.g., redshift independence) are severely diminished because X-ray data is needed to help constrain the shape of the surface brightness profiles. Therefore, an additional aim was to examine the ability of the next generation of SZ effect experiments to probe non-gravitational entropy in distant clusters. We have shown that the *SZA* and the upgraded *OVRO* array will produce high signal-to-noise data that will allow one to tightly constrain the surface brightness profiles of even very distant clusters and without the need for any X-ray results. As in the present study, these surface brightness profiles can then be compared to theoretical predictions in order to place stringent constraints on the level of the entropy floor. It will be very interesting to see if the trend of constant K_0 (with redshift) deduced here holds up and, if so, to determine how far back in redshift it extends.

Aside from the appearance and structure of individual clusters, our work has implications for universal SZ effect quantities, such as the SZ effect angular power spectrum, SZ effect cluster source counts, and the mean Compton parameter of the universe. These quantities can be used to measure cosmological parameters and test cluster formation scenarios (see Carlstrom, Holder, & Reese 2002 for a comprehensive review). A number of studies have already examined how non-gravitational gas physics modifies these quantities (e.g., Holder & Carlstrom 2001; Cavaliere & Menci 2001; da Silva et al. 2001; Springel et al. 2001; White et al. 2002). However, none of these studies have invoked entropy injection at the high

level estimated in the present analysis. Generally, low levels of entropy injection ($K_0 \sim 100$ keV cm^2), which are consistent with X-ray measurements from low mass groups (Ponman et al. 1999), were implemented. We are in the process of investigating how the power spectrum, source counts, and mean Compton parameter are modified by higher initial entropies.

We thank Erik Reese for making available his SZ effect data prior to publication. We also thank Ann Gower, John Carlstrom, Peng Oh, Kathy Romer, and Mark Voit for helpful discussions. A. B. would like to acknowledge the hospitality extended to him by the Canadian Institute for Theoretical Astrophysics during his tenure as CITA Senior Fellow. I. G. M. is supported by a postgraduate scholarship from the Natural Sciences and Engineering Research Council of Canada (NSERC). A. B. is supported by an NSERC operating grant, G. P. H. is supported by the W. M. Keck Foundation, and M. L. B. is supported by a PPARC rolling grant for extragalactic astronomy and cosmology at the University of Durham.

Chapter 5

On the Relationship between Cooling Flows and Bubbles

Abstract

A common feature of the X-ray bubbles observed in *Chandra* images of some "cooling flow" clusters is that they appear to be surrounded by bright, cool shells. Temperature maps of a few nearby luminous clusters reveal that the shells consist of the coolest gas in the clusters — much cooler than the surrounding medium. Using simple models, we study the effects of this cool emission on the inferred cooling flow properties of clusters. We find that the introduction of bubbles into model clusters that *do not* have cooling flows results in temperature and surface brightness profiles that resemble those seen in nearby "cooling flow" clusters. They also approximately reproduce the recent *XMM-Newton* and *Chandra* observations of a high minimum temperature of ~1-3 keV. Hence, bubbles, if present, must be taken into account when inferring the physical properties of the ICM. In the case of some clusters, bubbles may account entirely for these observed features, calling into question their designation as clusters with cooling flows. However, since not all nearby "cooling flow" clusters show bubble-like features, we suggest that there may be a diverse range of physical phenomena that give rise to the same observed features.

5.1 Introduction

Observations obtained with the *Chandra* and *XMM-Newton* X-ray Observatories have yielded a number of important results that have changed our view of galaxy groups and clusters, especially those systems that have been termed "cooling flow" clusters[1]. For example, *Chandra*'s exquisite spatial resolution has allowed for much more detailed analyses of the X-ray surface brightness depressions (referred to as "bubbles" or "holes") discovered in earlier *ROSAT* images of several nearby "cooling flow" clusters (Fabian et al. 2000; Schmidt et al. 2002; Heinz et al. 2002; Blanton et al. 2001; 2003). High quality *Chandra* data is also responsible for the discovery of many new bubbles (or bubble-like features) in a number of other groups and clusters (e.g., McNamara et al. 2000; 2001; Schindler et al. 2001; Mazzotta et al. 2002; Johnstone et al. 2002; Young et al. 2002; Sanders & Fabian 2002; Smith et al. 2002). It now seems that such bubbles are a fairly common constituent of "cooling flow" clusters.

Another important result, derived with *XMM-Newton* data, is the lack of spectral evidence for gas cooling to temperatures below a few keV (e.g., Peterson et al. 2001; 2003; Kaastra et al. 2001; Tamura et al. 2001). Possible explanations for this unexpected behavior include heating of the cooling flows by AGN outflows and/or thermal conduction, rapid mixing of the low temperature gas, and inhomogeneous metallicity distributions in the ICM (e.g., Peterson et al. 2001; Ciotti & Ostriker 2001; Narayan & Medvedev 2001; Fabian et al. 2002a; 2002b; Churazov et al. 2002; Ruszkowski & Begelman 2002; Kaiser & Binney 2003; Morris & Fabian 2003).

[1]The designation *"cooling flow" cluster* refers to a system that has a sharply rising surface brightness profile and a declining temperature profile towards the center. These observational characteristics have typically been interpreted as manifestations of an ICM that is radiatively cooling on short timescales. The cooling gas flows inward toward the cluster center (hence, the name cooling flow). When we use the phrase "cooling flow" (in quotation marks) we are referring to the observational characteristics and not a physical model.

The near simultaneous discovery of the connection between bubbles and "cooling flow" clusters, and the high minimum temperatures in clusters raises the question: are these phenomena related? As we already mentioned, it has been hypothesized that heating by a central AGN could quench the cooling flows. Recent numerical simulations show that heating the ICM near the cluster core can also give rise to bubble-like features that resemble those seen in the *Chandra* images (e.g., Churazov et al. 2001; Quilis et al. 2001; Brighenti & Mathews 2002a). However, it still is not clear *how* the AGNs or the bubbles they produce could heat up cooling flows, e.g. through shocks, cosmic rays, or Compton heating, or whether this heating would be sufficient to offset the radiative losses and establish the observed high minimum temperature (see, e.g., Fabian et al. 2002a; Brighenti & Mathews 2002b). We speculate that there could be an even simpler connection between the bubbles, "cooling flow" clusters, and the high minimum temperatures of clusters.

A common feature of the X-ray bubbles present in the *Chandra* images is that they appear to be partially or fully surrounded by cool, bright shells. In fact, high resolution cluster temperature maps of Perseus and A2052 (see Fig. 6. of Schmidt et al. 2002; Fig. 10. of Blanton et al. 2003), two nearby X-ray bright clusters which have probably yielded the best constraints on bubble properties, reveal that the shells consist of the coolest gas in the clusters; much cooler than surrounding ambient medium. What are the effects of these bright, cool shells on the inferred cooling flow properties of clusters? It is clear that if the emission from the bubbles is relatively important, it will have an impact on both the azimuthally-averaged surface brightness and emission-weighted temperature profiles. Since the cooling flow properties of clusters (e.g., the cooling time, mass deposition rate, age and size of the cooling flow) are deduced from these profiles, they will also be affected. To date, however, the effects that bubbles have on the inferred properties of gas in the cores of clusters have not been studied theoretically or observationally.

In this Letter, we explore how the presence of bubbles affects the surface bright-

ness and temperature (kT_{ew}) profiles of clusters. We show that the introduction of bubbles into non-cooling flow model clusters results in profiles that closely resemble those observed in nearby "cooling flow" clusters that clearly contain bubbles (but which have not been excised from the analysis of those clusters). This implies that the bubbles have a significant impact on the inferred cooling flow properties of these clusters and, in the case of some clusters, may account for the entire "cooling flow".

5.2 Model Clusters with Bubbles

To ascertain the effects of bubbles on the general appearance of clusters, we make use of analytic "preheated" cluster models developed in Babul et al. (2002). Since an in-depth discussion of the models can be found in that study, we give only a very brief description here.

The distribution of the dark matter in the model clusters is assumed to be the same as that found in recent high resolution numerical simulations. The intracluster gas, preheated to a uniform 'entropy' ($\equiv kT_e n_e^{-2/3}$) of 300 keV cm^2, is assumed to be in hydrostatic equilibrium within the cluster potential well. The preheated models (with entropy floors $\gtrsim$ 300 keV cm^2) have been shown to provide an excellent match to the observed *global* X-ray and thermal Sunyaev-Zeldovich effect properties of groups and clusters (Balogh et al. 1999; Babul et al. 2002; McCarthy et al. 2002a; 2003b). A welcome by-product of the high level of preheating is that the cooling timescale of the ICM is greater than the age of the Universe (for $H_0 =$ 75 km s^{-1} Mpc^{-1}, $\Omega_m = 0.3$, and $\Omega_\Lambda = 0.7$ at $z = 0$, which we assume throughout) for groups up to moderate mass clusters. Thus, the complicated effects of radiative cooling and cooling flows (which are neglected by the Babul et al. 2002 models) are unimportant for these model clusters. Because there are no cooling flows, it is straightforward to quantify the effects of the cool bubble shells on the surface brightness and emission-weighted temperature profiles.

For the bubbles, we use the *Chandra* images of Perseus and A2052 as a guide. Each model bubble consists of a spherical 'cavity' surrounded by a spherical shell[2]. Schmidt et al. (2002) and Blanton et al. (2001; 2003) argue that any gas filling the 'cavities' must be hot ($kT_e \gtrsim 20$ keV) and have a low density. We assume a constant cavity temperature of 20 keV. The density distribution of the cavities is set by requiring that they are in pressure equilibrium with the bubble shells and the ambient ICM. This, combined with the high temperature, insures that the density is quite low and, consequently, the cavities are X-ray-deficient (as observed). As expected, use of higher cavity temperatures (i.e., lower densities) gives very similar results. The radius of the cavities is assumed to be 7 kpc, approximately the mean value of the bubbles observed in Perseus and A2052 (scaled to our assumed cosmology). For the shells, Blanton et al. (2001; 2003) find a deprojected temperature of about 1 keV. We assume this temperature, although changing the temperature by up to 50% does not significantly modify the results (see Fig. 5.2). Again, the density distribution is set by requiring that the shells are in pressure equilibrium with the surroundings. A shell thickness of 3.5 kpc is assumed. Two of these (identical) bubbles are placed near the center of each model cluster. The bubbles are placed in opposite hemispheres with equal distances from the cluster center, and perpendicular to the line-of-sight. We have also experimented with other orientations (e.g., bubbles overlapping) but the qualitative results remain generally unaffected.

A surface brightness map of a typical model cluster with bubbles is displayed in Figure 5.1. As observed, the shells have been significantly 'limb-brightened' (especially near the cluster center). With an emission-weighted temperature of $\sim$ 3 keV at a projected radius of about 50 kpc, beyond the outer radius of the bubble shells, this particular model cluster roughly resembles A2052.

[2]For simplicity, we assume that the shells completely surround the cavities, even though this does not appear to be the case for all of the observed bubbles.

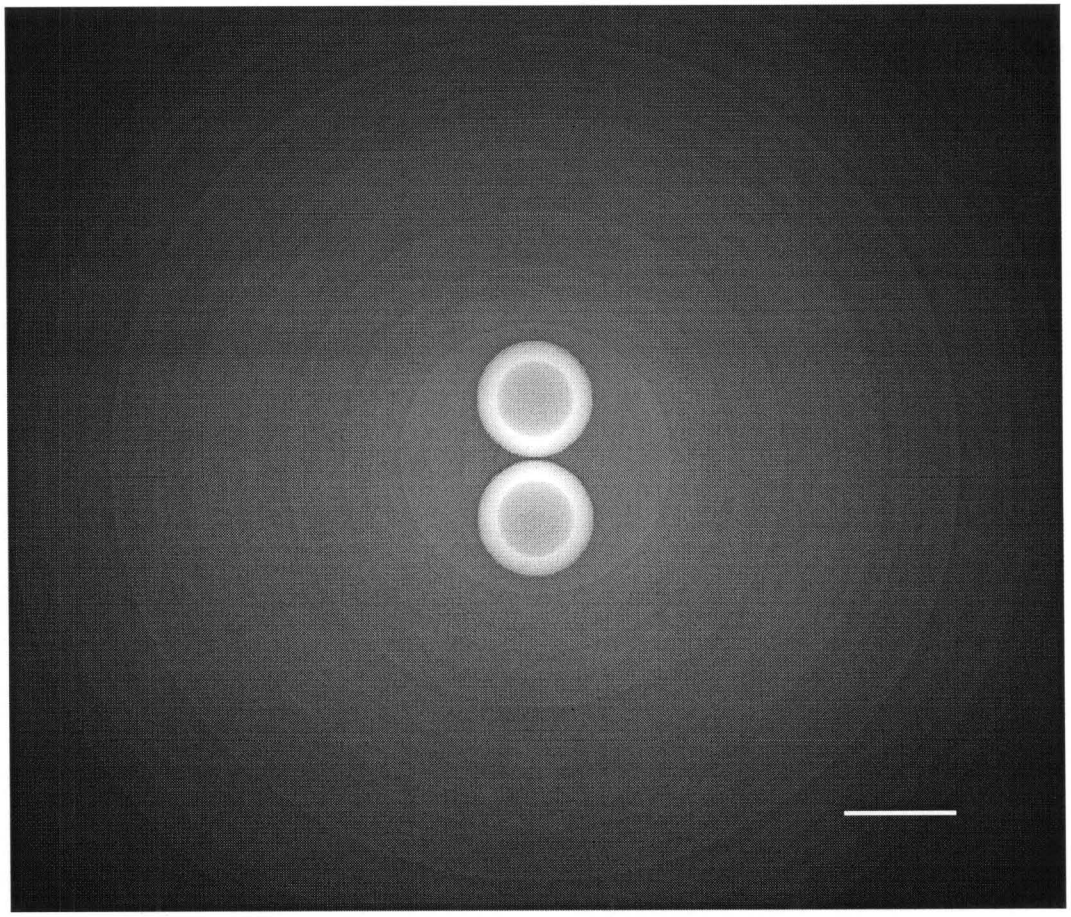

Figure 5.1: Bolometric surface brightness map of a typical model cluster. The surface brightness is displayed in logarithmic scale. The solid white line indicates a length of 20 kpc.

5.3 Results

In Figure 5.2, we plot the predicted emission-weighted temperature profiles of two model clusters. As expected, the addition of the bubbles with cool shells leads to a decrease in the emission-weighted temperature towards the center of the cluster. The magnitude and scale over which the drop occurs, however, is surprising. The temperature, kT_{ew}, declines from ≈ 3 keV to ≈ 2 keV in the case of the lower mass cluster and from ≈ 6 keV to ≈ 2.5 keV for the more massive cluster. Furthermore,

both model clusters (in fact, all of the model clusters that we examined) show a slow decline, almost a core, in the temperature profile near the very centers of the clusters and the minimum temperatures are quite similar ($\sim$ 2 keV). These predicted trends roughly match those seen in nearby "cooling flow" clusters (that contain bubbles). This is surprising since it implies that the cool shells alone could be entirely responsible for the observed temperature dips and the surface brightness peaks (i.e., cooling flows may not be necessary for these clusters). It should be kept in mind that the bubble shells have very low masses ($\sim 10^9 M_\odot$) and only occupy $\approx$ 18% (combined) of the total volume within the central 21 kpc. Any mass deposition rates inferred from such clusters that do not excise the cool shell emission will grossly overestimate the true cooling rate.

The temperature dips seen in Fig. 5.2 are obviously confined within the (projected) outer radius of the bubble shells (in this case about 21 kpc). An interesting question, therefore, is do the observed temperature gradients in clusters with bubbles extend beyond the outer radius of the observed bubbles? If so, this would immediately imply that the bubble shells cannot be *solely* responsible for the gradients. A close examination of Fig. 2 of Blanton et al. (2001) suggests that the gradient of A2052 does, indeed, begin very near the outer edge of the bubble shells. Similar, although somewhat less clear-cut, trends are seen in Virgo (Fig. 5 of Young et al. 2002), Hydra A (Figs. 1 & 3 of McNamara et al. 2000), A133 (Figs. 1 & 9 of Fujita et al. 2002), MKW3S (Figs. 1 & 3 of Mazzotta et al. 2002), Cygnus A (Figs. 1 & 8 of Smith et al. 2002) and A2199 (Figs. 2 & 3 of Johnstone et al. 2002). Thus, the simplistic model we have proposed seems to provide a viable explanation for the gradients in these clusters. However, the model does not appear to be compatible with the *Chandra* observations of Perseus (Schmidt et al. 2002). The gradient in that cluster extends well beyond the outer radius of the two bubbles situated near the center of the cluster. We note that there are at least two other bubbles at larger radii but they do not seem to have bright shells. Unless the bubbles *had* bright shells that somehow became dissociated from the

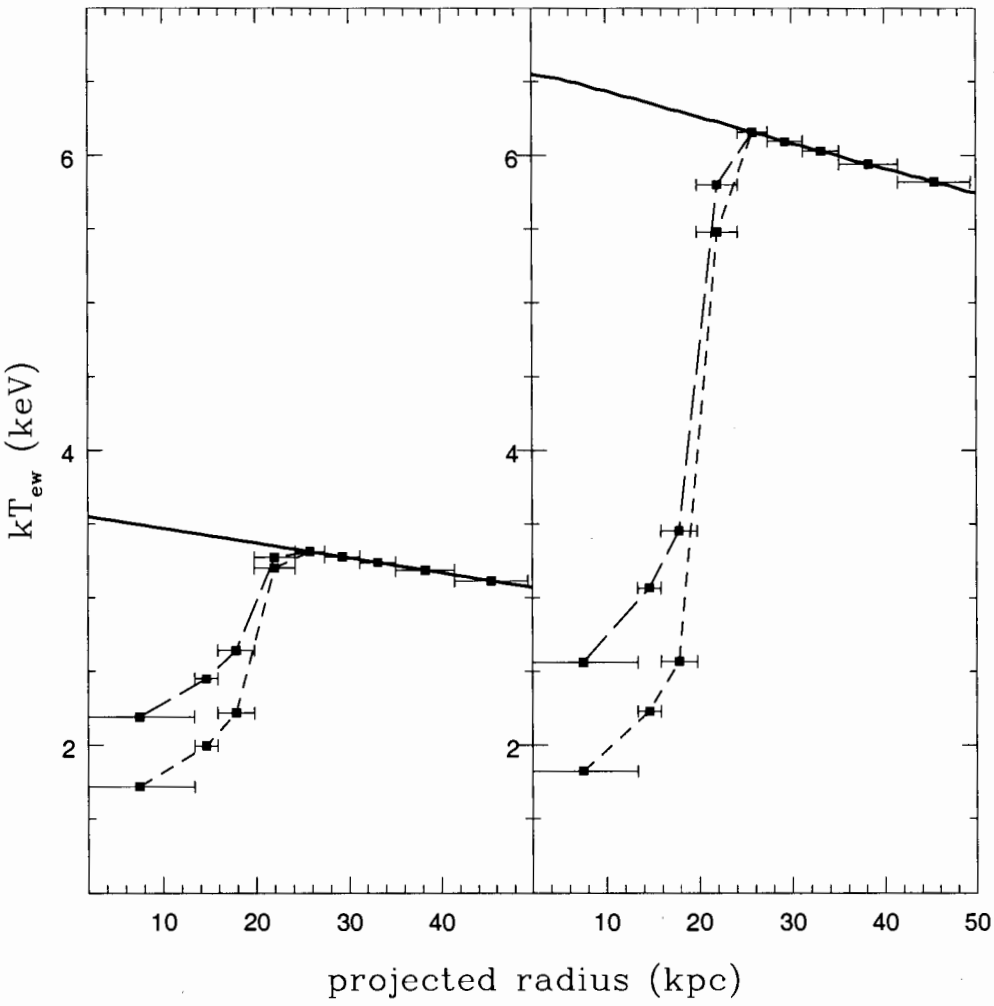

Figure 5.2: Predicted emission-weighted temperature profiles. *Left:* Profile of the cluster displayed in Fig. 5.1. *Right:* Profile of a more massive cluster. The thick solid lines are the profiles *prior* to placing the bubbles in the cluster. The long-dashed and short-dashed lines are the profiles assuming shell temperatures of 1 keV and 0.8 keV, respectively. The solid squares indicate the radial bins from which the temperatures were extracted, while the error bars indicate the bin widths (which are similar to those used in the analyses of Perseus and A2052).

cavities and were distributed throughout the ambient ICM, it is difficult to see how our model could reproduce the entire temperature gradient of Perseus. Even

so, the shells of the two interior bubbles certainly influence the gradient near the center of the cluster (note the temperature jump at 50 kpc in Fig. 2 of Schmidt et al. 2002).

What about the surface brightness profiles? Figure 5.3 is a plot of the predicted bolometric surface brightness profile of the model cluster displayed in Fig. 5.1. It is readily apparent that the addition of bubbles with bright shells results in a sharp peak in the surface brightness profile of the model cluster. This trend holds true for both higher and lower mass model clusters as well. Use of the isothermal β model reveals an emission excess at the cluster center. Near the cluster center, the surface brightness has been enhanced by a factor of three, which is very similar to what is observed in A2052. Such excess emission is often interpreted as an indicator for the presence of cooling flows (e.g., Blanton et al. 2003) but there are no cooling flows in our model clusters.

5.4 Discussion

We have developed a simple toy model that qualitatively reproduces the surface brightness and temperature trends of nearby "cooling flow" clusters that contain bubbles. Because our models do not have cooling flows, this suggests that the bubbles have significant effects on the observed profiles and perhaps explain them entirely (without the need for a massive cooling flow). Without taking into account the cool emission from the bubble shells, estimates of the total mass drop out due to radiative cooling would be orders of magnitude too high. Thus, our model potentially explains the longstanding problem of why only relatively small amounts of atomic and molecular gas have been found in the centers of "cooling flow" clusters (e.g., Donahue et al. 2000), at least for some clusters (such as A2052). However, there do exist some "cooling flow" clusters that do not have bubbles. Abell 2029, for example, is a seemingly relaxed cluster with a temperature gradient that extends out to nearly 260 kpc (Lewis et al. 2002). This suggests that observational

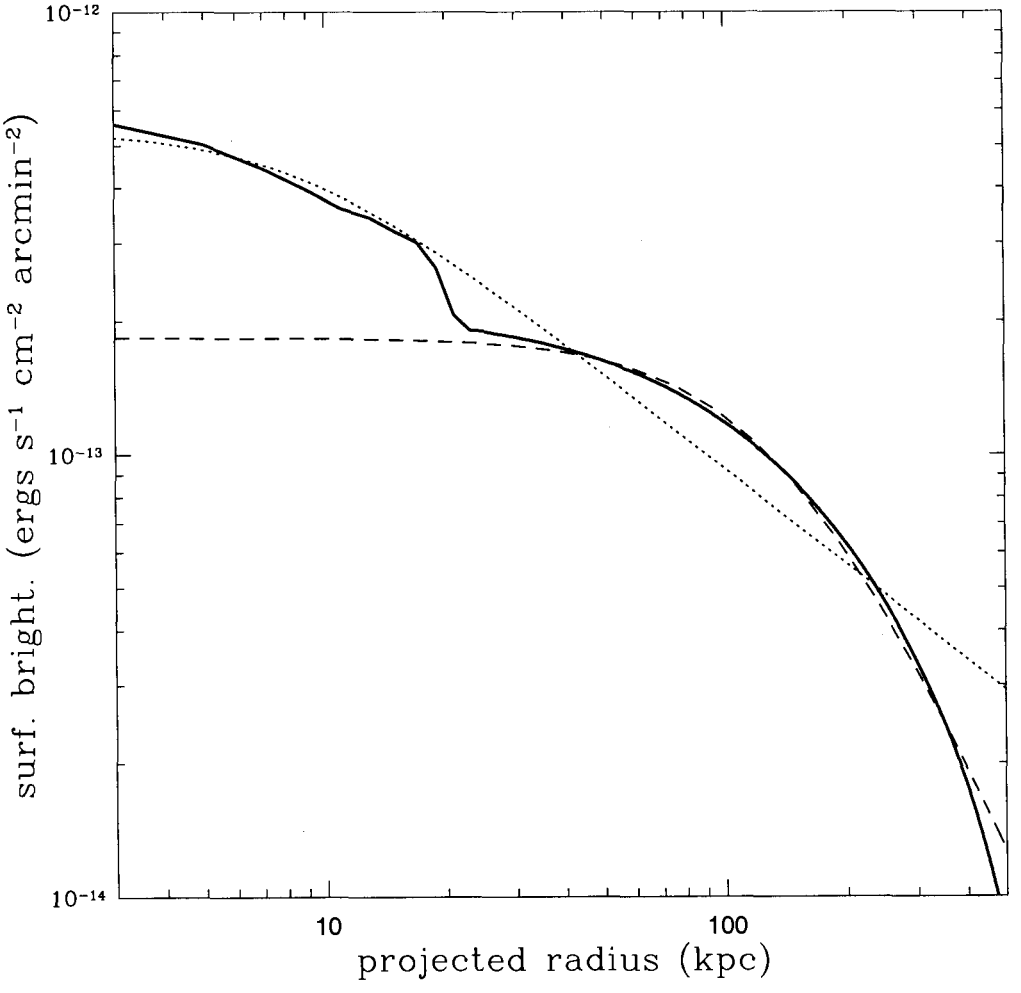

Figure 5.3: Predicted bolometric surface brightness profile of the cluster displayed in Fig. 5.1. The thick solid line is the resulting profile after the bubbles have been placed in the cluster. The dotted line is the best-fit isothermal β model, while the dashed line is the best-fit isothermal β model excluding the central 30 kpc. The sharp kink at $\approx$ 20 kpc is an artifact of the simplistic geometry we have assumed for the bubbles. A more realistic geometry would result in a smoother surface brightness profile.

features that have come to be characterized as manifestations of cooling flows may in fact be due to a wider range of physical phenomena. As noted earlier, the observed properties of Perseus, for example, may be due to several processes, of

which the bubbles are one.

The results of the present study hinge on the properties of our model bubbles and, in particular, their shells. For the purposes of simplicity, the shell properties (i.e., geometry, size, temperature) were *chosen* to roughly match the *Chandra* images of Perseus and A2052, probably the most clearcut cases. But what physical mechanism(s) can give rise to such cool shells? A number of proposals have recently been put forward. The shells could consist of low entropy gas that was lifted by the bubble from the cluster center and cooled through adiabatic expansion as the bubble floated to larger cluster radii (e.g., Churazov et al. 2001; Soker et al. 2002; Nulsen et al. 2002). Alternatively, the shells (or shell-like structures) could be cool gas from the central cD galaxy that was displaced by a recent merger event (Ricker & Sarazin 2001), the result of instabilities that were induced by the interaction between the gas around the cD galaxy and the ICM (Fujita et al. 2002), or the result of thermal instabilities that were triggered by radio jets. Whatever the mechanism, the shells should not be regarded as merely re-organized cooling flows, since the radiative cooling time of the gas in the shells is apparently larger than the age of the bubbles, at least for the limited number of bubbles studied in detail to date (Soker et al. 2002; Nulsen et al. 2002).

The cooling time of the gas in the shells may not necessarily be long relative to the age of the bubbles for all clusters. In the absence of a significant source of heating, the gas would cool quickly. This would obviously conflict with the lack of X-ray emission lines below ~ 1 keV or so in "cooling flow" clusters (e.g., Peterson et al. 2001). Thermal conduction has been proposed as a way of explaining the lack of very cool gas in clusters (e.g., Narayan & Medvedev 2001; Fabian et al. 2002b), but this is over large scales. In the case of cool shells, conduction would be more efficient since it would be acting over smaller scales with a much steeper temperature gradient. In addition, the process of bubble formation itself could help to disentangle the magnetic fields in and around the bubbles shells, perhaps allowing conduction to proceed near the Spitzer rate. We suggest the shells could

be reheated through conduction and eventually disappear when, for example, the jets causing the thermal instabilities cease or when the magnetic fields become disentangled enough to allow conduction to overwhelm the cooling.

Ultimately, any detailed model of the ICM must include the natural formation and evolution of bubbles with cool shells in realistic galaxy clusters. High resolution hydrodynamic simulations are required and we anticipate that a thorough check of our hypothesis will be possible in the not too distant future. A detailed and explicit accounting of the full instrumental response of *Chandra*, which has been ignored in the present study, should be included in such an analysis. Hence, we regard the present study as a first step towards understanding how bubbles influence the inferred properties of the gas in the cores of clusters. We expect that the results and conclusions presented here are generally robust, since the bubble models are based, to a large extent, on observations of *real* bubbles. Just how remarkably well this simplistic model works is, in our opinion, a strong testament to the hypothesis that bubbles significantly affect the observed properties of clusters and must be taken into account when inferring the physical properties of the ICM.

We thank the referee, Luca Ciotti, for very helpful comments and suggestions. I. G. M. is supported by a postgraduate scholarship from NSERC. A. B. is supported by an NSERC operating grant, N. K. is supported by NSF AST-9988146, NAG5-1203, and NSF AST-0205969 and M. L. B. is supported by a PPARC rolling grant for extragalactic astronomy and cosmology at the University of Durham.

Chapter 6

Models of the ICM with Heating and Cooling: Explaining the Global and Structural X-ray Properties of Clusters

Abstract

Non-radiative simulations which only include heating due to gravitational processes fail to match the observed mean X-ray properties of galaxy clusters. As a result, there has recently been increased interest in models in which either radiative cooling or entropy injection (and/or redistribution) play a central role in mediating the thermal and spatial properties of the intracluster medium. Both sets of models can account for the mean global properties of clusters. Radiative cooling alone, however, results in fractions of cold/cooled baryons in excess of observationally established limits. On the other hand, the simplest entropy injection models, by design, do not treat the "cooling core" structure present in many clusters and cannot account for declining entropy profiles towards cluster centers revealed by recent high resolution X-ray observations. We consider models that marry radiative cooling with entropy injection, and confront model predictions for the global and structural properties of massive clusters with the latest X-ray data.

The models successfully and simultaneously reproduce the observed $L-T$ and $L-M$ relations, yield detailed entropy, surface brightness, and temperature profiles in excellent agreement with observations, and predict a cooled gas fraction that is consistent with observational constraints. More interestingly, the model provides a possible explanation for the significant intrinsic scatter present in the $L-T$ and $L-M$ relations. The model also offers a natural way of distinguishing between clusters classically identified as "cooling flow" clusters and the relaxed "non-cooling flow" clusters. The former correspond to systems that experienced only mild levels ($\lesssim 300$ keV cm^2) of entropy injection, while the latter are identified as systems that had much higher entropy injection. The dividing line in entropy injection between the two categories corresponds roughly to the cooling threshold for massive clusters. This finding suggests that entropy injection may be an important, if not the primary, factor in determining the class a particular cluster will belong to. These results also suggest that the previously identified relationship between inferred cooling flow strength and the dispersion in the $L-T$ relation is a manifestation of the distribution of cluster entropy injection levels. This is borne out by the entropy profiles derived from *Chandra* and *XMM-Newton*. Finally, the model predicts a relationship between a cluster's central entropy and its core radius, the existence of which we confirm in the observational data.

6.1 Introduction

It has been made increasingly apparent in recent years that theoretical models of cluster formation and evolution that incorporate gravitationally-driven processes alone fail to match the observed global X-ray properties of clusters (e.g., Kaiser 1991, Tozzi & Norman 2001; Babul et al. 2002). More recently, McCarthy et al. (2003a, 2003b) showed that such models are also incompatible with the observed Sunyaev-Zeldovich (SZ) effect properties of distant clusters. This discord between theory and observations has motivated a number of authors to examine the potential role of *non*-gravitational gas physics, usually in the form of radiative cooling, entropy injection[1] (e.g., from AGN or galactic winds), or both cooling and entropy

injection (e.g., Kaiser 1991; Balogh, Babul, & Patton 1999; Bryan 2000; Tozzi & Norman 2001; Borgani et al. 2001; Voit & Bryan 2001; Babul et al. 2002; Wu & Xue 2002; Voit et al. 2002; Davé, Katz, & Weinberg 2002; Voit et al. 2003; Oh & Benson 2003). These models generally compare more favorably to the data [e.g., to the observed luminosity-temperature ($L-T$) and luminosity-mass ($L-M$) relations] than the standard 'non-radiative' model, but it still remains somewhat unclear as to which of these models — those with entropy injection alone, those with cooling alone, or those with entropy injection plus cooling — best reflect the true nature of clusters.

Part of the reason for the ambiguity undoubtedly arises from the fact that there is a relatively large amount of scatter present in the observed X-ray scaling relations of clusters, in particular the $L-T$ and $L-M$ relations. Because of the large scatter, the various non-gravitational models, which typically predict similar mean global properties, are essentially indistinguishable (see, e.g., Voit et al. 2002; Balogh et al. 2005).

The origin of the scatter in the observed relations is uncertain and has received very little attention from a theoretical modeling point of view. It is clear that at least some of the dispersion is due to real physical differences in the properties of clusters of a given mass (as the observed scatter cannot be explained by measurement uncertainty) and, therefore, any realistic theoretical model of cluster evolution that seeks to make precise predictions must account for it. Understanding the origin of the scatter is of considerable importance to studies seeking to use clusters for precision cosmological tests, such as the determination of the matter power spectrum normalization, σ_8 (see, e.g., Smith et al. 2003; Balogh et al. 2005).

An examination of whether or not the intrinsic scatter can be accounted for by

[1]We also regard mechanisms such as thermal conduction and turbulent mixing (e.g., Narayan & Medvedev 2001; Kim & Narayan 2003) as sources of 'entropy injection' since they transfer heat to the cluster center. Strictly speaking, however, these processes do not really introduce new entropy into the system, they merely *redistribute* the cluster's (pre-existing) entropy.

non-gravitational gas physics, therefore, is one of the primary goals of the present paper. We demonstrate below that *the scatter in the $L-T$ and $L-M$ relations is inconsistent with entropy injection only or cooling only models.* However, the scatter can be accounted for by a model that includes both entropy injection and radiative cooling. Moreover, our analysis indicates variations in the efficiency of entropy injection across the cluster population. Combined cooling + entropy injection models also have the advantage of not being subject to the "overcooling" problems that plague the purely radiative cooling models.

While detailed studies of the global properties of clusters have taught us much (and continue to teach us) about the intracluster medium (ICM) and clusters in general, a potentially much more powerful test is comparisons between observed and predicted *structural* properties, such as entropy, temperature, and surface brightness profiles. The influx of new high spatial and high spectral resolution X-ray data from *Chandra* and *XMM-Newton* now affords us the opportunity to make such comparisons. A second goal of this study, therefore, is to confront theoretical models that include entropy injection and/or cooling with new high resolution data. We note that early results from *Chandra* and *XMM-Newton* show no signs of the large isentropic cores in groups and clusters predicted by generic injection only models (e.g., David et al. 2001; Pratt & Arnaud 2003; Mushotzky et al. 2003). This implies that other processes, possibly radiative cooling, are also important, at least for some clusters. Indeed, we demonstrate that models with both radiative cooling and entropy injection are able to match the observed structural properties of massive clusters and simultaneously account for the $L-T$ and $L-M$ relations. Interestingly, the theoretical systems with only mild levels of entropy injection look remarkably like "cooling flow" (CF) clusters[2], whereas systems with high levels exhibit the typical characteristics of "non-cooling flow" (NCF) clusters.

[2]The designation *"cooling flow" cluster* refers to a system that has a sharply rising surface brightness profile and, normally, a declining temperature profile towards the center. These ob-

The present paper is organized as follows. In §6.2, we extend the models of Babul et al. (2002) to include a realistic treatment of radiative cooling. A general discussion of how radiative cooling modifies the properties of the models is given in §6.3. In §6.4, the physical origin of the scatter in the $L-T$ and $L-M$ relations is explored. Comparisons of structural properties between the various theoretical models and high quality *Chandra* and *XMM-Newton* data are made in §6.5. Finally, in §6.6 and §6.7, we summarize and discuss our results.

The models considered below were developed in a flat ΛCDM cosmology with $h = 0.75$, $\Omega_m = 0.3$ and $\Omega_b = 0.020h^{-2}$, which is a close match to current estimates, including those from *WMAP* (Spergel et al. 2003).

6.2 Cluster models with radiative cooling

The primary goal of this paper is to explore how entropy injection and radiative cooling influence the evolution of the ICM and to confront these models with new high quality X-ray data. We have already performed a thorough analysis of how entropy injection alone modifies the ICM (e.g., Balogh, Babul, & Patton 1999; Babul et al. 2002; McCarthy et al. 2002a, 2003a, 2003b, 2003c). This model sought to explain the properties of groups and clusters *minus* the "cooling flow" component, if any, and therefore, explicitly ignored radiative cooling. We refer the reader to Babul et al. (2002), in particular, for an in-depth discussion of the model, including an examination of the possible sources of the entropy injection. We re-examine the issue of sources of non-gravitational entropy in §6.6 of the present paper.

Since we have examined the effects of entropy injection in detail, the current

servational characteristics have typically been interpreted as manifestations of an ICM that is radiatively cooling on short timescales. The cooling gas flows inward toward the cluster center (hence, the name cooling flow). When we use the phrase "cooling flow" (in quotation marks) we are referring to the observational characteristics and not a physical model.

section is devoted to an examination of the effects of radiative cooling. First, however, a short discussion of the initial conditions prior to cooling is given so that we may gauge how cooling modifies things.

6.2.1 Initial conditions

There have been claims that radiative cooling alone may explain the deviations of clusters from self-similarity (e.g., Bryan 2000; Wu & Xue 2002; Davé, Katz, & Weinberg 2002) or, at least, that it plays the dominant role in the breaking of self-similarity (e.g., Voit & Ponman 2003). In order to explore this possibility, we examine the effects of cooling on the simple isothermal model of Babul et al. (2002). As its name implies, this isothermal model assumes that initially (i.e., before any cooling) the ICM has a constant temperature, which is set to the cluster virial temperature. The intracluster gas is in hydrostatic equilibrium within a gravitationally-dominant dark matter halo that has a density profile which matches those found in recent high resolution numerical simulations (e.g., Moore et al. 1999; Lewis et al. 2000). In order to solve for hydrostatic equilibrium, it is assumed that the cluster is a typical region of the universe in terms of the mixture of dark matter and baryons, i.e., the ratio of gas mass to total mass within cluster's maximum radius, $r_{\rm halo}$, is given by Ω_b/Ω_m. In terms of global properties, this simple model has been shown to be in excellent agreement with self-similar predictions (i.e., it predicts $L \propto T^2$ and $L \propto M^{4/3}$) and with the results of non-radiative simulations, such as those performed by Evrard, Metzler, & Navarro (1996). The simplicity of this model makes it particularly suitable for analysis. We, therefore, adopt it as the baseline model to gauge the impact of cooling.

While our simple isothermal model predicts *global* properties that are very similar to those seen in non-radiative simulations, it is clear that there are some differences between the two in terms of predicted *structural* properties. For example, Lewis et al. (2000) and, more recently, Loken et al. (2002) find non-isothermal temperature profiles in their non-radiative ("adiabatic") simulations, with the gas

temperature dropping by more than a factor of 2 from the cluster center to its periphery. Thus, it is reasonable to ask whether or not the isothermal model represents a fair baseline model. In order to test this, we turn to the study of Voit et al. (2003). Using the numerical simulations of Bryan & Voit (2001) (which were run with the same adaptive mesh refinement (AMR) code used by Loken et al. 2002), Voit et al. (2003) showed that the dimensionless entropy profiles of simulated non-radiative clusters are approximately self-similar. We use their self-similar entropy profile, which was kindly provided in electronic form by G. M. Voit and G. L. Bryan, together with a realistic dark matter density profile (the same profile used in the isothermal model) to construct a second baseline model to which we can compare our isothermal model. As expected, the global properties of the isothermal model and the non-radiative Voit & Bryan clusters are quite similar but there are some differences between the predicted temperature and density profiles. However, when we allow both baseline models to cool, we find very similar results (over a large range of masses), in the sense that both give rise to extremely high cooled gas fractions and both predict $L - T$ relations which are too luminous (at a fixed temperature) with respect to the observations (we demonstrate this explicitly in §6.3 and §6.4 for the isothermal model). *Therefore, we find that including the effects of radiative cooling but not those of entropy injection leads to failure in accounting for observed properties of clusters. This conclusion holds irrespective of which baseline model we use.* Throughout the paper, we present results for the isothermal plus cooling model only.

Perhaps a more physically plausible model is one which includes both the effects of radiative cooling and entropy injection (e.g., Voit et al. 2002, 2003; Oh & Benson 2003). In order to examine this scenario, we will cool the entropy injection model of Babul et al. (2002). Like the isothermal model, the entropy injection model also consists of intracluster gas in hydrostatic equilibrium within a realistic dark halo. The primary difference between this model and the isothermal model (aside from the fact that one model assumes isothermality and the other does

not) is that in the absence of cooling, the entropy injection model contains an isentropic core, which is presumed to have arisen through early heating events such as AGN outflows (e.g., Valageas & Silk 1999; Babul et al. 2002; Scannapieco & Oh 2004). The value of the entropy of this core is a free parameter and has been determined previously by fitting to observed scaling relations. Analysis of "cooling flow corrected" scaling relations, such as the $L - T$ relation (Babul et al. 2002), $M_{\rm gas} - T$ relation (McCarthy et al. 2002a), and various SZ effect scaling relations (McCarthy et al. 2003b), indicates that an entropy core of $\gtrsim$ 300 keV cm^2 gives the best fit. It is interesting to see whether or not such a high level of injection is required once the effects of radiative cooling are also included and the results compared to actual uncorrected X-ray data. Before moving on, it is also worth noting that the entropy profile at large radii (where entropy injection is unimportant) in this model is not identical to that of our baseline isothermal model. Instead, the profile at large radii is required to match the results of high resolution non-radiative simulations (Lewis et al. 2000). We verify that the slope and normalization of the entropy profile at large radii is also a close match to the self-similar entropy profile reported by Voit et al. (2003).

6.2.2 A treatment of radiative cooling

Voit et al. (2002) clearly demonstrated that how one chooses to model the effects of radiative cooling can have a significant impact on the predicted properties of clusters (compare the results of their 'truncated' cooling model with their more realistic 'radiative losses' cooling model, for example). Thus, we wish to treat the effects of radiative cooling as realistically as possible but without resorting to computationally expensive hydrodynamic simulations. The treatment developed below is similar to the physically-motivated analytic method of Oh & Benson (2003) and the reader is referred to that study for a more in-depth discussion of boundary conditions and how the relevant differential equations are solved. We give a description of this method below.

We start with the initial gas and dark matter radial profiles for the model clusters (i.e., the profiles predicted by the isothermal and entropy injection models described above) and subject these to radiative cooling. Radiative cooling reduces the specific entropy (s) of a parcel of gas according to

$$\frac{ds}{dt} = -\frac{\mu m_H n_i n_e \Lambda(T)}{\rho k_b T} \tag{6.1}$$

where $\Lambda(T)$ is the cooling function (which is modeled as a Raymond-Smith plasma with 0.3 solar metallicity), μ is the mean molecular weight (0.6 in this case), and the other symbols have their usual meanings.

Equation (1) can be re-written in terms of the gas pressure (P) and the more commonly used form of 'entropy' K, where $s = \ln K^{3/2} +$ constant (assuming an ideal gas and an equation of state $P = K\rho^{5/3}$),

$$\frac{dK}{dt} = -\frac{2}{3}\left(\frac{n_e n_i}{n^2}\right)\frac{1}{(\mu m_H)^2}\left(\frac{P}{K}\right)^{1/5}\Lambda(K,P) \tag{6.2}$$

The new gas entropy profile after cooling for a small time interval dt is calculated by integrating equation (2). The gas pressure is assumed to remain constant (i.e., isobaric cooling) over this short interval. After each time step, the properties of the gas (density and temperature and, therefore, pressure) are updated by placing the model clusters back in hydrostatic equilibrium by simultaneously solving the coupled differential equations

$$\begin{aligned} \frac{dr}{dM_{\rm gas}} &= \frac{1}{4\pi r^2}\left(\frac{K}{P}\right)^{3/5} \\ \frac{dP}{dM_{\rm gas}} &= -\frac{GM_{\rm DM}}{4\pi r^4} \end{aligned} \tag{6.3}$$

As the gas cools and the pressure at the cluster center preferentially decreases, an inward flow develops in order to re-establish hydrostatic equilibrium. Because

the gas flows inward, we must implement different boundary conditions than employed in setting up the initial cluster profiles (i.e., $M_{\rm gas,tot}/M_{\rm tot} = \Omega_b/\Omega_m$ at $r_{\rm halo}$). We solve for hydrostatic equilibrium after each cooling time step by applying the following boundary conditions (see Oh & Benson 2003):

$$\begin{aligned} r(0) &= 0 \\ r(M_{\rm gas,tot}) &= r_{\rm end} \\ P(M_{\rm gas,tot}) &= \left[P_{\rm halo}^{2/5} + \frac{2}{5K_{\rm halo}^{3/5}} \int_{r_{\rm end}}^{r_{\rm halo}} \frac{GM_{\rm DM}(r)}{r^2} dr\right]^{5/2} \end{aligned} \tag{6.4}$$

where $P_{\rm halo}$ and $K_{\rm halo}$ are the initial gas pressure and entropy at $r_{\rm halo}$, the maximum radius of cluster (see Babul et al. 2002 for a quantitative definition of $r_{\rm halo}$). The last boundary condition implies that the outermost gas mass shell is compressed adiabatically as it flows inward, which is appropriate since the cooling time of this shell greatly exceeds the age of the cluster. Since this is a two point boundary value problem (with $r_{\rm end}$ being the eigenvalue of the problem), we use a relaxation technique to solve the equations.

If cooled long enough, the temperature of the gas at the center of the model clusters will approach zero and cease to emit X-rays. This is referred to as 'dropping out'. For the purposes of the present model, we assume a parcel of gas drops out (and is then removed from the calculation) if its temperature falls below $\approx 10^5$ K or if its entropy decreases to zero during a time step. As the gas at the cluster center approaches this threshold, the time steps are chosen such that only a few mass shells drop out at a time. Typically, this corresponds to a temporal resolution of 20 Myr (depending on system mass), which is small compared to the age of the cluster and is more than sufficient to achieve convergent results. As the gas starts to drop out, a cooling flow is established. This flow is treated as an adiabatic process after the small time step dt by shifting the remaining (hot) gas, $K(M_{\rm gas})$, inward to replace the mass shells that dropped out. The properties of the gas are then updated via hydrostatic equilibrium (as described above) and the cluster

continues to cool. Similar to Oh & Benson (2003), we do not consider the effects of the cold gas on the gravitational potential of the cluster (e.g., adiabatic contraction of the dark matter halo). However, we do not expect this to significantly modify our results as our entropy injection + cooling model generally predicts small cooled gas fractions (which are consistent with observations).

An obvious but important question is how long should cooling be allowed to operate? For the sake of simplicity, it has become standard to allow the model clusters to cool for a Hubble time, t_h (e.g., Bryan 2000; Voit & Bryan 2001; Voit et al. 2002; Xue & Wu 2002; Oh & Benson 2003). Clearly, this represents the maximum amount of cooling a cluster can undergo. We show later (in §6.4) that if one focuses solely on explaining relaxed CF clusters, that in fact a wide distribution of times (in addition to an entropy injection level of $\lesssim 300$ keV cm^2) is required in order to account for the scatter in the $L-T$ and $L-M$ relations. The possibility of a connection between the intrinsic scatter in the $L-T$ relation and variations in the time available for cooling was previously suggested by Scharf & Mushotzky (1997). Throughout the paper, we plot results that span cooling from $t = 0$ to $t = t_h$.

6.3 The effects of radiative cooling

We examine here the general effects of radiative cooling on the global and structural properties of isothermal and entropy injection model clusters. This will aid the discussions in §6.4 and §6.5 of comparisons with the observations.

6.3.1 Cooled gas fractions

As discussed earlier, if a cluster is allowed to cool for a long enough time, eventually gas will drop out of the ionized X-ray emitting phase, become neutral, and possibly form stars. Since there are fairly good observational constraints on the fraction of a cluster's baryons that are in the form of neutral gas (e.g., Donahue et al.

2000; Edge 2001; Edge et al. 2002) and stars (e.g., Cole et al. 2001; Lin, Mohr, & Stanford 2003), a key prediction of the theoretical models is the fraction of gas that completely cools out.

Plotted in Figure 6.1 is the percentage of gas that completely cools out as a function of cluster mass, entropy injection level, and time (as the clusters cool). The various line types demonstrate how the cooled fraction evolves as a function of time, while the different panels show how entropy injection affects the amount of gas that is able to completely cool. The level of injection is characterized by S (what X-ray observers often call the "entropy"), which is related to the K via

$$S \equiv \frac{k_b T}{n_e^{2/3}} = K \left(\frac{n}{n_e} \right)^{2/3} (\mu m_H)^{5/3} \tag{6.5}$$

Concentrating for a moment on the upper left hand panel of Fig. 6.1, it can be seen that given nearly a Hubble time to cool, low mass clusters that have not been injected with entropy can cool out a substantial fraction ($\gtrsim$ 20%) of their baryons. Yet, observations indicate that, at most, only 10% of a cluster's baryons are in the form of stars (see Balogh et al. 2001). A negligible amount is in the form of neutral gas (see Edge et al. 2002). Simply reducing the amount of time that such systems can cool for (within reason) does not resolve this problem (see the dotted line, for example). This predicted overabundance of cooled material in groups and clusters has been dubbed the "cooling crisis" and has been taken as strong evidence in support of feedback/entropy injection (Balogh et al. 2001; Oh & Benson 2003). The requirement for large amounts of feedback/entropy injection also seems to be necessary in order to quench a similar problem found in semi-analytic and hydrodynamic studies of galaxy formation (Somerville & Primack 1999; Yoshida et al. 2002; Benson et al. 2003).

Encouragingly, the results for the isothermal plus cooling model are quite similar to those found from other analytic cluster models that include the effects of radiative cooling but not entropy injection (e.g., Voit et al. 2002; Oh & Benson

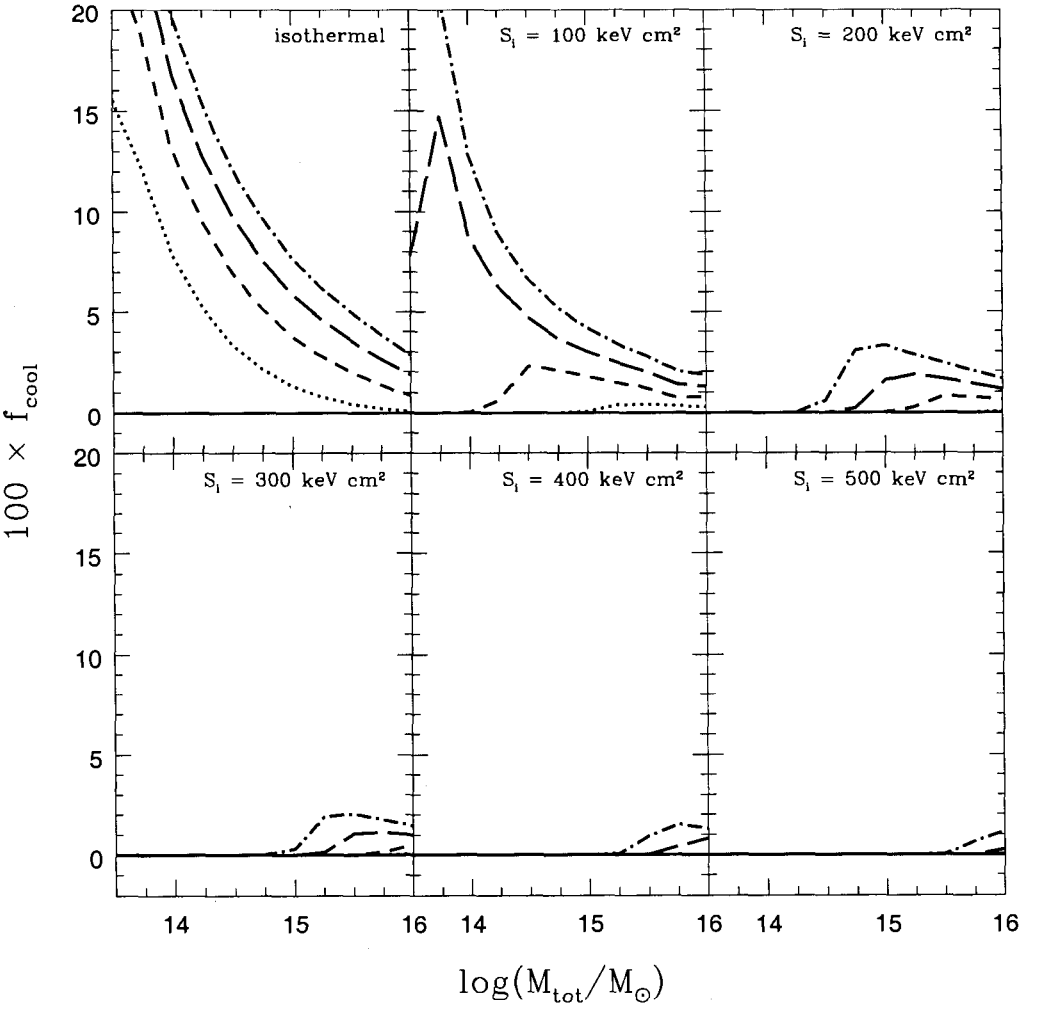

Figure 6.1: Percentage of the total gas mass that completely cools out as a function of total cluster mass, time, and entropy injection level S_i. The cooled gas fraction, $f_{\rm cool}$, is given by $M_{\rm cool}/(M_{\rm cool} + M_{\rm hot})$, where $M_{\rm cool}$ is the total mass of gas that has cooled out of the X-ray emitting phase and $M_{\rm hot}$ is the total mass of gas remaining in the hot ionized phase. The solid, dotted, short dashed, long dashed, and dot dashed lines represent cooling for 0, 3, 6, 9, and 12 Gyrs, respectively. The different panels indicate how various levels of entropy injection affect the amount of gas that is able to completely cool out.

2003). This is despite there being slight differences in the adopted initial cluster conditions and how one chooses to model the effects of cooling. This model also predicts cooled gas fractions which are comparable, although slightly lower, than those found from numerical simulations that include radiative cooling only (e.g., Muanwong et al. 2002; Davé, Katz, & Weinberg 2000).

Examination of the remaining panels in Fig. 6.1 clearly demonstrates that entropy injection has a large effect on the amount of gas that is able to cool out of the X-ray emitting phase. In particular, injecting the gas with $S_i \gtrsim 200$ keV cm^2 is sufficient to obtain cooled gas fractions consistent with the observations, while injecting more than 300 keV cm^2 essentially shuts off cooling in all but the most massive clusters. Hence, entropy injection offers a viable solution to the so-called cooling crisis (see Oh & Benson 2003 for a detailed discussion).

6.3.2 Entropy profiles

Through hydrostatic equilibrium, the properties of the hot X-ray emitting gas at any particular time are determined entirely by the entropy distribution of the gas and the structure of the cluster's dark matter halo (see eqns. 3 and 4). Since radiative cooling modifies the cluster's entropy profile (see eqn. 2) it must also effect the cluster's gas density and temperature. These, of course, set the cluster's appearance and dictate how efficiently the cluster can continue cooling. Understanding how cooling modifies the entropy distribution of a cluster, therefore, is of paramount importance in understanding how it influences the evolution of a cluster's global and structural

Figure 6.2 shows the evolution of the entropy profile of a cluster with $M_{\rm tot} = 10^{15} M_{\odot}$ as a function of time. The various panels demonstrate how varying levels of entropy injection influence this evolution.

Let us focus first on the upper right hand panel of Fig. 6.2, since it shows the full range of entropy profiles as a function time. The initial entropy profile (solid line) shows a central floor of 200 keV cm^2 (by design) and a power law of

$S \propto r^{\sim 1.1}$ at large radii, which matches the large radii results of semi-analytic smooth accretion models and high resolution non-radiative simulations (Lewis et al. 2000; Tozzi & Norman 2001; Voit et al. 2003). After approximately 3 Gyr of radiative cooling, the central entropy of the cluster has dropped to nearly 100 keV cm^2. At this point, a clear entropy floor persists. As the cluster continues to cool, the entropy core steepens until eventually the central entropy approaches zero. When this occurs, gas begins to drop out of the X-ray emitting phase and an inward cooling flow develops. However, even after 9 Gyr of cooling a remnant of the initial entropy is still present (note the kink in the entropy profile near 0.03 r_{200}), although the 'core' is now quite steep and very small in radial extent (since most of it has dropped out). Eventually, the entropy core completely drops out and what remains is essentially a pure power law, $S \propto r^{\sim 1.1}$, that extends all the way from the cluster center to its periphery. After this, the cluster continues to cool but approximately maintains this power law over all radii, reaching a quasi-steady state[3].

The remaining panels in Fig. 6.2 are now easily interpreted. Our baseline isothermal model, which has the lowest initial central entropy, starts cooling gas out the fastest and it is simple to see why this model predicts such large cooled gas fractions (Fig. 6.1). Injecting the gas with 100 keV cm^2 only slightly delays the development of a cooling flow. Injection levels of $S_i = 300$ keV cm^2 or higher, however, essentially prevent any gas from dropping out, although the central entropy of the gas is significantly lower after cooling for a Hubble time.

The above trends hold true for clusters with masses different than that considered in Fig. 6.2. as well. The only difference is the amount of time it takes for the entropy profile to evolve. For example, because low mass clusters have lower central densities than high mass clusters (and, therefore, are less luminous), they

[3]We use the phrase *quasi*-steady state instead of just steady state since, although the entropy profile maintains the same shape and normalization, it continues to decrease in radial extent with time as the gas flows inward to re-establish hydrostatic equilibrium.

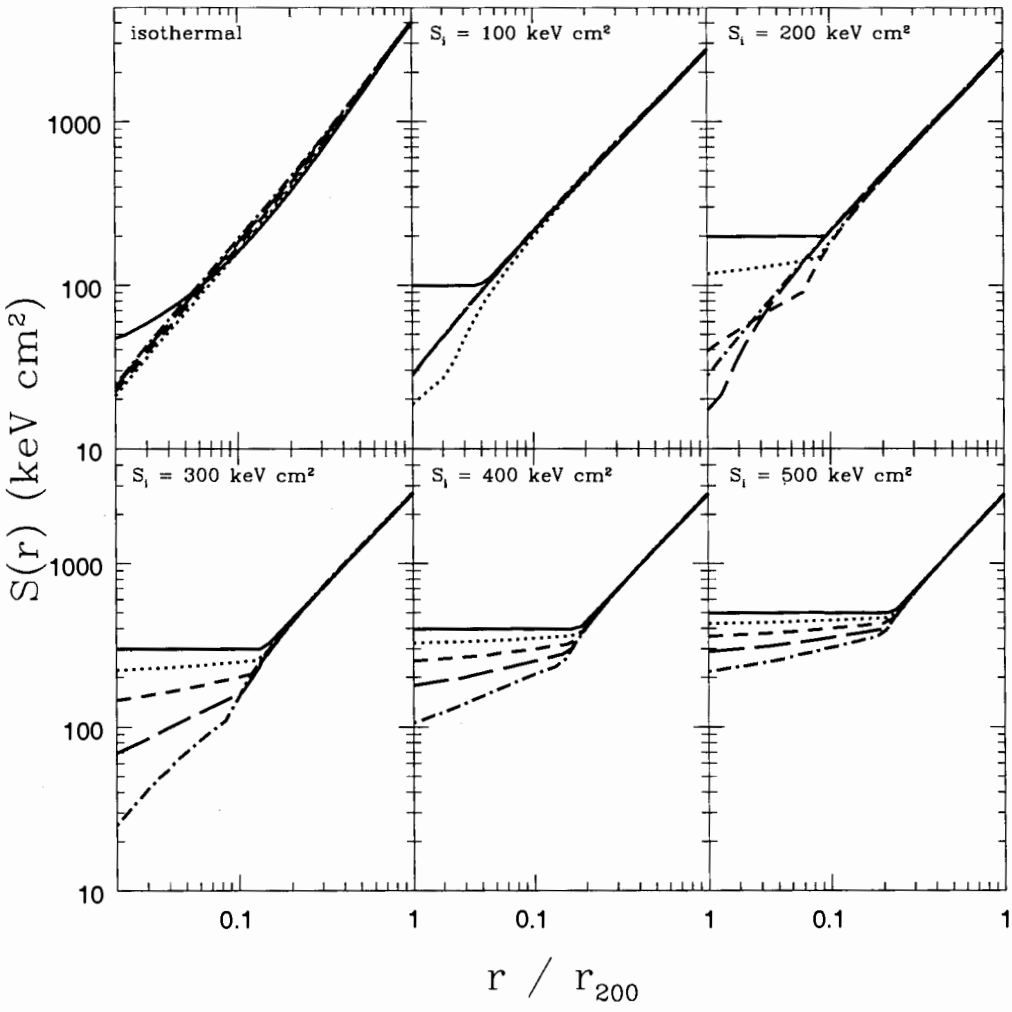

Figure 6.2: The entropy profile as a function of time and entropy injection level for a cluster with $M_{\rm tot} = 10^{15}$ $M_\odot$. The line types have the same meaning as in Fig. 6.1. The quantity r_{200} is defined as the radius within which the mean dark matter density is 200 times the critical density of the universe (1.68 Mpc in this case).

have a much more difficult time in cooling out their entropy cores. On the other hand, clusters more massive than the one considered in Fig. 6.2 cool out their cores more quickly and reach the quasi-steady state faster.

The fact that radiative cooling approximately maintains the initial power-law

entropy profile with time is interesting and deserves some investigation. First, it is worth noting that both the isothermal and entropy injection models approximately maintain their power-laws (once the elevated entropy at the center cools out). This is despite the fact that the power-law indices are not identical for these two cases. In particular, at large radii, the entropy injection model initially has $S \propto r^{1.1}$ while the isothermal model initially has $S \propto \rho^{-2/3} \propto r^{4/3}$ ($\rho \propto r^{-2}$ at large radii for this model). Therefore, the fact that the power-law remains essentially invariant with cooling appears to be independent of the power-law index. We have verified that this is roughly true for a range of different initial power-law indices. Interestingly, a very similar trend has recently been reported by Kaiser & Binney (2003). These authors demonstrated that radiative cooling does not significantly modify the initial power-law relationship between entropy and gas mass of their model clusters. Unfortunately, a straightforward analytic explanation for these (numerically-derived) trends is not easily obtained, at least at small radii. At large radii, however, we should expect the power-law to be maintained since the cooling time of the gas is long relative to the Hubble time. This implies that $S(M_{\rm gas})$ should remain roughly constant and, furthermore, the physical size of a mass shell should be fixed (since the shell will not have been compressed much). Understanding the evolution of the entropy profile at small radii is more difficult because both coordinates, $S(M_{\rm gas})$ and $r(M_{\rm gas})$, are being significantly modified by cooling. A more thorough investigation of entropy evolution of clusters will be presented in a forthcoming paper.

Given enough time, our models predict that all clusters should reach a quasi-steady state that is characterized by a near perfect power law entropy profile over all radii. However, since the age of the universe (which is an upper limit on the amount time available for cooling) is comparable to the predicted central cooling times of our model clusters, a general prediction of our model is that there should be a full range of central entropy distributions, depending on the initial injection level and how long each cluster is able to cool. Indeed, in §6.5 we demonstrate that

new published *Chandra* and *XMM-Newton* results show a large range of central entropies that compares quite favorably to those plotted in Fig. 6.2.

6.3.3 Surface brightness and emission-weighted temperature profiles

Plotted in Figure 6.3 is the evolution of the bolometric X-ray surface brightness (b_X) profile of a cluster with $M_{\rm tot} = 10^{15} M_{\odot}$ as a function of time. The panels and line types have the same meaning as in Figs. 6.1 & 6.2.

Again, we focus first on the model with an injection level of $S_i = 200$ keV cm^2 (upper right hand panel). It can clearly be seen that as the cluster cools the surface brightness near the center of cluster increases and becomes more peaked. This, of course, is due to the increasing central density which, in turn, is the result of the decreasing central entropy and the re-adjustment of the cluster gas to achieve hydrostatic equilibrium. Thus, there is a strong connection between the evolution of the surface brightness profile and the evolution of the entropy profile of a cluster. Indeed, comparison of Fig. 6.3 with Fig. 6.2 demonstrates that the central surface brightness is a strong function of the amount of low entropy gas near the cluster center. For example, the central surface brightness reaches its maximum value after roughly 9 Gyr of cooling (long dashed line), which coincides exactly with the time when the central entropy reaches its lowest value (i.e., just before the core drops out). Once the entropy core disappears, the surface brightness profile achieves a quasi-steady state (dot dashed line). This is expected given the results of §6.3.2. The same is true for other levels of entropy injection, the only difference being the time it takes to achieve this quasi-steady state (which are greater than a Hubble time for sufficiently high levels of entropy injection).

The trend of increasing central concentration of b_X as the cluster cools is an interesting one. For clusters that had a mild level of entropy injection (top three panels of Fig. 6.3), radiative cooling has a large effect on the central gradient

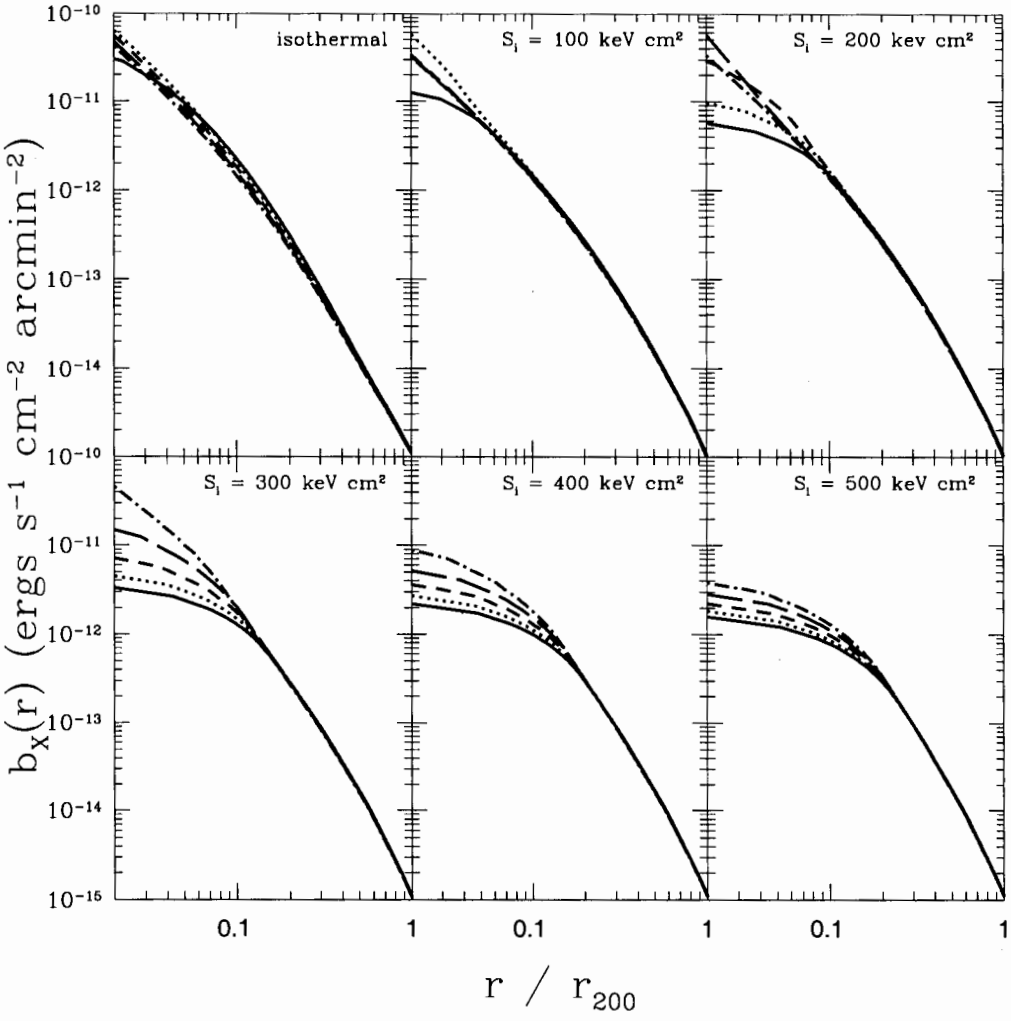

Figure 6.3: The bolometric X-ray surface brightness profile as a function of time and entropy injection level for a cluster with $M_{\rm tot} = 10^{15}$ M$_\odot$. The line types have the same meaning as in Fig. 6.1.

of the cluster's surface brightness. On the other hand, clusters that had a large injection of entropy are less affected by cooling, as expected. This difference in central concentration means we can qualitatively identify the two types of clusters (i.e. those with mild and strong heating) with CF and NCF clusters, respectively (see §6.5.2). In fact, we argue later, on the basis of the observed $L - T$ and

$L - M$ relations, that the origin of these two morphological classes of clusters can be explained in terms of the entropy injection level. This hypothesis is reinforced by the actual observed entropy profiles of these two classes of systems, which is presented in §6.5.

In Figure 6.4 we plot the evolution of the bolometric emission-weighted temperature ($kT_{\rm ew}$) profile of a cluster with $M_{\rm tot} = 10^{15} M_{\odot}$ as a function time. Again, the panels and line types have the same meaning as in the previous figures.

In the top three panels of Fig. 6.4, we see the rapid development of large positive temperature gradients at the cluster center. Like the surface brightness and entropy profiles discussed above, the emission-weighted temperature profile also reaches a quasi-steady state once the initial entropy core has dropped out. The predicted steady state temperature profile, which is characterized by a steep positive gradient at the cluster center and a gentle negative gradient at large radii, is qualitatively similar to that recently observed in CF clusters by Allen, Schmidt, & Fabian (2001) and De Grandi & Molendi (2002). On the other hand, clusters that had a high level of entropy injection ($S_i > 300$ keV cm^2) retain their sharp central negative temperature gradients even after cooling for more than 12 Gyr.

Lastly, it is also worth noting that the development of central positive temperature gradients in our models coincides almost exactly with the development of peaked surface brightness profiles. In other words, depending on the time elapsed since the entropy injection, one either has a cluster with a flat central surface brightness and a sharp central negative temperature gradient or a cluster with a peaked surface brightness profile and a central positive temperature gradient. These two types of clusters, which emerge naturally from our analytic model, match the main qualitative features of observed relaxed NCF and CF clusters.

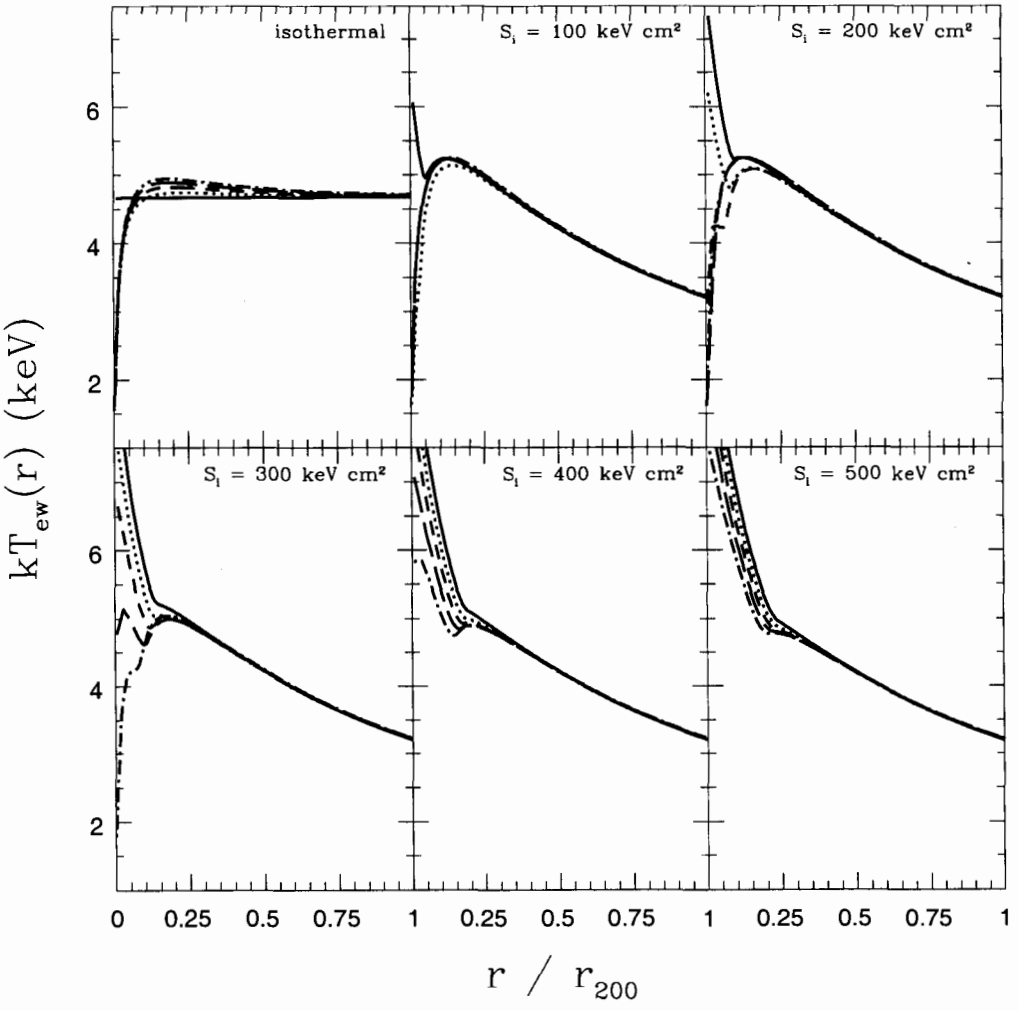

Figure 6.4: The emission-weighted temperature profile as a function of time and entropy injection level for a cluster with $M_{\rm tot} = 10^{15}$ $M_{\odot}$. The line types have the same meaning as in Fig. 6.1.

6.3.4 Integrated luminosities and mean cluster temperatures

Figures 6.3 and 6.4 illustrate how radiative cooling is expected to modify the observable radial properties of the intracluster medium. Here, we describe the effects of cooling on the integrated X-ray luminosity and the mean emission-weighted

temperature of the cluster.

As is evident from Figs. 6.2-6.4, cooling primarily affects only the central regions of the model clusters. Therefore, since cooling increases the central surface brightness and decreases the central temperature, we should expect that, in general, the integrated luminosity of the clusters will increase with the addition of radiative cooling while the mean temperature should decrease. This is exactly what the model predicts, as shown by the evolutionary $L-T$ tracks plotted in Fig. 6.5. Here, the tracks of six clusters of varying mass are shown (dashed and dotted lines, see figure caption). The clusters evolve from the initial $L-T$ relation predicted by the $S_i = 200$ keV cm^2 model without cooling (thick solid line) to higher luminosities. The open pentagons represent specific times of 0, 3, 6, 9, and 12 Gyr during the evolution.

To understand what this plot is telling us, let us focus for a moment on the tracks for the least massive (track A) and second most massive (track E) clusters. Track A shows that the least massive cluster starts off with a luminosity of $L_{\rm X,bol} \approx 6 \times 10^{43}$ ergs s^{-1} and evolves to higher luminosities. After approximately 13 Gyr of cooling (i.e., the end of the track), the cluster's luminosity has increased by roughly a factor of 3.3. Also, its temperature has decreased but not by nearly as much (only a factor of 1.19). Thus, the evolution in the $L-T$ plane is primarily driven by the influence of cooling on the luminosity rather than the temperature. It is important to note that even after 13 Gyr of cooling this low mass cluster has been unable to rid itself of its initial entropy core (see Fig. 6.1). Therefore, it is straightforward to understand why the $L-T$ relation evolves as it does: with time the central entropy decreases, giving rise to an increased central density which, in turn, dramatically increases the X-ray luminosity of the cluster. More massive clusters experience something slightly different. Focusing on track E, we see that just shortly after 6 Gyr of cooling the cluster begins to evolve back towards lower luminosities and higher temperatures (as indicated by the dotted line). Eventually, after approximately 9 Gyr, it reaches a more or less stable position on the $L-T$

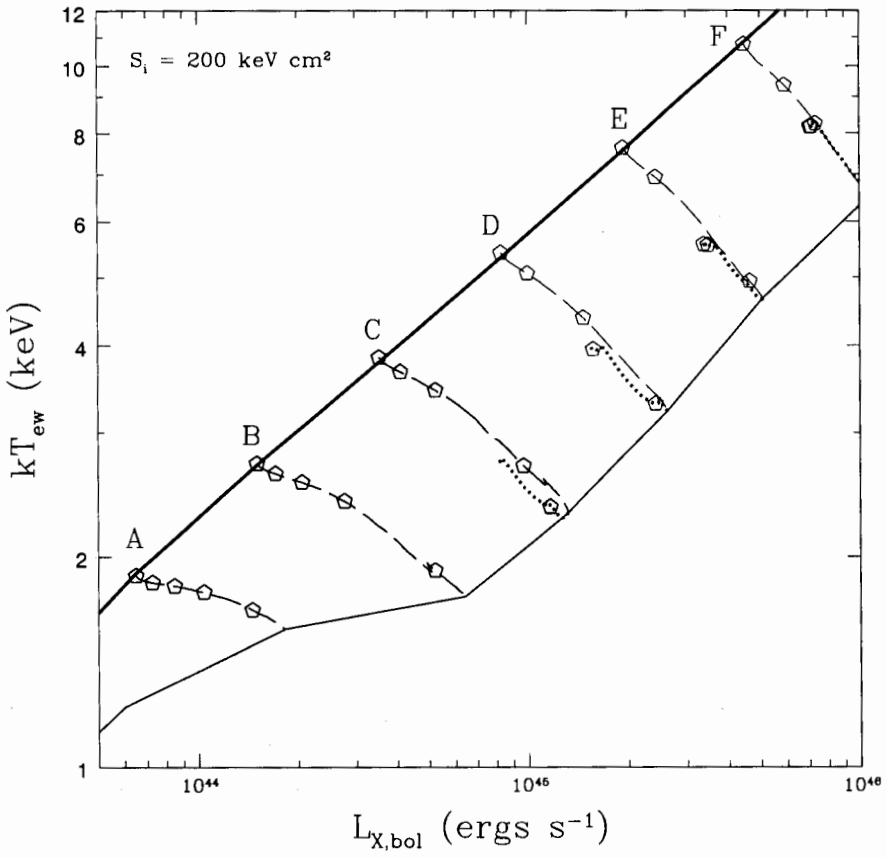

Figure 6.5: Evolutionary $L-T$ tracks for clusters that have been injected with S_i = 200 keV cm^2. Six different tracks are shown corresponding to clusters with masses of $log_{10}(M_{\rm tot})$ = 14.25 (A), 14.50 (B), 14.75 (C), 15.00 (D), 15.25 (E), and 15.50 (F) (in $M_\odot$). The thick solid line is the initial $L-T$ relation prior to including the effects of radiative cooling. The dashed and dotted lines are the evolutionary tracks as the cluster cools. The dashed lines show evolution towards high L and low T, which occurs prior to the removal of the isentropic core, while the dotted lines show the evolution towards low L and high T, which occurs after the core has dropped out (if it is able to drop out in less than 13 Gyr). Together, the thin and thick solid lines enclose the predicted range of $L-T$ values during cooling for 13 Gyr. For comparison with the previous figures, the open pentagons show the predicted $L-T$ relation at the discrete times of 0, 3, 6, 9, and 12 Gyr.

diagram. These trends can be understood by re-examining the results presented in §6.3.3. First, the fact that the cluster reaches a stable position on the $L-T$ diagram is expected since it has been shown that the surface brightness and temperature profiles reach quasi-steady states. Given the results of §6.3.3, it is also clear why this stable point happens to lie at a higher luminosity/lower temperature than the initial $L-T$ relation (i.e., the surface brightness is more peaked while the temperature profile shows a central positive gradient). Furthermore, we can also understand the origin of the turn-around of this massive cluster on the $L-T$ diagram as being due to the entropy core in its final days. Just prior to the dropping out of the entropy core, there exists a large amount of low entropy gas near the cluster center (since the core cools somewhat intact, see top right hand panel of Fig. 6.2). This gives rise to an extremely peaked surface brightness profile. However, once the core completely drops out, the surface brightness peak is diminished (so, too, is the integrated luminosity) and, hence, the result is the $L-T$ turn-around.

As might be expected, the above trends also hold true for clusters that have experienced different levels of entropy injection. Even clusters that were initially isothermal (and have no core per se) evolve towards higher luminosities and lower temperatures. This seems to be a very general prediction of our cooling model for massive clusters. Encouragingly, Voit et al.'s (2002) 'radiative losses' model, which is similar to our model in many aspects, also predicts an overall evolution of the $L-T$ relation towards higher luminosities and lower temperatures and by roughly the same magnitude (see their Fig. 27).

Figure 6.5 shows that the position of any given cluster on the L-T diagram is dictated by the initial level of entropy injection and how long radiative cooling has had to operate. (See also Figure 6.9 for predicted L-T relation for a range of entropy injection levels.) This implies a potential degeneracy in the sense that one can account for the observed location of any individual cluster on the $L-T$ diagram as being due to either a high level of initial entropy injection and a long subsequent

period of cooling, or a low level of initial entropy injection followed by a relatively short period of cooling. However, this degeneracy is bounded. There are regions of the $L-T$ plot (see Figure 6.9) that cannot be accessed by clusters with $K_0 > 300$ keV cm^2, even if they cooled for the entire lifetime of the Universe. Similarly, there are regions of the $L-T$ plot that cannot be accessed by clusters with low initial entropy injection. Jointly, these two bounds can be used to place rough constraints on the initial entropy injection of an individual cluster. On the other hand, as we discuss below, the distributions of present-day global and structural properties of the cluster population, collectively, provide a powerful probe of the initial *distribution* of entropy injection levels. Additional insights are also likely to be obtained from an analysis of a high-z cluster sample because radiative cooling will not have had much time to operate in these systems.

Before proceeding with a comparison of our models with the observational data, we stress that there is an important caveat to the results presented in this subsection. As noted earlier, if a cluster is able to cool out its initial entropy core, what remains is pure power law entropy profile with the cluster achieving a quasi-steady state. This gives rise to a more or less fixed position on the $L-T$ diagram. This is only true, however, if the radial extent of the entropy profile is not reduced by a significant amount after a Hubble time of cooling. Under the circumstances considered above, i.e., high mass clusters and fairly large amounts of entropy injection, this condition is approximately met. Because such clusters are only able to cool out a small fraction of their baryons, gas that was originally at the outskirts of the cluster only manages to flow inward by a relatively small amount. However, in the limit of low mass clusters that experience small amounts of entropy injection (and, therefore, extremely high cooled gas fractions), the shrinking entropy profile can significantly affect the evolution of the $L-T$ relation. The amount of gas that remains in the hot X-ray emitting phase after a Hubble time of cooling is reduced by a large fraction and so, too, is the X-ray luminosity of the cluster. The result is a position on the $L-T$ diagram that is actually at a lower luminosity and higher

temperature than the initial position (i.e., to the left of the initial curve). In fact, the same would be true of high mass clusters if they could somehow be forced to cool out $\gtrsim 15 - 20\%$ of their baryons. We have tested this by allowing our high mass clusters to continue cooling for several Hubble times until they reach this cooled gas fraction. Thus, the resulting $L - T$ relation is a strong function of the efficiency of cooling in clusters. It is, therefore, essential that the model retain consistency with the observed cooled gas fraction of clusters.

6.4 Comparison with Observed Global Properties

The luminosity-temperature relation has been known for roughly a decade now to deviate from simple self-similar predictions. This has been the primary motivating factor for the investigation of cluster models that incorporate non-gravitational gas physics, such as entropy injection and/or radiative cooling. While such models have generally been shown to provide better matches to the 'typical' cluster, the large amount of intrinsic scatter in the observed $L - T$ (e.g., Novicki, Sornig, & Henry 2002) and $L - M$ (e.g., Reiprich & Böhringer 2002) relations has yet to be addressed by these models. A primary goal of the present study is to see whether or not the scatter is consistent with theoretical models that include entropy injection and/or radiative cooling.

6.4.1 Observations

Essential to exploring the properties of the scatter are large, homogeneously analysed samples of clusters. Such samples guard against selection effects, differences in analysis procedures, differences in absolute flux calibration between various instruments, and other issues which could influence the physical interpretation of the scatter. Ideally, these samples should not have had any corrections applied

to them (e.g., "cooling flow" correction) other than the removal of obvious point sources (e.g., McCarthy, West, & Welch 2002b). Fortunately, such samples are now becoming available. We focus on two of the larger samples that now exist: the *ASCA* Cluster Catalog (ACC) of Horner (2001) and the extended *ROSAT* HIFLUGCS sample of Reiprich & Böhringer (2002).

The ACC of Horner (2001) contains roughly 270 clusters, the large majority of which are nearby systems ($z \leq 0.2$) (and, henceforth, we restrict ourselves to nearby clusters with $z \leq 0.2$). The wide bandpass and good spectral resolution of *ASCA* allows for the accurate determination of cluster mean temperatures and total bolometric X-ray luminosities. Unfortunately, because of *ASCA*'s rather poor spatial resolution, it is not possible to accurately measure surface brightness profiles and, therefore, quantities such as cluster mass. Thus, we use the ACC by itself to study the luminosity-temperature relation only. In order to study the luminosity-mass relation of clusters, we turn to the extended HIFLUGCS sample. Using surface brightness profiles from *ROSAT* and temperatures from *ASCA*, Reiprich & Böhringer (2002) deduced, through the assumption of hydrostatic equilibrium (and isothermality), the masses of 106 nearby ($z \lesssim 0.2$) clusters within three different radii: r_{500}, r_{200}, and a fixed physical radius of $3h_{50}^{-1}$ Mpc. In the present study, we focus only on the mass within r_{500}, which is typically the smallest of the three and, therefore, requires the least amount of extrapolation of the observed surface brightnesses (see Reiprich & Böhringer 2002). Unfortunately, many of the temperatures used by these authors were corrected for the effects of "cooling flows" and, therefore, in its current state, the sample cannot be fairly compared to our radiative cooling models. In order to address this issue, we have selected clusters in common between the ACC and the HIFLUGCS (≈ 80 systems). Using uncorrected temperatures from the ACC and surface brightness profiles from the HIFLUGCS, we recompute the cluster masses within r_{500}, taking care to correct for differences in the assumed cosmologies.

Before comparing the observed scaling relations to the models, it is instructive

to examine the properties of the data itself. Plotted in Figure 6.6 is the observed luminosity-temperature relation of nearby, massive clusters. Where possible, we indicate with symbols the cooling flow status of the clusters. In particular, triangles represent clusters that have an inferred cooling flow mass deposition rate, $\dot{M}$, consistent with zero, squares represent clusters with $\dot{M} \gtrsim 100\ M_{\odot}\ \mathrm{yr}^{-1}$, and squares with a surrounding open circle represent clusters with $\dot{M} \gtrsim 300\ M_{\odot}\ \mathrm{yr}^{-1}$. Cooling flow deposition rates were estimated by Allen & Fabian (1998) and Peres et al. (1998) based on a deprojection analysis of *ROSAT* surface brightness data. Those clusters that have published deprojected entropy profiles (or deprojected temperature and density profiles from which an entropy profile may be derived) inferred from new *Chandra* or *XMM-Newton* data have been explicitly labeled and will be examined in detail in §6.5.

First, there is the expected well-defined correlation between a cluster's luminosity and temperature. However, there is a large amount of scatter in the plot. As discussed by Allen & Fabian (1998), correcting for the central "cooling flow" dramatically reduces the scatter in the $L-T$ relation. Here, we have purposely left the data uncorrected for the effects of "cooling flows" in an attempt to ascertain whether models that include radiative cooling (either alone or in addition to some amount of entropy injection) can account for this scatter.

There is also a high degree of coherent structure present in the scatter of the $L-T$ relation. Namely, the clusters with large values of $\dot{M}$ preferentially lie on the high luminosity side of the scaling relation, while clusters with small values of $\dot{M}$ lie on the low luminosity side. This correlation between inferred cooling flow strength and dispersion in the scaling relation has been known for some time (Fabian et al. 1994; see also White, Jones & Forman 1997; Allen & Fabian 1998; Markevitch 1998). However, Fig. 6.6 is probably the cleanest, most clearcut illustration of this trend to date, with the high and low $\dot{M}$ systems occupying well-defined locii.

Recently, the standard isobaric cooling flow model has been shown to provide a poor description of *XMM-Newton* spectra of CF clusters (e.g., Peterson et al.

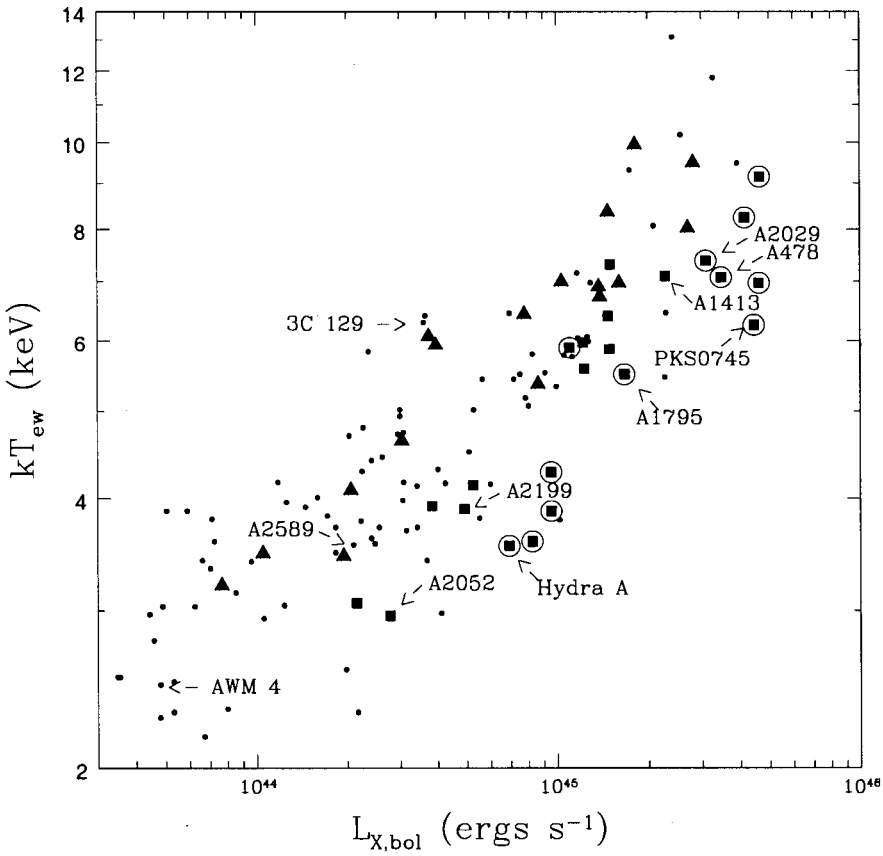

Figure 6.6: The observed $L - T$ relation of nearby, massive galaxy clusters. Data are from the ASCA Cluster Catalog of Horner (2001). Small filled circles represent clusters that have no published cooling flow status. Triangles represent clusters that have an inferred cooling flow mass deposition rate, $\dot{M}$, consistent with zero, squares represent clusters with $\dot{M} \gtrsim 100\ M_{\odot}\ \mathrm{yr}^{-1}$, and squares with a surrounding open circle represent clusters with $\dot{M} \gtrsim 300\ M_{\odot}\ \mathrm{yr}^{-1}$. Cooling flow deposition rates were estimated by Allen & Fabian (1998) and Peres et al. (1998) based on a deprojection analysis of *ROSAT* data. The clusters that have been labeled are those which now have published entropy profiles inferred from *Chandra* or *XMM-Newton* observations.

2001, 2003; Kaastra et al. 2004). Thus, the inferred mass deposition rates may not be perfect indicators of whether a cluster is a "cooling flow" cluster or not (i.e., whether or not it contains a peaked surface brightness and a central positive

temperature gradient). This is important if we wish to quantify comparisons between the models and CF or NCF clusters. In order to test this idea, we searched the literature for new *Chandra* and *XMM-Newton* observations of clusters in the Horner ACC and classified each system as either CF or NCF, and either relaxed or unrelaxed. Determination of CF versus NCF status is based primarily on the presence or absence of a well-defined central positive temperature gradient, while determination of the dynamical state is determined by the presence or absence of large-scale ($\sim$ a few hundred kpc) substructure in the X-ray images, which is presumably due to mergers. *Therefore, our classification scheme makes use of observed features rather than quantities inferred by fitting an assumed model.* The results of this classification are presented in Figure 6.7 for the $L-T$ relation and Figure 6.8 for the $L-M$ relation. Table 6.1 lists the clusters plotted in Figs. 6.7 and 6.8 along with their classifications.

An examination of Fig. 6.7 demonstrates that our "cooling flow" classification scheme correlates well with the results plotted in Fig. 6.6, although the results in Fig. 6.7 look less impressive since, to date, only a relatively small number of clusters in the ACC have been observed by *Chandra* or *XMM-Newton*. Furthermore, Fig. 6.7 indicates that there are apparently more unrelaxed NCF systems than relaxed systems. It is important to note, however, that the majority of NCF clusters observed with *Chandra* to date have been selected because they were known to be mergers (for the purposes of studying bow shocks, etc.). This is discussed further in §6.6 & 6.7. Interestingly, several of the clusters that lie roughly on the boundary between high and low $\dot{M}$ systems in Fig. 6.6 have switched "cooling flow" classification in Fig. 6.7 (e.g., A1413, A1689). More importantly is that, *in general, the dynamical status of a cluster does not seem to influence its position on the $L-T$ diagram* (note that the relaxed and unrelaxed NCF clusters lie together in one locus while relaxed and unrelaxed CF clusters lie together in another). This point is discussed further in §6.5 and 6.6.

The $L-M$ relation plotted in Fig. 6.8 has many of the same features present in

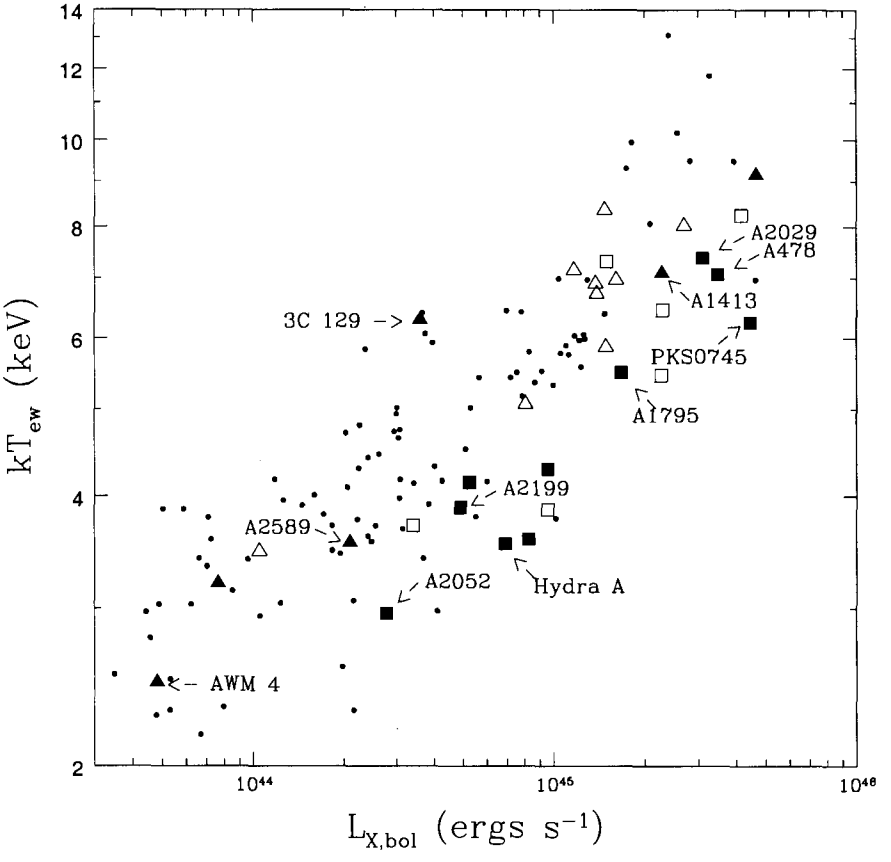

Figure 6.7: Same as Fig. 6.6 but using published *Chandra* and *XMM-Newton* data to classify the clusters according to CF status and morphology. Here, squares represent CF clusters, triangles represent NCF clusters, filled symbols represent relaxed systems, and open symbols represent unrelaxed systems.

the $L-T$ relation. Namely, NCFs and CFs are separated according to luminosity, and dynamical status does not seem to systematically affect this trend. As far as we are aware, this is the first time the dispersion in the luminosity-mass relation has been shown to depend on "cooling flow" status, although Reiprich & Böhringer (2002) hinted at the existence of such a trend (ApJ, 567, pg. 730). Below, we examine whether any of the theoretical models can account for this intrinsic scatter and the dichotomy between NCF and CF clusters.

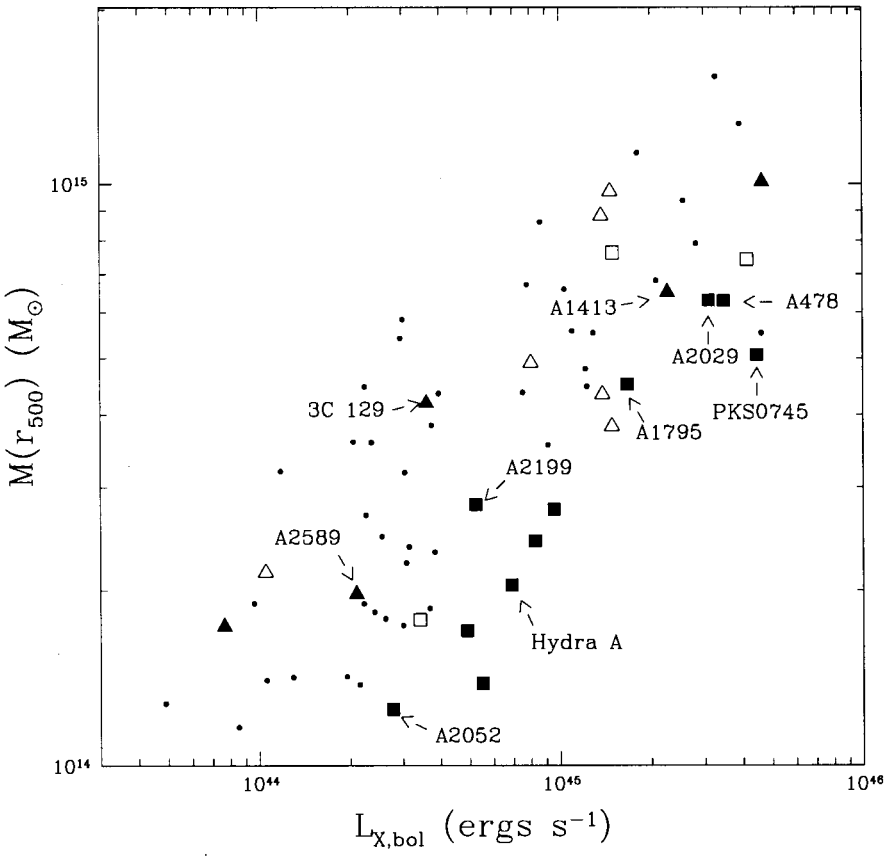

Figure 6.8: The observed $L - M$ relation of nearby, massive galaxy clusters. Luminosities are from Horner (2001) and masses are computed using the surface brightness profiles of Reiprich & Böhringer (2002) and uncorrected temperatures of Horner (2001). The symbols have the same meaning as in Fig. 6.7.

To begin with, we consider the issue of the cooling flow mass deposition rate, $\dot{M}$. The new *Chandra* and *XMM-Newton* high resolution X-ray data of massive CF clusters have been used to infer mass deposition rates typically ranging from $\dot{M} \sim 100 - 400 M_\odot$ yr^{-1} (e.g., Schmidt, Allen, & Fabian 2001; Ettori et al. 2002; Peterson et al. 2003), which is substantially lower than previous estimates based on *ASCA* and *ROSAT* data of the same clusters. Our model predicts mass drop out rates in range $300 - 500 M_\odot$ yr^{-1} once the initial entropy core has been radiated

Table 6.1: Properties of nearby clusters based on analysis of Chandra/XMM-Newton data

Cluster	CF/NCF	relaxed?	references
2A 0335+096	CF	yes	Mazzotta et al. (2003)
3C 129	NCF	yes	Krawczynski (2002)
A85	NCF	no	Kempner et al. (2002)
A115	CF	no	Gutierrez & Krawczynski (2005)
A133	CF	no	Fujita et al. (2002)
A478	CF	yes	Sun et al. (2003a)
A496	CF	yes	Dupke & White (2003)
A644	CF	no	Lewis & Buote (2002); Bauer & Sarazin (2000)
A665	NCF	no	Markevitch & Vikhlinin (2001)
A1060	NCF	yes	Yamasaki et al. (2002)
A1068	CF	no	Wise et al. (2004)
A1367	NCF	no	Sun & Murray (2002)
A1413	NCF	yes	Pratt & Arnaud (2002)
A1689	NCF	yes	Xue & Wu (2002)
A1795	CF	yes	Ettori et al. (2002)
A2029	CF	yes	Lewis et al. (2003)
A2034	NCF	no	Kempner et al. (2003)
A2052	CF	yes	Blanton et al. (2003)
A2142	CF	no	Markevitch et al. (2000)
A2199	CF	yes	Johnstone et al. (2002)
A2218	NCF	no	Machacek et al. (2002)
A2256	NCF	no	Sun et al. (2002)
A2589	NCF	yes	Buote & Lewis (2004)
A2597	CF	yes	McNamara et al. (2001)
A3112	CF	yes	Takizawa et al. (2003)
A3266	NCF	no	Henriksen & Tittley (2002)
A3667	NCF	no	Mazzotta et al. (2002)
A3921	NCF	no	Sauvageot et al. (2001)
AWM4	NCF	yes	O'Sullivan & Vrtilek (2004)
Hydra A	CF	yes	David et al. (2001)
MKW4	CF	yes	O'Sullivan & Vrtilek (2004)
PKS 0745-19	CF	yes	Chen et al. (2003)
RX J1720.0+2638	CF	no	Mazzotta et al. (2001)

Note.— "Cooling flow" status is based on the presence or absence of large declining temperature profiles towards the cluster center while dynamical status is based on the presence or absence of large-scale irregularities (presumably due to merging) in the X-ray images of the clusters.

away. To the extent that these two results can be compared, we are comforted by the reasonable agreement. Admittedly, the model results appear to be somewhat

larger than the "observed" values; however, we point out that the latter are inferred from the observations assuming an isobaric cooling flow model whereas our model values represent the actual physical cooling rate in the systems. Strictly speaking, a detailed comparison of the theoretical vs. "observed" mass drop out rates would entail making mock observations of our model clusters and then, use the isobaric cooling flow model to infer a mass drop out rate for the theoretical models, an exercise that is beyond the scope of the present study.

6.4.2 The $L - T$ relation

Plotted in Figure 6.9 is a comparison between the theoretical models and the observed $L - T$ relation. The various panels show the predicted relation for a range of entropy injection levels. The thick solid lines in each panel represent the luminosity-temperature relation prior to including the effects of radiative cooling. The hatched regions encompass the full range of $L - T$ values spanned by the model clusters during 13 Gyrs of cooling (similar to Fig. 6.5). The data is the same as that plotted in Fig. 6.7. We have not plotted error bars on the data as the statistical error bars on the luminosity are negligible and we have restricted ourselves to clusters with temperature determinations to better than 20% (i.e., $\Delta kT_{\rm ew}/kT_{\rm ew} \leq 0.2$). Thus, the intrinsic scatter in the relation dominates the statistical scatter.

The top left hand panel of Fig. 6.9 demonstrates why there has been so much effort invested in researching the role of non-gravitational gas physics in clusters. The thick solid line in this panel, which represents a model with no cooling and no entropy injection, clearly fails to match the observational data. It should be noted that there is essentially no freedom in the isothermal model, unless one is willing to resort to a drastically different dark matter profile than the one currently being considered. Cooling the isothermal model over the course of 13 Gyr (hatched region) does not improve the situation. If anything, it makes things worse, as the clusters' luminosities increase with the inclusion of cooling. In addition, the model

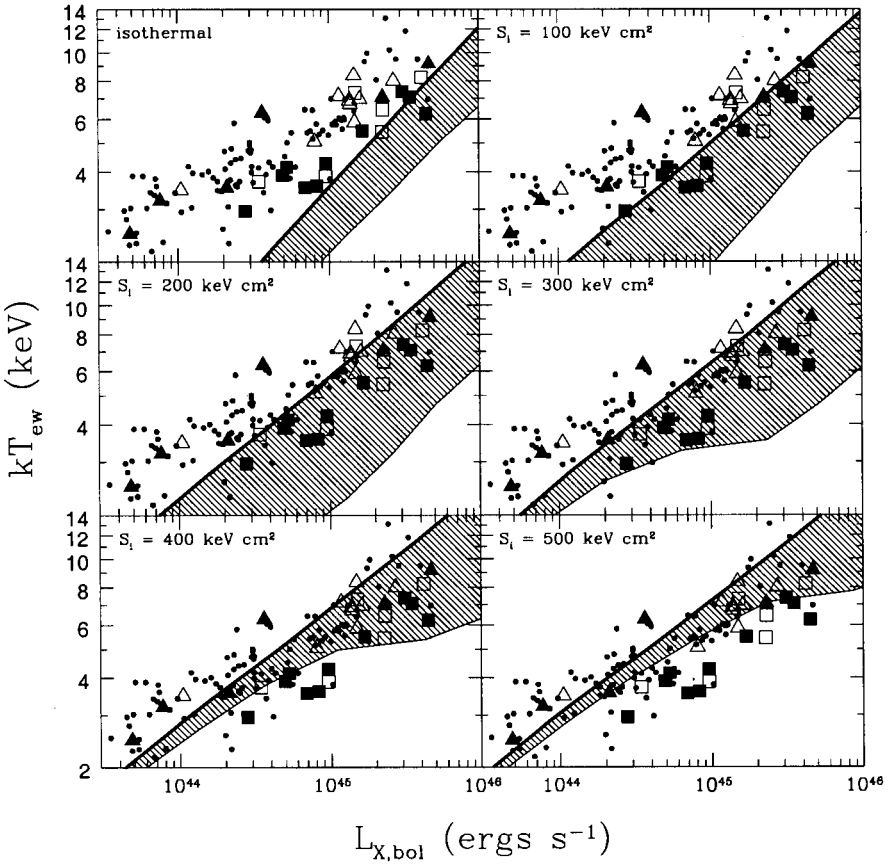

Figure 6.9: Comparison of theoretical models to the observed $L - T$ relation. The thick solid line represent the initial models prior to including the effects of cooling. The hatched region represents the full range of predicted $L - T$ values during cooling for 13 Gyr. The symbols have the same meaning as in Fig. 6.7.

also violates the observed cooled gas fraction of clusters reported by Balogh et al. (2001) (see Fig. 6.1). As noted in §6.2.1, very similar results are obtained if, instead of using the isothermal model, we make use of the non-radiative self-similar entropy profile of Voit et al. (2003) to construct an alternative baseline model. This is compelling evidence that some form of entropy injection is required.

First we investigate models with only a single, fixed entropy injection level. For example, we have previously reported that an entropy injection level of > 300

keV cm^2 provides a good fit to the data (e.g., Babul et al. 2002; McCarthy et al. 2003b). The aim of these studies was to account for the properties of groups and clusters minus any "cooling flow" component and, therefore, the effects of radiative cooling were neglected by these models. A better approach (which we have adopted in the present study), however, is to include the effects of radiative cooling and explicitly try to model uncorrected data. Surveying the thick solid lines in each of the panels (i.e., entropy injection only models), it is seen that injecting the ICM with ≈ 200 keV cm^2 gives the best fit to the *uncorrected* X-ray data (in the sense that the predicted relation falls more or less in the middle of the data). Injecting > 300 keV cm^2 tends to skew the predicted $L - T$ relation towards lower luminosities (i.e., the region occupied by NCF clusters), confirming our previous results for fits to "cooling flow" corrected data. However, with the large amount of intrinsic scatter present in the new uncorrected X-ray data, it is clear that no single entropy injection level can account for the uncorrected $L - T$ relation.

Alternatively, we could consider a range of entropy injection levels. As with any physical process, a variation in efficiency is likely to be the norm. However, in order to explain systems on the high-luminosity side of the $L - T$ relation (i.e., where CF clusters live), entropy injection levels of $S_i \lesssim 300$ keV cm^2 are required. The predicted central cooling time of massive clusters with this amount of injection is comparable to the Hubble time (see, e.g., Fig. 6.1) and, therefore, the effects of cooling need to be factored in. Additionally, as pointed out recently by Mushotzky et al. (2003), among others, simple entropy injection models cannot account for the observed entropy profiles of (some) groups and clusters, most likely because of the effects of radiative cooling. Central positive temperature gradients observed in many massive "cooling flow" clusters (e.g., Allen, Schmidt, & Fabian 2001) also attest to the importance of radiative cooling. In other words, the observations are unlikely to be explained by a model which includes a range of injection levels but not the effects of radiative cooling.

The alternative is to consider a model that includes both entropy injection and radiative cooling. Physically, this is probably the most plausible scenario anyway. However, as demonstrated by Fig. 6.9, it doesn't seem possible to explain all of the data with a single entropy injection level plus radiative cooling. An entropy injection level of $S_i \approx 300$ keV cm^2 probably comes the closest to explaining the data, but it is clear that a significant fraction of the clusters on the low luminosity side of the relation are not explained by this model. Increasing the injection level improves the situation but at the expense of losing agreement with the relaxed CF clusters. This makes sense since increasing the injection level mitigates the effects of radiative cooling. We are again forced to consider a model with a range of entropy injection levels but this time with the effects of radiative cooling included. With no constraints on the source of the entropy injection, indeed it can be seen from the trends in Fig. 6.9 that the data (including both relaxed CF and NCF clusters) can be accounted for by such a model. In particular, the CF clusters can typically be explained by entropy injection levels of $S_i \lesssim 300$ keV cm^2, while NCF clusters require higher injection levels.

6.4.3 The $L - M$ relation

While we place more weight on the $L - T$ relation (because it is based on essentially WYSIWYG observables), it is still useful to examine the $L - M$ relation as a consistency check. Figure 6.10 presents a comparison between the observed and predicted luminosity-mass relations[4]. Reassuringly, the same general trends may be derived from this plot as well; i.e., clusters on the low luminosity side of the relation can be explained by high levels of entropy injection, while clusters on the high luminosity side can be explained by low levels of entropy injection (plus radiative cooling). There are some slight differences, however, in the exact constraints placed on the injection levels by the $L-T$ and $L-M$ relations. These are probably due to issues associated with the analysis of the observational data as well as simplifying assumptions in the modeling [assumptions for the *observed*

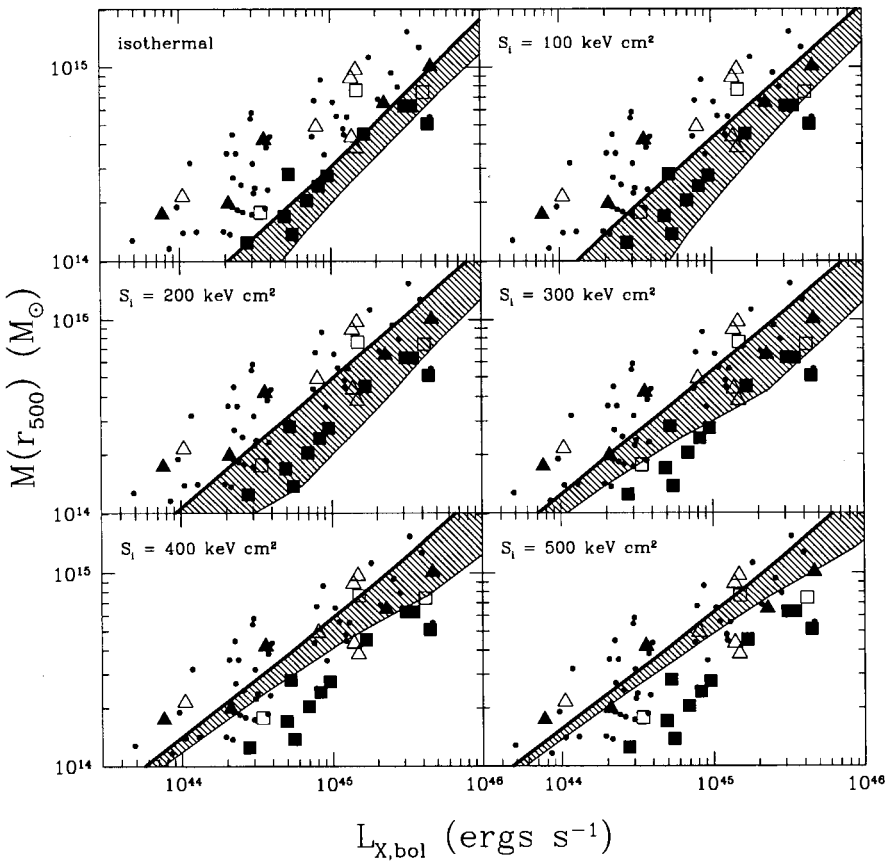

Figure 6.10: Comparison of theoretical models to the observed $L - M$ relation. The thick solid line represent the initial models prior to including the effects of cooling. The hatched region represents the full range of predicted $L - M$ values during cooling for 13 Gyr. The symbols have the same meaning as in Fig. 6.7.

mass calculation include isothermality, an assumed form for the surface brightness profiles (i.e., beta model), and spherical symmetry].

[4]The observed values of $M(r_{500})$ refer to the total mass (baryons and dark matter), whereas the model values neglect the baryon contribution. We have ignored the baryonic component in the models as hydrostatic equilibrium is computed using the dark matter potential only. However, this is a small effect that we can neglect since, at worst, the model masses are incorrect by a factor of $\Omega_b/\Omega_m \approx 0.119$ while the measurements uncertainties are typically $\sim 20\%$ (Reiprich & Böhringer 2002).

6.4.4 Summary

We have found that cooling only and entropy injection only models fail to reproduce the observed uncorrected luminosity-temperature and luminosity-mass relations of nearby massive, clusters. However, a model that includes a distribution of entropy injection levels and radiative cooling can account for these relations, including their intrinsic scatter and the dichotomy between relaxed NCF and CF clusters. In particular, NCF and CF clusters require relatively large and small amounts of additional entropy, respectively, with $S_i \approx 300$ keV cm^2 essentially being the dividing line between the two classes of clusters. In retrospect, this result is not surprising, since the cooling threshold, assuming cooling for roughly a Hubble time, for a typical massive cluster with $kT_{ew} \sim 6$ keV is ~ 300 keV cm^2 (see Fig. 1 of Voit & Bryan 2001).

Immediately below, we examine whether or not such a model can account for the observed structural properties of clusters, as deduced from new *Chandra* and *XMM-Newton* data.

6.5 Comparison with Observed Structural Properties

6.5.1 Entropy profiles

Presented in Figure 6.11 are the observed entropy profiles of the *relaxed* clusters labeled in Figs. 6.7 & 6.8 as derived from new *Chandra* and *XMM-Newton* data. These clusters include 3C 129 (Krawczynski 2002; *Chandra* data), A1413 (Pratt & Arnaud 2002; *XMM-Newton* data), AWM4 (O'Sullivan & Vrtilek 2003; *XMM-Newton* data), A2589 (Buote & Lewis 2004; *Chandra* data), A2199 (Johnstone et al. 2002; *Chandra* data), A1795 (Ettori et al. 2002; *Chandra* data), A2052 (Blanton et al. 2003; *Chandra* data); A478 (Sun et al. 2003a; *Chandra* data), A2029 (Lewis, Buote, & Stocke 2003; *Chandra* data), PKS0745 (Chen, Ikebe, &

Böhringer 2003; *XMM-Newton* data) and Hydra A (David et al. 2001; *Chandra* data). In some cases, the actual deprojected entropy profile was not published but could be easily derived from the published deprojected temperature and density (or pressure) profiles. In such cases, we assume a $0.3Z_{\odot}$ metallicity if none was listed. The hatched region is the predicted zone of entropy profiles from clusters with emission-weighted temperatures ranging from $3\,\mathrm{keV} \lesssim kT_{\mathrm{ew}} \lesssim 9\,\mathrm{keV}$ (roughly matching the observed range) and whose *initial entropy core has dropped out.* The value of the initial core is irrelevant since, once the core has dropped out, the resulting entropy profiles for clusters of a given mass are identical in the model of Babul et al. (2002). In other words, the hatched region illustrates where clusters that are actively cooling gas out should live. If, however, the gas was injected with entropy and has not had enough time since to cool out the resulting entropy core, we should expect to see elevated entropy levels near the cluster center (see Fig. 6.2). At large radii, however, all of the profiles should converge to the hatched region, as this is the regime where shock heating becomes much more important than the non-gravitational entropy injection.

One of the first features that leaps out of Fig. 6.11 is that essentially all of the observed entropy profiles converge to the hatched region at large radii, where non-gravitational physics is less important. This suggests that high resolution numerical simulations are doing an excellent job of capturing the gravitational gas physics of cluster formation (again, we note that the entropy profile at large radii in our models has been forced to match the results of non-radiative simulations).

But how does the entropy injection plus cooling model measure up to the observed entropy profiles at small radii? The answer is surprisingly well. A comparison of Fig. 6.11 to Figs. 6.7 & 6.8 shows that there is a clear trend between central entropy and dispersion in the $L-T$ and $L-M$ relations. Namely, the central entropy increases as one goes from the high luminosity side to the the low luminosity side of these relations. This is quite reminiscent of the trend between dispersion in the $L-T$ and $L-M$ relations and "cooling flow" status plotted

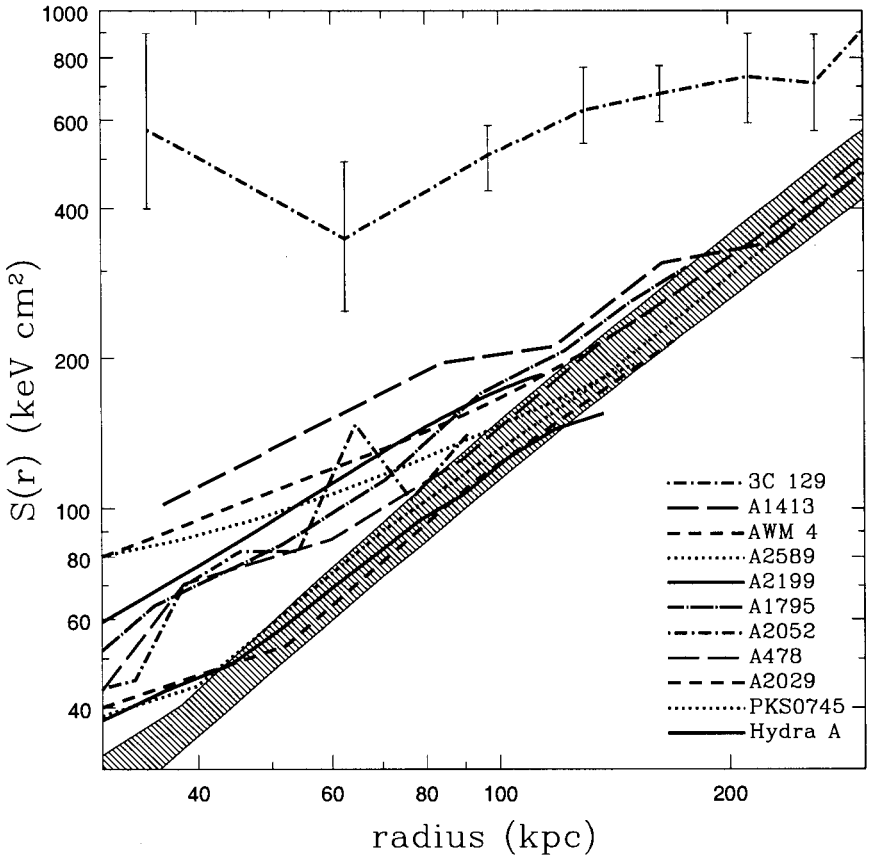

Figure 6.11: The entropy profiles of 11 nearby, massive clusters observed with *Chandra* or *XMM-Newton*. The key in the bottom right hand corner is ordered according to the central entropy values of these clusters in descending order (i.e., 3C 129 is the top long dashed line, A1413 is the long dashed line immediately below, and so on). With the exception of 3C 129, errors on the derived entropy profiles are typically 10%. The hatched region represents the model predictions for clusters that are actively cooling gas out (see text).

in Figs. 6.6-6.8. In fact, based on the present results, we would argue that the latter is a direct consequence of the former. For example, in order to explain an 'extreme' (relaxed) NCF cluster like 3C 129 on the basis of the results presented in §6.4, we require an extraordinarily large entropy injection level of $S_i > 500$ keV cm^2 (see Fig. 6.9). This may seem unlikely, but Fig. 6.11 indeed demonstrates

that 3C 129 has a very high central entropy. Also consistent with this trend are intermediate clusters such as A2589, AWM 4, and A1413 (which lie more or less in the middle of the $L-T$ and $L-M$ relations), that show elevated central entropies, and massive "cooling flow" clusters, such as PKS0745 and Hydra A, which show almost no excess entropy in their cores.

So the entropy injection plus cooling model we have proposed works fairly well in terms of explaining the observed entropy profiles of massive clusters. However, the current sample of 11 profiles is obviously too small to be definitive. It should also be noted that the majority of clusters with published entropy profiles were selected on the basis of prior (i.e., *ROSAT/ASCA*) evidence for "cooling flows" (see Figs. 6.7 & 6.8). Therefore, it is reasonable to expect that the current data set is biased towards clusters with low central entropies. This may be partially responsible for earlier claims that large amounts of entropy injection are ruled out (e.g., Pratt & Arnaud 2003; Mushotzky et al. 2003). A simple way of testing this model would be to obtain the entropy profiles for a large, *representative* sample of clusters. It should be kept in mind that NCF clusters could make up 30% (or more) of all nearby clusters (Peres et al. 1998). We expect that such samples will soon be available as more and more *Chandra* and *XMM-Newton* data become public.

6.5.2 Surface brightness profiles

X-ray observers often parameterize the observed X-ray surface brightness profiles by fitting the observed profile to assumed analytic functions. The simplest and most commonly used of these is the β model (Cavaliere & Fusco-Femiano 1976). This family of curves is characterized by two parameters: r_c, which measures the size of the constant surface brightness X-ray core, and β, which measures how rapidly the X-ray flux falls off with radius beyond the core. While we recognize that the simple β model does not provide a perfect match to *either* the observed profiles or the predicted profiles of our model clusters, the approach does provide a useful

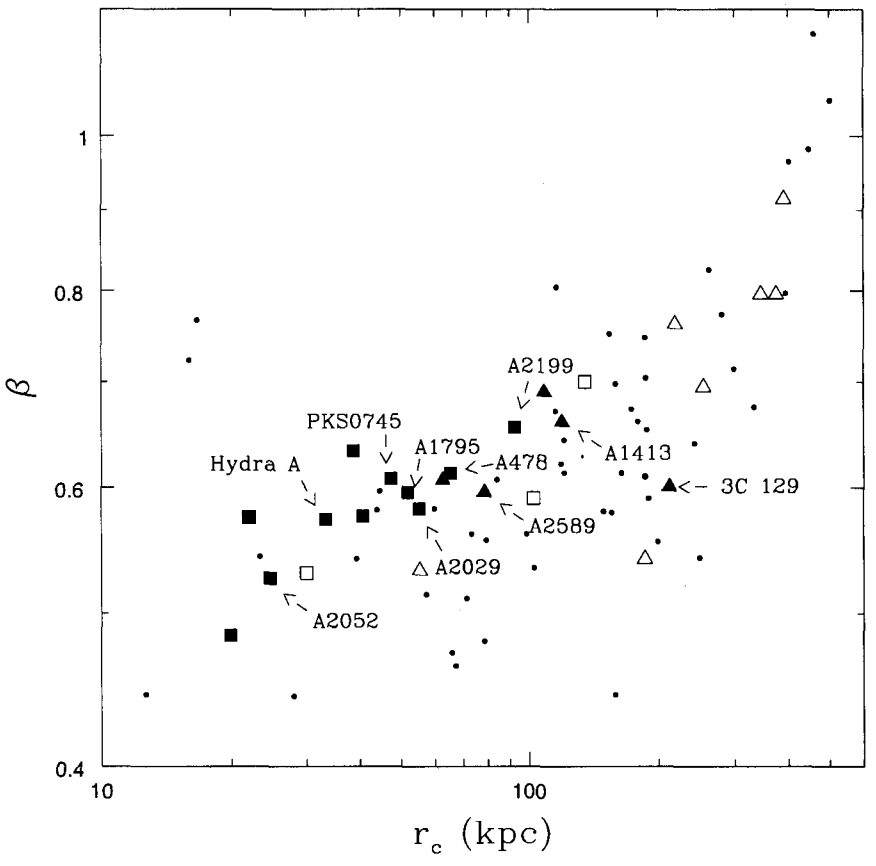

Figure 6.12: The $\beta - r_c$ relation for nearby, massive clusters observed with *ROSAT* by Reiprich & Böhringer (2002). The symbols have the same meaning as in Fig. 6.7. Labeled clusters are those with published entropy profiles (see Fig. 6.11).

characterization of the data/models for the purposes of comparison especially since the values of β and r_c for the observed profiles are readily available in literature.

Plotted in Fig. 6.12 is the observed relationship between the surface brightness shape parameters, β and r_c, as determined by Reiprich & Böhringer (2002) by fitting the single β model to clusters in the extended *ROSAT* HIFLUGCS sample. Only those clusters in common with the ACC have been plotted. For clarity, we have not plotted measurement error bars. Typically, measurement uncertainty on β and r_c is $\lesssim 10\%$.

One immediately noticeable trend is that the "cooling flow" and "non-cooling flow" clusters are separated according to core radius size and, to a much lesser extent, by the value of β. This trend between core radius size and "cooling flow" status has been known for some time (e.g., Mohr, Mathiesen, & Evrard 1999; Ota & Mitsuda 2002). More interestingly, the unrelaxed systems (particularly the unrelaxed NCF clusters) appear to be separated from the relaxed systems, in the sense that systems that are undergoing (or have recently undergone) mergers have larger core radii than those systems which appear relaxed. Given the results of §6.4.1, therefore, it would seem that mergers tend to influence the structural profiles of clusters (within the central regions) but not the overall global properties. This is consistent with the fact that "cooling flow correction" of relaxed CF clusters results in global properties typical of (relaxed and unrelaxed) NCF clusters (e.g., the "cooling flow corrected" $L - T$ relation; Markevitch 1998).

In §6.5.1, we found a correlation between dispersion in the $L - T$ and $L - M$ relations and the central entropy of clusters. Comparison of Fig. 6.12 with Figs. 6.7 and 6.8 illustrates that there is also a correlation between dispersion in the scaling relations and the size of a cluster's core radius. Therefore, we should expect an observed relationship between the size of a cluster's core radius and its central entropy. These quantities are plotted in Fig. 6.13 for the *relaxed* clusters explicitly labeled in Figs. 6.11 and 6.12. In the top panel of Fig. 6.13, we plot the entropy at a radius of 40 kpc versus core radius size, while in the bottom panel we plot the entropy at the core radius versus the core radius size.

With the exception of A2052, the results plotted in the top panel of Fig. 6.13 clearly demonstrate that the core radius of a cluster increases with increasing central entropy. The dashed lines show the best fit power-law relationship between the central entropy and core radius excluding A2052. The bottom panel, which instead plots the entropy at the core radius versus core radius size, shows an even tighter relationship with $\log S(r_c) = 1.65 \log r_c - 1.05$ (with r_c in kpc and $S(r_c)$ in keV cm^2).

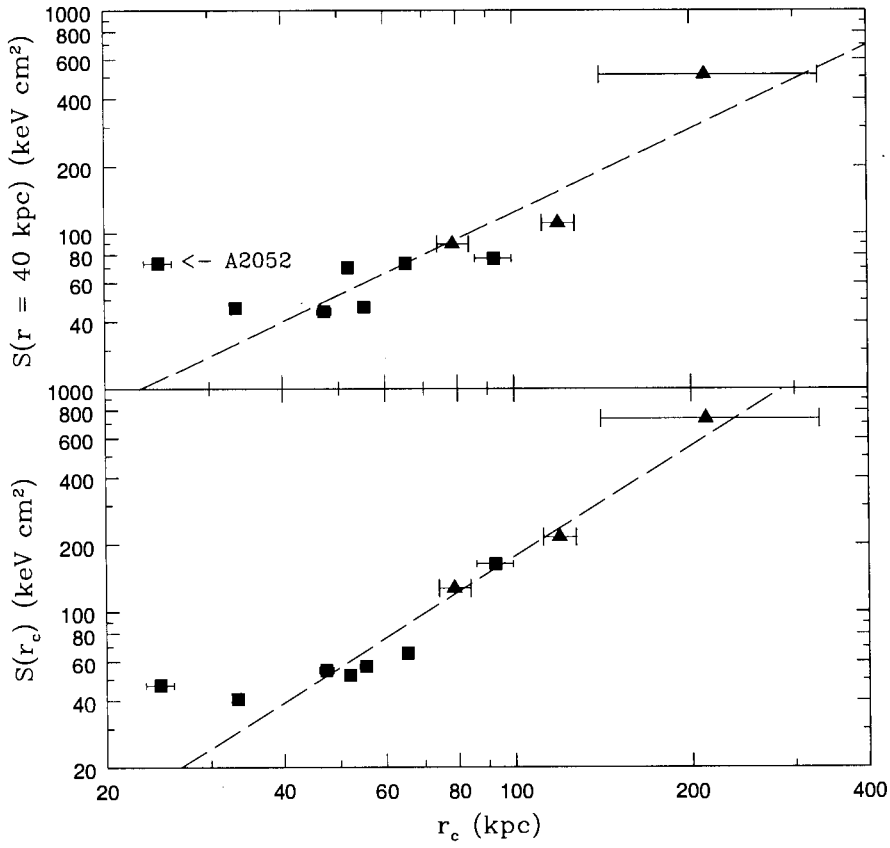

Figure 6.13: The observed relationship between core radius size and central entropy for the clusters plotted in Fig. 6.11. *Top*: Entropy at 40 kpc. *Bottom*: Entropy at the core radius. Measurement uncertainty in the entropy is typically 10%. Symbols have the same meaning as in Fig. 6.7. Dashed lines indicate the best fit power-laws to the relations (excluding A2052, see text). Namely, $\log[S(r = 40\text{kpc})] = 1.24 \log r_c - 0.39$ and $\log[S(r_c)] = 1.65 \log r_c - 1.05$.

A possible explanation for why A2052 is scattered away from the trend traced out by the rest of the clusters in Figure 6.13 is the presence of prominent bubbles in the core of this cluster (Blanton et al. 2003). While it is true that a number of other CF clusters plotted in Figure 6.13 also show evidence for bubbles in central regions (eg. A2199 and Hydra A), the bubbles in these clusters are relatively small compared to size of the region over which the gas is cooling (i.e., region within

which the gas temperature declines towards the cluster center). A2052, by contrast, has "large" bubbles and the impact of these features is such that one can account for the "cooling flow" properties of A2052 by azimuthally averaging over the X-ray bright, cool, bubble shells (McCarthy et al. 2003c). We hypothesize that the anomalous values of β and r_c for A2052 are the result of contamination from these bubbles. This illustrates a potential pitfall of characterizing the surface brightness profiles of clusters with simple β models, in that substructure can potentially throw off the fit to the data and give misleading results. Nonetheless, we find it quite remarkable that, within the context of the small sample we have examined, most systems follow a tight trend between core radius size and central entropy.

It is interesting to see whether or not the models can explain the $\beta - r_c$ relation plotted in Fig. 6.12 and also account for the relationship between the central entropy and r_c as well. Plotted in Fig. 6.14 is a comparison of the observed and predicted $\beta - r_c$ relations. The symbols have the same meaning as in Fig. 6.7 with exception of the diagonal crosses, which represent the model predictions. The crosses are the result of fitting single β models to the model surface brightness profiles as a function of time (as the cluster cools) for a suitable range of cluster masses [i.e., $M(r_{500}) \gtrsim 10^{14} M_{\odot}$]. As the clusters cool, both β and (especially) r_c decrease (i.e., with time, the model predictions typically move from upper right hand side of the plot to the lower left hand side; see arrow in upper right hand panel).

The results of Fig. 6.14 illustrate that models with entropy injection levels of $S_i \lesssim 200$ keV cm^2 + radiative cooling can account for relaxed CF clusters, while higher levels of entropy injection are typically required to explain relaxed NCF clusters. This is in excellent agreement with the results of §6.5. Not surprisingly, the unrelaxed NCF systems have core radii that are much larger than can be accounted for by the model clusters (which, by definition, are relaxed). Therefore, core radius size is a potentially promising way of distinguishing between relaxed and unrelaxed systems. In addition, the crosses in Fig. 6.14 indicate that as one

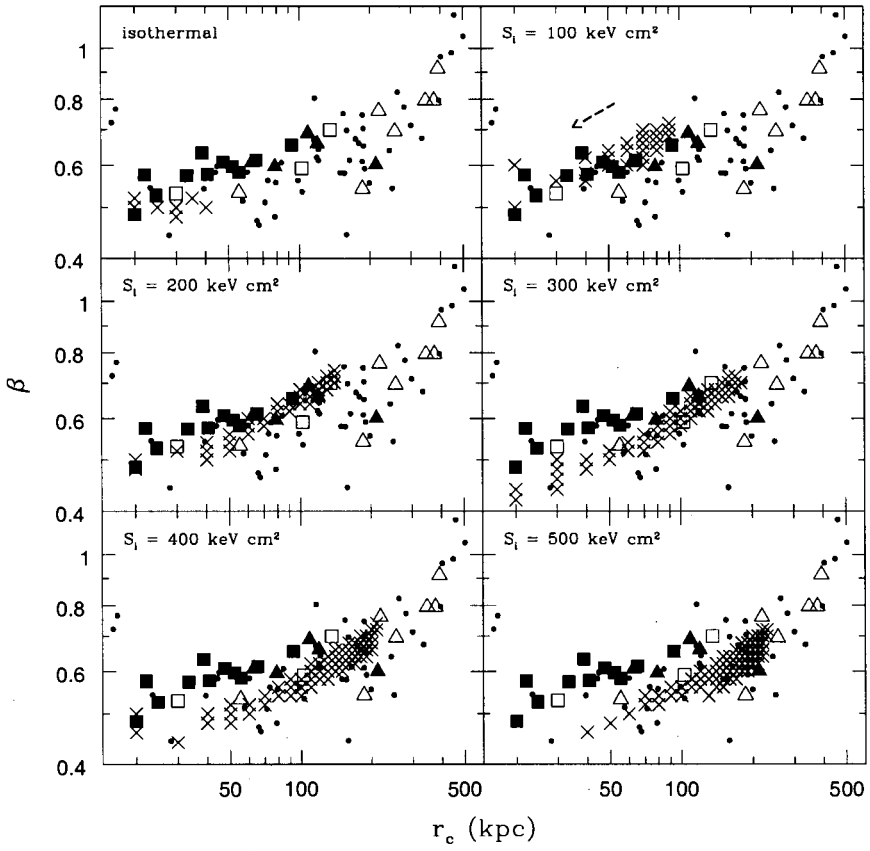

Figure 6.14: Comparison of theoretical models to the observed $\beta - r_c$ relation. The symbols have the same meaning as in Fig. 6.7 with the exception of the diagonal crosses, which represent the model predictions (see text). The arrow in the upper right hand panel indicates which way the model predictions evolve as the clusters cool.

injects more and more entropy into a system the larger its core becomes (as is also evident from Figs. 6.2 and 6.3). This qualitatively matches the trends seen in Fig. 6.13. Because the central entropy and core radius evolve with time in the models, a more direct comparison between theory and observations would require knowledge about how long each observed system has been able to cool for.

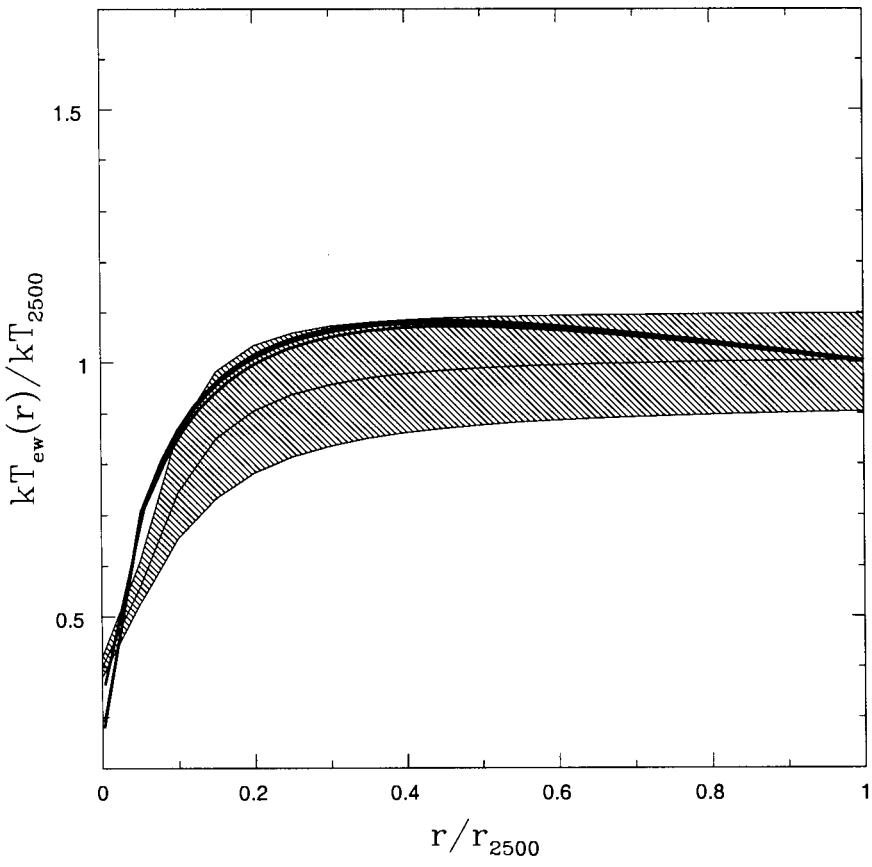

Figure 6.15: Comparison of observed and predicted temperature profiles for "cooling flow" clusters. The hatched region represents the observational results of Allen, Schmidt, & Fabian (2001) from a sample of 6 massive, "cooling flow" clusters. The solid black lines represent the predictions of our model *after the entropy core has dropped out* for a range of high mass clusters.

6.5.3 Temperature profiles

Finally, we make a comparison between observed and predicted temperature profiles. Plotted in Fig. 6.15 is the so-called universal temperature profile of Allen, Schmidt, & Fabian (2001). This was derived from a sample of 6 clusters observed with *Chandra* and classified as relaxed, massive "cooling flow" clusters by these authors. Also shown (solid lines) are the predictions of our entropy injection plus

cooling model *after the initial core has dropped out* for a range of cluster masses. The model profiles have been normalized the same way as the observational results; i.e., radii have been normalized to r_{2500} and temperatures have been normalized to the temperature at that radius.

Overall, the fit to observational data is quite good. There is a hint of some slight differences at very small radii, although the hatched region (which represents Allen, Schmidt, & Fabian's best fit to their data) does not encompass all of the scatter in the observed temperature profiles (see Fig. 1 of Allen, Schmidt, & Fabian 2001). Thus, so long as there is enough time to cool out the initial entropy core, the model does a very good job of matching relaxed, massive CF clusters.

Unfortunately, there are very few relaxed NCF clusters with published *Chandra* or *XMM-Newton* temperature profiles. Furthermore, comparison with observations is made difficult by the fact that our model does not predict a quasi-steady state "non-cooling flow" temperature profile but, rather, a full distribution of profiles (see Fig. 6.4). We do note, however, that 3C 129 has a sharp *negative* temperature gradient at its center (i.e., sharp rise towards the center; see Fig. 2 of Krawczynski 2002), which is qualitatively what we should expect from a system that had a large injection of entropy (see Fig. 6.4).

6.6 Discussion

A major result of the present study is that a relatively wide range in entropy injection levels combined with subsequent radiative cooling is required to explain the observed global and structural properties of massive clusters. That cooling is an essential process is the least surprising result. The very fact that clusters are radiating in X-rays is evidence that they are cooling. However, the large scatter in their global and structural properties suggests large cluster-to-cluster variations in cooling efficiency. We have shown that this can be accounted for as a by-product of variations in the level of entropy injection. Regardless of the source of the entropy

injection, cluster-to-cluster variations in injection efficiency are to be expected. A similar suggestion was recently put forward by Sun et al. (2003b) in order to explain scatter in the observed entropy profiles of 6 low mass groups.

Variations in the injection level can also naturally account for the dichotomy between NCF and CF clusters. The prevailing view is that NCF clusters are systems that have been disrupted by recent major mergers. This picture is often supported by images of NCF clusters which show disturbed X-ray morphologies (although, admittedly, NCF clusters typically have flatter surface brightness profiles and, therefore, it should be easier to pick out irregularities in these systems than in CF clusters). Indeed, it is likely that some of the NCFs are the result of mergers, and such systems should be removed from consideration[5], but, as we have already discussed, there are several NCF clusters that look remarkably relaxed and do not show any obvious signs of ongoing mergers (e.g., 3C 129, A2589, A1060, A1651, A1689, AWM 4, A3571, A1413, RX J1200.8-0328, RX J1120.1+4318). Such systems need to be accounted for. Moreover, in the currently favored hierarchical model for structure formation, *all massive systems* are formed through mergers and accretion of smaller objects. Therefore, CF clusters should also experience major mergers, since they are a ubiquitous feature of the ΛCDM cosmology. In fact, Loken, Melott, & Miller (1999) showed that CF clusters tend to occupy more crowded regions of the universe than NCF clusters. Perseus, RX J1347.5-1145, A2142, A1644, and A644 are all examples of clusters which are believed to be undergoing mergers (or have recently undergone a merger) and yet have retained their "cooling flow" identity. This argues against merging being the only difference

[5]Since only a small fraction of the clusters examined in the present study have high quality *Chandra* or *XMM-Newton* images available, we have not explicitly excluded merger systems from the first part of this study. As we have shown, mergers do not seem to significantly influence *global* properties such as the $L-T$ and $L-M$ relations (see §6.4.1) and, therefore, we do not expect a significant bias to be present. When investigating *structural* properties (§6.5), on the other hand, only the profiles of relaxed systems were considered, as azimuthally-averaged profiles for highly asymmetric (merging) clusters are essentially meaningless.

between CF and NCF clusters.

In order to explore these ideas more explicitly, we have carried out a series of numerical simulation experiments involving the merging of clusters of various mass ratios and impact parameters. In addition, the effects of radiative cooling have been included. The results of this study will be presented in a forthcoming paper (Poole et al. in preparation). We briefly note, however, that the recent hydrodynamic study of Motl et al. (2004) shows that it is extremely difficult to disrupt the dense cores of cooling clusters and, subsequently, form a system that resembles a NCF cluster. Typically, the clusters regain their CF status on a very short time scale. Similar conclusions were reached by Gómez et al. (2002). This lends further credence to the hypothesis that some other mechanism, in addition to merging, may be required in order to explain the relatively large fraction of NCF clusters observed in the local universe. Based on the results of the current study, we would argue entropy injection is the required mechanism.

But what is the source of the additional entropy? This is perhaps the single most important outstanding issue of models which implement entropy injection. A whole host of entropy injection mechanisms (a number of which are discussed in detail in §1 of Babul et al. 2002) have been proposed to explain the overcooling/cooling flow problem and also the global X-ray scaling relations of clusters. The most commonly proposed mechanism is galactic winds driven by supernovae, which are expected to transfer relatively large amounts of thermal energy into the ICM (e.g., Loewenstein 2000; Voit & Bryan 2001). However, in order to explain the scaling relations of clusters, the efficiency of the supernovae must be extremely high (probably unreasonably high) and even then one requires a top-heavy stellar initial mass function (e.g., Balogh et al. 1999; Valageas & Silk 1999). As such, supernovae by themselves are unlikely to be the source of the entropy/energy injection. Heating via quasars and active galactic nuclei (AGN), either prior to or following cluster formation, is a currently popular (proposed) mechanism, since such objects potentially contain vast reservoirs of energy. While it seems there is

plenty of energy available, it is still unclear exactly how the AGN heat the gas. Possibilities include Compton heating of intracluster electrons via high energy UV and X-ray photons emitted by the AGN accretion disk (e.g., Ciotti & Ostriker 1997, 2001), shock heating by transonic or supersonic jets (e.g., Binney & Tabor 1995; Omma et al. 2004), entrainment, transport, and subsequent mixing of low entropy gas via buoyantly rising bubbles of hot plasma inflated by the AGN (e.g., Quilis, Bower, & Balogh 2001; Mathews et al. 2003; Dalla Vecchia et al. 2004), and viscous dissipation of the kinetic energy of the rising bubbles (e.g., Fabian et al. 2003; Ruszkowski, Bruggen, & Begelman 2004). Detailed calculations, which are beyond the scope of this paper, are required in order to assess whether AGN are able to give rise to the distribution of entropy injection levels required to account for the X-ray properties discussed above.

Entropy injection into the central regions of the clusters can also be achieved via heat transport from outer regions. Two transport mechanisms have been proposed: thermal conduction (e.g. Narayan & Medvedev 2001) and turbulent mixing (e.g. Kim & Narayan 2003). Until recently it was thought that conduction would be an inefficient heat transport mechanism, since the presence of intracluster magnetic fields should strongly suppress conduction. However, Narayan & Medvedev (2001) demonstrated that if the magnetic fields are tangled it is still possible to achieve conductivities of up to one-third the Spitzer conductivity. Zakamska & Narayan (2003) subsequently demonstrated with simple models that conduction could offset radiative losses in some (but not all) CF clusters. However, through the use of hydrodynamical simulations that include radiative cooling and conduction, Dolag et al. (2004) showed that while conduction may be important for the most massive clusters, it does not significantly modify the properties of lower mass clusters (since the conductivity has a strong temperature dependence). Thus, thermal conduction is unlikely to be solely responsible for the distribution of entropy injection levels inferred in the present study. On the other hand, turbulent mixing of the intracluster gas, which is likely caused by stirring due to infalling and or-

biting substructure, is perhaps more promising (El-Zant et al. 2004; Bildfell et al. in preparation). For example, Kim & Narayan (2003) have demonstrated that one can reproduce the slope of the $L - T$ relation for high mass clusters with a simple mixing model. However, it has yet to be demonstrated whether such a model can account for the normalization of the relation and its associated scatter.

Finally, we note that our estimates for the amount of non-gravitational entropy required to explain the observed x-ray properties of relaxed clusters — and our subsequent evaluation of the possible sources of this entropy — implicitly assumed that in the absence of any entropy injection, the cluster gas will exhibit a very small entropy core, if any. The reason for making this assumption is because if one places isothermal gas in the cluster potential well (i.e., the standard model), the gas density distribution will have an exponential form and, correspondingly, the entropy profile will have a small core (both in size and amplitude). This implicitly assumes the underlying (dark matter) potential is similar to those found from high resolution numerical simulations. For a singular isothermal sphere, there is no entropy core whatsoever.

The above analytic result is borne out by SPH non-radiative simulations of galaxy clusters. Although there is some evidence for an entropy core in low resolution simulations, this core decreases in size and amplitude with increasing resolution (e.g., Frenk et al. 1999; Lewis et al. 2000), indicating that the core in the low-resolution simulations is a numerical artifact.

More recently, though, high-resolution mesh-based (e.g., AMR) non-radiative simulations show substantial entropy cores that persist even when the simulation resolution is increased, while agreeing with SPH results at large radii (e.g., Voit et al. 2003). Moreover, there appears to be a coupling between the magnitude and the size of the entropy core in individual cluster and the cluster's merger history. The origin of the core, and in fact whether the core is indeed real has yet to be ascertained. In fact, there is no clear explanation available as to why the SPH and mesh-based codes give such different result. Clearly, though, a more careful study

is warranted because if the AMR results are correct, then the stringent constraints on the amount of non-gravitational entropy injection required is correspondingly reduced. Quite independent of how the entropy core arises, our present study demonstrates that a distribution in magnitudes of the central entropy cores in galaxy clusters is key to understanding their global and structural properties.

Finally, in the present study, we have purposely focused on high mass clusters since temperatures and luminosities are fairly straightforward quantities to measure for these systems. However, a complete picture must also address the intragroup medium. The low X-ray luminosity of poor groups makes this a difficult challenge. Not only are there much poorer statistics, in terms of low signal-to-noise ratios, but a significant fraction of the flux can originate from point sources and the ISM of the central galaxy, making disentanglement of the ICM that much harder. A good example of just how difficult it is to obtain reliable results from group data is presented in the recent study of Osmond & Ponman (2004). By simply increasing the number of low temperature systems in their data set, and also correcting the luminosity to a fixed overdensity, these authors found that the evidence for steepening of the $L-T$ relation in groups (e.g., Mulchaey & Zabludoff 1998; Helsdon & Ponman 2000), relative to self-similar predictions, is no longer solid. In order to make a fair comparison between the models and group data, one needs to fold the instrumental response of the X-ray satellite into the theoretical models. Furthermore, the models should be analysed the same way as the observational data (Poole et al. 2004b in preparation). A future project, therefore, is to 'observe', with a mock X-ray satellite (which mimics *Chandra* or *XMM-Newton*), a realistic population of groups and clusters that includes the effects of radiative cooling and specific entropy injection processes such as conduction, mixing, and AGN heating.

6.7 Conclusions

Recent X-ray observations have highlighted the lack of large isentropic cores in groups and clusters and have led some to suggest that radiative cooling is the dominant mechanism in the breaking of self-similarity. However, radiative cooling alone leads to a predicted overabundance of cooled gas in theoretical models (the so-called "cooling crisis"). In order to explain the observed entropy profiles and also retain consistency with the observed fraction of cold baryons (stars) in clusters, it is likely that both radiative cooling and some form of entropy injection are required. We have performed a thorough investigation of this scenario by adding a realistic treatment of the effects of radiative cooling to the entropy injection model of Babul et al. (2002). A comparison to the current suite of X-ray observations was then made with a particular emphasis on assessing whether or not the model could account for the large amount of intrinsic scatter in the observed scaling relations and, simultaneously, account for the observed entropy, surface brightness, and temperature profiles of clusters. The main results can be summarized as follows:

- Injecting the ICM with $S_i \gtrsim 200$ keV cm^2 prevents significant mass drop out due to radiative cooling and insures the observed fraction of cold baryons ($\lesssim 10\%$; Balogh et al. 2001) is not violated.

- Radiative cooling approximately maintains the initial power-law between entropy and radius, $S \propto r^{1.1}$, at large radii and extends it to small radii as well, so long as there is enough time for cooling to wash out the effects of any non-gravitational entropy injection.

- Depending on the time elapsed since entropy injection (i.e., the time available for the cluster to cool radiatively), the model naturally predicts either clusters with flat central surface brightnesses and sharp central negative temperature gradients or clusters with peaked surface brightnesses and central positive temperature gradients. These match the main qualitative features of NCF

and CF clusters, respectively.

- Radiative cooling tends to have a larger effect on the luminosity of a cluster than its temperature. So long as only a small fraction of the cluster's baryons are cooled out ($\lesssim 10\%$), the result is that cooling moves the predicted $L-T$ relation to higher luminosities at a fixed temperature.

- An analysis of the $L-T$ and $L-M$ relations derived from the ACC of Horner (2001) and the extended HIFLUGCS of Reiprich & Böhringer (2002) demonstrates that there is a strong correlation between dispersion in these relations and "cooling flow" status. Although this trend has been illustrated before for the $L-T$ relation (although probably not as clearly), this is the first time it has been demonstrated for the $L-M$ relation.

- We find that a distribution of entropy injection levels combined with the effects of radiative cooling can account for the observed $L-T$ and $L-M$ relations and the large amount of intrinsic scatter associated with each. This is the first time a theoretical model has been shown to account for this intrinsic scatter. We also find that so-called "cooling flow" clusters typically require 'mild' amounts of entropy injection ($S_i \lesssim 300$ keV cm^2), whereas "non-cooling flow" clusters require larger amounts of injection. Interestingly, this dividing line is essentially equal to the cooling threshold for massive clusters (Voit & Bryan 2001; Babul et al. 2002), implying that the amount of entropy injection dictates which class (CF or NCF) a particular cluster will fall under. Moreover, so long as the CF clusters were injected with $S_i \gtrsim 200$ keV cm^2, their predicted cold gas fractions do not violate observational constraints.

- A natural consequence of our explanation for the scatter of the $L-T$ and $L-M$ relations is that the central entropy of clusters should increase as one goes from the high-luminosity side of these scaling relations to the low-

luminosity side. An examination of the deprojected entropy profiles of 11 relaxed massive CF and NCF systems observed with *Chandra* and/or *XMM-Newton* reveals just such a correlation between central entropy and dispersion in these scaling relations. It is this trend which likely gives rise to the previously identified relationship between $L-T$ dispersion and inferred cooling flow strength (see Fabian et al. 1994).

- The model predicts surface brightness profiles that are consistent with those of relaxed CF clusters when mild amounts of entropy are injected ($S_i \lesssim 200$ keV cm^2) and with relaxed NCF clusters when higher amounts of entropy are injected. This is in good agreement with the constraints placed on S_i from analysis of the $L-T$ and $L-M$ relations. The model also qualitatively explains the observed (newly discovered) relationship between a cluster's central entropy and the size of its core radius.

- We demonstrate that the model can also successfully explain the observed universal temperature profile (for relaxed, massive CF clusters) of Allen, Schmidt, & Fabian (2001).

- At present, there is a dearth of structural information (e.g., entropy and temperature profiles) of relaxed NCF clusters from *Chandra* and *XMM-Newton* data. A large number of the NCF clusters observed with these satellites are the sites of ongoing mergers (e.g., Govoni et al. 2004). It is important to note, however, that in most cases *these clusters were selected because they were known to be mergers* (for the purposes of studying 'cold fronts', bow shocks, etc.). However, there are examples of relaxed NCF clusters observed previously with *ROSAT* and *ASCA* (e.g., Buote & Tsai 1996, see also §6.6 of the present study). A simple way of testing the present model, therefore, would be to obtain deprojected entropy profiles for these systems (using the current generation of satellites) and see whether or not they possess elevated entropy levels at the centers.

The authors wish to thank the referee for useful comments which improved the quality of the paper, particularly the discussion of observational results. We thank Alastair Edge, Gilbert Holder, James Binney, and Greg Bryan for useful comments on an earlier version of the manuscript. We also thank Steve Allen, Roderick Johnstone, Henric Krawczynski, Ewan O'Sullivan, and Ming Sun for providing their Chandra/XMM-Newton results in electronic form and Greg Bryan and Mark Voit for providing the entropy profiles of their numerically simulated clusters. I. G. M. is supported by a postgraduate scholarship from Natural Sciences and Engineering Research Council of Canada (NSERC). A. B. is supported by an NSERC Discovery Grant and M. L. B. is supported by a PPARC fellowship.

Chapter 7

The Effects of Radiative Cooling on the Entropy Distribution of Intracluster Gas

Abstract

A number of theoretical explorations of the effects of radiative cooling in clusters find that radiative cooling naturally produces powerlaw entropy profiles in the cores of clusters. However, the origin of this behavior and its dependence on initial conditions have yet to be elucidated. In the present study, we explain this trend in the context of the self-similar cooling wave model developed previously by Bertschinger (1989). It is shown that the logarithmic slope of the entropy profile in the cores of cooling clusters is given by a simple analytic function that depends only on the logarithmic slopes of the local gravitational potential and the cooling function. Interestingly, high resolution X-ray observations indicate that, perhaps with the exception of the very central regions, the entropy profiles in the cores of massive "cooling flow" clusters are well approximated by powerlaws. A comparison to our pure radiative cooling models demonstrates that it is possible to account for the entropy and temperature profiles of such systems. Furthermore, the inferred gravitational potentials are relatively steep and are consistent with hydrostatic analyses of X-ray data and also with the predictions of cosmological numer-

ical simulations. We present a detailed discussion of the implications of our results for the non-gravitational heating of "cooling flow" clusters. Finally, we propose a few useful applications of our results, including a simple method for constructing realistic analytic cluster models that include the effects of radiative cooling and a test of the reliability of cooling routines implemented in analytic models and hydrodynamic simulations.

7.1 Introduction

The entropy distribution of the intracluster medium (ICM) is set by gravitational shock heating during the assembly of the cluster as well as non-gravitational processes such as radiative cooling and heating via AGN outflows and supernovae (both prior to and following cluster formation), thermal conduction, and perhaps heating from a variety of other sources as well. In terms of non-gravitational heating, the resulting entropy distribution will obviously depend sensitively on the level of heating and how it is distributed throughout the ICM. As such, a detailed understanding of the heating source is likely required. Radiative cooling, on the other hand, is potentially a more straightforward process to model, since the cooling rate depends only on the gas density of the ICM and the well-known cooling function, $\Lambda(T)$.

An interesting result that has come out of detailed studies of the effects of radiative cooling on the ICM (e.g., Kaiser & Binney 2003; Dalla Vecchia et al. 2004; McCarthy et al. 2004, hereafter M04; Voit & Donahue 2005) is that cooling naturally tends to establish powerlaw entropy profiles in the cores of clusters. Furthermore, this trend appears to be independent of the initial entropy distribution of the gas (see, e.g., §3.2 of M04). It would be interesting to understand from a physical perspective what is driving this trend.

Unfortunately, a rigorous calculation of the effects of radiative cooling and the subsequent (quasi-hydrostatic) inflow of intracluster gas can only formally be obtained by numerically solving the time-dependent hydrodynamic equations (as

approximately done, e.g., in M04). This makes it a challenge to understand physically why the above trend is established by cooling. Despite this inconvenience, there are, however, analytic tools at our disposal that can help to establish a physical picture. For example, Bertschinger (1989) (hereafter, B89) used a self-similarity analysis to derive the behavior of cooling gas in clusters. One of the interesting results derived by Bertschinger is that the logarithmic slopes of the gas density and temperature profiles for $r \ll r_{\rm cool}$ (where $r_{\rm cool}$ is the radius at which the cooling time of the gas equals the age of the cluster) depend only on the shapes of the cluster gravitational potential and of the cooling function. The behavior of the gas density and temperature profiles can be used to infer how radiative cooling influences the distribution of intracluster entropy, which is perhaps a more fundamental quantity since convection will strive to prevent the establishment of a rising entropy profile towards the cluster center. [Furthermore, entropy is a more sensitive probe of non-gravitational heating and cooling in clusters; see, e.g., Voit et al. (2002).] Thus, the study of B89 is a good starting point for our investigation of the effects of cooling on intracluster entropy.

Although our primary goal is to explore the physics of radiative cooling, our investigation is not merely academic. Recent high resolution X-ray observations from *Chandra* and *XMM-Newton* indicate that, perhaps with the exception of the very central regions, the entropy profiles in the cores of relaxed "cooling flow" clusters appear to be near powerlaws (e.g., David et al. 2001; Pratt & Arnaud 2002; M04; Piffaretti et al. 2005; Donahue et al. 2005). Thus, it would seem that pure radiative cooling models may be able to provide an accounting of relaxed "cooling flow" clusters. We explore this hypothesis in more detail below and discuss what implications this has for non-gravitational heating in such clusters.

An outline of the present study is as follows. In §2, we briefly review the self-similar analysis of B89, including the basic assumptions made in that study and their validity, and use his results to derive how radiative cooling modifies the entropy profiles of clusters. In §3, we compare the self-similar solution to the

results of the 1-D cooling model of M04 for clusters with powerlaw dark matter profiles and that cool via thermal bremsstrahlung. We then assess whether or not the solution of B89 is valid for clusters with more realistic dark matter profiles and that cool via both bremsstrahlung and line emission. In §4, we present a comparison of the theoretical models to X-ray observations of relaxed "cooling flow" clusters. Finally, in §5, we present a discussion of our results, including a description of a few potentially interesting applications of our results.

7.2 Cooling and Self-Similarity: The Solution of B89

As noted above, in general, the time-dependent hydrodynamic equations must be solved numerically in order to obtain a detailed picture of the effects of radiative cooling on cluster gas. However, when the time dependence is due to a single physical process that can be characterized by a unique scale length [in this case, the cooling radius[1], $r_{\rm cool}(t)$], it is possible to construct similarity solutions, which have the obvious advantage of offering useful, physical insight. Adopting this approach, B89 derived the general behavior of cooling gas in clusters of varying gravitational potentials (and varying cooling functions as well). We are especially interested in the properties of his solution for $r \ll r_{\rm cool}$, where cooling quickly establishes steady-state distributions for the properties of the gas that are independent of the initial conditions. (Outside the cooling radius the initial conditions of the gas are of crucial importance since radiative cooling hasn't had enough time to significantly modify the gas there.) Before examining the solution itself, let us first review the

[1]The cooling radius grows larger with time. Unfortunately, the self-similar solution in B89 is expressed in terms of the *initial* cooling radius. Thus, it might be expected that comparison to observations, which are used to infer the *present* cooling radius, is somewhat ambiguous. However, as noted by B89, this leads to only a small error since, over the course of a cluster's life, the cooling radius grows by only a small amount.

basic assumptions made in B89 and their validity.

Since self-similar solutions can be characterized by only a single scale length, some simplifying assumptions are required in order to obtain a solution for the properties of the cooling gas. In particular, Bertschinger assumed that the gravitational potential and the cooling function could be characterized by simple powerlaws that remained fixed as a function of time. Of course, in reality, neither of these assumptions are strictly valid. High resolution numerical simulations indicate that the dark matter density profiles of clusters (and halos of other masses as well) have a characteristic scale length (the so-called scale radius, r_s), where the index of the powerlaw profile changes from relatively shallow (between ~ -1 and -1.5; e.g., Navarro, Frenk, & White (NFW) 1997; Moore et al. 1999) to relatively steep (~ -3). The cooling function is not scale-free either, owing primarily to line emission. Thus, one is justified in questioning the physical relevance of a model that invokes these assumptions. We examine in §3.2 whether relaxing these assumptions significantly affects the shapes of the resulting entropy profiles in the cores of *massive* clusters.

Other assumptions made in the analysis of B89 include spherical symmetry, subsonic inflow, and single-phase cooling. Spherical symmetry is expected to be approximately valid, at least in an average sense for a reasonably large relaxed cluster sample. Likewise, subsonic flow should hold for the bulk of the gas within $r_{\rm cool}$, except possibly near the very center where the gas may cool on a timescale shorter than the dynamical time, possibly fragment, and flow inward transsonically. It has yet to be determined whether or not multi-phase cooling is important in clusters. Recent spatially-resolved *Chandra* and *XMM-Newton* spectra of the central regions "cooling flow" clusters have confirmed that, probably with the exception of the very central radial bin, single-phase models provide at least as good a fit as multi-phase models (e.g., David et al. 2001; Matsushita et al. 2002). For the present study, we assume single-phase cooling.

Finally, it is implicitly assumed that there are no significant sources of non-

gravitational heating (such as AGN feedback, thermal conduction, and turbulent mixing) present in the ICM. Again, our primary focus is to understand why radiative cooling tends to establish powerlaw entropy profiles in the cores of clusters. However, a discussion of non-gravitational heating is presented in §4.

Implementing the above assumptions, we follow B89 and renormalize the hydrodynamic equations by removing any time dependence arising through $r_{\rm cool}(t)$. A self-similar solution is obtained if one neglects the acceleration terms (which is valid since the inflow of gas is highly subsonic) in the renormalized hydro equations. It is straightforward to derive the behavior of the gas density and temperature profiles for $r \ll r_{\rm cool}$ under these conditions (see eqns. 2.30 of B89):

$$\frac{d\log\rho_g}{d\log r} = \frac{(2-\alpha)(1-\beta)-3}{2} \quad , \quad \frac{d\log T}{d\log r} = 2-\alpha \tag{7.1}$$

where we have assumed that dark matter dominates the gravitational potential and $\rho_{\rm dm} \propto r^{-\alpha}$, $\Lambda(T) \propto T^{\beta}$, and an adiabatic index for the gas of $\gamma = 5/3$. Note that the definitions of α and β differ from the definitions of these symbols in B89. In particular, $(\alpha-\beta)$ in the notation of B89 is equivalent to $(2-\alpha)$ in our notation.

In recent studies of the ICM, the following combination of observable quantities is often adopted as a proxy for the entropy of the gas: $S \equiv kTn_e^{-2/3}$. With a bit of manipulation, equation (1) can be used to yield the logarithmic slope of the entropy profile within $r_{\rm cool}$:

$$\epsilon \equiv \frac{d\log S}{d\log r} = \left[1-\frac{1}{3}(1-\beta)\right](2-\alpha)+1 \tag{7.2}$$

Thus, for $\beta = 1/2$ (i.e., cooling dominated by thermal bremsstrahlung),

$$\epsilon = \frac{5}{6}(2-\alpha)+1 \tag{7.3}$$

which yields $\epsilon = 1$ for a singular isothermal sphere ($\alpha = 2$), $\epsilon \approx 1.4$ for a Moore et al. profile ($\alpha = 1.5$ for $r \ll r_s$), and $\epsilon \approx 1.8$ for a NFW profile ($\alpha = 1$ for

$r \ll r_s$). Note, however, that the value of ϵ in equation (2) depends only weakly on the shape of the cooling function (that is, for typical values of β ranging from $-1/2$ to $1/2$) for $\alpha \gtrsim 1$.

Below, we compare this simple analytic result with the 1-D cooling model of M04.

7.3 Self-Similarity in the Context of Realistic ICM Models

7.3.1 Powerlaw clusters

A number of models have been proposed for the evolution of the ICM to explain the observed X-ray properties of galaxy clusters. As alluded to in §1, the majority of these models illustrate that radiative cooling, if effective, tends to establish a powerlaw entropy distribution for the gas in the cores of clusters. In order to test whether this trend is a manifestation of the self-similar behavior discussed in §2, we make use of the cooling model developed by M04. Briefly, the M04 cooling model is an improved version of the Babul et al. (2002) ICM entropy model, in that it explicitly accounts for the time-dependent effects of radiative cooling (see Babul et al. 2002 and M04 for a detailed discussion of the model). The model is able to successfully and simultaneously reproduce the luminosity-temperature and luminosity-mass relations (including their associated intrinsic scatter) and yield detailed fits to the entropy, surface brightness, and temperature profiles of clusters as inferred from recent high resolution X-ray observations.

We use the model of M04 to track the effects of cooling for a set of clusters with arbitrary initial conditions (recall that the solution of B89 within the cooling radius does not depend on initial gas conditions). As a starting point, we consider cluster-scale dark matter halos with powerlaw density profiles $\rho_{\rm dm} \propto r^{-\alpha}$. The halos are populated with gas with varying entropy profiles (see Figs. 7.1-7.2). The

initial gas density and temperature profiles are determined by placing the gas in hydrostatic equilibrium within the dark matter halos. For specificity, we present results for clusters that have a total dark matter mass of $10^{15} M_{\odot}$, a total gas mass of $\approx 1.5 \times 10^{14} M_{\odot}$, and a maximum radius, $r_{\rm halo}$, of 2.06 Mpc.

The cluster gas is allowed to evolve via radiative cooling and inflow until stable entropy profiles are achieved. To calculate the cooling rate, we use a pure thermal bremsstrahlung cooling function with $\Lambda(T) \propto T^{1/2}$. Finally, as in M04, we remove any gas that is able to cool below a threshold temperature of 10^5 K from the calculation and assume that its dynamical effects on the cluster gravitational potential are negligible. Clearly, if a significant amount of gas is able to completely cool this assumption will be violated. However, in this case, we expect the effects of mass accumulation will be relevant only for the very central regions of the cluster and will have a minor effect on the overall entropy distribution within the cooling radius.

To show how the effects of cooling are linked to the underlying gravitational potential, we present Figure 7.1. We start with a cluster that is initially characterized by an entropy profile that contains a core and a logarithmic slope of $\epsilon = 1.1$ outside the core. This is the initial slope adopted by Babul et al. (2002) and M04 and is what one expects if the gas is in hydrostatic equilibrium and if its density profile traces that of the dark matter (e.g., Voit et al. 2002; Williams et al. 2004), an expectation that is supported by high resolution hydrodynamic simulations (e.g., Lewis et al. 2000; Voit et al. 2003; Ascasibar et al. 2003; Voit 2005). As can be clearly seen, the slope of the dark matter profile, α, is important in determining the slope of the steady-state entropy profile within $\sim 0.1 r_{\rm halo}$ (which corresponds roughly to $r_{\rm cool}$ for these clusters). In particular, as the dark matter profile steepens the resulting entropy profile becomes more shallow, agreeing qualitatively and quantitatively with equation (3).

Figure 7.2 shows the results for clusters that have steeper entropy profiles outside the entropy core. A comparison of the various panels with each other

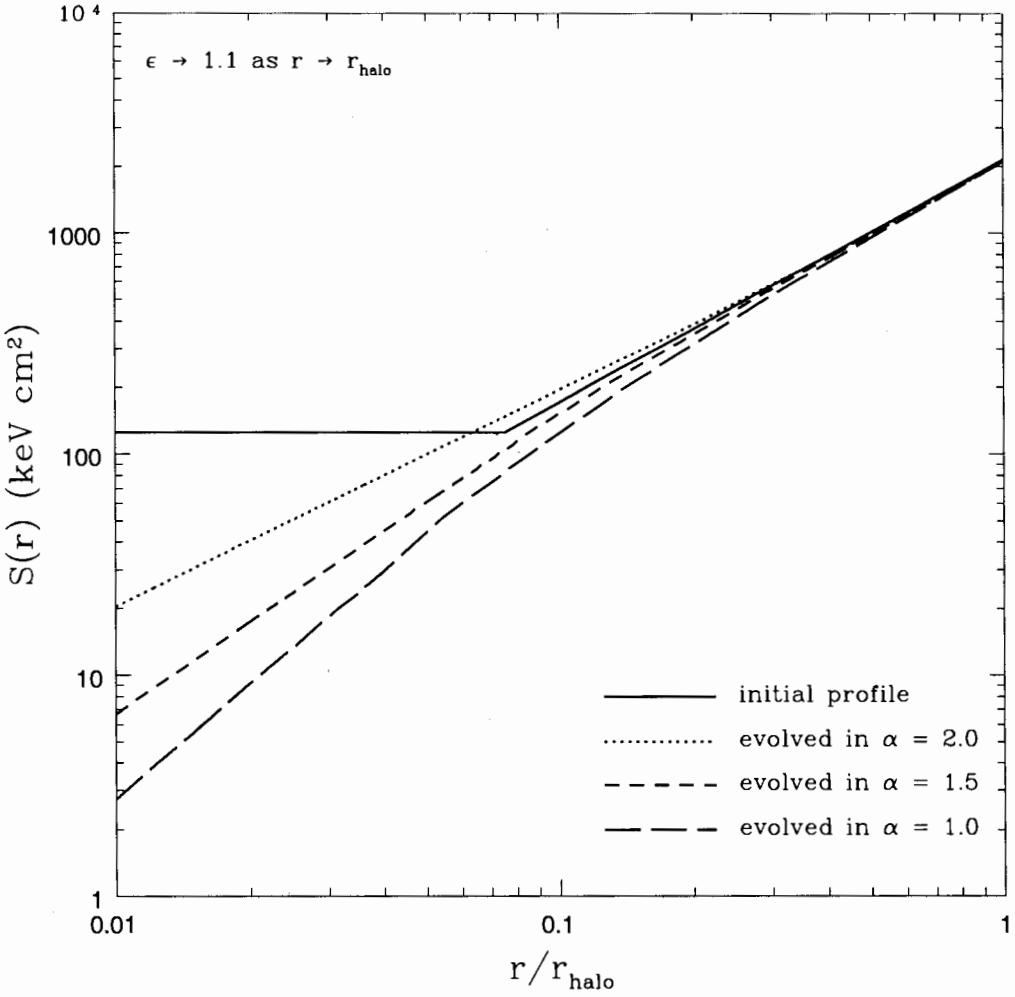

Figure 7.1: The effects of cooling and inflow on the entropy distribution of clusters. The solid line represents the initial entropy profiles. The dotted, short dashed, and long dashed lines represent the resulting steady-state entropy profiles when the ICM is evolved in dark matter halos that have density profiles characterized by powerlaw indices of $\alpha = 2.0$, 1.5, and 1.0, respectively. Figure 7.3 presents a comparison of the central logarithmic entropy slopes to the solution of B89.

and with Figure 7.1 illustrates that the initial conditions of the ICM have no effect on the resulting steady-state entropy profile within $r_{\rm cool}$. Likewise, what happens in the interior of the cluster does not significantly influence gas outside of $r_{\rm cool}$, as

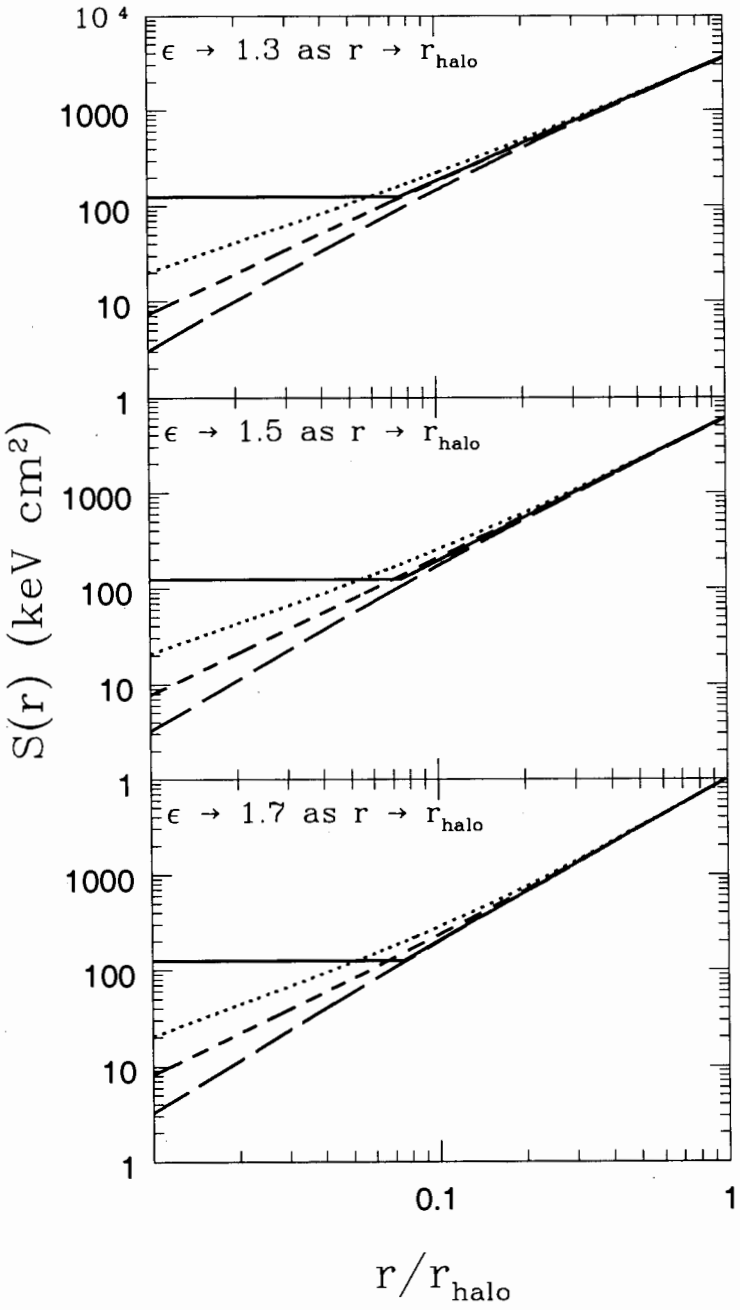

Figure 7.2: Same as Figure 7.1 but for clusters that have steeper entropy profilesoutside the core.

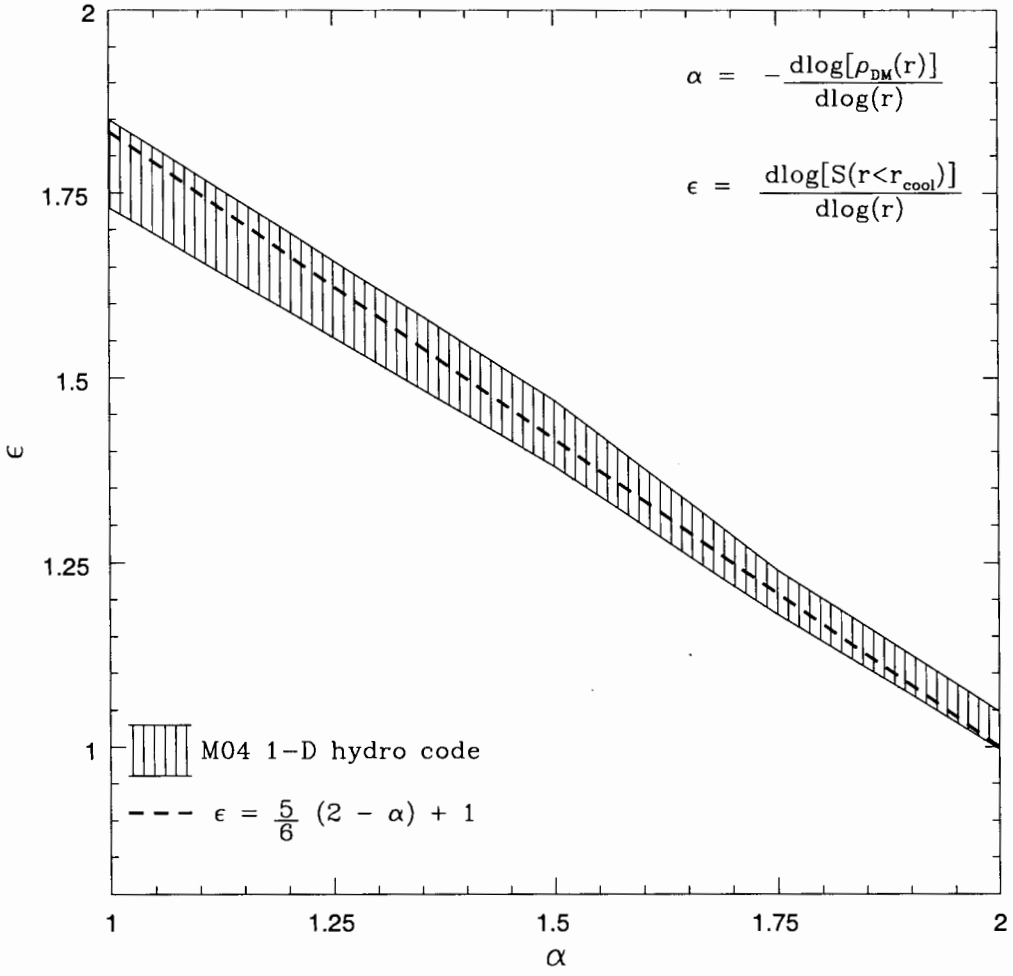

Figure 7.3: Comparison of the self-similar solution of B89 with the results of M04's cooling model. The shaded region reflects the uncertainty in the best fit powerlaw indices of the entropy profiles (within $r_{\rm cool}$) shown in Figs. 7.1-7.2.

expected.

We have fitted the steady state entropy profiles plotted in Figs. 7.1-7.2 with simple powerlaws. However, we find that the entropy profiles within $r_{\rm cool}$ are not exact powerlaws and there is some "wiggle" room in the best fit logarithmic slope, depending on the range of radii over which the profiles are fitted. Figure 7.3

presents a comparison between the analytic self-similar solution of B89 and the fits to the entropy profiles shown in Figs. 7.1-7.2. The shaded region roughly reflects the uncertainty in the best fit powerlaw indices for the profiles predicted by M04's cooling model.

Reassuringly, excellent agreement between the self-similar solution and the 1-D cooling code is obtained. Thus, the self-similar cooling wave model of B89 provides a physical basis for the powerlaw trends found by M04 and others. In addition, the agreement in Figure 7.3 gives us confidence in the reliability of the 1-D cooling model developed in M04.

7.3.2 Realistic clusters

Observed clusters and clusters formed in cosmological numerical simulations do not have pure powerlaw gravitational potentials. Furthermore, the ICM contains a significant quantity of metals and, consequently, cools not only through thermal bremsstrahlung but also through line emission. Line emission has the effect of distorting the cooling function away from the powerlaw form that is characteristic of bremsstrahlung. For these two reasons, the physical relevance of the results presented in §3.1 may be questioned. Below, we investigate the extent to which the shape of the resulting entropy profile is affected by these assumptions.

Since we are introducing additional scales into the problem, it is important that we construct realistic cluster models. We consider two different systems: one with a NFW dark matter profile and one with a Moore et al. dark matter profile. Both systems have been chosen to have the same total gas and dark matter masses; specifically, $M_{\rm gas}(r_{200}) \approx 1.5 \times 10^{14} M_{\odot}$ and $M_{\rm dm}(r_{200}) = 10^{15} M_{\odot}$, where $r_{200} \approx 2.06$ Mpc. We use a typical cluster dark matter concentration of $c_{\rm NFW} \equiv r_{200}/r_s \approx 3.4$ for the NFW halo (e.g., Eke et al. 1998; Bullock et al. 2001) and $c_{\rm Moore} \equiv r_{200}/r_{(-2)} = c_{\rm NFW}/0.630 \approx 5.4$ for the Moore et al. halo (see Keeton 2001). The above implies a scale radius of $r_s \approx 600$ kpc. As for the intracluster gas, we turn to the studies of Voit et al. (2003) and Voit (2005). These authors found

that the entropy profiles of a large sample of clusters generated with a numerical simulation of a ΛCDM cosmology including hydrodynamics (e.g., shock heating) but not radiative cooling are approximately self-similar over a wide range of masses (see Fig. 11 of Voit 2005). With the exception of a small modification (see below), the initial entropy distributions of our model clusters are assumed to be identical to Voit's best fit to his simulated clusters. The initial gas density and temperature distributions are determined through the equation of hydrostatic equilibrium by applying the boundary condition that the total amount of gas within r_{200} is equal to that specified above [i.e., $M_{\rm gas}(r_{200})/M_{\rm dm}(r_{200}) = \Omega_b/(\Omega_m - \Omega_b)$].

As mentioned above, we have made a slight modification to Voit's self-similar entropy profile. At large radii, i.e., for $r > 0.1r_{200}$, Voit (2005) reports a best fit entropy profile of $S(r) \propto r^{1.1}$. At small radii, however, there is an apparent entropy core whose origin remains uncertain (as is the relatively large amount of cluster-to-cluster scatter in the amplitude of this core; see §6 of M04 for a discussion of this). We have shrunk this core for computational convenience, since the model clusters reach steady state more quickly if they have small initial entropy cores. For example, for the NFW cluster it takes ≈ 5 and 8 Gyrs to remove cores (and reach steady state) with amplitudes of 130 keV cm^2 and 220 keV cm^2 (which are typical amplitudes for Voit's simulated clusters), respectively. This modification does not affect our results or conclusions since the entropy core is contained entirely within the cooling radius (assuming cooling for a Hubble time). As discussed above, the resulting steady-state entropy profile within $r_{\rm cool}$ depends only on the shapes of the gravitational potential and the cooling function (and not on the initial properties of the gas within $r_{\rm cool}$).

To compute the effects of cooling, we again make use of the model developed by M04. In order to gauge the effects of line emission, we explore two different cooling functions: the pure thermal bremsstrahlung function implemented in §3.1 and a Raymond-Smith plasma with a metallicity set to $0.3Z_\odot$. As in the case of the powerlaw models, we neglect the dynamical effects of mass drop out and we run the

cooling model until steady-state entropy profiles are achieved. At steady state, we find that both clusters have similar global emission-weighted temperatures, with $kT_{\rm ew} \approx 5$ keV, and cooling radii, with $r_{\rm cool}/r_{200} \approx 0.07$ (i.e., $r_{\rm cool} \approx 150$ kpc).

In Figure 7.4 (top panels), we plot the initial and final entropy profiles of our model clusters. In both panels, the dotted lines represent the initial entropy distributions, the thick solid lines represent the final distributions when cooled using a pure bremsstrahlung cooling function, and the thick dashed lines represent the final distributions when cooled using the $0.3Z_{\odot}$ Raymond-Smith plasma cooling function. In the left panel, the thin dashed and dot-dashed lines indicate the slope predicted by B89's self-similar solution assuming $\alpha = 1.5$ and $\alpha = 1.55$, respectively (assuming $\beta = 1/2$). In the right panel, the thin dashed and dot-dashed lines indicate the slope predicted by B89's self-similar solution assuming $\alpha = 1.0$ and $\alpha = 1.19$, respectively (again assuming $\beta = 1/2$). All of the thin lines representing the self-similar solution of B89 have been normalized to the thick solid lines at the cluster centers.

We focus first on the role of the gravitational potential. A comparison of the thick solid line with the thin dashed line in the top left panel of Fig. 7.4 demonstrates that the final ICM entropy profile of the Moore et al. halo is approximated fairly well within the central ≈ 70 kpc by the self-similar solution assuming $\alpha = 1.5$ and $\beta = 1/2$. Analogously, the final ICM entropy profile of the NFW halo is reasonably well approximated within the central ≈ 40 kpc by the B89 solution assuming $\alpha = 1.0$ and $\beta = 1/2$ (see top right panel). Recall that for $r \ll r_s$, the logarithmic slopes of the Moore et al. and NFW halos asymptote to $\alpha = 1.5$ and 1.0, respectively. It is important to note, however, that the self-similar solution with $\alpha = 1.5$ and 1.0 does not match the entropy profiles of the Moore et al. and NFW halos, respectively, all the way out to their cooling radii. In fact, with these choices for α, the self-similar solution only matches the central $\approx 0.5r_{\rm cool}$ of the Moore et al. halo and to the central $\approx 0.25r_{\rm cool}$ of the NFW halo. The reason for this is that logarithmic slopes of the dark matter density profiles of the Moore et

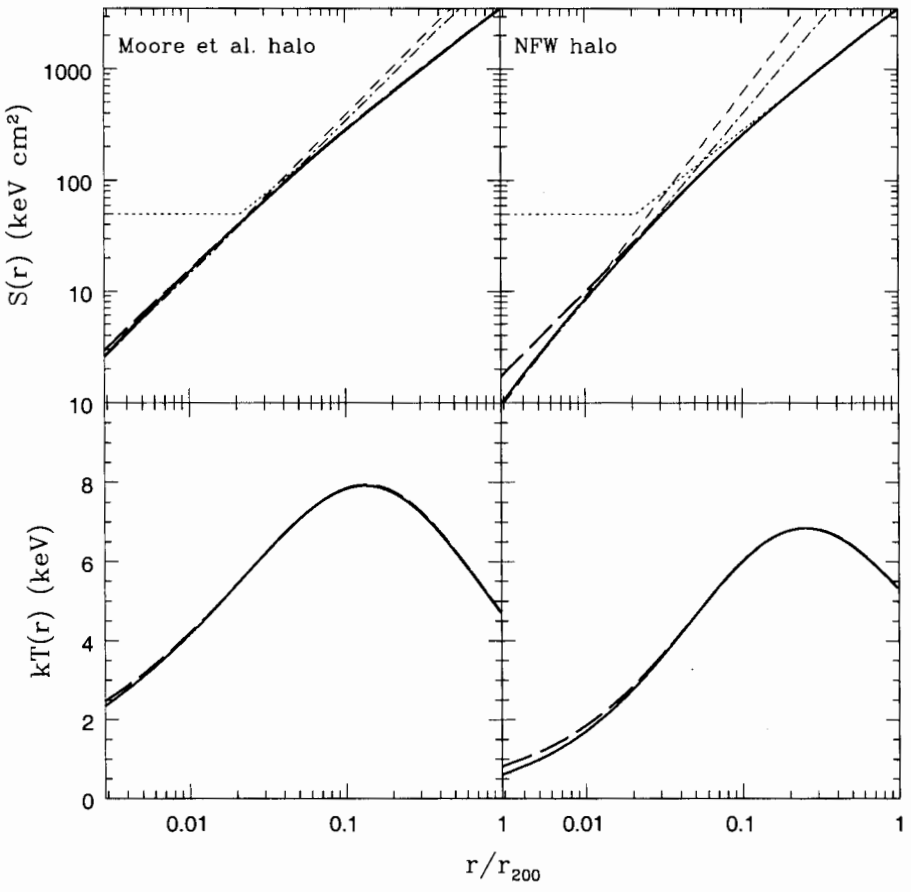

Figure 7.4: The effects of including line emission and more realistic dark matter halos on the steady-state cooling entropy profile. The thick solid and dashed lines represent the final entropy (top panels) and temperature (bottom panels) distributions assuming cooling with a pure thermal bremsstrahlung cooling function and a Raymond-Smith plasma model with $Z = 0.3Z_{\odot}$, respectively. *Top left:* The cluster with a Moore et al. dark matter halo. The thin dashed and dot-dashed lines represent the slope predicted by B89's self-similar solution with $\alpha = 1.5$ and 1.55, respectively (assuming $\beta = 1/2$). The dotted line represents the initial entropy distribution. *Top right:* The cluster with a NFW dark matter halo. The thin dashed and dot-dashed lines represent the slope predicted by B89's self-similar solution with $\alpha = 1.0$ and 1.19, respectively (assuming $\beta = 1/2$). The dotted line represents the initial entropy distribution.

al. and NFW halos have not fully asymptoted to $\alpha = 1.5$ and 1.0, respectively, at radii of $r \sim r_{\rm cool}$ (i.e., we are not strictly in the $r \ll r_s$ regime). Fitting the dark matter density profiles of the two halos, we find that simple powerlaw models with effective powerlaw indices of $\alpha_{\rm eff} = 1.55$ and 1.19 match the Moore et al. and NFW halos, respectively, quite well. Setting $\alpha = \alpha_{\rm eff}$ and plugging this into equation (3) yields much better agreement with final steady-state entropy distributions (as evidenced via a comparison of the thick solid and thin dot-dashed lines in the two top panels). In fact, using these more appropriate values for α, the self-similar solution describes well the final entropy distributions of the ICM in the Moore et al. and NFW halos out to radii in excess of 100 kpc. Therefore, the top panels of Fig. 7.4 illustrate that what is relevant is the shape of the *local* gravitational potential (i.e., at $r \lesssim r_{\rm cool}$), not the shape of the overall potential.

We now examine the role of the cooling function. For the Moore et al. halo, a comparison of the thick solid and dashed lines demonstrates that there is only a very weak dependence on which cooling function we use. The ICM entropy distribution of the NFW halo, however, is shallower if we include line emission. This difference can be understood as follows. The gravitational potential of the Moore et al. halo is steeper than that of the NFW halo. Consequently, gas flowing into the center of the Moore et al. halo requires more thermal support to remain in quasi-hydrostatic equilibrium. We demonstrate this in the bottom panels of Fig. 7.4, where the final steady-state temperature distributions of the two model clusters are plotted. Note that the gas near the center of the Moore et al. halo is significantly hotter than that of the NFW halo. In fact, for the Moore et al. halo, at any particular time there is virtually no gas below 2 keV (except within the central few kpc, where gas rapidly cools below our temperature threshold of $\approx 10^5$ K). The shallower NFW potential, however, permits some gas below 2 keV to exist in steady state out to radii of $r \sim 0.01 r_{200}$. An examination of the cooling function of a Raymond-Smith plasma with $Z = 0.3 Z_\odot$ (see Figure 7.5) shows that for temperatures of $kT \gtrsim 2$ keV, the cooling function is dominated by thermal

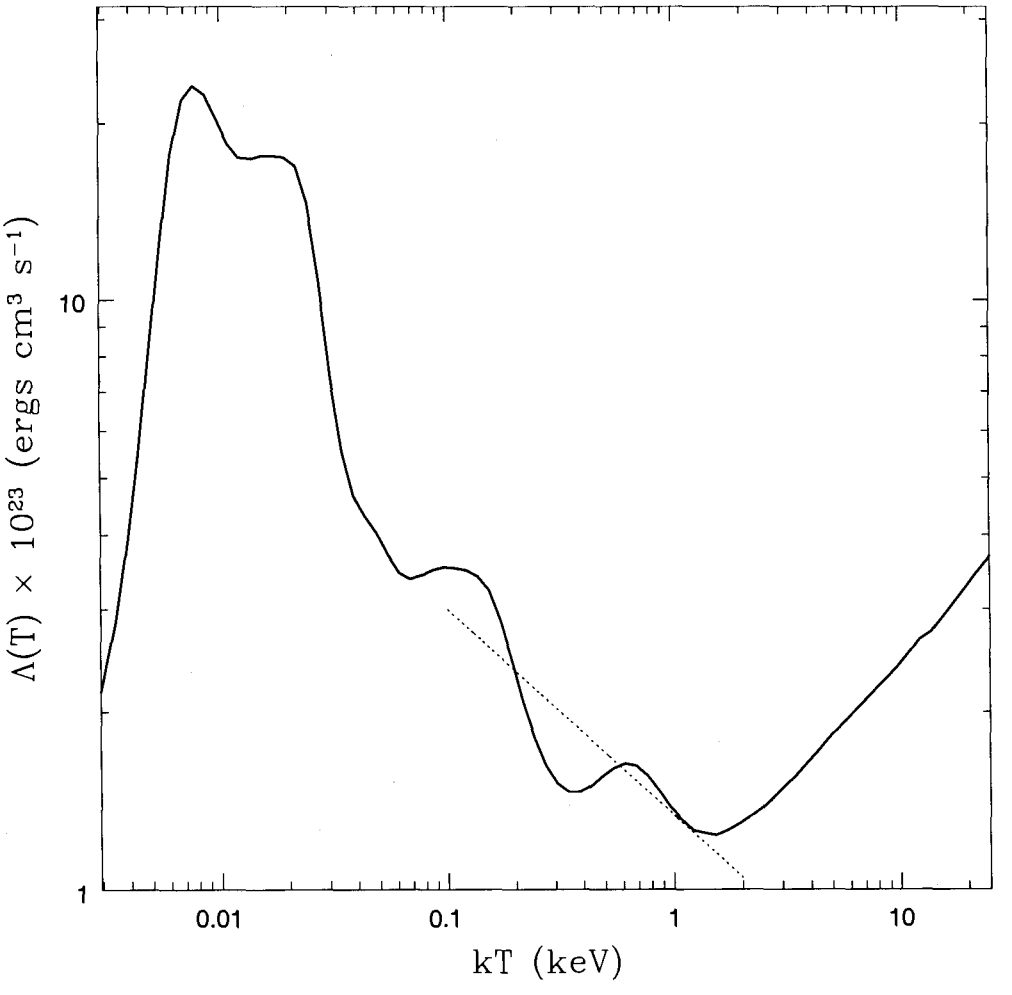

Figure 7.5: The cooling function for a Raymond-Smith plasma with $Z = 0.3Z_{\odot}$. The dotted line represents the best fit powerlaw (with $\beta \approx -0.35$) to the function over the range 0.1 keV $\leq kT \leq$ 2.0 keV.

bremsstrahlung and is well approximated by a powerlaw; $\Lambda(T) \propto T^{1/2}$. At lower temperatures, however, line emission begins to dominate. The thin dotted line in Fig. 7.5 shows the best fit powerlaw to the cooling function between 0.1 keV $\leq kT \leq$ 2 keV, which has an index of $\beta \approx -0.35$. Using this value for β in equation (2), it is possible to account for the small deviation in the shape of the entropy

profile within the central regions of the NFW halo. For the massive clusters under consideration, this deviation due to cool $kT \lesssim 2$ keV gas is restricted to the central ~ 30 kpc, but in less massive systems we would expect it to extend out to larger radii and, hence, explicit accounting of this deviation may become important.

We conclude that the introduction of more realistic dark matter halos, with shapes motivated by high resolution cosmological simulations, and the inclusion of radiative cooling via line emission do not result in significant violations of self-similarity. For massive clusters, the dark matter scale radius is typically two to four times larger than the cooling radius. Over the range $r \lesssim r_{\rm cool}$, we find that the gravitational potentials of massive clusters can be represented quite well by simple powerlaws, as assumed by B89. Furthermore, because structure formation proceeds hierarchically, resulting in an inside-out halo growth scenario, we expect that the central gravitational potential of clusters have been in this relaxed state for a significant fraction of the age of the Universe. As for cooling via line emission, we find that the deep potential wells of massive clusters ensure that most of the gas, even within $r_{\rm cool}$, is quite hot with $kT \gtrsim 2$ keV. For such high temperatures, thermal bremsstrahlung, which gives rise to a scale-free cooling function, dominates the X-ray emissivity. We note, however, that for lower mass systems (i.e., groups of galaxies) self-similarity will likely be significantly violated. For such systems, the cooling radius will be comparable to (or even exceed) the dark matter scale radius and, consequently, the gravitational potential within $r_{\rm cool}$ will most likely not be adequately represented by a simple powerlaw. Furthermore, line emission will play a comparable, if not dominate, role to that of thermal bremsstrahlung for the cluster X-ray emissivity.

7.4 Comparison to "Cooling Flow" Clusters

As alluded to §1, recent high resolution X-ray observations have indicated that the central entropy profiles of some "cooling flow" clusters appear to be near powerlaws.

This raises the interesting possibility that these clusters are in (or very nearly in) a cooling steady state as per B89 (see §3.2). Here, we explore this possibility further by examining the observational data and comparing it to our theoretical models[2].

Using *XMM-Newton* data, Piffaretti et al. (2005) derived the entropy profiles of a relatively large sample of "cooling flow" clusters using a standard deprojection technique. We consider a subset of the most nearby ($z < 0.1$), massive clusters in their sample. This selection criterion was motivated by the necessity of resolving the central regions ($r \lesssim r_{\rm cool}$) with multiple radial bins. In particular, we examine the entropy profiles of 7 massive "cooling flow" clusters: A1795, A2052, A3112, A4059, A426, A496, and MKW 3S.

In order to compare the entropy profiles of clusters with various mean temperatures (i.e., various masses) on an equal footing, it is necessary to scale the profiles. One physically-motivated way to scale the profiles is according to the standard self-similar model, which is based on the assumption that only gravitational processes are important in the formation of the cluster (this is not be confused with the B89 self-similar cooling solution). As such, the ICM traces the dark matter in this model. Consequently, like the dark matter, the ICM has a universal density profile that does not depend on halo mass. Thus, the entropy scales as $S \equiv kTn_e^{-2/3} \propto T$ and the radius, through the virial theorem, scales as $r \propto T^{1/2}$. Scaling the profiles accordingly should line the profiles up at large radii (where gravitational shock heating dominates any entropy modification due to radiative cooling or non-gravitational heating) and bring out any differences in the profiles at small radii. However, because the mean temperatures of the 7 clusters that we focus on are all fairly similar, ranging from 3 keV $\lesssim kT_{\rm ew} \lesssim$ 6 keV, scaling the profiles in this way amounts to only a small adjustment. But we do so for

[2]Our comparison between the observational data and the theoretical models will be restricted to $r \gtrsim 25$ kpc. At smaller radii it is expected that both the self-similar solution of B89 and the 1-D cooling model of M04 will break down owing to multi-phase cooling, transsonic flow, and strong deviations from spherical symmetry because of the increasing importance of angular momentum.

completeness.

In Figure 7.6, we plot the scaled entropy profiles of the 7 massive "cooling flow" clusters together (solid squares). As expected, the data points form a tight scatter at large radii. At smaller radii there is an apparent increase in the amount of scatter, but there are no obvious signs of a core or of significant deviations from the slope of the profile at large radii. We have also inspected the entropy profiles of the individual clusters (as opposed to plotting all of them together) and verify that none of their profiles show evidence for central cores or inversions.

To help aid the eye, we also show in Figure 7.6 the B89 self-similar solution for a halo with $\alpha = 1$ (solid line), $\alpha = 1.5$ (short-dashed line), and $\alpha = 2$ (long-dashed line) representing NFW, Moore et al. and singular isothermal potentials, respectively (assuming $\beta = 1/2$). The lines have been normalized to the data points near the cooling radius, assuming $r_{\rm cool} \approx 150$ kpc for all of the clusters. The dotted line shows a continuation from the cooling radius to large radii assuming a logarithmic slope of $\epsilon = 1.1$.

From this rough comparison we confirm that the observed profiles are nearly powerlaws at small radii. Interestingly, the inferred gravitational potentials are fairly steep with $1 < \alpha \lesssim 2$ or so. This constraint agrees well with the recent hydrostatic analyses of relaxed "cooling flow" clusters by Arabadjis & Bautz (2004) using *Chandra* data of ten clusters and by Pointecouteau et al. (2005) using *XMM-Newton* data of a different set of ten systems.

Temperature profiles provide another useful test of the applicability of pure radiative cooling models to observed "cooling flow" clusters. Using a sample of relaxed clusters observed with *Chandra*, Allen et al. (2001) uncovered a 'universal' projected temperature profile for "cooling flow" clusters. This profile is plotted in Figure 7.7 along a variety of model temperature profiles. In particular, the hatched region represents the Allen et al. 's observed profile and the thin and thick long-dashed and solid lines represent the steady-state projected profiles for the Moore et al. and NFW halos with and without line emission included that were plotted

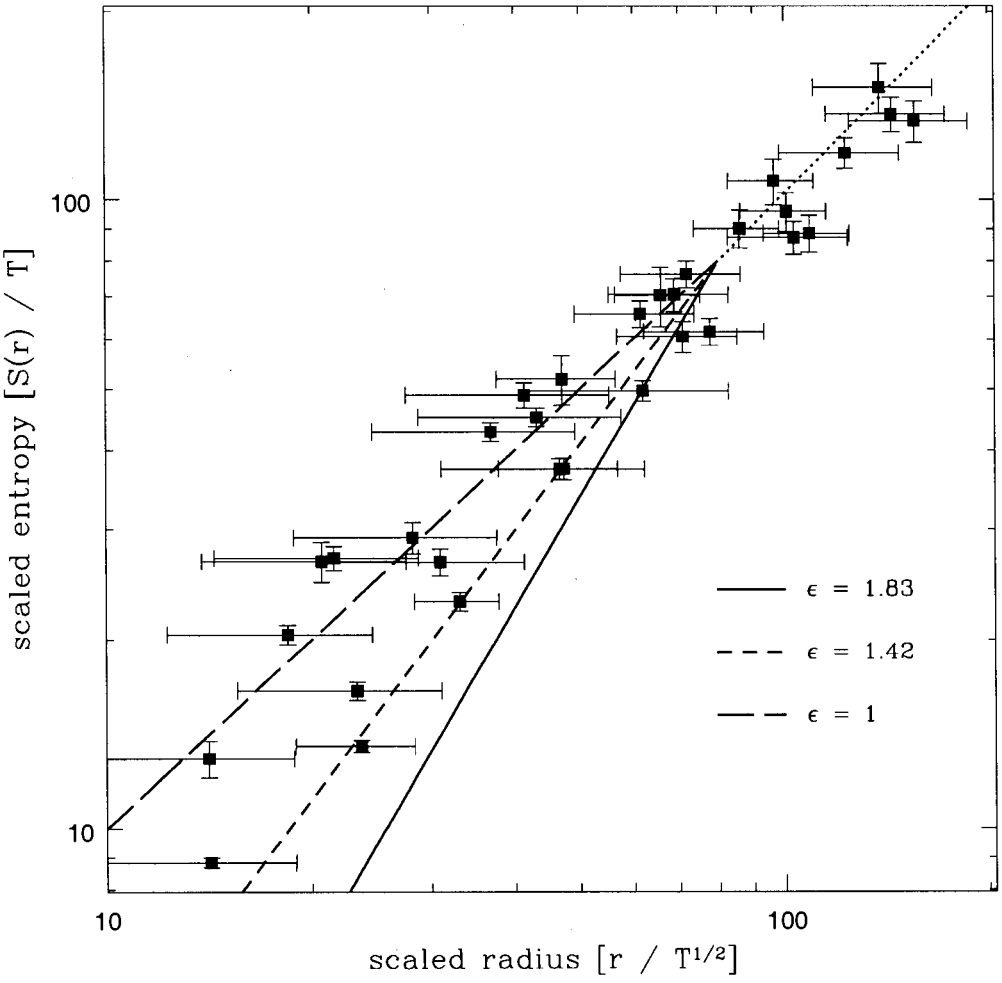

Figure 7.6: The scaled entropy profiles of 7 massive "cooling flow" clusters from Piffaretti et al. (2005). The solid, short-dashed, and long-dashed lines represent entropy profiles with logarithmic slopes of $\epsilon = 1$, 1.42, and 1.83 which corresponds to the self-solutions for a NFW halo, a Moore et al. halo, and a singular isothermal sphere, respectively (assuming $\beta = 1/2$). The lines have been normalized to the data points near the cooling radius (assuming $r_{\rm cool} \approx 150$ kpc for all of the clusters). The dotted line shows a continuation from the cooling radius to large radii assuming a logarithmic slope of $\epsilon = 1.1$.

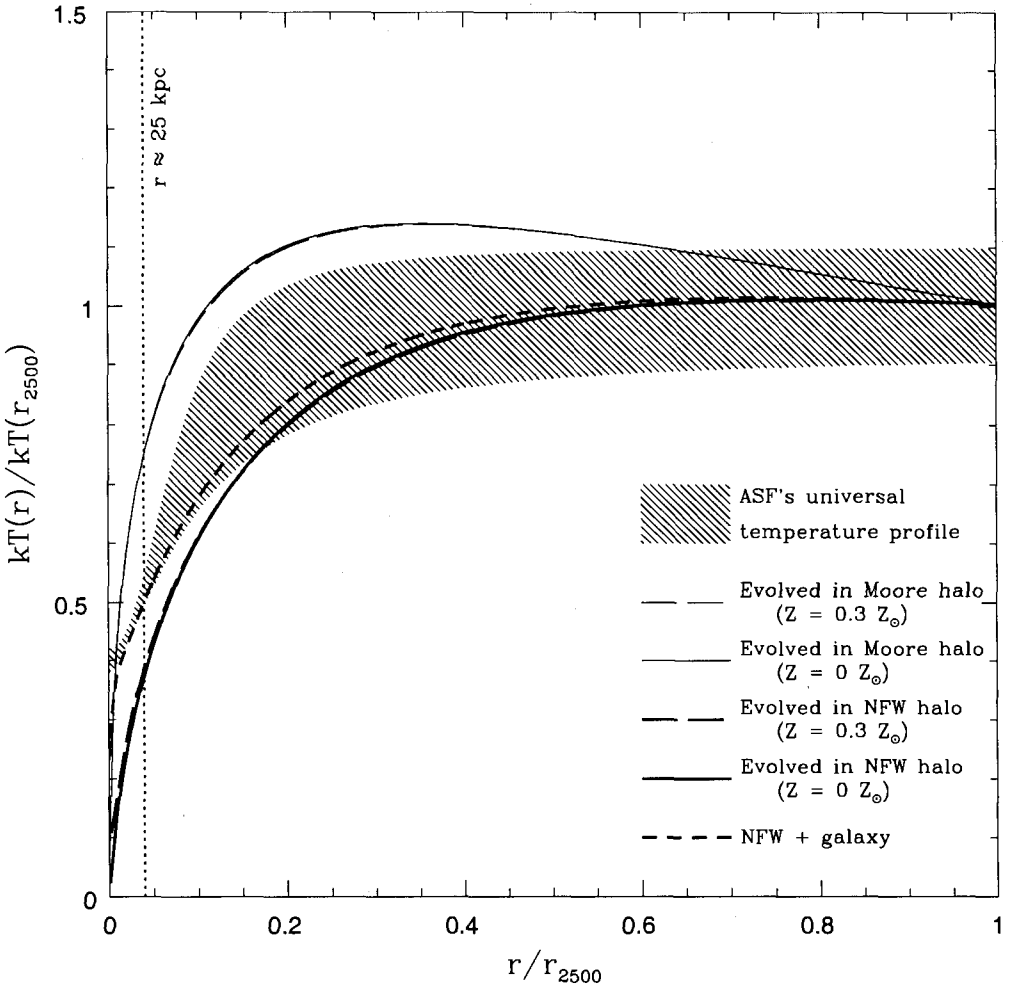

Figure 7.7: The universal projected temperature profile of "cooling flow" clusters. The shaded region corresponds to the observed 'universal' profile of Allen et al. (2001). The thin long-dashed and solid lines correspond to the steady-state projected temperature profiles for a Moore et al. halo with and without line emission included, respectively. The thick long-dashed and solid lines correspond to the steady-state projected temperature profiles for a NFW halo with and without line emission included, respectively. The short-dashed line represents a NFW cluster (line emission turned on) with the addition of a central elliptical Hernquist galaxy that is characterized by a scale radius of 5 kpc and a total mass of $\approx 3 \times 10^{12} M_{\odot}$ (see text).

in Figure 7.4.

A comparison of the thin long-dashed and solid lines to the hatched region indicates that the gravitational potential of Moore et al. halo is a bit too steep to be consistent with the observations. On the other hand, the NFW halo (represented by the thick lines) appears to be a bit too shallow. A dark matter profile in between these two cases (i.e., $1 < \alpha < 1.5$), therefore, should capable of explaining the observations. Recently, through detailed convergence tests of numerically-simulated galaxy clusters (which were simulated using a variety of different codes), Diemand et al. (2004) have argued for this type of universal cluster dark matter profile with $\alpha = 1.16 \pm 0.14$.

Another possibility is that the dark matter potential may be NFW-like ($\alpha = 1$) but that the *total* gravitational potential, including the stellar mass of central elliptical galaxy, is steeper. Up to this point, we have neglected the gravitational influence of a central elliptical galaxy. We have experimented with this scenario by allowing the formation of such a galaxy at the center of the NFW halo through the accumulation of cold baryons. In particular, we distribute gas that drops below 10^5 K at the cluster center in a galaxy that is characterized by a Hernquist density profile with a scale radius of 5 kpc, which is typical of observed massive elliptical galaxies. Furthermore, we contract the dark matter halo of cluster adiabatically in response to the build up of the cold baryons, although in practice it is the addition of the cold baryons, not the contraction of the dark halo, that has the most important effects on the projected temperature profile[3]. We find that the addition of a central galaxy with a mass of a few times $10^{12} M_{\odot}$, which is typical of brightest cluster galaxies, is capable of bringing the temperature profile of the NFW halo into excellent agreement with the observations. Finally, we note that

[3]Because the baryons dominate the central gravitational potential irrespective of whether we contract the cluster dark matter halo or not, this implies that the exact formation history of the central galaxy is unimportant. For example, if instead of forming the galaxy slowly from the accumulation of cold baryons we simply place a central galaxy at the cluster center by hand (say as part of our initial conditions), an almost identical projected X-ray temperature profile results.

by fitting a simple powerlaw to the combined dark matter + stellar density profile of this cluster, we retrieve an effective powerlaw index, $\alpha_{\rm eff}$, of ≈ 1.30.

We have shown that models that include radiative cooling but no sources of non-gravitational heating are capable of reproducing the observed entropy and projected temperature profiles of "cooling flow" clusters, at least outside the central ≈ 25 kpc or so. Furthermore, the inferred shape of underlying gravitational potential from these two tests are roughly consistent with each other and also with analyses that make use of the standard hydrostatic equilibrium method (Arabadjis & Bautz 2004; Pointecouteau et al. 2005). What does this imply about the role of non-gravitational heating in "cooling flow" clusters?

The first possibility worth considering is that non-gravitational heating is absent (or insignificant) in "cooling flow" clusters. As demonstrated above, it appears (perhaps surprisingly) that it is possible to account for the observed temperature and entropy profiles of such clusters with this model (at least beyond ≈ 25 kpc). However, there are two potentially serious, well-known problems associated with this scenario. The first is that new high spatial and high spectral resolution data from *Chandra* and *XMM-Newton* demonstrate that there is very little (or possibly no) X-ray emitting gas with temperatures below $kT \approx 1-2$ keV (e.g., Fabian et al. 2002; Peterson et al. 2003; Kaastra et al. 2004). This observational trend is sometimes recast in terms of an inferred mass deposition rate for low temperature gas. In particular, assuming that the standard isobaric cooling flow model holds true, one can, for example, use the observed fluxes of various low energy iron lines to calculate a mass deposition rate. New *Chandra* and *XMM-Newton* data of "cooling flow" clusters typically indicate mass deposition rates of $\sim 10-100\ M_{\odot}$ yr^{-1}, roughly a factor of $\sim 5-50$ smaller than that found in our cooling models (and, coincidentally, smaller by a similar factor than that of calculations based on previous *ROSAT* and *ASCA* data). However, it is important to note that this is not a self-consistent comparison, in that we are comparing a mass deposition rate that has been inferred, by applying the standard isobaric cooling flow model, from

observations with a real physical cooling rate from our theoretical models (which, for example, does not assume isobaric cooling and takes into account the work done by the gravitational potential). A more appropriate comparison would entail comparing the inferred values from the observational data with that found from fitting the standard cooling flow spectral model to synthetic spectra generated from our theoretical clusters, an exercise that is beyond the scope of the present study. Instead, we comment on the amount of cool X-ray-emitting gas present in our theoretical clusters. As noted above, the steepness of the NFW and Moore et al. potentials ensures that the majority of the ICM is quite hot, even within the cooling radius. In fact, at steady state we find that the X-ray-emitting gas with a temperature below 1 keV contributes only about 10% of the total X-ray luminosity within the central (projected) 150 kpc of the NFW halo considered above (an even smaller contribution is obtained for the Moore et al. halo). The X-ray luminosity is reduced further, by roughly a factor of 2, if one employs a threshold of 0.5 keV instead of 1 keV. In short, we find the vast majority of the gas within the cooling radius is either hot, with $kT \gtrsim 1$ keV, or quite cold (i.e., below the X-ray-emitting threshold of 10^5 K) with very little in between, as observed. Thus, it is not immediately clear to us that this issue is as serious as commonly reported.

The second issue with pure radiative cooling models is what is commonly referred to as the classic cooling flow problem; i.e., the fact that the large amounts of cold neutral gas and enhanced star formation rates expected to be present in cores of "cooling flow" clusters have not been found. Actually, this statement is not entirely accurate. There is evidence for *some* cold gas and dust in central galaxies of "cooling flow" clusters (see, e.g., Edge 2001; Edge et al. 2002). However, it is clear that there is a sizeable discrepancy between what is predicted by pure cooling models (e.g., the standard cooling flow model, the cooling model of M04, the cooling model of Voit et al. 2002) and what is observed. For this reason, pure radiative cooling models cannot provide a complete description of the formation and evolution of "cooling flow" clusters. The most obvious resolution to this problem

is non-gravitational heating, which we now focus on.

For ease of discussion, we seperate the various non-gravitational heating models into three broad classes. It is important to note, however, than more than just one may be relevant/operating in cluster. The three broad classes are: (i) continuous, distributed heating that results from transport processes such as thermal conduction (e.g., Narayan & Medvedev 2001) and turbulent mixing/stirring of the ICM due, for example, to the orbital motions of cluster galaxies (e.g., El-Zant et al. 2004); (ii) episodic heating from a central AGN (e.g., Kaiser & Binney 2003); and (iii) the heating of the ICM prior to cluster formation; i.e., preheating during the epoch of galaxy formation, possibly by high-z AGN (see, e.g., Babul et al. 2002). We now discuss each of these broad classes in turn.

Continuous, distributed heating mechanisms represent an interesting possibility. For example, the idea that thermal conduction may be offsetting a large fraction of the radiative losses of the ICM has recently been revived and has received some attention. It was previously thought that conduction would be highly suppressed due to the presence of intracluster magnetic fields, but recent theoretical calculations by Narayan & Medvedev (2001) and others have demonstrated that this is not necessarily the case, particularly if the field lines are chaotically tangled. Furthermore, *distributed* heating mechanisms, such as conduction, naturally meet the observational constraint that there appears to be no evidence for cold gas piling up *anywhere within the cooling radius* of "cooling flow" clusters (see, e.g., Fabian et al. 2002). However, it is much less clear if continuous, distributed heating mechanisms can explain the fact that the observed entropy and temperature profiles of "cooling flow" clusters appear to be in (or near) a steady state that looks remarkably like the cooling steady state predicted by B89. In fact, it is quite difficult, but perhaps not impossible, how this can be so while, at the same time, such mechanisms would provide a solution to the classic cooling flow problem. Indeed, high resolution cosmological hydrodynamic simulations that invoke thermal conduction show that it is insufficient to prevent the classic cooling flow problem

(Dolag et al. 2004). However, it may be possible that conduction combined with other sources of heating (e.g., AGN) could resolve this problem (e.g., Ruszkowski & Begelman 2002). Heating via turbulent mixing remains an open possibility as well.

The second class of heating models that we consider are episodic in nature. In this case, the heating of the ICM likely occurs following shortly after the accretion of cold gas onto a supermassive black hole at the center of cluster. Kaiser & Binney (2003) have recently developed such a model. The duty cycle of the central AGN, which is expected to be linked to the central cooling time of the ICM, ensures that the probability of finding a cluster with appreciable cold gas is quite low (since the cooling time of cold, dense gas is quite short). Instead, one is much more likely to find a system that has a core temperature of $kT \gtrsim 1-2$ keV, as observed. Observational support for this general heating scenario has recently been uncovered in the form of X-ray-deficient, buoyantly-rising bubbles of hot plasma in the cores of many "cooling flow" clusters (e.g., Heinz et al. 2002; Blanton et al. 2003). Thus, episodic heating is occurring at some level. It is important, however, that the heating episodes are not so efficient as to prevent "cooling flow" clusters from quickly settling back to a (at least near) steady state, as demonstrated above, or to prevent the build-up of *some* cold neutral gas, as observed by Edge et al. (2002) and others. To test this, the exact heating mechanism by which the AGN heats the ICM must be understood and explored.

The last class models that we consider are the preheating models. Here, the proto-ICM is heated by an unspecified source during the epoch of galaxy formation. High redshift AGN would be a likely candidate for preheating, since it is well known AGN outflows are more powerful and common in the early universe than they are today (e.g., REFS.). Whether or not the preheated cluster will achieve a cooling steady state depends on the level of preheating. M04 demonstrated that if the level of entropy injection is below roughly 300 keV cm^2 then the cluster will reach cooling steady state over the course of a Hubble time. If the level of heating is

significantly above this threshold, a low density, high temperature core will persist for the cluster's lifetime. M04 argued that, in this way, a distribution of initial heating levels would naturally give rise to the two broad classes of observed clusters; i.e., "cooling flow" and "non-cooling flow" clusters[4]. For low levels of preheating, we further demonstrated that it is possible to achieve clusters with steady state cooling properties but that are not subject to the classic cooling flow problem. In particular, initial heating levels of $\sim 100 - 200$ keV cm^2 ensure that most clusters have only reached the cooling steady state recently and, therefore, have not had sufficient time to build up large amounts of cold gas at the cluster center. Thus, with this model, it seems it may be possible to explain why "cooling flow" clusters appear to be in steady state and yet only have small amounts of cold gas present in their cores. Furthermore, it is consistent with the fact there appears to be no cold gas piling up at larger radii. However, a detailed examination of whether or not this model is consistent with the inferred mass deposition rates of cool X-ray-emitting gas of "cooling flow" clusters is required before clean bill of health can be assigned. We leave this for a future study. Finally, we suggest that a further test of this model can be made by probing the properties of high redshift clusters. If it is found that many clusters at high redshift are in (or near) steady state (and have some amount of cold gas at their cores) this would be inconsistent with the prediction that "cooling flow" clusters have only recently reached steady state.

Finally, while we have shown that B89's self-similar solution is, at least, approximately applicable to "cooling flow" clusters, it is clear that this model *cannot* provide a reasonable description of relaxed "non-cooling flow" clusters. Such sys-

[4]We note that the energetics for turning a (potential) "cooling flow" cluster into a "non-cooling flow" cluster are much more favorable at high redshift than they are today because the cores of clusters are much denser now. In fact, theorists have a difficult time finding sources that are energetic enough just to compensate for cooling, nevermind elevating the gas to such high entropies that its cooling time exceeds a Hubble time. However, it is clear that some source of non-gravitational heating is required in order to explain the existence of relaxed "non-cooling flow" clusters. This is a compelling argument in support of the preheating scenario (see M04).

tems have large entropy cores (see, e.g., Fig. 11 of M04) and, therefore, must have been severely heated in the past. Presumably this extreme level of heating has prevented the development of self-similar cooling flows in such systems.

7.5 Discussion & Conclusions

Using the self-similar solution of B89, we have shown that radiative cooling and inflow lead to a characteristic entropy profile within the cooling radius that depends only on the shapes of the cooling function and the gravitational potential. We have compared the self-similar solution to the cooling model of M04 and, reassuringly, find excellent agreement for clusters with powerlaw potentials and that cool via thermal bremsstrahlung. Furthermore, we have demonstrated that the self-similar solution is also approximately valid for more realistic dark matter potentials and cooling functions that include line emission. This result explains the numerically-derived powerlaw trends found by M04 and others.

We have presented a comparison of our pure radiative cooling models to the entropy and temperature profiles of observed relaxed "cooling flow" clusters. With the exception of the central $\approx$ 25 kpc or so (where our models are expected to break down), the models are able to approximately account of the properties of the gas within the cooling radii of these clusters. Furthermore, the inferred gravitational potentials are fairly steep and are roughly consistent with both the results of cosmological numerical simulations and with hydrostatic analyses of observed clusters. In §4, we presented a thorough discussion of the implications of our results for the non-gravitational heating of "cooling flow" clusters. In particular, we examined three broad classes of heating models; (i) continuous, distributed heating (e.g., thermal conduction); (ii) episodic heating by a central AGN; and (iii) and preheating. We have argued that continuous, distributed heating mechanisms are unlikely to be the sole solution to the cooling flow problem. The latter two heating models remain open possibilities that require further detailed examination.

It also should be noted that pure radiative cooling models, such as those explored in the present study fail to explain relaxed "non-cooling flow" clusters or systems which are classified as intermediate between "cooling flow" and "non-cooling flow" clusters. To account for these systems, both radiative cooling and large amounts of non-gravitational heating (perhaps injected prior to cluster formation) are required (see M04).

Quite independent of how well it describes observed clusters, the self-similar solution also has a number of interesting applications for theoretical modelling of clusters. We briefly discuss but two here.

1.) A simple method for calculating initial conditions of analytic model clusters with radiative cooling. This could serve as a "poor man's alternative" to a model that explicitly takes into account the effects of radiative cooling and inflow on intracluster gas. For example, a realistic set of initial conditions could be generated by using the results of non-radiative simulations (e.g., Lewis et al. 2000; Loken et al. 2002; Voit 2005) to describe the gas at large radii ($r > r_{\rm cool}$) while using the self-similar solution of B89 to describe the properties of the gas within $r_{\rm cool}$. The normalization of the entropy profile within $r_{\rm cool}$ (which is not specified by the self-similar solution) could be set by matching the non-radiative simulation results near $r_{\rm cool}$. One example of where such initial conditions might be useful is for models that explore the ability of various heating mechanisms to offset radiative losses of the ICM. For example, a number of recent AGN heating simulations (e.g., Quilis, Bower, & Balogh 2001; Ruszkowski & Begelman 2002) have invoked initial conditions such as isothermality or temperature profiles derived from non-radiative simulation (as opposed to that expected for a cluster that is cooling radiatively) and this may have some effect on the estimates of the energetic requirements for the prevention of catastrophic cooling at the cluster center. It would be interesting to see whether the estimates of the amount of required heating change significantly when more realistic initial conditions (such as those proposed above) are implemented.

2.) A test of the reliability of cooling routines implemented in analytic models and hydrodynamic simulations. Because the self-similar solution is a simple function, it can easily be used to test, for example, how well various formulations of smoothed particle hydrodynamics (SPH) or mesh-based techniques [such as adaptive mesh refinement (AMR)] treat the effects of cooling (see, e.g., Abadi, Bower, & Navarro 2001). We are currently undertaking such a study using a variety of popular analytic and hydrodynamic codes (Dalla Vecchia et al. in preparation).

The authors would like to thank Steve Allen, Megan Donahue, and Mark Voit for helpful discussions. I. G. M. also thanks Rocco Piffaretti for providing his *XMM-Newton* cluster results in electronic form. I. G. M. is supported by a postgraduate scholarship from the Natural Sciences and Engineering Research Council of Canada (NSERC) and A. B. is supported by an NSERC Discovery Grant. A. B. would also like to acknowledge support from the Leverhulme Trust (UK) in the form of the Leverhulme Visiting Professorship.

Chapter 8

Conclusions & Future Work

We have developed physically-motivated analytic models of the ICM in order to assess the role that non-gravitational processes, such as radiative cooling and heating from AGN, play in mediating the observed properties of clusters. We have carried out detailed and systematic comparisons between our models and the observed global and structural X-ray and SZ effect properties of clusters. From this comparison we conclude the following. As expected, a pure gravitational model (i.e., the standard self-similar model) fails to match the observed properties of clusters. A model that invokes radiative cooling but no sources of non-gravitational heating also fails, as it has no hope of accounting for the "cooling crisis" or of explaining the origin of "non-cooling flow" clusters. On the other hand, a model that includes non-gravitational heating but that does not take into account the effects of radiative cooling fails to account for the observed global and structural properties of "cooling flow" clusters and obviously has no hope of explaining galaxy or star formation in clusters. We find that in order to account for the global X-ray and SZ effect scaling relations (including their intrinsic scatter), it is necessary to invoke both radiative cooling and a distribution in the level of non-gravitational heating experienced by clusters. Under this scenario, clusters that were severely heated early on likely evolved into "non-cooling flow" clusters, whereas clusters that were

heated by only mild amounts likely evolved into "cooling flow" clusters. This conclusion is reinforced by comparisons to new spatially-resolved entropy, temperature, and surface brightness profiles derived from *Chandra* and *XMM-Newton* data.

Although the above exploration has yielded many new and interesting results, a number of important details still need clarification. Perhaps the most fundamental of these is identifying the source(s) of non-gravitational heating in clusters and understanding why the level of heating varies as much as it does from cluster to cluster. This requires detailed and systematic examinations of all of the potentially relevant heating sources, including thermal conduction, AGN heating, turbulent mixing, cosmic ray heating, and so on. A combination of analytic models and idealized numerical simulations probably represent the best venue for this type of exploration. This will be one of the central themes of the research I will perform in the coming years at the University of Durham.

Perhaps the main technical shortcoming of the analytic models explored in this thesis is that they do not properly account for the hierarchical formation of clusters. In essence, our model clusters are balls of gas evolving according to a simple set of rules (meant to approximately account for the effects of cooling and non-gravitational heating) in basically static dark matter potentials. While treating the dark matter potential of clusters as static may be reasonable for present-day clusters (as the majority of the cluster mass has been in place for roughly 5-7 Gyr), it is clearly not reasonable for high redshift systems. Furthermore, radiative cooling, and other non-gravitational processes as well, depends sensitively on the properties of the gas which, in turn, are dictated by gravitational processes. So, for example, it's not at all obvious whether cooling gas in a static massive cluster for a Hubble time will result in the same fraction of gas being converted into stars as in the case where the cluster is built up from smaller subhalos that merge to form the cluster. Preliminary comparisons between analytic models and numerical simulations that both include radiative cooling but no sources of non-gravitational

heating indicate that the results are not hugely discrepant, but there are differences. There are a variety of other reasons as well, especially concerning using clusters as probes of cosmology, why one should attempt to treat the hierarchical build-up of clusters accurately.

Detailed cosmological hydrodynamic simulations may seem like the obvious solution to this problem. However, as outlined in Chapter 1, such simulations are extremely computationally-expensive. It therefore becomes extremely difficult simulate large, representative volumes of the universe in adequate detail. One way to get around this problem is to analytically populate dark matter-only simulations with baryons. Dark matter-only simulations are much less computationally-expensive than hydrodynamic simulations. In fact, there now exist a few moderately high resolution simulations whose computational volumes approach that of the observable universe (e.g., the so-called "Hubble Volume" and "Millenium" simulations carried out by the Virgo consortium). Populating the dark matter halos in these simulations with baryons according to some physically-motivated prescription is something I look forward to doing in the coming years.

Semi-analytic models of structure formation also potentially solve the above problem by tracking hierarchical formation through computationally-inexpensive analytic statistical methods. While it is certainly possible to explore many random realizations using this approach (i.e., to 'simulate' large volumes of the universe), the accuracy of this method is questionable. For example, it is well-known that the mass function predicted by extended Press-Schechter theory deviates strongly from the results of numerical simulations at both very large and very small halo masses. However, new semi-analytic models, such as PINOCCHIO and PThalo, have been explicitly calibrated to match typical merger trees found in cosmological simulations and, therefore, should resolve many of these issues. It would quite interesting to compare and contrast the results of combining such semi-analytic models with the analytic hydro code developed in this thesis to cosmological hydrodynamic simulations or dark matter-only simulations populated analytically

with baryons (as described above).

Bibliography

[1] Abadi, M. G., Bower, R. G., & Navarro, J. F.: 2000, *M. N. R. A. S.*, 314, 759

[2] Akritas, M. G., & Bershady, M. A.: 1996, *Astrophys. J.*, 470, 706

[3] Allen, S. W.: 1998, *M. N. R. A. S.*, 296, 392

[4] Allen, S. W.: 2000, *M. N. R. A. S.*, 315, 269

[5] Allen, S. W., & Fabian, A. C.: 1998, *M. N. R. A. S.*, 297, L57

[6] Allen, S. W., Schmidt, R. W., & Fabian A. C.: 2001, *M. N. R. A. S.*, 328, L37

[7] Allen, S. W., Schmidt, R. W., & Fabian A. C.: 2002, *M. N. R. A. S.*, 335, 256

[8] Arnaud, M., & Evrard, A. E.: 1999, *M. N. R. A. S.*, 305, 631

[9] Arabadjis, J. S., & Bautz, M. W.: 2004, *Astrophys. J.*, submitted (astro-ph/0408362)

[10] Ascasibar, Y., et al.: 2003, *M. N. R. A. S.*, 346, 731

[11] Athreya, R. M., et al.: 2002, *Astronomy and Astrophysics*, 384, 743

[12] Babul, A., et al.: 2002, *M. N. R. A. S.*, 330, 329

[13] Balogh, M. L., Babul, A., & Patton, D. R.: 1999, *M. N. R. A. S.* 307, 463

[14] Balogh, M. L., et al.: 2001, *M. N. R. A. S.*, 326, 1228

[15] Balogh, M. L., et al.: 2005, *M. N. R. A. S.*, submitted

[16] Bauer, F., & Sarazin, C. L.: 2000, *Astrophys. J.*, 530, 222

[17] Benson, A. J., et al.: 2003, *Astrophys. J.*, 599, 38

[18] Bertschinger, E.: 1989, *Astrophys. J.*, 340, 666 (B89)

[19] Bialek, J. J., Evrard, A. E., & Mohr, J. J.: 2001, *Astrophys. J.*, 555, 597

[20] Binney, J., & Tabor, G.: 1995, *M. N. R. A. S.*, 276, 663

[21] Birkinshaw, M.: 1999, *Phys. Rep.*, 310, 97

[22] Blanton, E. L., et al., 2001, *Astrophys. J.*, 558, L15

[23] Blanton, E. L., Sarazin, C. L., & McNamara, B. R.: 2003, *Astrophys. J.*, 585, 227

[24] Borgani, S., et al.: 2001, *Astrophys. J.*, 559, L71

[25] Bower, R. G.: 1997, *M. N. R. A. S.*, 288, 355

[26] Brighenti, F., & Mathews, W. G.: 2002a, *Astrophys. J.*, 567, 130

[27] Brighenti, F., & Mathews, W. G.: 2002b, *Astrophys. J.*, 573, 542

[28] Bryan, G. L.: 2000, *Astrophys. J.*, 544, L1

[29] Bullock, J. S., et al.: 2001, *Astrophys. J.*, 550, 21

[30] Buote, D. A., & Lewis, A. D.: 2004, *Astrophys. J.*, 604, 116

[31] Buote, D. A., & Tsai, J. C.: 1996, *Astrophys. J.*, 458, 27

[32] Burles, S., & Tytler, D.: 1998, *Astrophys. J.*, 499, 699

[33] Burles, S., Nollett, K. M., & Turner, M. S.: 2001, *Astrophys. J.*, 552, L1

[34] Cantalupo, C. M., et al.: 2003, *Astrophys. J.*, submitted (astro-ph/0212394)

[35] Carlstrom, J. E., Holder, G. P., & Reese, E. D.: 2002, *Annual Review of Astronomy and Astrophysics*, 40, 643

[36] Carlstrom, J. E., Joy, M., & Grego, L.: 1996, *Astrophys. J.*, 456, L75

[37] Cavaliere, A., & Fusco-Femiano, R.: 1976, *Astronomy and Astrophysics*, 49, 137

[38] Cavaliere, A., & Fusco-Femiano, R.: 1978, *Astronomy and Astrophysics*, 70, 677

[39] Cavaliere, A., & Menci, N.: 2001, *M. N. R. A. S.*, 327, 488

[40] Cavaliere, A., Menci, N., & Tozzi, P.: 1997, *Astrophys. J.*, 484, L21

[41] Cavaliere, A., Menci, N., & Tozzi, P.: 1998, *Astrophys. J.*, 501, 493

[42] Cavaliere, A., Menci, N., & Tozzi, P.: 1999, *M. N. R. A. S.*, 308, 599

[43] Chen, Y., Ikebe, Y., Böhringer, H.: 2003, *Astronomy and Astrophysics*, 407, 41

[44] Churazov, E., et al.: 2001, *Astrophys. J.*, 554, 261

[45] Churazov, E., et al.: 2002, *M. N. R. A. S.*, 332, 729

[46] Ciotti, L, & Ostriker J. P.: 1997, *Astrophys. J.*, 487, L105

[47] Ciotti, L., & Ostriker, J. P.: 2001, *Astrophys. J.*, 551, 131

[48] Clowe, D., & Schneider, P.: 2001, *Astronomy and Astrophysics*, 379, 384

[49] Cole, S., et al.: 2001, *M. N. R. A. S.*, 326, 255

[50] Cotter, G., et al.: 2002, *M. N. R. A. S.*, 334, 283

[51] da Silva, A.C., et al.: 2001, *Astrophys. J.*L, 561, 15

[52] Dalla Vecchia, C., et al.: 2004, *M. N. R. A. S.*, 355, 995

[53] Davé, R., et al.: 2001, in Sesto 2001 - Tracing Cosmic Evolution with Galaxy Clusters (astro-ph/0109394)

[54] Davé, R., Katz, N., & Weinberg, D. H.: 2002, *Astrophys. J.*, 579, 23

[55] David, L. P., et al.: 2001, *Astrophys. J.*, 557, 546

[56] De Grandi, S., & Molendi, S.: 2002, *Astrophys. J.*, 567, 163

[57] Diemand, J., Moore, B., & Stadel, J.: 2004, *M. N. R. A. S.*, 353, 624

[58] Di Matteo, T., Springel, V., & Hernquist, L.: 2005, *Nature*, 433, 604

[59] Dolag, K., et al.: 2004, *Astrophys. J.*, 606, L97

[60] Donahue, M. E., et al..: 2000, *Astrophys. J.*, 545, 670

[61] Donahue, M. E., et al.: 2005, *Astrophys. J.*, submitted

[62] Dupke, R. A., & Bregman, J. N.: 2001, *Astrophys. J.*, 562, 266

[63] Dupke, R., & White, R. E., III 2003, *Astrophys. J.*, 583, L13

[64] Edge, A. C.: 2001, *M. N. R. A. S.*, 328, 762

[65] Edge, A. C., et al.: 2002, *M. N. R. A. S.*, 337, 49

[66] Eke, V. R., Navarro, J. F., & Frenk, C. S.: 1998, *Astrophys. J.*, 503, 569

[67] El-Zant, A., Kim, W.-T., & Kamionkowski, M.: 2004, *M. N. R. A. S.*, 354, 169

[68] Ettori, S., & Fabian, A. C.: 1999, *M. N. R. A. S.*, 305, 834

[69] Ettori, S., et al.: 2002, *M. N. R. A. S.*, 331, 635

[70] Evrard, A. E., & Henry, J. P.: 1991, *Astrophys. J.*, 383, 95

[71] Evrard, A. E., Metzler, C. A., & Navarro, J. F.: 1996, *Astrophys. J.*, 469, 494

[72] Finoguenov, A., Reiprich, T. H., & Böhringer, H.: 2001, *Astronomy and Astrophysics*, 368, 749

[73] Fitchett, M., & Merritt, D.: 1988, *Astrophys. J.*, 335, 18

[74] Fabian, A. C., et al..: 1994, *M. N. R. A. S.*, 267, 779

[75] Fabian, A. C., et al.: 2000, *M. N. R. A. S.*, 318, L65

[76] Fabian, A. C., et al.: 2002a, *M. N. R. A. S.*, 332, L50

[77] Fabian, A. C., et al.: 2002b, *M. N. R. A. S.*, 335, L71

[78] Fabian, A. C., et al..: 2003, *M. N. R. A. S.*, 344, L43

[79] Fixsen, D. J., et al.: 1996, *Astrophys. J.*, 473, 576

[80] Frenk, C. S., et al.: 1999, *Astrophys. J.*, 525, 554

[81] Fujita, Y., et al..: 2002, *Astrophys. J.*, 575, 764

[82] Furusho, T., et al.: 2001, *P. A. S. J.*, 53, 421

[83] Gómez, et al.: 2002, *Astrophys. J.*, 569, 122

[84] Govoni, F., et al.: 2004, *Astrophys. J.*, 605, 695

[85] Grainge, K., et al.: 2002a, *M. N. R. A. S.*, 329, 890

[86] Grainge, K., et al.: 2002b, *M. N. R. A. S.*, 333, 318

[87] Gray, M. E., et al.: 2002, *Astrophys. J.*, 568, 141

[88] Grego, L. et al.: 2000, *Astrophys. J.*, 539, 39

[89] Grego, L., et al.: 2001, *Astrophys. J.*, 552, 2

[90] Gutierrez, K., & Krawczynski, H.: 2005, *Astrophys. J.*, 619, 161

[91] Heinz, S., et al..: 2002, *Astrophys. J.*, 569, L79

[92] Herbig, T., et al.: 1995, *Astrophys. J.*, 449, L5

[93] Helsdon, S. F., & Ponman, T. J.: 2000, *M. N. R. A. S.*, 315, 356

[94] Henriksen, M. J., & Tittley, E. R.: 2002, *Astrophys. J.*, 577, 701

[95] Holder, G. P., & Carlstrom J. E., 2001, *Astrophys. J.*, 558, 515

[96] Holder, G. P., et al.: 2000, *Astrophys. J.*, 544, 629

[97] Holzapfel, W.: 1996, PhD thesis, Univ. California

[98] Holzapfel, W., et al.: 1997, *Astrophys. J.*, 480, 449

[99] Holzapfel, W., et al.: 2000, *Astrophys. J.*, 539, 57

[100] Horner, D. J.: 2001, PhD Thesis, University of Maryland

[101] Horner, D. J., Mushotzky, R. F., & Scharf, C. A.: 1999, *Astrophys. J.*, 520, 78

[102] Hughes, J. P., & Birkinshaw, M.: 1998, *Astrophys. J.*, 501, 1

[103] Itoh, N, Kohyama, Y., & Nozawa, S.: 1998, *Astrophys. J.*, 502, 7

[104] Johnstone, R. M., et al.: 2002 *M. N. R. A. S.*, 336, 299

[105] Jones, M. E., et al.: 1993, *Nature*, 365, 320

[106] Jones, M. E., et al.: 2005, *M. N. R. A. S.*, 357, 518

[107] Joy, M., et al.: 2001, *Astrophys. J.*, 551, L1

[108] Kaastra, J. S., et al.: 2001, *Astronomy and Astrophysics*, 365, L99

[109] Kaastra, J. S., et al.: 2004, *Astronomy and Astrophysics*, 413, 415

[110] Kaiser, C. R., & Binney, J. J.: 2003 *M. N. R. A. S.*, 338, 837

[111] Kaiser, N.: 1991, *Astrophys. J.*, 383, 104

[112] Katz, N.: 1992, *Astrophys. J.*, 391, 502

[113] Keeton, C. R.: 2001, *Astrophys. J.*, 561, 46

[114] Kempner, J. C., Sarazin, C. L., & Markevitch, M.: 2003, *Astrophys. J.*, 593, 291

[115] Kempner, J. C., Sarazin, C. L., & Ricker, P. M.: 2002, *Astrophys. J.*, 579, 236

[116] Kim, W. T., & Narayan, R.: 2003, *Astrophys. J.*, 596, L139

[117] Klypin, A. A., et al.: 1999, *Astrophys. J.*, 516, 530

[118] Kneissl, R., et al.: 2001, *M. N. R. A. S.*, 328, 783

[119] Komatsu, E., et al.: 1999, *Astrophys. J.*, 516, L1

[120] Krawczynski, H.: 2002, *Astrophys. J.*, 569, L27

[121] Lamarre, J. M., et al.: 1998, *Astrophys. J.*, 507 L5

[122] LaRoque, S. J., et al.: 2003, *Astrophys. J.*, 583, 559

[123] Lewis, A. D., & Buote, D. A.: 2002, in American Physical Society, April Meeting, Jointly Sponsored with the High Energy Astrophysics Division (HEAD) of the American Astronomical Society April 20 - 23, 2002 Albuquerque Convention Center Albuquerque, New Mexico

[124] Lewis, A. D., Buote, D. A., & Stocke, J. T.: 2003, *Astrophys. J.*, 586, L135

[125] Lewis, A. D., Stocke, J. T., & Buote, D. A.: 2002, *Astrophys. J.*, 573, L13

[126] Lewis, G. F., et al.: 2000, *Astrophys. J.*, 536, 623

[127] Lin, Y. T., Mohr, J. J., & Stanford, S. A.: 2003, *Astrophys. J.*, 591, 749

[128] Lloyd-Davies, E. J., Bower, R. G., & Ponman, T. J.: 2002, *M. N. R. A. S.*, submitted (astro-ph/0203502)

[129] Lloyd-Davies, E. J., Ponman, T. J., & Cannon, D. B.: 2000, *M. N. R. A. S.*, 315, 689

[130] Lo, K., et al.: 2000 (astro-ph/0012282)

[131] Loewenstein, M.: 2000, *Astrophys. J.*, 532, 17

[132] Loken, C., Melott, A. L., & Miller, C. J.: 1999, *Astrophys. J.*, 520, L5

[133] Loken, C., et al.: 2002, *Astrophys. J.*, 579, 571

[134] Machacek, M. E., et al.: 2002, *Astrophys. J.*, 567, 188

[135] Markevitch, M.: 1998, *Astrophys. J.*, 504, 27

[136] Markevitch, M., et al.: 2000, *Astrophys. J.*, 541, 542

[137] Markevitch, M., & Vikhlinin, A.: 2001, *Astrophys. J.*, 563, 95

[138] Mason, B. S., Myers, S. T., & Readhead, A. C. S.: 2001, *Astrophys. J.*, 555, L11

[139] Mathews, W. G., et al.: 2003, *Astrophys. J.*, 596, 159

[140] Matsushita, K., et al.: 2002, *Astronomy and Astrophysics*, 386, 77

[141] Mauskopf, P. D., et al.: 2000, *Astrophys. J.*, 538, 505

[142] Mazzotta, P., et al..: 2001, *Astrophys. J.*, 555, 205

[143] Mazzotta, P., et al.: 2002, *Astrophys. J.*, 567, L37

[144] Mazzotta, P., Fusco-Femiano, R., & Vikhlinin, A.: 2002, *Astrophys. J.*, 569, L31

[145] Mazzotta, P., Edge, A. C., Markevitch, M.: 2003, *Astrophys. J.*, 596, 190

[146] McCarthy, I. G., Babul, A., & Balogh, M. L.: 2002a, *Astrophys. J.*, 573, 515

[147] McCarthy, I. G., West, M. J., & Welch, G. A.: 2002b, *Astrophys. J.*, 567, 762

[148] McCarthy, I. G., et al.: 2003a, *Astrophys. J.*, 591, 515

[149] McCarthy, I. G., et al.: 2003b, *Astrophys. J.*, 591, 526

[150] McCarthy, I. G., et al.: 2003c, *Astrophys. J.*, 587, L75

[151] McCarthy, I. G., et al.: 2004, *Astrophys. J.*, 613, 811

[152] McCarthy, I. G., Fardal, M. A., & Babul, A.: 2005, *Astrophys. J.*, submitted (astro-ph/0501137)

[153] McNamara, B. R., et al.: 2000, *Astrophys. J.*, 534, L135

[154] McNamara, B. R., et al.: 2001, *Astrophys. J.*, 562, L149

[155] Miralda-Escudé, J., & Babul, A.: 1995, *Astrophys. J.*, 449, 18

[156] Mohr, J.J., Mathiesen, B., & Evrard, A.E.: 1999, *Astrophys. J.*, 517, 627

[157] Moore, B., et al.: 1998, *Astrophys. J.*, 499, L5

[158] Moore, B., et al.: 1999, *M. N. R. A. S.*, 310, 1147

[159] Morris, R. G., & Fabian, A. C.: 2003, *M. N. R. A. S.*, 338, 824

[160] Motl, P. M., et al.: 2004, *Astrophys. J.*, 606, 635

[161] Muanwong, O., et al.: 2001, *Astrophys. J.*, 552, L27

[162] Muanwong, O., et al.: 2002, *M. N. R. A. S.*, 336, 527

[163] Mulchaey, J. S.: 2000, *Annual Review of Astronomy and Astrophysics*, 38, 289

[164] Mulchaey, J. S., & Zabludoff, A. I.: 1998, *Astrophys. J.*, 496, 73

[165] Mushotzky, R. F., & Scharf, C. A.: 1997, *Astrophys. J.*, 482, L13

[166] Mushotzky, R., et al.: 2003, *Astrophys. J.*, submitted (astro-ph/0302267)

[167] Myers, S. T., et al.: 1997, *Astrophys. J.*, 485, 1

[168] Narayan, R., & Medvedev, M. V.: 2001, *Astrophys. J.*, 562, L129

[169] Nath, B. B., & Roychowdhury, S.: 2002, *M. N. R. A. S.*, 333, 145

[170] Navarro, J. F., Frenk, C. S., & White, S. D. M.: 1997, *Astrophys. J.*, 490, 493

[171] Neumann, D. M., & Arnaud, M.: 2001, *Astronomy and Astrophysics*, 373, 33

[172] Nevalainen, J., Markevitch, M., & Forman, W.: 2000, *Astrophys. J.*, 532, 694

[173] Novicki, M. C., Sornig, M., & Henry, J. P.: 2002, *Astron. J.*, 124, 2413

[174] Nozawa, S., et al.: 2000, *Astrophys. J.*, 536, 31

[175] Nulsen, P. E. J., et al.: 2002, *Astrophys. J.*, 568, 163

[176] Oh, S. P., & Benson, A. J.: 2003, *M. N. R. A. S.*, 342, 664

[177] Omma, H., et al.: 2004, *M. N. R. A. S.*, 348, 1105

[178] Osmond, J. P. F., & Ponman, T. J.: 2004, *M. N. R. A. S.*, 350, 1511

[179] O'Sullivan, E., & Vrtilek, J. M.: 2003, in The Riddle of Cooling Flows in Galaxies and Clusters of Galaxies, ed. T. Reiprich, J. Kempner, & N. Soker, published electronically at http://www.astro.virginia.edu/coolflow/

[180] Ota, N., & Mitsuda, K.: 2002, *Astrophys. J.*, 567, L230

[181] Ota, N., et al.: 2004, *Astrophys. J.*, 601, 120

[182] Patel, S. K., et al.: 2000, *Astrophys. J.*, 541, 37

[183] Pearce, F. R., et al.: 2000, *M. N. R. A. S.*, 317, 1029

[184] Peres, C. B., et al.: 1998, *M. N. R. A. S.*, 298, 416

[185] Peterson, J. R., et al.: 2001, *Astronomy and Astrophysics*, 365, L104

[186] Peterson, J. R., et al.: 2003, *Astrophys. J.*, 590, 207

[187] Piffaretti, R., et al.: 2005, *Astronomy and Astrophysics*, 433, 101

[188] Pointecouteau, E., et al.: 1999, *Astrophys. J.*, 519, L115

[189] Pointecouteau, E., et al.: 2001, *Astrophys. J.*, 552, 42

[190] Pointecouteau, E., et al.: 2002, *Astronomy and Astrophysics*, 387, 56

[191] Pointecouteau, E., Arnaud, M., & Pratt G. W.: 2005, *Astronomy and Astrophysics*, 435, 1

[192] Ponman, T. J., Cannon, D. B., & Navarro, J. F.: 1999, *Nature*, 397, 135

[193] Pratt, G. W., & Arnaud, M.: 2002, *Astronomy and Astrophysics*, 394, 375

[194] Pratt, G. W., & Arnaud, M.: 2003, *Astronomy and Astrophysics*, 408, 1

[195] Press, W. H., et al.: 1992, Numerical Recipes in Fortran: The Art of Scientific Computing, (Cambridge: Cambridge Univ. Press)

[196] Quilis, V., Bower, R. G., & Balogh, M. L.: 2001, *M. N. R. A. S.*, 328, 1091

[197] Ricker, P. M., & Sarazin, C. L.: 2001, *Astrophys. J.*, 561, 621

[198] Reese, E. D., et al.: 2000, *Astrophys. J.*, 533, 38

[199] Reese, E. D., et al.: 2002, *Astrophys. J.*, 581, 53

[200] Reiprich, T. H., & Böhringer, H.: 2002, *Astrophys. J.*, 567, 716

[201] Roussel, H., Sadat, R., & Blanchard, A.: 2000, *Astronomy and Astrophysics*, 361, 429

[202] Ruszkowski, M., & Begelman, M. C.: 2002, *Astrophys. J.* 581, 223

[203] Ruszkowski, M., Bruggen, M., & Begelman M. C.: 2004, *Astrophys. J.*, 615, 675

[204] Sanders, J. S., & Fabian, A. C.: 2002, *M. N. R. A. S.*, 331, 273

[205] Saunders, R., et al.: 2003, *M. N. R. A. S.*, 341, 937

[206] Sauvageot, J. L., et al.: 2001, in Clusters of galaxies and the high redshift universe observed in X-rays, Recent results of XMM-Newton and Chandra, ed. D. M. Neumann, & J. T. T. Van, published electronically at http://www-dapnia.cea.fr/Conferences/Morion_astro_2001/index.html

[207] Scannapieco, E., & Oh, S. P.: 2004, *Astrophys. J.*, 608, 62

[208] Scharf, C. A., & Mushotzky, R. F.: 1997, *Astrophys. J.*, 485, L65

[209] Schindler, S., et al.: 2001, *Astronomy and Astrophysics*, 376, L27

[210] Schmidt, R. W., Allen, S. W., & Fabian, A. C.: 2001, *M. N. R. A. S.*, 327, 1057

[211] Schmidt, R. W., Fabian, A. C., & Sanders, J. S.: 2002, *M. N. R. A. S.*, 337, 71

[212] Smith, D. A., et al.: 2002, *Astrophys. J.*, 565, 195

[213] Smith, G. P., et al.: 2003, *Astrophys. J.*, 590, L79

[214] Soker, N., Blanton, E. L., & Sarazin, C. L.: 2002, *Astrophys. J.*, 573, 533

[215] Somerville, R., & Primack, J. R.: 1999, *M. N. R. A. S.*, 310, 1087

[216] Spergel, D. N., et al.: 2003, *Astrophys. J.*S, 148, 175

[217] Springel, V., White, M., & Hernquist, L.: 2001, *Astrophys. J.*, 549, 681

[218] Stanford, S. A., et al.: 2001, *Astrophys. J.*, 552, 504

[219] Sun, M., & Murray, S. S.: 2002, *Astrophys. J.*, 576, 708

[220] Sun, M., et al.: 2002, *Astrophys. J.*, 565, 867

[221] Sun, M., et al.: 2003b, *Astrophys. J.*, 598, 250

[222] Sun, M., et al.: 2003a, *Astrophys. J.*, 587, 619

[223] Sunyaev, R., & Zeldovich, Y.: 1972, *Comments Astrophys. Space Phys.*, 2, 66

[224] Sunyaev, R., & Zeldovich, Y.: 1980, *M. N. R. A. S.*, 190, 413

[225] Takizawa, M., et al.: 2003, *Astrophys. J.*, 595, 142

[226] Tamura, T., et al.: 2001, *Astronomy and Astrophysics*, 365, L87

[227] Thomas, P. A., et al.: 2002, *M. N. R. A. S.*, 330, L48

[228] Tozzi, P., & Norman, C.: 2001, *Astrophys. J.*, 546, 63

[229] Valageas, P., & Silk, J.: 1999, *Astronomy and Astrophysics*, 350, 725

[230] Vikhlinin, A., Forman, W., & Jones, C.: 1999, *Astrophys. J.*, 525, 47

[231] Vikhlinin, A., et al.: 2002, *Astrophys. J.*, 578, L107

[232] Voit, G. M.: 2005, *Rev. Mod. Phys.*, 77, 207

[233] Voit, G. M., & Bryan, G. L.: 2001, *Nature*, 414, 425

[234] Voit, G. M., & Donahue, M. E.: 2005, *Astrophys. J.*, submitted

[235] Voit, G. M., & Ponman, T. J.: 2003, *Astrophys. J.*, 549, L75

[236] Voit, G. M., et al.: 2002, *Astrophys. J.*, 576, 601

[237] Voit, G. M., et al.: 2003, *Astrophys. J.*, 593, 272

[238] White, D. A.: 2000 *M. N. R. A. S.*, 312, 663

[239] White, D. A., Jones, C., & Forman, W.: 1997, *M. N. R. A. S.*, 292, 419

[240] White, M., et al.: 1999, *Astrophys. J.*, 514, 12

[241] White, M., Hernquist, L., & Springel, V.: 2002, *Astrophys. J.*, 579, 16

[242] Williams, L. R. L., et al.: 2004. To appear in the Proceedings of "Baryons in Dark Matter Haloes", Novigrad, Croatia, 5-9 October 2004; Editors: R.-J. Dettmar, U. Klein, P. Salucci (astro-ph/0412442)

[243] Wise, M. W., McNamara, B. R., & Murray, S. S.: 2004, *Astrophys. J.*, 601, 184

[244] Wu, K. K. S., Fabian, A. C., & Nulsen, P. E. J.: 2000, *M. N. R. A. S.*, 318, 889

[245] Wu, X. P., & Fang, L. Z.: 1997, *Astrophys. J.*, 483, 62

[246] Wu, X., & Xue, Y.: 2002, *Astrophys. J.*, 572, L19

[247] Xue, S.-J., & Wu, X.-P.: 2002, *Astrophys. J.*, 576, 152

[248] Yamasaki, N. Y., Ohashi, T., & Furusho, T.: 2002, *Astrophys. J.*, 578, 833

[249] Yoshida, N., et al.: 2002, *M. N. R. A. S.*, 335, 762

[250] Young, A. J., Wilson, A. S., & Mundell, C. G.: 2002, *Astrophys. J.*, 579, 560

[251] Zakamska, N. L., & Narayan, R.: 2003, *Astrophys. J.*, 582, 162